Natural core material based Vacuum Insulation Panels for application at up to 70 ℃

A thesis submitted for the degree of Doctor of Philosophy

by

Tarek Raad

College of Engineering, Design and Physical Sciences

Department of Mechanical and Aerospace Engineering

Brunel University London

January 2025

Abstract

Energy costs are rising and environmental concerns are gaining prominence in today's society, where the significance of effective insulation in the pursuit of energy efficiency cannot be overstated. The need to reduce heat transmission has emerged as a driving force for technical advancements across several domains including buildings, transportation, industrial processes, cold chain logistics, and energy storage. Vacuum Insulation Panels (VIPs) have generated a huge interest in recent years due to their ability to achieve a thermal conductivity of less than 7 $mW.m^{-1}.K^{-1}$. Fumed Silica (FS) and Glass Fibres (GF) are often used as core materials in VIPs owing to their inherent characteristics that enhance the panels' insulation performance. Primary drawbacks associated with these core materials are their significant impact on the environment and the high costs involved in their preparation.

The aim of this study was to develop an alternative core material from tree-based waste to partially or completely replace fumed silica and to thoroughly characterise it for its suitability in vacuum insulation panels. Three materials developed from tree-based waste, namely Tree-based Natural Fibres of varying sizes (TNFm and TNFs) and Tree-based Natural Ash (TNA). Subsequently, ten composites with FS were produced, followed by laboratory experimental characterisations. The materials microstructure was examined using a Scanning Electron Microscope (SEM) and image analysis, revealing that TNFm and TNFs had an average fibre length of 0.82 mm and 0.22 respectively, and TNA had an average particle size of 9.37 μm. SEM revealed that small agglomerates of FS particles infiltrated the interior pores of both TNFm and TNFs particles, thereby reducing the pore size. The pore size and porosity of materials and composites were analysed using Mercury Intrusion Porosimetry (MIP). Only fumed silica exhibited pores smaller than 0.1 μm, attributable to the diminutive size of primary particles and their aggregation behaviour, whereas the tree-based samples displayed an average pore size between 0.7 and 2.43 μm, with porosity ranging from 77.34% to 84.93%. The average pore diameter of all FS with tree-based natural fibre composite samples was determined to be smaller than 0.26 μm, which significantly contributes to achieving low gaseous conductivity, even under high VIP pressure. The infrared (IR) transmission spectra of the materials were acquired by Fourier Transform Infrared (FTIR) spectroscopy. Both TNF and TNA had a better spectrum extinction coefficient than FS within the 2.5 to 7.5 μm range, indicating decreased radiative leakage over the analysed wavelength spectrum. FS-TNFm1 (30 wt.% TNFm) showed the lowest thermal conductivity of 8.28 $mW.m^{-1}.K^{-1}$at 70 ℃ among all FS-TNFm composites. FS-TNFs1 (30 wt.% TNFs) showed the lowest thermal conductivity of 8.25 $mWm^{-1}K^{-1}$ at 70 ℃ among all FS-TNFs composites.

FS-TNA1 (30 wt.% TNA) showed the lowest thermal conductivity among all composites studied with a value of 7.41 $mW.m^{-1}.K^{-1}$at 70 ℃.

The results were utilised to create a COMSOL Multiphysics model of a Car Painting Booth (CPB) operating at 70 ℃. The energy consumption over a decade was analysed using three optimal composites along with FS VIP, considering the ageing effects of VIPs with various core materials, and was compared to EPS, the most common insulation employed in CPBs. Car painting booth insulated with FS-TNA1 exhibited the lowest energy consumption at 42.5 GJ over 252 days, succeeded by FS-TNFm1 at 42.7 GJ, FS-TNFs1 at 42.8 GJ, FS at 43.3 GJ, and EPS at 55.1 GJ over one year. After ten years of operation, CPBs insulated with FS VIP exhibited a reduction of 14 GJ and 11 GJ compared to FS-TNFm1 and FS-TNFs1, respectively. Following two years of operation, FS-TNFs1 and FS-TNFm1 exhibited superior thermal conductivity compared to FS, resulting in this reduction. The minimum energy consumption was 434 GJ for FS-TNA1, while the maximum was 551 GJ for EPS throughout a ten-year period.

The CPB results were used to evaluate a cradle to cradle Life Cycle Assessment (LCA) of VIPs, comprising primary material extraction, production, usage phase, and transportation of VIPs. LCA approaches Cut-off and APOS were used alongside two environmental impact assessment methods: Cumulative Energy Demand (CED) and EN15804 + A2. Impact categories were adjusted according to electricity consumption in the UK. FS-TNFm1 and FS-TNFs1 had the highest non-renewable impact at 848 GJ and 846 GJ, respectively, whereas FS had 837 GJ and FS-TNA1 had 829 GJ. The FS-TNA-insulated CPB used the least energy over a decade. The pyrolysis of TNA during early material processing prevented TNA composites from reducing their climate change impact below TNFm composites. When assessing acidification, climate change, and renewable and non-renewable resource impacts, FS was the "Green core" for substitution. Reusing core materials like FS and FS-TNA reduced environmental impacts by 74%, whereas FS-TNFm1 and FS-TNFs1 reduced impacts by 57%-59%, albeit increased energy requirements. Additionally, the cost per R-value of all manufactured VIPs at 20 ℃ and 70 ℃. FS yielded the greatest cost value of £5.13 kg^{-1} per R-value, surpassing FS-TNFm1, FS-TNFs1, and FS-TNA1, which had values of £2.70, £3.07, and £2.39 kg^{-1} per R-value, respectively.

These results demonstrate that tree-based waste materials can be transformed into sustainable, cost-effective alternatives to conventional VIP cores, reducing energy consumption by up to 7 GJ over 10 years of operation in a car painting booth and core cost by up to 29% when replacing up to 30 wt.% of tree-based waste with fumed silica, while also lowering environmental impact in both high/ low-temperature applications such as car painting booths, buildings, and cold storage.

Acknowledgments

I would like to begin by expressing my sincere appreciation to Professor Harjit Singh, my supervisor, for his invaluable guidance, unwavering support, and thoughtful advice throughout this journey. His mentorship has been a fundamental component of my development, and I am deeply appreciative of all the lessons I have acquired under his guidance.

I would also like to express my heartfelt gratitude to my friends and colleagues at the CSEF Laboratory for their shared knowledge and for creating a work environment that is both inspiring and enjoyable. Particularly, I am extremely thankful to Dron Kaushik, Leyli Vahid, Dr. Anshul Paneri, Dr. Sankarshan Verma, Dr. Hadi Tannous, Dr. Hassan Mroue, Aman Dhiman, Jose Tavares, and Maureen Senatore for their encouragement and support.

My family deserves a special and heartfelt appreciation for the continuous support, which has been the foundation of this journey. To my mother and sister, for their unwavering support, faith in me and endless love. To my partner, I am grateful for her consistent support and confidence in me throughout this journey. Most especially, to my father, Dr. Haytham Raad, whose boundless guidance, sacrifices, and financial support have made this milestone possible. His constant confidence in my capabilities has been a source of enormous strength and I am profoundly grateful to him.

List of Publications

Three peer reviewed journal publications have been produced (one published, two under review) with additional four papers accepted and presented at peer-reviewed international conferences.

Journal papers

- T.Raad, S.Verma and H.Singh, Tree waste based advanced thermal insulation – Vacuum insulation panels – For application at up to 70 ℃. International Journal of Thermal Sciences, 200, 108971 (2024). https://doi.org/10.1016/j.ijthermalsci.2024.108971
- T.Raad, D.Kaushik, V.Panara and H.Singh, "On the reusability of expanded perlite cores- A critical step towards green". Submitted to Journal of Material Cycles and Waste Management (under review).
- T.Raad and H.Singh, "A Comprehensive Life Cycle Assessment of Vacuum Insulation Panels (VIPs) for Applications at up to 70 ℃". Submitted to Journal of Building Engineering (under review).

Conference papers

- T. Raad and H. Singh "Effect of compaction and particle size distribution on the reusability of expanded perlite vacuum insulation panel cores". Paper accepted and will be presented at International Vacuum Insulation Symposium 2025 in Tennessee, USA.
- T. Raad and H. Singh "Life cycle assessment of various core materials for vacuum insulation panels used at temperatures up to 70 ℃". Paper accepted and will be presented at International Vacuum Insulation Symposium 2025 in Tennessee, USA.
- T. Raad and H. Singh "Date Palm Fibre (DPF) as core material for vacuum insulation panels for car painting booths operating at 70 ℃". Paper presented at International Vacuum Insulation Symposium 2023 in Chennai, India.
- T. Raad and H. Singh "Novel application for utilisation of Date Palm Fibre as core material in Vacuum Insulation". Paper presented at International Vacuum Insulation Symposium 2022 in London, UK.

Table of Contents

List of Figures

List of Tables

Nomenclature

Al_2O_3	Aluminium Oxide
ALCA	Attributional LCA
AP	Acidification Potential
APOS	Allocation at the Point of Substitution
CaO	Calcium Oxide
CC	Complete Cycle pyrolysis
CED	Cumulative Energy Demand
CLCA	Consequential LCA
CO	Carbon Monoxide
CO_2	Carbon Dioxide
CPB	Car Painting Booth
C-to-C	Cradle to Cradle
C-to-G	Cradle to Gate
D	Direct Pyrolysis
EE	Embodied Energy
EF	Environmental Footprint
EP	Eutrophication Potential
EPBD	Energy Performance of Buildings Directive
EPDs	Environmental Product Declarations
EPS	Expanded Polystyrene
ETC	Experimental Techniques Centre
Fe_2O_3	Iron Oxide
FeS_2	Iron Disulphide
FS	Fumed Silica
FTIR	Fourier Transform Infrared
FU	Functional Unit
GEC	Gross Energy Consumption
GF	Glass Fibres
GLO	Global
GWP	Global Warming Potential
H_2O	Water

HCl	Hydrochloric Acid
HFM	Heat Flow Meter
IBCs	Intermediate Bulk Containers
IEA	International Energy Agency
IPCC	Intergovernmental Panel on Climate Change
IR	Infrared
K_2O	Potassium Oxide
KBr	Potassium Bromide
LCA	Life Cycle Assessment
LCI	Life Cycle Inventory
LCIA	Life Cycle Impact Assessment
MgO	Magnesium Oxide
MIP	Mercury Intrusion Porosimetry
Na_2O	Sodium Oxide
NaCl	Sodium Chloride
NFs	Natural Fibres
ODP	Ozone Depletion Potential
P_2O_5	Phosphorus Pentoxide
PCRs	Product Category Rules
Re	Reynold Number
SEM	Scanning Electron Microscope
$SiCl_4$	Silicon Tetrachloride
SiO_2	Silicon Dioxide
TNA	Tree-based Natural Ash
TNF	Tree-based Natural Fibres
TNFm	Tree-based Natural Fibres medium
TNFs	Tree-based Natural Fibres small
VIPs	Vacuum Insulation Panels

λT	Overall Thermal Conductivity
λG	Gaseous Conductivity
λR	Radiative Conductivity
$\lambda Coup$	Coupling Effect
λS	Solid Conductivity
λ_S^*	Bulk Thermal Conductivity
E	Elastic Modulus
v	Poisson Number
p	External Pressure
Kn	Knudsen Number
ϕ	Pore Size
l	Mean Free Path of Gas Molecules
$\mathrm{k}B$	Boltzmann Constant
T	Temperature
$\mathrm{d}pa$	Diameter of Gas Molecule
$\lambda g0$	Gaseous Conductivity
β	Gas Coefficient
n	Refractive Index
σ	Stephan Boltzmann Constant
$\mathrm{E}R$	Rosseland Mean Extinction Coefficient
$\mathrm{T}h$	Hot Temperature
$\mathrm{T}c$	Cold Temperature
ρ	Density
$\mathrm{e}R*$	Rosseland Mean Mass Specific Extinction Coefficient
D	Pore Diameter
γ	Surface Tension between Fluid and Air
κ	Shape Factor
θ	Angle of Contact of Fluid and Wall Interface
φ	Porosity
$\mathrm{V_P}$	Pore Volume
$\mathrm{V_B}$	Bulk Volume

τ	Transmission
e_T^*	Total Spectral Extinction Coefficient
e_i^*	Spectral Extinction Coefficient of the ith component
XW	Water Constant
q	Heat Flux
th	Thickness
ΔT	Difference in Temperature
λ_{g0}	Gaseous Conductivity of Free Gas
ϕ	Average Pore Size of the Material
α	Optical Thickness
r	Rate of Increase of Thermal Conductivity
$\lambda 0$	Thermal Conductivity measured after Manufacturing
t	Time
$\mathrm{E_{Ms}}$	Energy Consumption at Maximum Capacity
$\mathrm{P_{Ms}}$	Maximum Power
$\mathrm{T_s}$	Time Required to Sieve TNFm and TNFs
E_g	Energy Consumption of the Grinder
P_g	Power of the Grinder
T_g	Time Required to Grind TNF
E_f	Energy Consumption of Furnace
P_f	Power of Furnace
T_f	Time Required for Pyrolysis
E_{OR}	Energy Consumption of Oven
P_{OR}	Power of the oven
T_{OR}	Time Required to dry the Raw Material
$E_{(TNFm)t}$	Total Energy Consumption of Processing TNFm
$E_{(TNFs)t}$	Total Energy Consumption of Processing TNFs
$E_{(TNA)tc}$	Total Energy Consumption of the Pyrolysis of TNA (CC)
$E_{(TNA)td}$	Total Energy Consumption of the Pyrolysis of TNA (D)
E_{core}	Actual Energy Consumed of Various Core Materials
E_{OC}	Energy Consumption
P_{OC}	Power of the Oven

T_{OC}	Time Required to Dry the Raw Material
E_{Mx}	Energy Consumption of Mixer
P_{Mx}	Power of the Mixer
T_{Mx}	Time Required to Mix the Composites
NR_T	Total Non-Renewable Energy Consumed
R_T	Total Renewable Energy Consumed
CC	Combined Effect of Three Factors: CC_F, CC_B and CC_L
CC_F	Climate Change Associated with Fossil Fuels
CC_B	Climate Change Associated with Biogenic Sources
CC_L	Climate Change Associated with Land Use
HT	Total Human Toxicity
HT_{Co}	Organic Total Human Toxicity
HT_{Ci}	Inorganic Total Human Toxicity
TNF_p	Cost of the Processed Fibres
TNA_p	Material Cost for TNA
e	Average Price of Electricity
RM	Raw Material Price
Ca_{max}	Total Amount of Material Filled at Maximum Capacity
C_{core}	Core Cost per Unit Mass
C_p	Material Specific Heat
u	Velocity Field
Q	Heat Energy
ϵ	Emissivity
G	Irradiance
$e_b(T)$	Blackbody Hemispherical Total Emissive Power
T_{in}	Inlet Temperature
T_{out}	Outlet Temperature
P_{heater}	Heater Power
T_C	Sensor Temperature

CHAPTER 1: Introduction

1.1 Background

The United Kingdom has established ambitious decarbonisation objectives, pledging to decrease greenhouse gas emissions by 68% by 2030 in relation to 1990 levels and to attain net zero by 2050 (BEIS, 2022). The UK Government has aims to completely decarbonise electricity generation by 2035 and to decrease energy usage in buildings by a minimum of 15% by 2030 by adopting improved energy efficiency measures (DESNZ, 2024).

Insulation is seen as a crucial element in reaching these goals by enhancing energy efficiency in buildings through the reduction of energy demand for heating and cooling, hence decreasing greenhouse gas emissions. Several insulation materials are presently utilised in the UK, including Expanded Polystyrene (EPS), fibreglass, and mineral wool, exhibiting thermal conductivities ranging from 30 to 40 $mW \cdot m^{-1} \cdot K^{-1}$ (Al-Sallal, 2003; Ramli Sulong et al., 2019; Väntsi and Kärki, 2014). It is increasingly becoming more and more evident that these materials would struggle in meeting the newly set environment targets, particularly concerning their thermal conductivity during usage phase and impacts on the environment during production and disposal phases.

For example, policy drivers such as Energy Performance of Buildings Directive (EPBD), require the European Union to achieve a 32.5% increase in energy efficiency by 2030 in all sectors (EPBD, 2019). Moreover, the UK prohibited the use of EPS in food-related applications as of November 2023 (DEFRA, 2023). This legislative change indicates a possibility of similar restriction(s) in industry sector as well. This legislative change suggests a trajectory toward more stringent regulation of EPS across broader applications, including its industrial use. In this context, industrial thermal enclosures, such as Car Painting Booths (CPBs), are increasingly being scrutinised through the same lens as building. Although CPBs are technically process equipment, they are enclosed, thermally regulated spaces located within or attached to buildings. As such, they are increasingly subject to the same principles that govern energy performance in buildings, particularly under UK Part L regulations and EU lifecycle-based environmental product declarations. Thus, the development of alternative insulation materials with enhanced thermal performance and better environment credentials is essential.

Vacuum Insulation Panels (VIPs) have generated a huge interest in recent years due to their ability to achieve a thermal conductivity of less than 0.007 $W.m^{-1}. K^{-1}$ (Verma and Singh, 2019a), which is 3-7 times smaller than that of conventional insulation. Understandably, they possess a

notable advantage in terms of space economy, since VIPs require a relative smaller thickness compared to conventional insulation (Alam et al., 2011) to deliver a given U-value (Chang et al., 2016).

The central element of VIPs, known as core, plays a crucial role in their performance by allowing the vacuum to be drawn and providing mechanical strength against collapsing under external forces caused by the atmosphere. The core is surrounded by a barrier, which serves the purpose of preserving vacuum inside the panel. Fumed Silica (FS) and Glass Fibres (GF) are often used as core materials owing to their inherent characteristics that enhance the thermal performance of VIPs.

The main disadvantages of these core materials include the limited durability of glass fibre and the high cost of fumed silica (Chang et al., 2016). Core material accounts for approximately 60% of the overall cost and 90% of the overall environmental impact (Resalati et al., 2021) in the case of VIPs. Several studies have reported the use of organic materials such as natural fibres, including bamboo fibre, flax fibre, straw and wood fibre, as primary core material (Dong et al., 2022; Wang et al., 2019a, 2020). Natural fibres as core materials have potentially favourable characteristics, such as affordability, minimal environmental impact and notable mechanical properties. However, it is important to note that the historical and contemporary research is limited to reporting experimental measurements performed under specific conditions, such as average temperature of ≤30 ℃. It is in this context that a comprehensive investigation into the impact of new organic materials' properties at elevated temperatures (up to 70 ℃) is needed to potentially identify economically and environmentally sustainable core materials.

While VIPs have been extensively explored in the building sector, their application in industrial settings remains underdeveloped. One promising area is the automotive sector. In 2023, the UK automotive sector consumed 3.128 TWh of electricity and a total of 603,319 tonnes of CO_2 emission during the vehicle production phase (SMMT, 2024). Out of the total energy consumed 20-30% is attributed to the oven process, primarily CPB, which necessitate maintaining precise temperature (about or up to 70 ℃) within the booth(Rao and Gopinath, 2013). These booths resemble thermally controlled building enclosures in both form and function, and thus, are increasingly relevant within discussions of building-integrated energy efficiency and decarbonisation strategies. Replacing conventionally used EPS insulation with VIPs in CPBs could enable the automotive industry to reduce energy usage and CO_2 emissions, hence helping in achieving UK's net-zero aim for 2050.

1.2 Aim and objectives

Aim:

The aim of this study is to develop and demonstrate performance of alternative, low-cost, and environmentally friendly core materials based on tree based organic materials (fibres and/or ash) for vacuum insulation panels for use in car painting booths operating at high-temperature (70 ℃).

Specific Objectives:

I. Analyse the historical and present developments in order to comprehend the fundamentals behind material selection, physics, and production of the core materials for vacuum insulation panels, as well as determining the factors affecting their thermal performance.

II. Test the properties (fibre length, particle size, pore size, porosity) of tree based natural fibres and ash to use as core material for vacuum insulation panel and optimisation. Techniques for material characterisation used in this study include Scanning Electron Microscopy, Fourier Transform Infrared spectroscopy, Mercury Intrusion Porosimetry, Energy-Dispersive X-Ray spectroscopy, Thermo-gravimetric analysis and Thermal conductivity measurement.

III. Manufacture and test vacuum insulation panels made of the optimised tree based natural fibres and ash, and their composites with fumed silica.

IV. Develop a COMSOL Multiphysics based system scale model for a typical car painting booth using vacuum insulation panels as insulation developed in this study.

V. Perform a comprehensive Life Cycle Assessment of vacuum insulation panels made of tree based organic materials developed in this study on cradle to cradle basis.

1.3 Thesis structure

This thesis has been divided into seven chapters where:

Chapter 1 introduces readers with the primary motivation behind the work and defines the aim and subsequent objectives.

Chapter 2 provides an in-depth review of various types of materials used in vacuum insulation panels, including organic (such as natural fibres), inorganic, and hybrid core materials. It also explores heat transfer phenomena, factors that influence thermal performance, the environmental impact of insulation, previous life cycle assessments on VIPs and knowledge gaps.

Chapter 3 presents an overview of the processes involved in preparing materials, developing composite samples, and characterising them. It also discusses the experimental techniques used

to measure various properties of different core materials, such as TNF, TNA, FS, and composite core materials.

Chapter 4 presents the experimental results of the manufactured VIP of different core materials at different temperature range (20-70℃) and different pressure range (0.1-1000 mbar) form the experiments planned from chapter 3.

Chapter 5 provides a comprehensive life cycle assessment of VIPs with various core materials. This assessment covers the extraction of raw materials, their preparation, production, usage, and disposal at the end of their life (cradle to cradle). This chapter offered comprehensive explanations of the functional units employed, along with the system boundaries and the importance of choosing suitable LCA approaches and methods.

Chapter 6 presents a new application for VIPs at elevated temperatures, specifically in car painting booths. A three-dimensional COMSOL Multiphysics model was created to analyse and compare the energy consumption, and CO_2 emissions of a car painting booth when insulated with vacuum insulation panel compared to expanded polystyrene. Moreover, the results of the full life cycle assessment of VIPs with various core materials in relation to the findings from the car painting booth model was discussed in depth. Additionally, an economic evaluation of the different core materials of VIP was conducted and compared to EPS.

Chapter 7 provides the conclusions of the study, as well as suggestions for future research.

1.4 Addition to the knowledge

The primary contribution of this work to the existing knowledge is summarised as follows:

I. A framework for material preparation and characterisation of organic materials (fibres and ash) for use as cores of vacuum insulation panels has been developed and presented.
II. Techno-econo-enviro performance of the produced organic materials and their composites with fumed silica at high temperature (70 ℃) is fully characterised, understood and presented.
III. A life cycle, cradle to cradle, environmental impact of VIPs made of developed organic materials and conventional materials has been performed and the results presented. Critical input parameters (material and process driven) needed for a reliable LCA analysis have been identified and presented along with the detailed methodology.

CHAPTER 2: Literature Review

2.1 Introduction

Insulation is essential to the UK's decarbonisation strategy, as it directly tackles the issue of diminishing energy usage and related greenhouse gas emissions across several sectors. Efficient insulation reduces heat transfer, resulting in substantial decreases in the energy used for heating, cooling, and maintaining temperature consistency across diverse applications. In buildings, high-performance insulation is essential for meeting the energy efficiency objectives established by the government's Heat and Buildings Strategy (HBS, 2021). This approach prioritises the retrofitting of existing buildings and enhancing the thermal efficiency of new constructions to comply with more stringent energy performance criteria and decrease heating and cooling requirements (Palmer and Cooper, 2012).

Vacuum Insulation Panels (VIPs) represent revolutionary technology, providing unparalleled thermal efficiency that aligns with the UK's decarbonisation objectives. VIPs can lower U-values to a minimum of 0.10 W/m²K in buildings, significantly surpassing the UK's existing building regulation standards of 0.18 W/m²K for walls in new constructions (Changes to Approved Document L 2021 (England), 2022). Their streamlined design facilitates thinner walls and roofs, which is especially beneficial in space-limited urban environments or when renovating historic structures where preserving interior space is crucial.

Besides their role in building, VIPs are being utilised in other areas essential to the UK's decarbonisation objectives. In cold chain logistics, where low temperatures are essential for food preservation or vaccine storage, VIPs minimise heat loss and substantially decrease the energy required for refrigeration. Thiessen et al., (2016) documented a 21% decrease in energy consumption when 56% of the refrigerator surface was insulated with VIPs instead of polyurethane (PU) foam.

The advantages of VIPs have been thoroughly examined, especially regarding their use in construction and various other industries. Nonetheless, considerable disadvantages are linked to the primary materials utilised in VIPs, namely Fumed Silica (FS) and Glass Fibre (GF). These materials are frequently utilised for their superior thermal insulation characteristics; nonetheless, their manufacture is marked by substantial costs and significant embodied energy. Fumed silica accounts for around 90% of the environmental effect of VIPs, highlighting its significant influence on the life-cycle energy requirements of these panels (Karami and Gudmundsson 2015).

In response to these issues, there is an increasing emphasis on discovering alternative core materials that are economically viable and environmentally friendly. Researchers globally have explored cost-effective alternatives to partially or completely substitute fumed silica and glass fibre in VIPs. Natural Fibres (NFs) are gaining considerable interest among these alternatives because to their cost-effectiveness, minimal environmental impact, and remarkable mechanical characteristics. Investigating these different types of materials involves classifying them, reviewing the conditions of their study, and evaluating the thermophysical processes that affect their performance in VIPs. The objective is to create core materials with improved characteristics that ensures reliable performance at the minimal feasible expense. This study systematically evaluates several core materials, encompassing both organic and inorganic alternatives, to identify viable alternatives for sustainable VIP production.

Following the evaluation of alternative core materials, it is essential to examine the life-cycle assessments (LCA) of VIPs. This includes the examination of research that define functional units, identify system boundaries, and assess critical parameters affecting environmental impacts. LCAs provide the quantification of advantages and disadvantages associated with various core materials, hence informing the selection process for sustainable alternatives. Additionally, it is crucial to investigate the reusability of VIP core materials, as they significantly influence both the cost and the environmental impact of VIPs. Initiatives that improve recyclability and diminish waste can substantially elevate the overall sustainability of these panels.

Finally, this research investigates the applicability of VIPs in many areas and temperature ranges. Comprehending the performance of VIPs under distinct situations helps in pinpointing the sectors where they deliver maximum value and guides the development of VIPs customised for various operational environments. This comprehensive strategy seeks to overcome the key constraints of VIPs, facilitating the development of more economical and environmentally friendly insulation alternatives.

2.2 VIP core materials and components

Vacuum insulation panels (VIPs) consist of many primary components, including core material and envelope, along with additional components such as getters, desiccants, and opacifiers, see Figure 2.1. The core material, constituting the internal component of the VIP, is composed of porous materials with varying pore dimensions, such as powders, fibres, and porous foams. These porous materials reduce heat transmission by minimising gaseous conduction, which is further suppressed by the evacuation process.

The VIP envelope serves as an external barrier that contains the core and preserves the vacuum at a low-pressure level. The envelope additionally provides mechanical strength to withstand stress during handling and installation. These barriers typically comprise metallised polymer films, aluminium foils, or steel, which can maintain the internal vacuum for a duration of 30 to 50 years, depending on the core material and the storage climatic conditions (Tenpierik and Cauberg, 2007). The essential features needed for the envelope encompass low thermal conductivity, flexibility, minimal water vapour and oxygen transmission.

Additional components, including getters and desiccants like synthetic zeolites, are employed to absorb water vapour and gases that may infiltrate the panel, hence potentially prolonging the VIP's service life. Opacifiers, like silicon carbide and carbon black, are incorporated into the core material to minimise radiative heat transfer. Optimising the quantity of opacifiers is crucial, since an increased proportion might significantly raise solid conductivity (Li et al., 2019).
The next two parts examine conventional non-organic core materials utilised for VIP and outline the alternative organic core materials investigated in recent years.

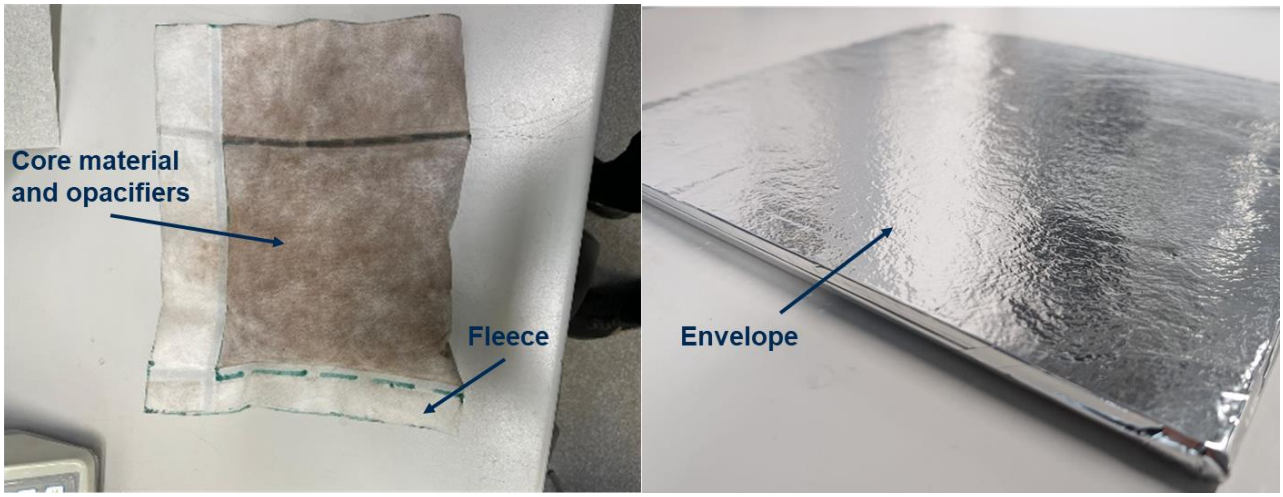

Figure 2.1 Vacuum insulation panels components.

2.2.1 Non-organic core materials

Fumed silica, aerogel, expanded perlite, and glass fibres are considered among the most often employed core materials for vacuum insulation panels. Fumed silica, originally developed by Evonik Industries in Germany in 1942 (Evonik Industries, 2006), is the predominant core material for VIPs owing to its distinctive properties that enhance the insulation performance of the panels. Fumed silica possesses a fused spherical structure arranged in branching chains, with an average aggregate size of 0.2–0.3 μm, distinguished by an exceptionally small particle size of 300 nm,

high porosity, and low density (Wang et al., 2007). However, fumed silica has two significant drawbacks: the high cost of manufacture (Barthel et al., 1996) and reduced thermal resistance to radiative heat transfer (Singh et al., 2015).

Aerogel incurs a prohibitively high cost, exceeding that of fumed silica, with a price of $2000 for a tile measuring 50 mm x 75 mm x 7 mm (Liu et al., 2017a). Aerogel, characterised by its small pore size typically ranging from 1 to 100 nm and its low density, provides exceptional thermal insulation, with heat conductivity not surpassing 4 $mW.m^{-1}.K^{-1}$at 50 mbar pressure, proving it suitable for VIP applications (Fricke et al., 1992). A proposed method involved utilising aerogel and expanded perlite as a composite to enhance mechanical stability and reduce the cost of the expensive aerogel, while also observing a little decrease in thermal conductivity compared to pure expanded perlite VIP (Wang et al., 2019a).

Expanded perlite is seen as an attractive alternative to partially or completely substitute fumed silica or aerogel, since it provides a more affordable solution due to its cheap cost of £0.27 per kilogramme (Alam et al., 2014). Historically, expanded perlite has been utilised in various construction applications owing to its low thermal conductivity and minimal bulk density, which can reach as low as 35 $kg.m^{-3}$ (Verma and Singh, 2022). Furthermore, researchers began utilising expanded perlite as a substitute core material for VIPs because of its porous characteristics, which are ideal for application in vacuum environments (Modest and Mazumder, 2021). When expanded perlite is compacted and subjected to vacuum, the core density increases, resulting in a substantial rise in overall thermal conductivity due to enhanced solid conduction. Expanded perlite VIP exhibits a thermal conductivity value of 11 $mW.m^{-1}.K^{-1}$ at a pressure of 0.1 mbar and mean temperature of 20℃ (Verma and Singh, 2019). Furthermore, the pore size of expanded perlite is comparatively larger than that of fumed silica, averaging 3 μm, necessitating a vacuum level below 0.01 mbar to mitigate the influence of gaseous conductivity. Maintaining this pressure for prolonged applications is challenging, which is a significant downside of utilising expanded perlite. The resolution of these concerns can be achieved by filling the large pores of perlite with nanomaterials, such as aerogels or fumed silica, which can lead to a decrease in gaseous conductivity even at atmospheric pressure (Beikircher and Demharter, 2013).

Another frequently utilised core material is glass fibre, particularly for high-temperature applications due to its exceptional thermal stability (Kwon et al., 2009). The fibre diameter generally varies from 0.5 to 0.7 μm, with a bulk density of 250 $kg.m^{-3}$. The solid conductivity of glass fibre VIP has been reported as 2.1 $mW.m^{-1}.K^{-1}$, radiative conductivity as 0.7 $mW.m^{-1}.K^{-1}$, and gaseous conductivity as 0.78 $mW.m^{-1}.K^{-1}$ at a mean temperature of 300 K and a pressure of

0.1 mbar. The thermal conductivity of 3.6 $mW.m^{-1}.K^{-1}$ can only be attained at low pressure, as it increases exponentially with rising pressure due to the substantial pore size of glass fibre. The two primary disadvantages of glass fibre are its limited lifespan, estimated at 15 years (Kallel et al., 2019), and the environmental concerns associated with its production (Kan et al., 2020).

2.2.2 Organic core materials and composites

The disadvantages of the traditional core materials are the limited durability, in case of glass fibre, and the considerably high expense in the production stage such as fumed silica (Verma and Singh, 2020). As a result, numerous researchers report a global effort to develop lower-cost alternative core materials that can partially or entirely substitute glass fibre and fumed silica.

Moreover, some researchers have documented studies on the utilisation of Natural Fibres (NFs), including bamboo fibre, flax fibre, straw, and wood fibre, as core materials for VIPs. NFs are experiencing a surge in popularity owing to their advantageous traits like as cost-effectiveness, less environmental impact, and significant mechanical properties. Table *2.1* displays fourteen alternative core materials collected from 2012 to 2022.

Table 2.1: Fourteen researches on alternative organic core materials (2012 to 2022)

Authors	Core Material	Main Findings
(Dong et al., 2022)	Bamboo Fibre (BF) and Glass Fibre (GF)	λ= 12.62 $mW.m^{-1}.K^{-1}$for complete bamboo fibre VIP at 0.0005 mbar λ= 4.81 $mW.m^{-1}.K^{-1}$for glass fibre and bamboo composites at 0.0005 mbar λ= 7.96 $mW.m^{-1}.K^{-1}$ f at 0.0005 mbar or composite after 500 days of storage at 30 ℃ and 60 % RH
(Zhao et al., 2022)	Wood Pulp (WP) and Glass Fibre (GF)	λ= 6.48 $mW.m^{-1}.K^{-1}$ for complete wood pulp fibre VIP at 0.0005 mbar and 25 ℃ λ= 4.69 $mW.m^{-1}.K^{-1}$ for complete wood pulp fibre and glass fibre composites at 0.0005 mbar and 25 ℃ λ= 7.42 $mW.m^{-1}.K^{-1}$ at 0.0005 mbar and 25 ℃ for composite after 365 days of storage at 70 ℃ and 90 % RH

(Wang et al., 2020)	Straw (St)	λ= 3.8 mW.m^{-1}.K^{-1} at 0.1 mbar for complete straw VIP with an optimum drying of the straw fibre for 60 minutes at temperature of 120 ℃
(Zach et al., 2019)	Cotton (Co)	λ= 5.14 mW.m^{-1}.K^{-1} for complete cotton VIP at 0.05 mbar and 10 ℃ and λ= 41.9 mW.m^{-1}.K^{-1}at atmospheric pressure and 10 ℃
	Flax (Fl)	λ= 4.45 mW.m^{-1}.K^{-1}for complete flax VIP at 0.05 mbar and 10 ℃ and λ= 43.42 mW.m^{-1}.K$^{-1\ 1}$at atmospheric pressure and 10 ℃
(Wang et al., 2019b)	Wood Fiber (WF)	λ= 9.4 mW.m^{-1}.K^{-1} at 0.03 mbar and 20 ℃ for complete wood fibre VIP with density of 200 kg.m^{-3}
(König et al., 2019)	Foamed Glass (FG)	λ= 54.3 mW.m^{-1}.K^{-1} for foamed glass VIP at atmospheric pressure and 20 ℃ with density of 117 kg.m^{-3} λ= 26.7 mW.m^{-1}.K^{-1}for foamed glass VIP at 0.0001 mbar and 20 ℃
(ChunXin et al., 2017)	Sawdust (Sd)	λ= 10.5 mW.m^{-1}.K^{-1} for complete sawdust VIP at 1 mbar and 23 ℃ with density of 200 kg.m^{-3} and a porosity of 83.1%
(Alam and Singh, 2019)	Sawdust, Fumed Silica (FS) and Silicon Carbide (SiC)	λ= 5.52 mW.m^{-1}.K^{-1} for composite VIP containing 30% sawdust at 0.5 mbar and 20 ℃ λ= 21.12 mW.m^{-1}.K^{-1} for composite VIP containing 80% sawdust at 0.5 mbar and 20 ℃
(Zhuang et al., 2017)	Expanded Cork (EC) and Fumed Silica (FS)	λ= 45.5 mW.m^{-1}.K^{-1} for composite VIP containing 100% expanded cork at atmospheric pressure and 20 ℃ λ= 28.7 mW.m^{-1}.K^{-1} for composite VIP containing 50% expanded cork at atmospheric pressure and 20 ℃

		λ= 6.3 mW.m^{-1}.K^{-1} for composite VIP containing 50% expanded cork at 1 mbar and 20 ℃
(Tetlow et al., 2017)	Cellulosic Crystals (CC) and Fumed Silica (FS)	λ= 11.7 mW.m^{-1}.K^{-1} for cellulosic crystals VIP containing with density of 127 kg.m^{-3} at 1 mbar
(Prachayawarakorn, 2005)	Rice Husk ash (RH), Fumed Silica (FS), and Opacifiers (O)	λ= 5.5 mW.m^{-1}.K^{-1} at 1 mbar and 24 ℃for an optimum composition of 26% rice husk ash VIP with density of 255 kg.m^{-3}
(Nemanič et al., 2014)	Melamine-formaldehyde Fibres (MF)	λ= 33 mW.m^{-1}.K^{-1} at atmospheric pressure and 20 ℃
(Kim et al., 2012)	Phenolic Foam (PF)	λ= 5 mW.m^{-1}.K^{-1} at 0.01 mbar and 20 ℃

2.3 Thermal performance of VIPs

Thermal conductivity is widely recognised as a key performance characteristic of thermal insulation materials. It encompasses the combined effect of solid, gaseous and radiative conductivity. This comprehensive metric can be mathematically stated equation (2.1), as described in (Fricke et al., 1992):

$$\lambda_T = \lambda_S + \lambda_G + \lambda_R + \lambda_{Coup} \quad (2.1)$$

where λ_T is the overall thermal conductivity of VIPs, λ_S the solid conductivity, λ_G the gaseous conductivity, λ_R the radiative conductivity and λ_{Coup} is the thermal conductivity due to the effect of coupling.

Factors such as density, pore size, porosity, mean operating temperature, sealing pressure, particle size, and relative humidity each contribute to the total conductivity of the VIPs. These key components are discussed in the four-coming sections.

2.3.1 Solid conductivity

Solid conductivity is considered the dominant heat transfer mode when the VIP is evacuated and assessed at low mean temperatures, where gaseous and radiative conductivity, along with coupling effects, exert limited influence. The core density and porosity of materials significantly influence solid conductivity, as heat is transmitted by direct particle contact. The density indicates the quantity of solid material per unit volume; in denser materials, the solid structure is more compact, resulting in shorter and more direct heat transmission paths, which leads to a higher

solid conductivity. On the other hand, porosity quantifies the proportion of a material's volume occupied by voids, which restrict heat transfer. Materials with higher porosity compel heat to travel around these holes over a longer and more tortuous pathway, resulting in reduced solid conductivity. However, obtaining accurate values of λ_S and validating them requires extensive experimental data due to the complexities involved.

Rottmann and Beikircher (2022) observed that an increase in porosity results in a nearly double decrease in solid conductivity, highlighting the significant impact of porosity on solid conductivity. This phenomenon occurs because the thermal conductivity of the solid phase typically exceeds that of the gas phase, thus augmenting porosity (or gas volume) reduces the effective thermal conductivity of porous structures. The thermal conductivity of a porous media is typically proportional to the thermal conductivity λ_s^* of the solid, non-porous material component (Rottmann and Beikircher, 2022) and can be determined using equation (2.2).

$$\lambda_{s,powders} = G\lambda_s^*(T) \tag{2.2}$$

where G denotes the influence of reduced density in a porous medium and encompasses all thermal resistances attributable to the material's structural properties.

The solid conductivity of fibrous materials can be determined using a straightforward model based on elastic contact theory (Kwon et al., 2009) using equation (2.3).

$$\lambda_{s,fibres} = \frac{16\lambda_s^*}{\pi^2}\left(\frac{E^{\frac{1}{3}}}{\{3\pi^2(1-v^2)(1-\prod)^4 p\}^{\frac{1}{3}}} + \frac{1}{4(1-\prod)^3}\right)^{-1} \tag{2.3}$$

Where; λ_s^* is the bulk thermal conductivity, E the elastic modulus, v the Poisson number, $\prod$ the porosity and p the external pressure.

It was anticipated that ideal stacked layers with uniform diameter and cross-oriented fibres were positioned over the preceding layer to maximise separation between adjacent neighbour contacts. The pathway for heat transfer is thereby optimised. Nonetheless, real-world materials frequently display inconsistencies in fibre alignment, contact areas, and packing density, resulting in deviations from the idealised model. Experimental data for solid conductivity can be acquired by assessing the total thermal conductivity under conditions of reduced pressure and low mean temperature, to minimise the impact of gaseous and radiative conductivity.

2.3.2 Gaseous conductivity

Heat transfer in gases occurs by convection and conduction. The conduction intensity in gases depends on the Knudsen Number (Kn), which is defined by the pore size (ϕ) and the ratio of the mean free path of gas molecules (l), representing the mean distance a gas molecule travels prior colliding with another molecule, as indicated in equation (24) (Simmler and Brunner, 2005). The mean free path is determined by equation (2.5).

$$Kn = \frac{l}{\phi} \tag{2.4}$$

$$l = \frac{k_B T}{\sqrt{2}\, p\pi d_{pa}^2} \tag{2.5}$$

where k_B is the Boltzmann constant (1.3807 x 10^{-23} JK^{-1}), T the temperature (K), p the gas pressure (Pa) and d_{pa} the diameter of gas molecule (m).

At reduced pressure, the mean free path outweighs the pore size, resulting in a Knudsen number that is higher than one. The substantial mean free path results in no energy transfer between gas molecules and solid surfaces, hence reducing gaseous conductivity. As internal pressure rises, the mean free path decreases, resulting in a Knudsen number of less than one. This indicates that when the mean free path decreases the collisions among molecules of gases increases, hence raising gaseous conductivity. The correlation between gaseous conductivity and the Knudsen number can be seen in equation (2.6) (Swimm et al., 2009).

$$\lambda_g = \frac{\lambda_{g0}}{1 + 2\beta Kn} \tag{2.6}$$

where λ_{g0} is the gaseous conductivity of free gas and β the gas coefficient.

The equation (2.6) clearly indicates that as pore sizes of the materials increase, gaseous conductivity would also rise with increasing pressure. Materials such as fumed silica, with a pore size of 300 nm, exhibit low gaseous conductivity even at elevated pressures (up to 50 mbar), whereas natural fibres, with pore sizes reaching 10 µm, experience a substantial increase in gaseous conductivity when internal pressure surpasses 10 mbar. This relation illustrates the significance of using nanoparticle materials when utilising materials with large average pore sizes.

2.3.3 Radiative conductivity

At low vacuum, gaseous conductivity becomes insignificant, rendering radiative conductivity a prominent mode of heat transfer. Radiative heat transfer encompasses the emission, absorption,

and scattering of thermal infrared radiation within porous core materials, determined using equation (2.7) (Reiss, 1988).

$$\lambda_r = \frac{16\, n^2 \sigma T^3}{3\, E_R\ (T)} \tag{2.7}$$

where *n* is the refractive index, σ the Stephan Boltzmann constant (5.67 x 10^{-8} $Wm^{-2}K^{-4}$), *T* the mean temperature and $E_R(\mathrm{T})$ the Rosseland mean extinction coefficient.

For minor differences between the hot (T_h) and cold (T_c) temperatures, the arithmetic mean temperature, as indicated in equation (2.8), serves as an adequate approximation of the mean radiation temperature T. Conversely, for high-temperature applications, the cubic mean of the temperature distribution must be computed using equation (2.9) (Roland Caps et al., 1984; Caps and Fricke, 2000).

$$T = \frac{(T_h + T_c)}{2} \tag{2.8}$$

$$T = \sqrt[3]{\frac{1}{4}(T_h^2 + T_c^2)(T_h + T_c)} \tag{2.9}$$

At elevated temperatures, the radiative thermal conductivity increases the cubic mean of the temperature, as shown in equation (2.7), and consequently dominates all other modes of heat transfer, especially when VIP is sealed at low pressure. As a result, it must be kept to a minimum in order to achieve low effective thermal conductivities.

The Rosseland mean extinction coefficient can be determined by the relation between the density (ρ) and the Rosseland mean mass specific extinction (e_R^*) coefficient using the equation (2.10).

$$E_R(T) = e_R^*\ \times \rho \tag{2.10}$$

e_R^* can be quantified by obtaining the transmission values by Fourier Transform Infrared Spectroscopy (FTIR) utilising two methodologies. The initial procedure was delineated wherein loose powder was spread on a base of potassium bromide (KBr) and positioned in a horizontal orientation (Kuhn et al., 1993). This method was employed to prevent the mixing of the material with KBr, hence avoiding alterations in scattering behaviour. A complex configuration of mirrors was utilised to divert the infrared beam onto the horizontal specimen. Nonetheless, a significant problem lies in the homogeneous dispersion of the powder layer on the KBr base surface, which may impact the reliability of the obtained spectral data.

The second method was set by employing the KBr technique, which involved combining a small proportion of the powder sample with KBr powder and compressing it into a disc (Intini and Kühtz, 2011). To mitigate the impact of KBr on infrared light scattering losses, they deducted a background measurement of a pure KBr disc. This method reduces the scattering effects induced by KBr, which is particularly significant in infrared analysis where precise transmission and scattering data are crucial.

2.3.4 Coupling effect

The coupling effect in thermal conductivity refers to the heat transmission between particles through gas molecules within a material's pores. This phenomenon functions as a shortcut for thermal transfer, with the gas acting as a medium connecting the solid particles. The importance of the coupling effect is contingent upon the material type and its structure. The impact is negligible for foam cores with undamaged structures, as solid channels mostly govern heat conduction, while the gas within the pores exerts less influence (Fricke et al., 2006). Nonetheless, in the case of porous powders, the coupling effect becomes significant at atmospheric pressure, since the elevated density of gas molecules enhances the interaction among solid particles. The coupling effect is pressure dependent, decreasing at low pressures when fewer gas molecules are available to enable heat transmission (Zhao et al., 2012). Direct measurement of the coupling effect is difficult due to its overlap with other modes of heat transfer, such as solid and gas conduction. Researchers have employed semi-empirical models to quantify this impact, which can also be implicitly computed by comparing thermal conductivity in atmospheric and evacuated circumstances, while considering gaseous conductivity.

2.3.5 Ageing of VIPs

The thermal conductivity measurements of the centres of panels from post-manufactured VIPs are utilised by most studies for predicting energy savings in various applications. It is essential to understand that the value of heat conductivity tends to grow over time. This is ascribed to either the gradual rise in internal air pressure or the moisture level within the VIP. The principal elements driving this rise are the materials used for the envelope and the core. For instance, fumed silica is hydrophobic and resists moisture absorption, while cellulosic materials are hydrophilic, enabling them to absorb moisture, especially when subjected to fluctuations in temperature and humidity. (Schwab et al., 2005) hypothesised that thermal conductivity increases over time, accounting for variations in both internal pressure and moisture content, as described by equation (2.11).

$$\lambda_T = \lambda_{T\,evac} + \lambda_G\big(p(t)\big) + b.X_W(t) \quad (2.11)$$

where $\lambda_{T\,evac}$ is the total thermal conductivity in evacuated condition, the pressure, t the time, b the sorption isotherm constant and X_W water constant.

2.3.6 Reported microstructural characteristics of different cores

As discussed in the preceding sections, the thermal conductivity of VIPs results from the combined contributions of solid conduction, gaseous conduction, and radiative heat transfer. These mechanisms are governed by the material's microstructural properties, particularly pore size, porosity, bulk density, and sometimes fibre morphology (length and diameter). This section consolidates these parameters from previous literature to establish reference benchmarks that inform the evaluation of new VIP core materials.

Table *2.1*Table *2.1* presents the thermal conductivity values of several natural, synthetic, and composite materials previously used in VIP cores. When this data is examined alongside microstructural parameters from Figure 2.2 to Figure 2.6, a clear pattern emerges: at ambient or low temperatures, materials with finer pores, higher porosity, and lower bulk density generally achieve lower total thermal conductivity. For example, fumed silica, which exhibits Nano-scale pores (0.3 μm) and porosity above 90%, routinely achieves thermal conductivity values in the range of 4.2–6.3 $mW{\cdot}m^{-1}{\cdot}K^{-1}$, primarily due to strong suppression of gas-phase conduction and limited solid conduction pathways.

Natural fibres such as straw, bamboo, or wood pulp, which tend to exhibit larger pore sizes (20–100 μm) and more variable porosities, typically fall in the 20–35 $mW{\cdot}m^{-1}{\cdot}K^{-1}$ range, similar to conventional insulation. These materials allow more gaseous conduction and may exhibit higher solid conduction depending on density and fibre contact area. Hybrid composites, often display improved performance, reaching values below 10 $mW{\cdot}m^{-1}{\cdot}K^{-1}$, by leveraging Nano-structured fillers or opacifiers to reduce radiation.

However, this relationship is not absolute, particularly at elevated operating temperatures. As temperature increases, radiative heat transfer becomes a dominant contributor, and in such cases, materials with slightly higher bulk density or solid content may perform better by enhancing infrared scattering or absorption. Consequently, a higher bulk density does not necessarily lead to poorer performance at high temperatures; instead, it may contribute to lower radiative conductivity if the material structure enhances extinction efficiency.

These insights underscore the importance of optimising core material properties to match the operating environment. This multi-parameter comparison supports a more rational and environmentally grounded approach to identifying sustainable and cost-effective alternatives for VIP core materials. Figure 2.2 to Figure 2.6 visually represent how materials compare across these parameters, offering a reference framework for material screening.

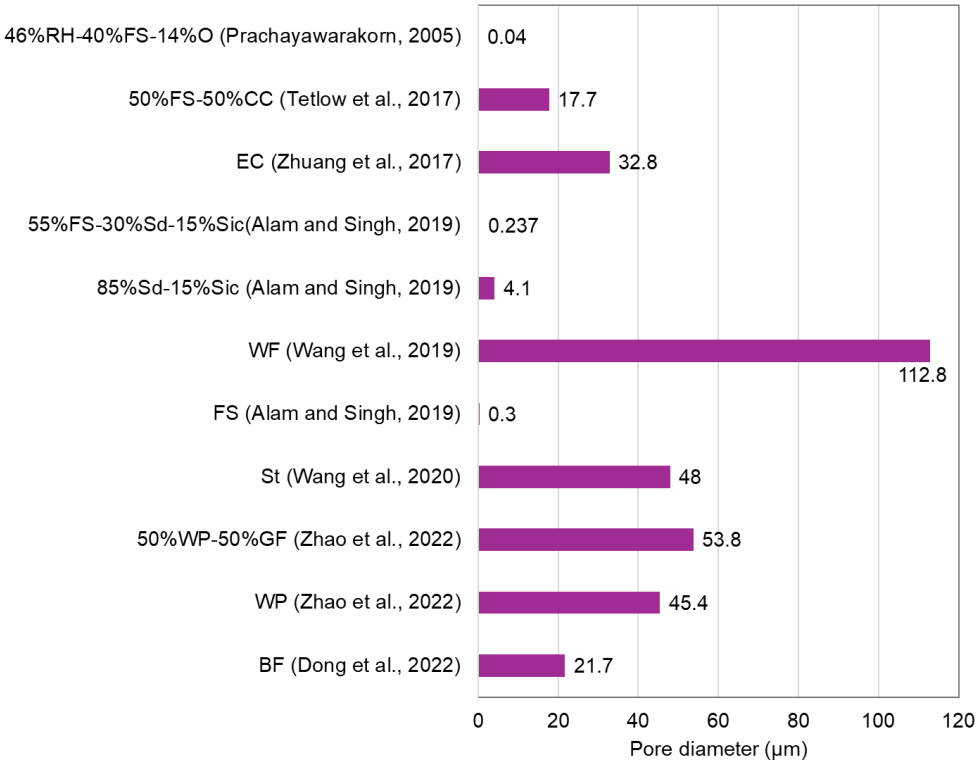

Figure 2.2 Reported pore diameter of VIP core materials from literature

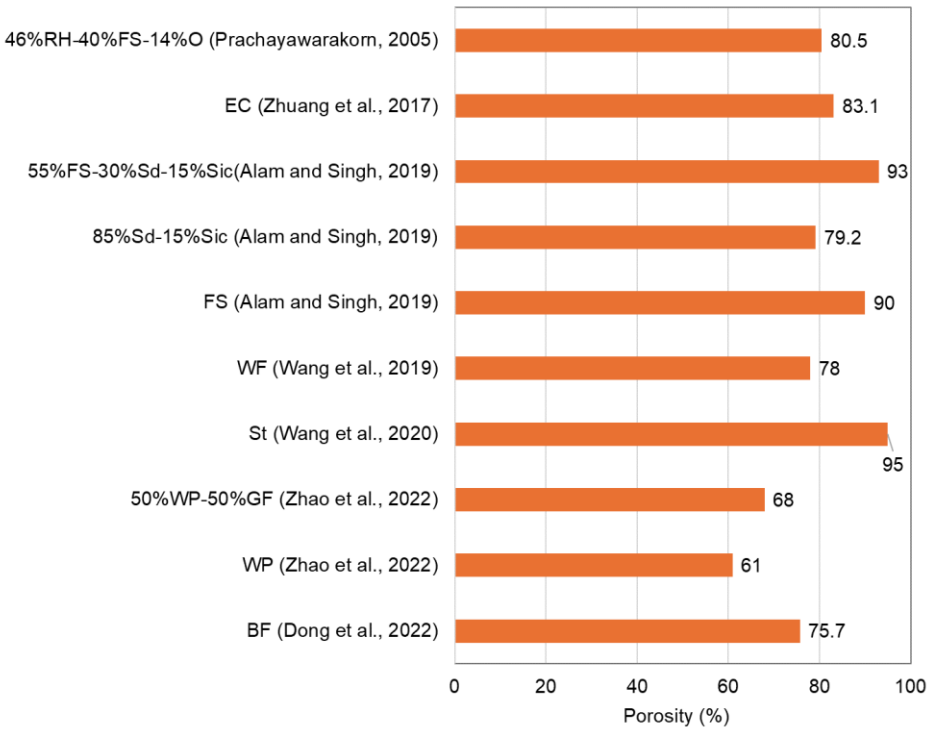

Figure 2.3 Reported porosity of VIP core materials from literature

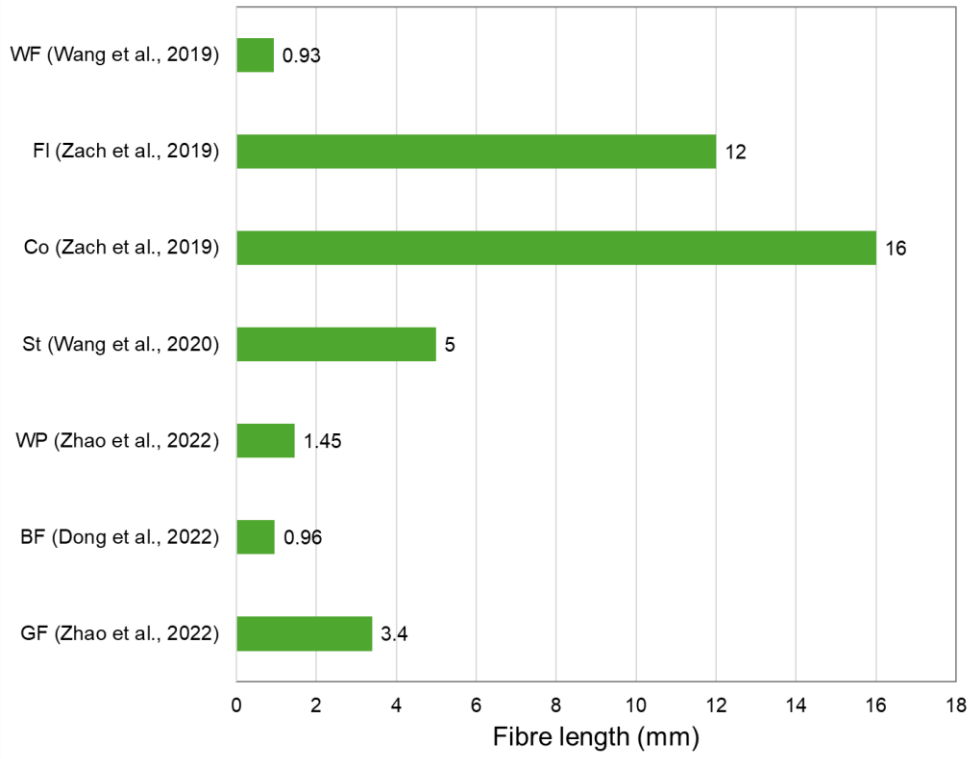

Figure 2.4 Reported fibre length of VIP core materials from literature

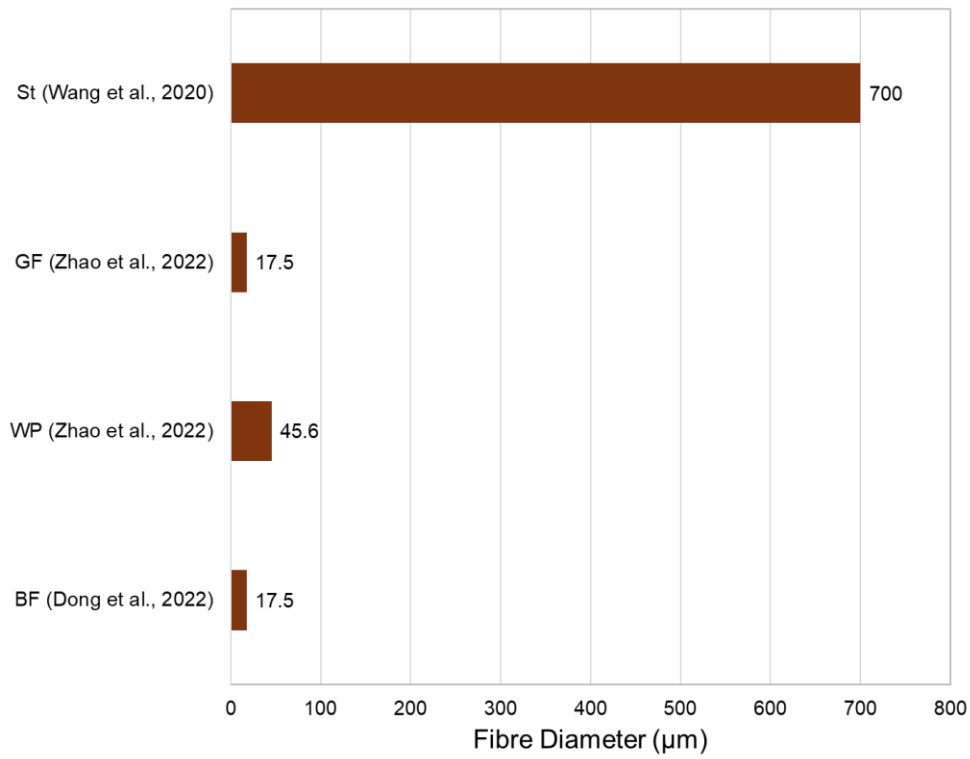

Figure 2.5 Reported fibre diameter of VIP core materials from literature

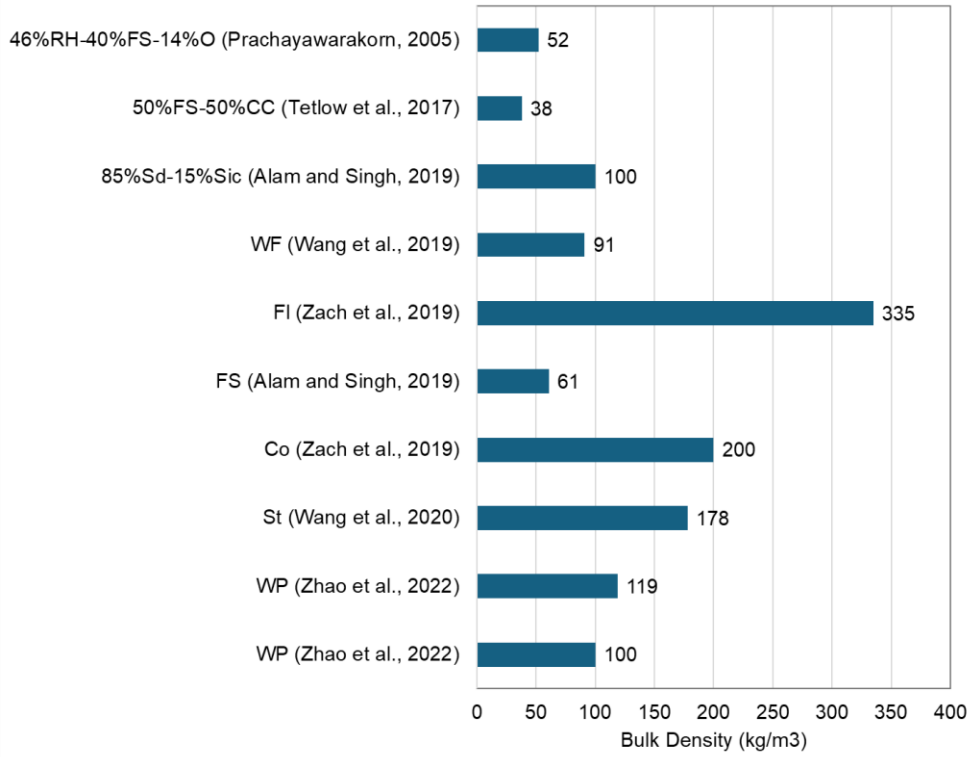

Figure 2.6 Reported bulk density of VIP core materials from literature

2.4 Environmental impacts of VIPs

The environmental impacts of VIPs section are categorised into three parts. The initial section delineates the general framework of Life Cycle Assessment (LCA), its various methodologies, the significance of functional units, the employed techniques, and their impact categories. The second part presents previous LCA study conducted by different researchers regarding vacuum insulation panels and their primary findings. The third part emphasises the research conducted on the recyclability of VIPs.

2.4.1 Life Cycle Assessment (LCA)

Life cycle assessment is a methodical strategy employed to examine the environmental impacts, including emissions, associated with the whole life cycle of a product or a process. The primary objective of the LCA is to ascertain methods for improving the environmental performance of products throughout various phases of their life cycle. Also, it helps in informing decision makers in various sectors such as industry, government or non-government organisations in improving their strategic planning for their products or process design. The LCA investigation follows the methodological framework of ISO14040:2006. According to this standard the LCA analysis is composed to four main phases as presented in Figure *2.7* :

(1) Goal and scope definition phase

Define the main purpose and boundaries of the work conducted, including the system boundaries and functional units.

(2) Life Cycle Inventory (LCI) analysis phase

Collect data associated with the product or system (input/output) from raw materials to waste generation.

(3) Life Cycle Impact Assessment (LCIA) phase

Asses the environmental impact of the LCI by the addition information/categories of the LCIA such as climate change, acidification, etc.

(4) Interpretation of the results phase

Analyse the results to make to draw conclusions and interpret recommendations for improvements.

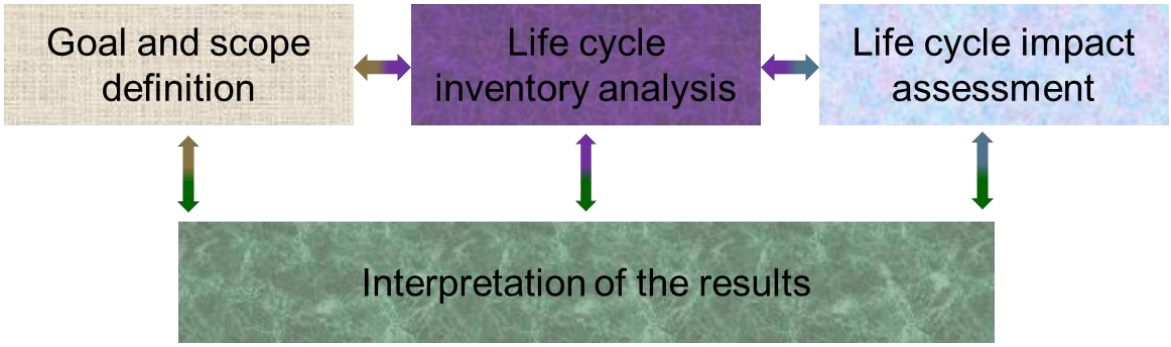

Figure 2.7 LCA framework of ISO14040:2006

The first essential phase in a life cycle evaluation is choosing the suitable approach, which determine the methodological decisions such as selecting input data and modelling algorithms for different output processes (Finnveden et al., 2009). Several LCA methodologies have been developed, each designed to address distinct research enquiries. The various methodologies used in LCA have a substantial impact on the limits of the system, either expanding or contracting them. This in turn, affects the compilation of the life cycle inventory and ultimately leads to changes in the final results of the study. Attributional LCA (ALCA) and Consequential LCA (CLCA) are two separate methodological techniques employed in LCA. These approaches were developed in the late 1990s to tackle different components of the decision-making process and environmental evaluations (Tillman, 2000).

The main focus of ALCA is to measure and describe the environmental inputs and outputs related to the whole life cycle of a product. The focus deceits on the present condition or "status quo" of the product's environmental effects within its specified system boundaries. ALCA utilises actual values or average data to assess the physical flows of materials, energy, and pollutants emitted throughout the many stages of a product's life cycle, from extraction of materials to disposal or recycling (Schrijvers et al., 2016). CLCA adopts a dynamic perspective that considers both direct (changes in production technology) and indirect (shifts in market behaviour) effects that may occur as a result of specific actions (political decisions) or changes in market demand. CLCA examines the environmental advantages as well as any further effects that may happen beyond the life cycle of the product being investigated, whereas ALCA concentrates on the immediate impact on the environment related to a particular activity within its defined limits (Danish EPA, 2003).

Figure 2.8 illustrates two distinct methodologies of LCA. The circles represent the overall global environmental interactions. The left circle depicts a portion of an activity in the process, such as human activity, that has been eliminated. The dotted line represents this removal. On the other

hand, the patterned spheres in the right circle aim to capture the alterations in environmental interactions by either including or eliminating activities, such as human activity.

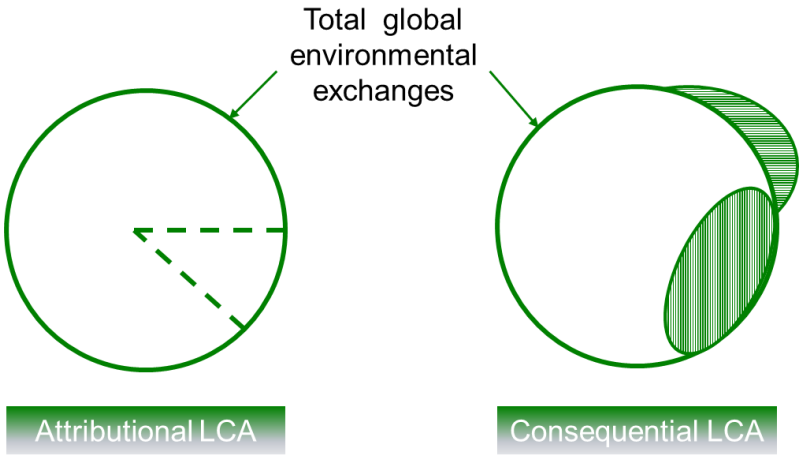

Figure 2.8 Difference between two approaches: attributional and consequential. Adopted from (Danish EPA, 2003)

Within the context of Ecoinvent's system models, the cut-off and Allocation at the Point of Substitution (APOS) models are in accordance with ALCA. The cut-off system model assigns full waste management responsibilities to the producer, without considering any credit for recyclable components. This approach provides a direct and clear evaluation of the environmental impacts linked to the whole life cycle of a product. The APOS system model, which operates within the attributional framework, allocates environmental burdens in proportion to the different processes involved in a product's life cycle. This technique considers the interdependence of processes and allocates impacts according to their contribution to the entire system.

The next important step following the selection of the primary objective of the study and the methodology is to determine the Functional Unit (FU).

The functional unit, as defined by ISO 14040 and 14044 standards, establishes the reference flow that is used as the foundation for quantifying all inputs and outputs in the assessment (Finnveden et al., 2009). This guarantees that the system remains aligned with its intended goals and boundaries.

Finally, it is essential to identify the impact categories relevant to the objective of the task. LCA programs like SimaPro, Gabi, OpenLCA, and Ecoinvent provide comprehensive databases and several globally standardised methodologies that assist users in comprehending diverse environmental impact assessments. The methods, including the European standard for environmental product declarations for construction products (EN15804), the European standard for assessing environmental performance at the building level (EN15978), the Institute of

Environmental Sciences at the University of Leiden in the Netherlands (CML), Gross Energy Consumption (GEC), and Cumulative Energy Demand (CED), encompass various impact categories. The main impact categories include Global Warming Potential (GWP), Ozone Depletion Potential (ODP), Acidification Potential (AP), land usage, water use, Eutrophication Potential (EP), non-renewable energy use and renewable energy use.

2.4.2 Previous LCA on VIPs

Various studies were conducted over the years on the Life cycle assessment of buildings, with only a few studies focussing on vacuum insulation panels as an alternative insulation method. This literature presents five studies in Table *2.2* from 2015 to 2021, wherein the authors examined the LCA of VIPs.

Resalati (2021) assessed and compared the environmental impact of five distinct VIP core materials: pyrogenic silica, glass fibre, expanded polystyrene, aerogel, and a hybrid composite of pyrogenic silica and sawdust, employing two methodologies. The functional units employed were 1 m² and 20 mm VIP, with just the Cradle to Gate (C-to-G) phase of the manufacture of various VIP cores being evaluated. The primary finding indicated that pyrogenic silica VIP exhibited the greatest environmental impact among the analysed cores.

The study by (De Masi and Vanoli (2021) mostly focused on a nearly zero energy building under various climatic scenarios, where VIP panels were utilised on the exterior of the roof and wall assemblies, and compared with traditional insulation utilising only one method. The functional unit comprised 1 m² of insulation, and the Cradle to Cradle (C-to-C) phase was analysed over a duration of 50 years. The study did not fully investigate the production stages of VIP, its end-of-life scenarios, or the core materials utilised, as their primary emphasis was on the application phase. The primary finding indicated that VIP lowered the total energy consumption of the building. However, the overall life cycle assessment impact increased in comparison to the other insulation materials examined.

Padopski (2019) examined the environmental performance of VIPs and PCMs insulation materials operating under the climatic conditions of Southern Europe, reporting an overall thermal conductivity of 0.019 W/mK. The functional unit selected was 1 m3, and the Cradle to Cradle (C-to-C) phase was examined over a duration of 25 years. As with the prior study, no specific production stages were referenced in this investigation. The primary finding of the study indicated that the overall environmental footprint during the production phase increased by 34% due to the application of PCM and VIPs. Nevertheless, over a duration of 25 years, coupled with the energy

savings provided by the VIPs, the total environmental footprint is reduced by 57% in comparison to building without insulation.

Zhuk (2018) compared the use of vacuum insulation panels composed of fumed silica with glass wool and expanded polystyrene. The functional unit was 1 m², and only the cradle to gate aspect of VIP manufacturing was studied. Among the five impact categories analysed by the gross energy consumption method, the findings indicated that VIP exhibits greater embodied energy than EPS and glass wool, with 90% of the energy utilised in VIP attributed to core production.
(Karami and Gudmundsson (2015) aimed to evaluate the environmental performance of three building types: a non-insulated structure, one insulated with traditional materials (wool and EPS), and another insulated with vacuum insulation panels. The key finding indicated that buildings insulated with conventional insulation exhibit superior GWP and more favourable primary energy impacts compared to buildings insulated using VIPs. The elevated embodied energy of VIP is attributable to the incorporation of fumed silica, which constitutes 90% of its environmental impact. It is essential to note that none of these studies demonstrated the approaches employed in the LCA, nor included information on transportation, which might significantly influence the final output.

Table 2.2: Previously studied LCA on VIPs form year 2015 to year 2021

Author	Core material	Method	Impact Category	Stages	Software
Resalati (2021)	5	EN 15978 and EN 15804	9	C-to-G	GaBi LCA
(De Masi et al., 2021)	-	CML –IA 2012	5	C-to-C	One Click LCA
Padopski (2019)	1	ReCiPe	9	C-to-C	SimaPro
Zhuk (2018)	1	GEC	5	C-to-G	-
(Karami and Gudmundsson (2015)	1	EN 15804	6	C-to-G	-

2.4.3 Recyclability of VIPs

Renato Sarc (2013) discussed the process for recycling the VIPs used in the cooling and refrigeration applications within an existing recycling plant. It was concluded that VIPs can be recycled in the existing recycling plants with modifications to be done to the filtration systems

used in the plants to meet health and safety requirements due to the fine powder-based core materials used in the VIP cores. Sonnemann (2013) discussed the development of a system to detect VIPs in the end-of-life refrigerators in a recycling plant. VIPs are detected by outer wall perforation and pressure measurement. These studies narrowly focus on the procedural challenges in recovering different VIP components, thus completely overlooking the potentially resulting changes in the core material properties and therefore their likely impact on the thermal performance of VIPs.

2.5 Applications of VIPs

Vacuum insulation panels (VIPs) have garnered significant academic and industrial interest over recent years due to their exceptional insulating performance and their potential to substantially improve energy efficiency across a range of sectors. A comprehensive bibliometric analysis conducted by Božiček (2024) reviewed 423 peer-reviewed publications from 1993 to 2022, covering various aspects of VIP development, including core materials, ageing effects, structural designs, and application domains. Of these, 238 publications (approximately 56%) focused on VIP applications in the building sector, underscoring their established role in enabling compliance with increasingly stringent thermal performance standards in construction. A further 139 studies examined the material science and engineering aspects of VIP core constituents, reflecting ongoing efforts to optimise thermal conductivity, mechanical integrity, and long-term stability. Only 46 studies (approximately 11%) addressed the deployment of VIPs in sectors beyond the built environment, as illustrated in Figure 2.9.

Among these alternative applications, 61% of the studies concentrated on cold chain logistics, indicating a growing emphasis on thermal regulation in refrigeration systems, thermal packaging, and vaccine transport. This surge in interest, particularly following the COVID-19 pandemic, highlighted the role of VIPs in maintaining cold-chain integrity for temperature-sensitive pharmaceuticals. The remaining 18 studies explored VIP integration in vehicles, pipelines, and thermal storage systems, areas that remain underrepresented in the literature despite their potential for significant energy savings

Despite the technological promise of VIPs, several critical limitations constrain their broader commercialisation and long-term functionality. Firstly, the high production cost, primarily associated with the use of fumed silica cores and multilayer gas barrier envelopes, remains a major barrier to market scalability, particularly in cost-sensitive sectors. Secondly, VIPs are structurally fragile due to their evacuated core and rigid envelope, rendering them vulnerable to

puncture or compression damage during transport, installation, or operation, which can lead to an irreversible loss of vacuum and rapid performance degradation. Thirdly, thermal ageing effects, often driven by gas permeation through envelope materials and core settling, gradually increase effective thermal conductivity over time, thereby reducing insulation efficiency and design predictability in long-term applications. Additionally, limited formability and cuttability make VIPs difficult to adapt on-site without compromising integrity, restricting their flexibility in retrofitting scenarios.

Furthermore, the vast majority of studies have focused on moderate-temperature applications (typically <50 ℃), leaving a significant research gap in understanding VIP behaviour under elevated temperatures, such as those encountered in thermal storage units or automotive sectors requiring higher temperature environment. In such environments, the thermal stability of the core material, binder degradation, and envelope material integrity are critical factors yet to be adequately explored. This underrepresentation not only limits innovation in thermally demanding industries but also impedes the development of robust design standards and lifecycle performance models tailored to high-temperature VIP applications. Consequently, there is a clear need for systematic investigation into the thermal, mechanical, and environmental durability of alternative VIP core materials under a broader range of operating conditions.

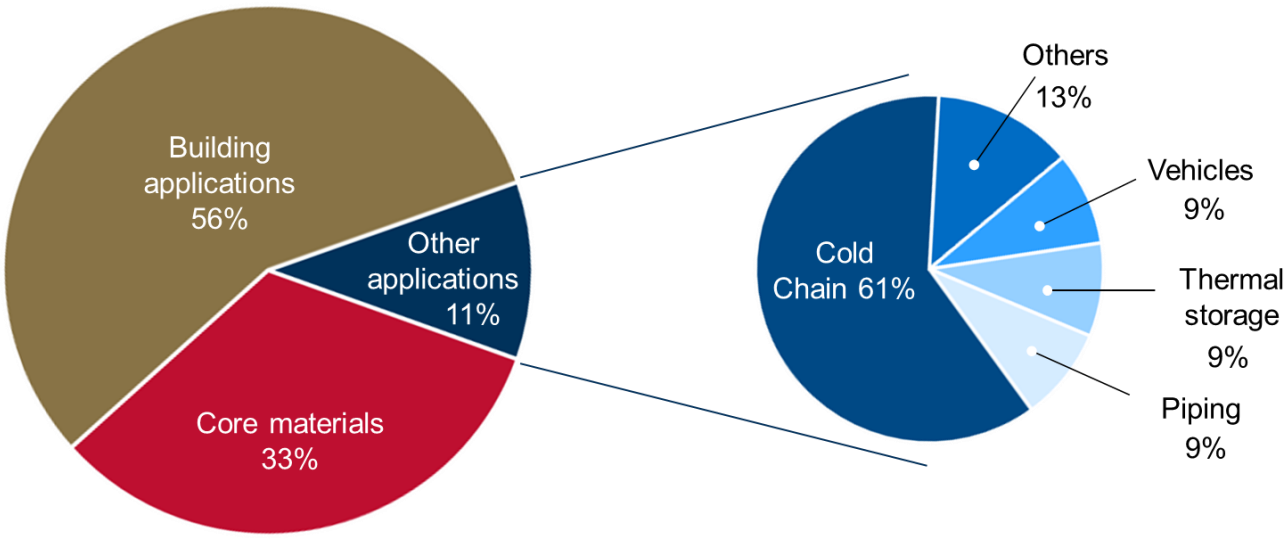

Figure 2.9 Studies on VIPs in different sectors. Adopted from (Božiček et al., 2024)

2.6 Summary

The main aim of this literature review is to examine the historical and current progress in the development of core materials for Vacuum Insulation Panels (VIPs). This review aims to reveal the principal parameters affecting the thermal performance of VIPs by analysing the principles of material selection, the physics of heat transmission, and the manufacturing processes. VIPs are essential technology for improving energy efficiency, notably acknowledged for their capacity to minimise heat loss in many applications. The enhancements in energy efficiency immediately facilitate the reduction of energy use and CO_2 emissions, so aiding the UK's objective of attaining net-zero emissions by 2050. Nevertheless, despite their great potential, VIPs encounter numerous obstacles that impede their adoption, as well as significant unexplored opportunities. The following gaps were identified:

- A significant obstacle is the elevated production cost, particularly for core materials, which can account for up to 60% of the total cost of a VIP. Recently, organic core materials, particularly those derived from natural fibres, have garnered attention as substitutes for fumed silica and glass fibre. These organic materials obtained from waste are more sustainable and diminish the production costs and environmental impact for VIPs. These organic materials have not yet reached their full potential due to limited studies and characterisations specially at higher temperature (up to 70℃).
- Multiple studies indicate that VIPs possess significantly more embodied energy than alternative insulation materials, with the core material representing over 90% of the energy utilised. The increased energy consumption results in a higher environmental impact. A significant concern with current researches is the absence of transparency in Life Cycle Assessment (LCA) studies of VIPs, which frequently lack to encompass the entire lifespan from material extraction to production, utilisation and disposal. The absence of transparency creates misleading environmental impacts of VIPs, hence restricting their adoption in different sectors.
- The reusability of core materials is an area that remains inadequately investigated. Most research have concentrated on the procedural difficulties in recovering various VIP components and neglecting the potential changes in the core material properties and their probable effects on the thermal performance of VIPs.
- Under 2% of the research on VIPs has focused on high-temperature applications, a domain where VIPs might potentially provide substantial advantages in sectors such as automotive, aerospace, and high-temperature industry.

To address these gaps in VIP research, it is essential to investigate additional alternative core materials sourced from waste that can reduce production costs and enhance sustainability while maintaining high thermal performance, particularly at elevated temperatures (up to 70℃), where existing data is limited. Furthermore, it is essential to create a thorough LCA model that assesses each phase of the product's lifecycle. This model must encompass resource extraction, energy consumption throughout manufacture, transportation, disposal, and recycling operations with appropriate functional unit, system boundary and approaches. A cradle to cradle life cycle assessment yield a more precise evaluation of environmental effect, facilitating informed decisions regarding the sustainability of VIP technology. Moreover, examining the viability of repurposing core components in future production cycles may prolong VIP lifespans, diminish waste, and improve sustainability. This should be empirically investigated and incorporated into the new LCA model. These efforts improve VIP sustainability, expand their uses, and help achieve energy efficiency goals.

CHAPTER 3: Core Material Development and Characterisation

Three novel core materials, were produced from Tree-based Natural Fibres (TNF) waste, were experimentally evaluated for their potential as substitutes for the costly and widely used FS. This investigation involved the preparation and characterisation of two distinct varieties of tree-based natural fibres – Tree based Natural Fibres medium (TNFm) with an average length of 0.82 mm and Tree based Natural Fibres small (TNFs) with an average length of 0.22 mm. Additionally, the waste by-products were pyrolysed into Tree-based Natural Ash (TNA) in order to optimally utilise the raw material.

This chapter discusses material and composite preparation and characterisation methodologies, utilised for TNFm, TNFs, TNA and FS composite. The microstructure of the materials, including their shape, morphology, size, and pores, was analysed using a Scanning Electron Microscope (SEM) and image analysis. The elemental composition of TNA was analysed using Energy-Dispersive X-ray Spectroscopy (EDS). The particle size distribution of TNA was measured using laser diffraction and SEM images. The pore size and porosity of materials and composites was analysed by using Mercury Intrusion Porosimetry (MIP). Thermogravimetric analysis (TGA) was performed to determine the temperature threshold for drying TNF and to examine any chemical degradation with temperature increase. The infrared (IR) transmission spectrum of the materials was obtained using Fourier Transform Infrared (FTIR) spectroscopy. Lastly, fourteen different VIPs samples were manufactured (between pure samples and composites), see Figure *3.1*.

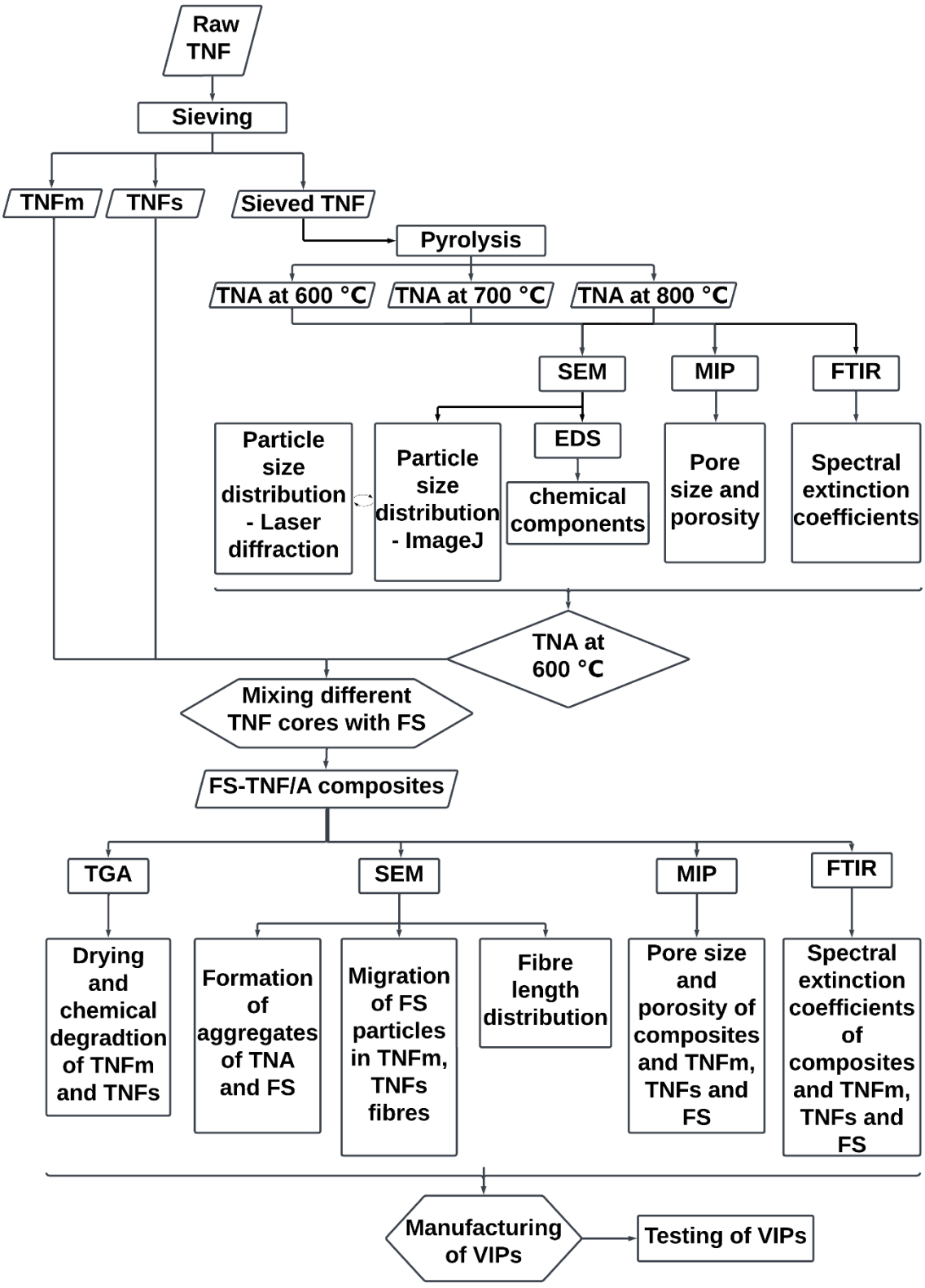

Figure 3.1 Flow chart detailing all steps involved in the development and characterisation of VIPs

3.1. Core material development

Three novel core materials, which were produced from Tree-based Natural Fibres (TNF) waste, were developed in Brunel lab facilities. Tree-based Natural Fibres, which are naturally occurring lignocellulosic materials, are extensively available globally and specifically in regions such as the Middle East and North Africa. They are known for their low cost, biodegradability, and high tensile strength. This investigation involved the preparation and characterisation of two distinct varieties of tree-based natural fibres - TNFm and TNFs. Additionally, the waste by-products were pyrolysed into Tree-based Natural Ash (TNA) in order to optimise the utilisation of the raw material.

For this investigation Aerosil 300, a specific type of fumed silica manufactured by Evonik, was used (Evonik Industries, 2006). In larger- scale industrial applications, the typical price range for bulk purchases of fumed silica is between £6 kg^{-1} and £10 kg^{-1}. Fumed silica is generated during the ongoing process of flame hydrolysis of silicon tetrachloride ($SiCl_4$). During this procedure, $SiCl_4$ undergoes a transition into the gaseous state and undergoes a reaction with hydrogen and oxygen in a flame, usually at a temperature of approximately 1800 ºC. This chemical reaction yields fumed silica and releases gaseous hydrochloric acid (HCl) as a secondary product equation (3.1).

$$2H_2 + O_2 + SiCl_4 \rightarrow SiO_2 + 4HCl \quad (3.1)$$

3.1.1. Production of Tree-based Natural Fibres (TNF)

TNF is lignocellulosic material obtained from tree waste. These fibres are renowned for their excellent tensile strength, ability to decompose naturally, and economical value (£0.024 kg^{-1}). The fibres consist mostly of cellulose, hemicellulose, and lignin, which are responsible for their mechanical characteristics (Kriker et al., 2008), see Table *3.1*.

Table 3.1**:** Chemical composition of tree-based natural fibres (Kriker et al., 2008)

Chemical element	Wt (%)
Cellulose	43.71
Lignin	29.43
Hemicellulose	18.66
Ash	4.81
Others	3.39

TNF were cleaned using distilled water to remove any accumulated dust particles following which they were dried in an oven at 60 ℃ for 24 hours, ground using a mechanical grinder and sieved with two different mesh sizes to achieve a particular grade. TNF were grinded using a Retsch

cutting mill (SM 100, Germany) that had a 2 mm mesh and then sieved using the Endecott EFL 2000/2, see Figure *3.2*a. Two distinct fibres, namely TNFm and TNFs, were produced, exhibiting average fibre length of 0.82 mm and 0.22 mm, respectively.

The grinded TNF were thereafter passed through a sequence of sieves (1000, 500, 250 and 125 µm) in order to attain a precise geometry, see Figure *3.2*b. It was noted that 97% of the grinded TNF were able to pass through a sieve with a mesh size of 1000 µm, see Figure *3.3*a. The remaining 3% were found to be the largest in terms of length and diameter range among all the sieved TNF, as shown in Figure *3.3*b. A mere 12% fibres remained on the 500 µm sieve with 85% passing through, see Figure *3.3*c. Afterwards, 46% of the TNF was retained on the 250 µm sieve, whereas 39% went through. This was the most quantity of fibres that were kept on this specific mesh size, as shown in Figure *3.3*d. Out of the material that went through the 250 µm sieve, 28% was held back by the 125 µm sieve, while the remaining 11% went through. Fibre sizes used in this study were TNFm (125-250 µm) and TNFs (<125 µm), as presented in Figure *3.3*e and Figure *3.3*f respectively. The selection of these specific sizes was based on the presence of both fibres and powders in this mesh size. Moreover, these two fibre sizes possess the finest fibres in comparison to those kept on other mesh sizes. Figure *3.3*g presents TNA and its production is discussed in the section 3.1.2.

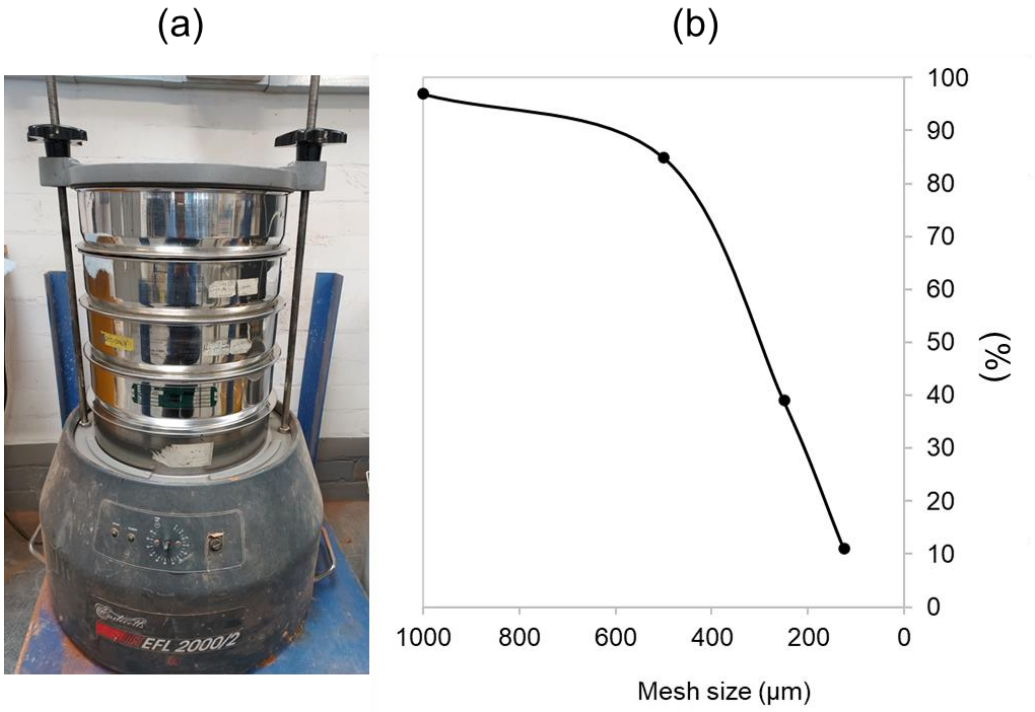

Figure 3.2 (a) Endecotts EFL 2000/2 sieving machine used for TNF and (b) the proportion of the fibres passing through each mesh size

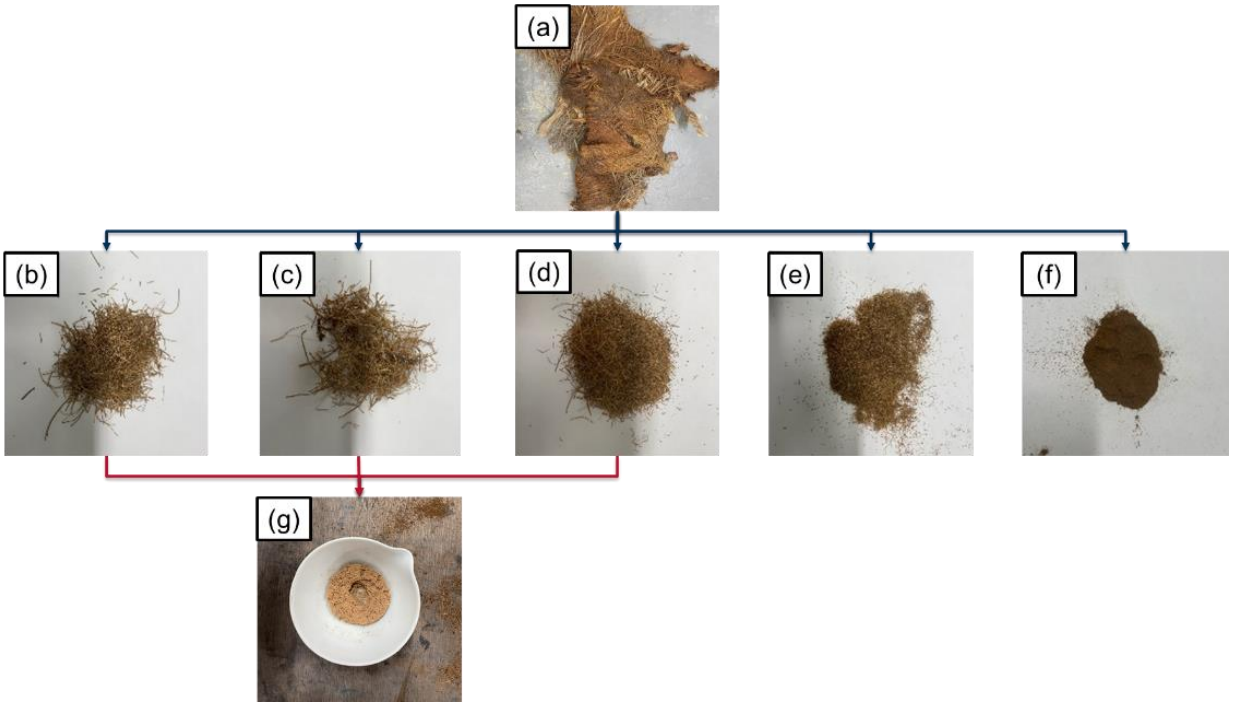

Figure 3.3 Visuals of the different sizes of sieved materials (a) sheath;(b) fibre size greater than 1000 µm, (c) fibre size between 500-1000 µm, (d) fibre size between 250-500 µm, (e) fibre size between 125-250 µm labelled in this research as TNFm, (f) fibre size less than 125 µm labelled in this research as TNFs and (g) pyrolysed TNF from (b,c and d) labelled in this research as TNA

3.1.2 Production of Tree-based Natural Ash (TNA)

In order to make the most of the waste produced from tree-based natural fibres, both the non-grinded fibres and those that were too large for sieving (mesh >250 µm) were partially pyrolysed into TNA using an industrial furnace. The TNA production process involved pyrolysis at three specific temperatures, 600 ℃, 700 ℃, and 800 ℃, identified in this study as TNA, TNA-700, and TNA-800, respectively. All produced TNA were sieved using a 63 µm mesh to remove any remaining rocks that were attached to the waste fibres and ensure a uniform consistency. Consequentially, all waste generated from the tree-based natural fibres was efficiently utilised to manufacture cores and composites for VIPs, see Figure *3.4*.

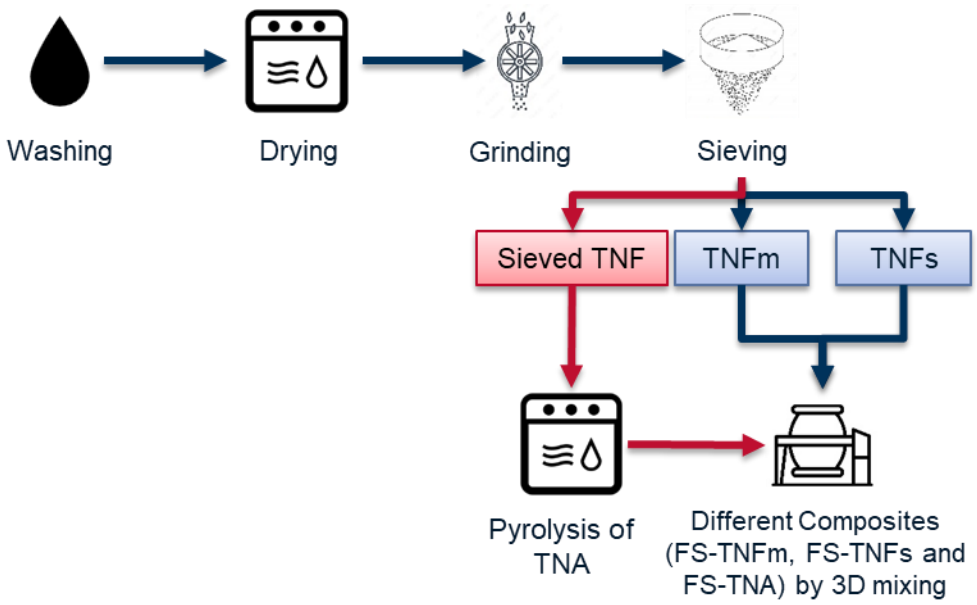

Figure 3.4 Production of TNF and TNA employed in this study

Only 39% of sheath could be processed into TNF (28% TNFm and 11% TNFs). The remaining 61% of tree sheath was pyrolysed into ash using a compact electric furnace shown as in Figure *3.5*a. The furnace was equipped with an XMTG-7000 programmable temperature controller, seen in Figure *3.5*b.

Figure 3.5 The furnace used to process the TNA at three different temperatures: (a) furnace chamber and (b) XMTG-70000 programmable temperature controller

The furnace functions by going through three primary phases: heating, isothermal hold, and cooling.

A pyrolysis process (heating rate 10 ℃ min^{-1}) was adopted. This heating rate also helped to avoid any damage to the ceramic sample holder. The heating period was evenly distributed among the three target temperatures, see Figure *3.6*.

The duration of the isothermal hold was initially assessed at a temperature of 600℃. It was noted that maintaining the temperature for less than 100 minutes led to incomplete pyrolysis, where a proportion of TNF remained unburnt, shown as blackish material in the blue circle in Figure *3.7*a. By extending the duration of the hold period to 120 minutes, a complete conversion of TNF into ash was achieved at a temperature of 600 ℃ as well as at 700 ℃ and 800 ℃. This led to a consistent reddish/brownish colour, which was a clear indication of complete pyrolysis.

The cooling down stage was not effectively controlled due to the absence of an active cooling feature in the furnace and the need to keep the door closed for safety purposes. Removing the sample directly was not possible since it could cause thermal shock and potentially damage the ceramic holder. Therefore, the samples were left to cool down inside the furnace for 80 minutes before being taken out.

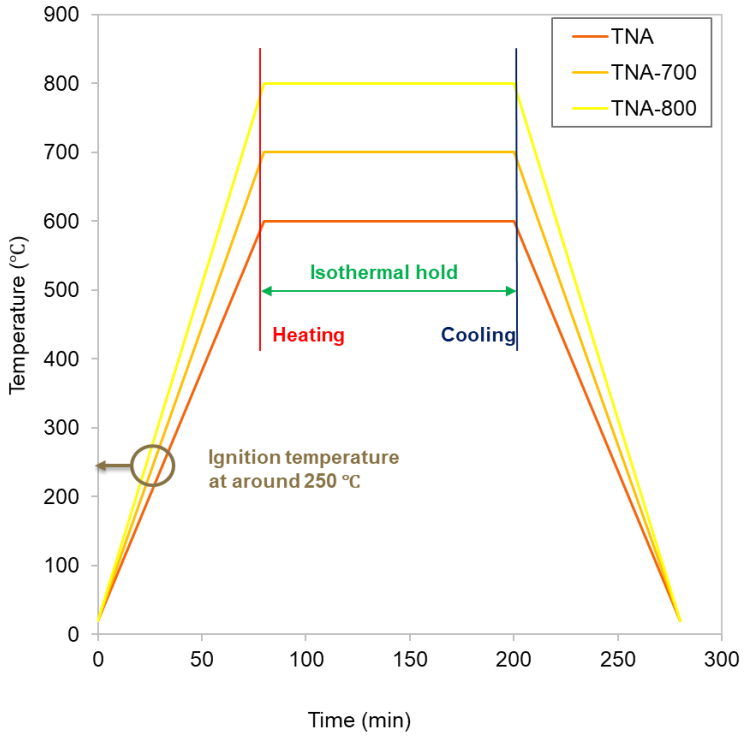

Figure 3.6 Heating parameters employed in the production of TNA at three different temperatures 600 ℃, 700℃ and 800℃

Another experiment conducted at a temperature of 500 ℃ demonstrated that the TNF was not fully pyrolysed, as the material still had a black and grey colour, suggesting that the conversion to ash was not fully observed, see Figure *3.7*b. The incomplete transformation noticed in this study can be attributed to two main factors. Firstly, the pyrolysis temperature used was not high enough, this reasoning is further discussed in the section 3.3.10. Secondly, a small furnace size required the fibres to be compacted to maximise material pyrolysed. Extra compaction is thought to have impeded uniform heat distribution and pyrolysis through the material layer.

The selection of 600℃ as the temperature for beginning the pyrolysis of TNA in this work was based on the specific limits and conditions of the experimental setup, however it does not definitively establish it as the optimum temperature. Further characterisation was conducted and are further elaborated upon in the following sections. Based on the findings, the choice was made to not increase the temperature beyond 800 ℃ or decrease it below 600 ℃.

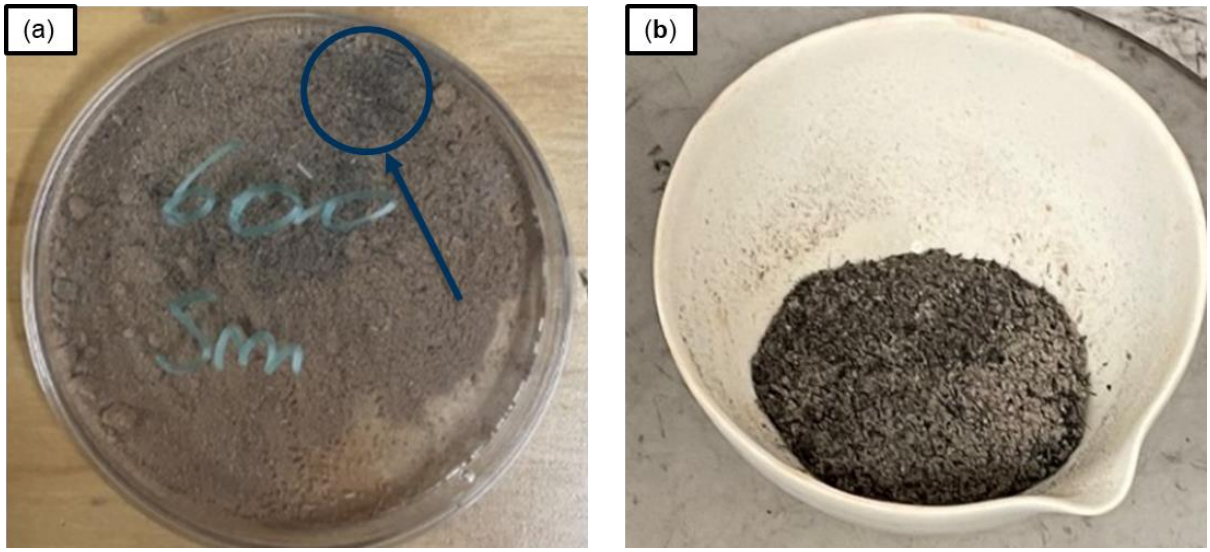

Figure 3.7 (a) TNA pyrolysed at 600 ℃ with an isothermal hold of 100 minutes and (b) TNA pyrolysed at 500℃

3.1.3 Mixing of composites

Achieving uniform mixing of core materials is crucial in the development of composite materials. Proper mixing ensures even distribution of components, which is essential for consistent properties throughout the material. For instance, well-controlled mixing allows smaller particles to migrate into larger pore sizes, leading to a reduction in gaseous conductivity. On the other hand, inconsistent mixing can result in variations in density, mechanical strength, and other important properties, negatively impacting the performance of the composite, such as the overall thermal conductivity.

A three-dimensional mixer was used in this study to combine the core materials at 50 RPM for a duration of 10 minutes. The selection of this procedure was made in order to attain a comprehensive and uniform blend, which is crucial for the reliability and strength of the final composite. Ten composite samples were produced, each including different combinations of FS with TNA, TNFm, or TNFs, listed in Table *3.2*.

Table 3.2: Sample ID and description of FS and tree-based natural fibres (TNFm, TNFs and TNA) composites

Sample ID	Description
FS-TNA	80% FS + 20% TNA
FS-TNA1	70% FS + 30% TNA
FS-TNA2	60% FS + 40% TNA
FS-TNA3	50% FS + 50% TNA
FS-TNA4	40% FS + 60% TNA
FS-TNFm1	70% FS + 30% TNFm
FS-TNFm2	60% FS + 40% TNFm
FS-TNFm3	50% FS + 50% TNFm
FS-TNFs1	70% FS + 30% TNFs
FS-TNFs2	60% FS + 40% TNFs

3.2 Characterisation of materials/composites produced

Materials were analysed for shape, morphology, size of the particles and fibres and pores using SEMs. Additionally, the migration of composites, the length distribution of the fibres and the size distribution of the powders was assessed as well. The analyses were conducted using the ImageJ software, and the results are discussed in section 3.3.4 and 3.3.6.

Two equipment were used. The Leo 1455 VP, which has a maximum magnification capability of 1,000,000x, was mostly employed for most of the samples. However, as a result of a malfunction in the Leo 1455VP, the Zeiss Supra 35VP equipment which has a maximum magnification capacity of 900,000x was used instead for the remaining samples. In order to address the electrical non-conductivity of samples, a gold coating with a thickness of 10 nm was applied prior to testing.

3.2.1 SEM images of individual materials –TNFm, TNFs, TNA, and FS

As shown in Figure *3.8* the two tree-based natural fibres exhibited particles with irregular shapes. The TNFm sample (Figure *3.8*a) exhibited a considerable number of fibres, including both small and large fibres. Conversely, TNFs sample (Figure *3.8*b) exhibited a greater number of dust particles (or crushed fibres), while a minor quantity of fibres was still seen. The variation in morphological form may be attributed to the process of sieving, whereby a lower quantity of fibres was able to pass through the sieve as its size decrease, but a greater amount of fibre dust was able to pass through smaller sieve sizes.

During pyrolysis all fibres were converted into ash, taking the shape of small flakes. The TNA particles underwent agglomeration, resulting in the formation of a bigger porous spherical particle, as depicted in Figure *3.8*c. This processing alters its structure from fibrous to flaky, resulting in improved thermal insulation by lowering heat transfer through the solid phase. All the samples of TNA pyrolysed at different temperatures showed similar shape.

The SEM images of FS (Figure *3.8*d) exhibited similar characteristics to those of TNA, but with smaller spherical particles that were agglomerating. Due to the smaller size of the primary particles of fumed silica compared to TNA, they tend to form chain-like structures termed aggregates when they come together. These aggregates then interact with each other to form larger structures known as agglomerates. This structure is known for its exceptional thermal insulation capabilities, which are attributed to its high porosity and minimal solid paths for heat conduction. The reduced size of the main particles and the subsequent formation of a chain-like structure improve the material's ability to capture air and reduce heat conductivity.

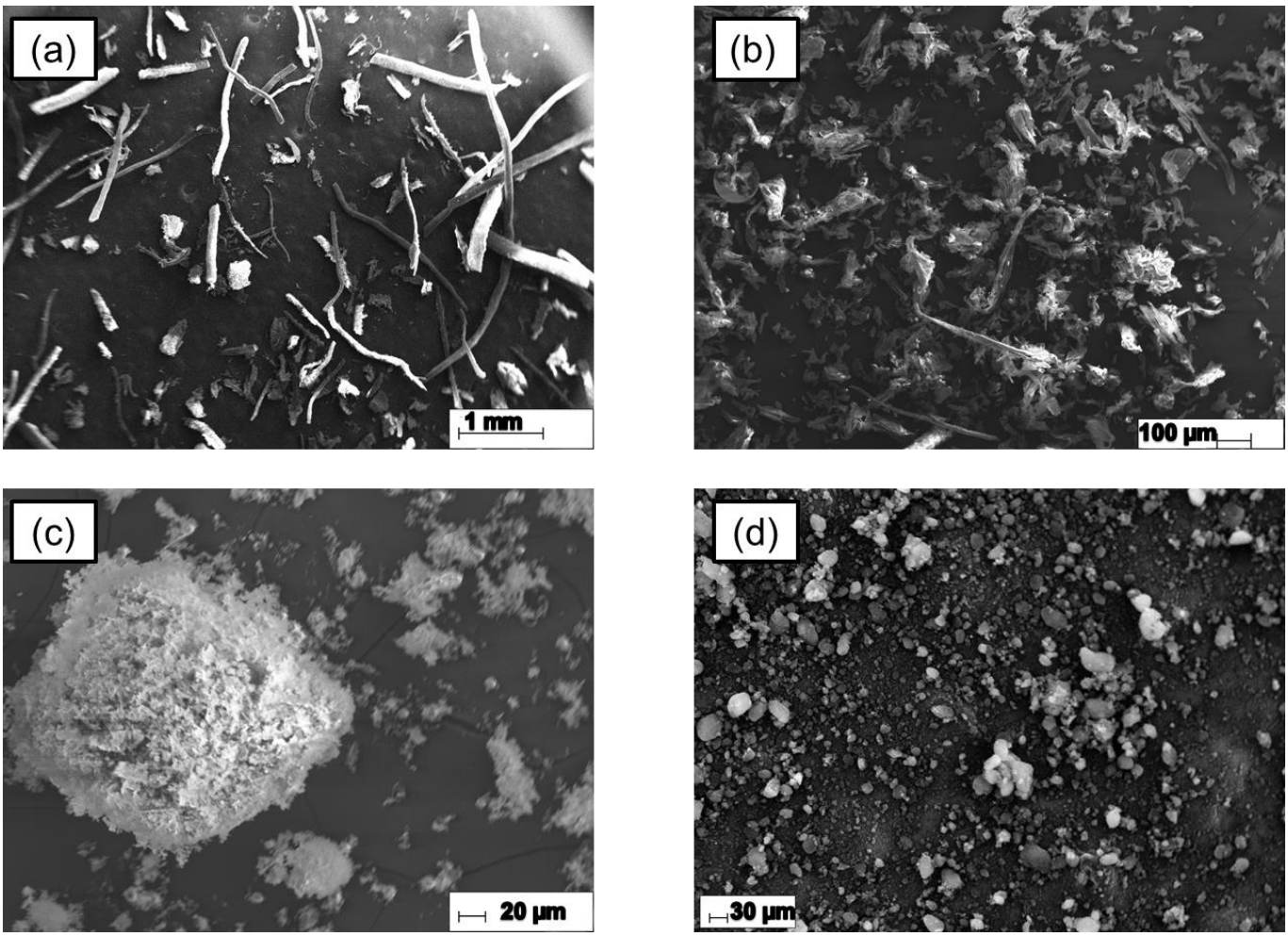

Figure 3.8 SEM images of (a) TNFm, (b) TNFs, (c) TNA pyrolysed at 600 ℃ and (d) FS

3.2.2 SEM images of composites

In the investigation of composites, three samples were analysed, consisting of 70% FS mixed with 30% TNA, TNFm and TNFs by weight. Significantly, samples FS-TNFm1 and FS-TNFs1, depicted in Figure *3.9*a and Figure *3.9*b, respectively, displayed a significant phenomenon. Small agglomerates of FS particles not only settled near the fibres, but also migrated the inner pores of both TNFm and TNFs particles. The migration of these particles has the capacity to reduce the overall pore size, an aspect that is further discussed in section 3.2.8.

The FS-TNA1 sample, shown in Figure *3.9*c, exhibited noticeable features, with the formation of aggregates consisting of tiny particles of TNA and FS. The aggregation of particles can cause the creation of smaller cavities within the FS-TNA1 sample, which may lead to reduced gas conductivity even at high sealing pressures. As a result, this could lower thermal conductivity especially at high sealing pressure due to the reduced pore size.

These observations highlight the complexity of composite behaviour and its influence on thermal conductivity. The movement and interaction of particles within the composites have a substantial impact on the structure of the pores, which in turn influences the thermal performance. Further characterisation is required to comprehend the optimal quantity of composites.

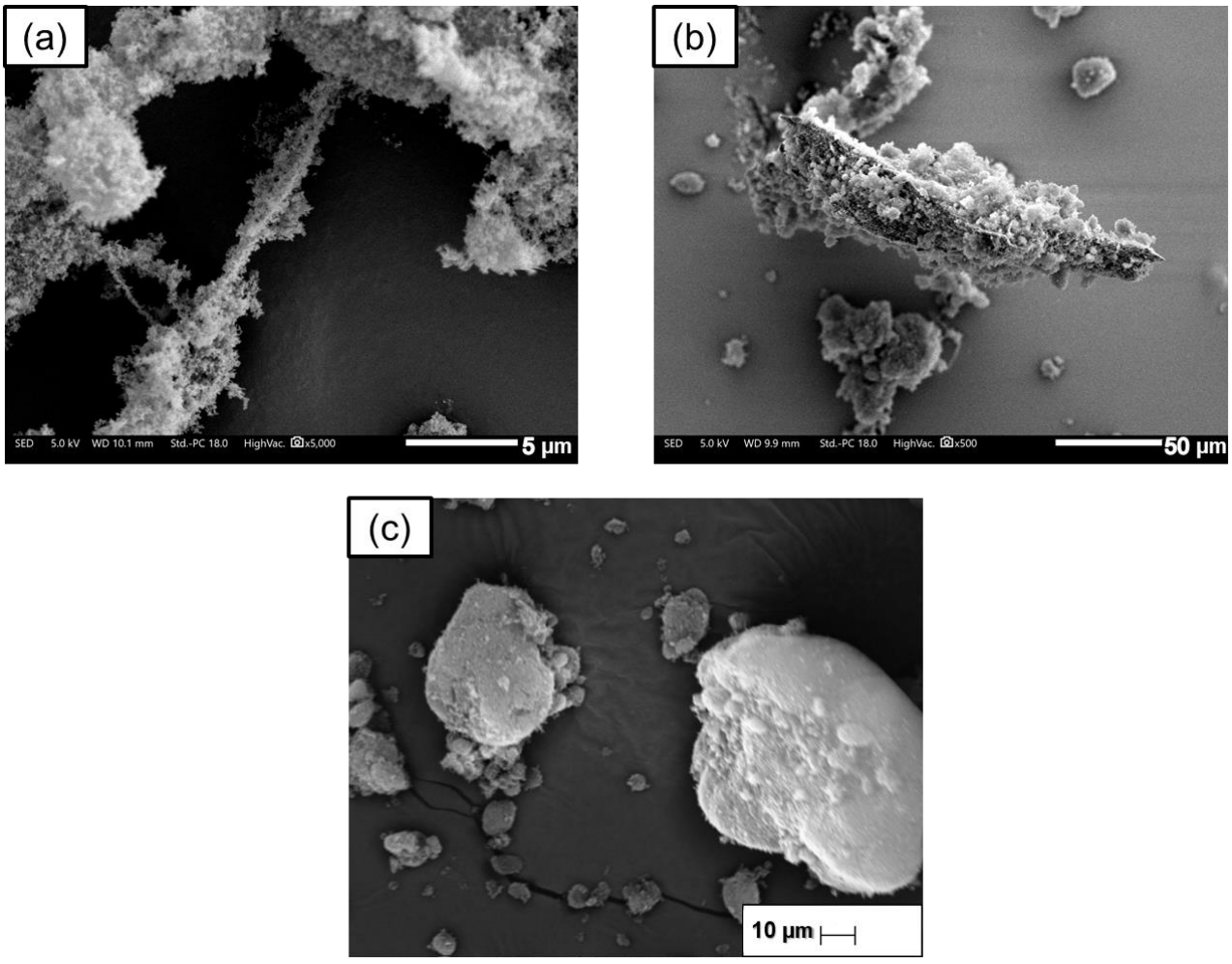

Figure 3.9 SEM images of (a) FS-TNFm1, (b) FS-TNFs1 and(c) FS-TNA1

3.2.3 Energy-Dispersive X-ray Spectroscopy (EDS)

Energy-Dispersive X-ray Spectroscopy (EDS) was used to analyse the elemental composition of TNA pyrolysed at temperatures of 600℃, 700℃, and 800℃, employing the "map sum spectrum" method for comprehensive analysis. Elemental maps visualised the spatial distribution of elements are presented in Figure *3.10*, correlating this distribution with the sample's morphology. The VIP performance is affected by the chemical composition of pyrolysed fibres at different temperatures. During pyrolysis, organic compounds like cellulose, lignin, and hemicellulose undergo decomposition, leading to the formation of carbon dioxide (CO_2), carbon monoxide (CO),

and water (H_2O). The breakdown process results in a significant decrease in the mass of the material (around 93% reduction from the initial weight), leaving concentrated inorganic components that combine with oxygen to produce various oxides. The EDS study revealed a notable change in the chemical composition, which included a reduction in organic substances and an increase in inorganic residues and newly formed oxides, see Table *3.3*.

The VIP performance is influenced by key elements with concentrations above 10%, such as silicon dioxide (SiO_2), potassium oxide (K_2O), and calcium oxide (CaO), as well as by other elements with concentrations below 10%, including sodium chloride (NaCl), magnesium oxide (MgO), aluminium oxide (Al_2O_3), phosphorus pentoxide (P_2O_5), sodium oxide (Na_2O), iron disulfide (FeS_2), and iron oxide (Fe_2O_3). SiO_2, due to its low thermal conductivity, improves insulation properties, whereas components such as NaCl, which have higher thermal conductivity, have a detrimental effect on performance. Nevertheless, the presence of NaCl, which rises from 5.56% at 600℃ to 6.71% at 800℃, can have a negative impact on thermal performance due to its elevated thermal conductivity. The thermal conductivity can also be influenced by K_2O and CaO, which similarly rise with temperature, although their effect is not as strong as that of SiO_2 and NaCl.

Additional trace elements that are produced through oxidation processes during pyrolysis also have an impact on VIP performance. As temperature increases, the amount of P_2O_5 drops, which in turn reduces its potential negative effect on thermal conductivity. Optimising the balance of these elements is essential for maximising the efficiency of insulation. In addition, raising the pyrolysis temperature can result in smaller particles, which in turn improves the thermal performance of VIPs by increasing the density of the packing and reducing the thermal conductivity of gases within the core material.

The thermal conductivity of the material should exhibit consistent stability across various pyrolysed temperatures, since minimal percentage variations in these elements was deducted. However, additional characterisation is required. Additionally, it is important to examine a balance between the thermal properties and energy consumption (pyrolysis) while selecting the optimal pyrolysis temperature for TNA.

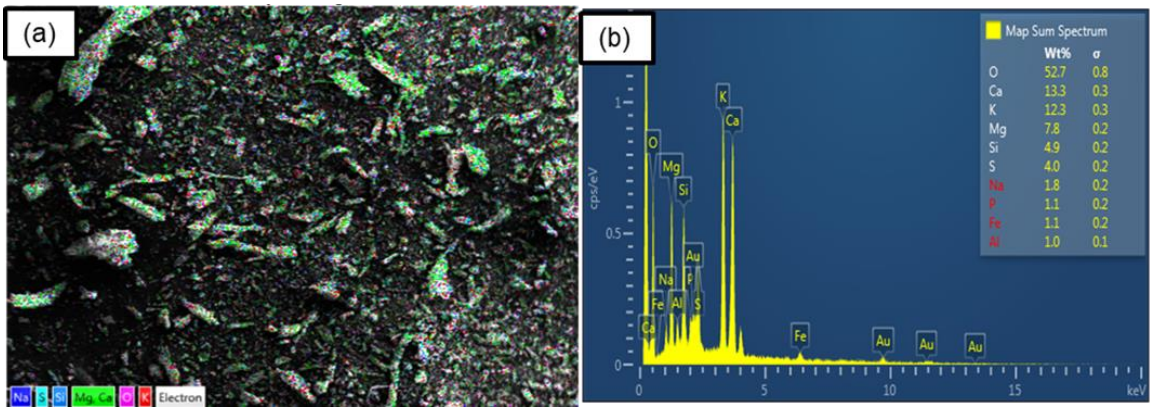

Figure 3.10 (a) SEM image of TNA pyrolysed at 700 ℃ and (b) results of the EDS

Table 3.3: Chemical composition of processed TNA at 600, 700 and 800 ℃ using EDS

Chemical Composition	Content (%)			
	Pyrolysed fibres 600 ℃	Pyrolysed fibres 700 ℃	Pyrolysed fibres 800 ℃	Pyrolysed fibres 700 ℃ (2nd study)
SiO_2	53.9	55.5	56.9	53.9
K_2O	10.6	11.2	11.3	11.1
CaO	10.8	11.8	12.1	11.1
NaCl	5.5	5.8	6.7	-
MgO	4.7	4.4	4.9	5.4
Al_2O_3	2.8	2.9	3.1	3.7
P_2O_5	4.9	2.7	1.1	1.2
Na_2O	2.9	2.3	2.5	2.2
FeS_2	2.3	1.9	1.6	-
Fe_2O_3	1.7	1.5	1.5	2.7
others	-	-	-	8.8

In order to verify the accuracy of the findings acquired by the EDS map spectrum approach, a supplementary analysis was conducted on TNA produced at 700℃. The second study aims to validate the results obtained from the initial EDS assessment, so confirming the accuracy and reliability of the chemical composition values. The comparison of the two approaches revealed similar values, notably for significant elements like as SiO_2, K_2O, and CaO, which are essential for understanding the material's properties. The SiO_2 concentration is 55.51% as determined by EDS and 53.95% in the validation test. Similarly, the values of K_2O and CaO were comparable using both approaches. The results of the EDS map spectrum data support the

reliability of the primary analysis in accurately representing the composition of the material. This comprehensive validation assures that the findings are reliable in potential employment in thermal performance studies.

3.2.4 TNA particle size distribution using ImageJ

Two techniques were utilised in this part of the research to measure the particle size distribution of TNA pyrolysed at 600℃, 700℃, and 800℃. The initial approach involved the utilisation of ImageJ software after doing SEM, while the second approach used was laser diffraction exclusively for TNA pyrolysed at 600℃ and 800℃ which is discussed in the next section.

Three high-resolution SEM images were captured for each sample. The process employing ImageJ was as follows:

I. *Image import and preparation:* The high-resolution SEM image, shown in Figure *3.11*a, was imported into ImageJ by simply dragging and dropping the image into the software. As the SEM pictures were already in grayscale, there was no need for any conversion.
II. *Brightness and contrast adjustment:* The visibility of the particles was enhanced by adjusting the brightness and contrast, as depicted in Figure *3.11*b.
III. *Thresholding:* Thresholding was utilised to generate a binary image (black and white) which effectively separated the particles from the background. This can be shown in Figure *3.11*c. It was essential to ensure that the particles were black and the background was white.
IV. *Scale setting:* The scale was established by use the known distance provided by the scale bar in the SEM image, enabling precise measurements in micrometres.
V. *Noise reduction:* Image clarity was enhanced by eliminating noise with noise reduction techniques.
VI. *Particle size range settings:* Two approaches were investigated for setting the particle size range:
    - An open size range was initially tried during the experiment. Nevertheless, this occasionally led to the software mistakenly combining several particles, resulting in inaccuracies. For example, the largest particle measured 109.87 μm, while the range of sizes observed went above 200 μm.
    - Range Limitation was adopted in order to prevent this issue, where a specific range of up to 200 μm was employed, considering the possibility of agglomeration. The average particle size difference between the open and set ranges was negligible (less than 1 μm), hence the set range was uniformly applied to all samples.

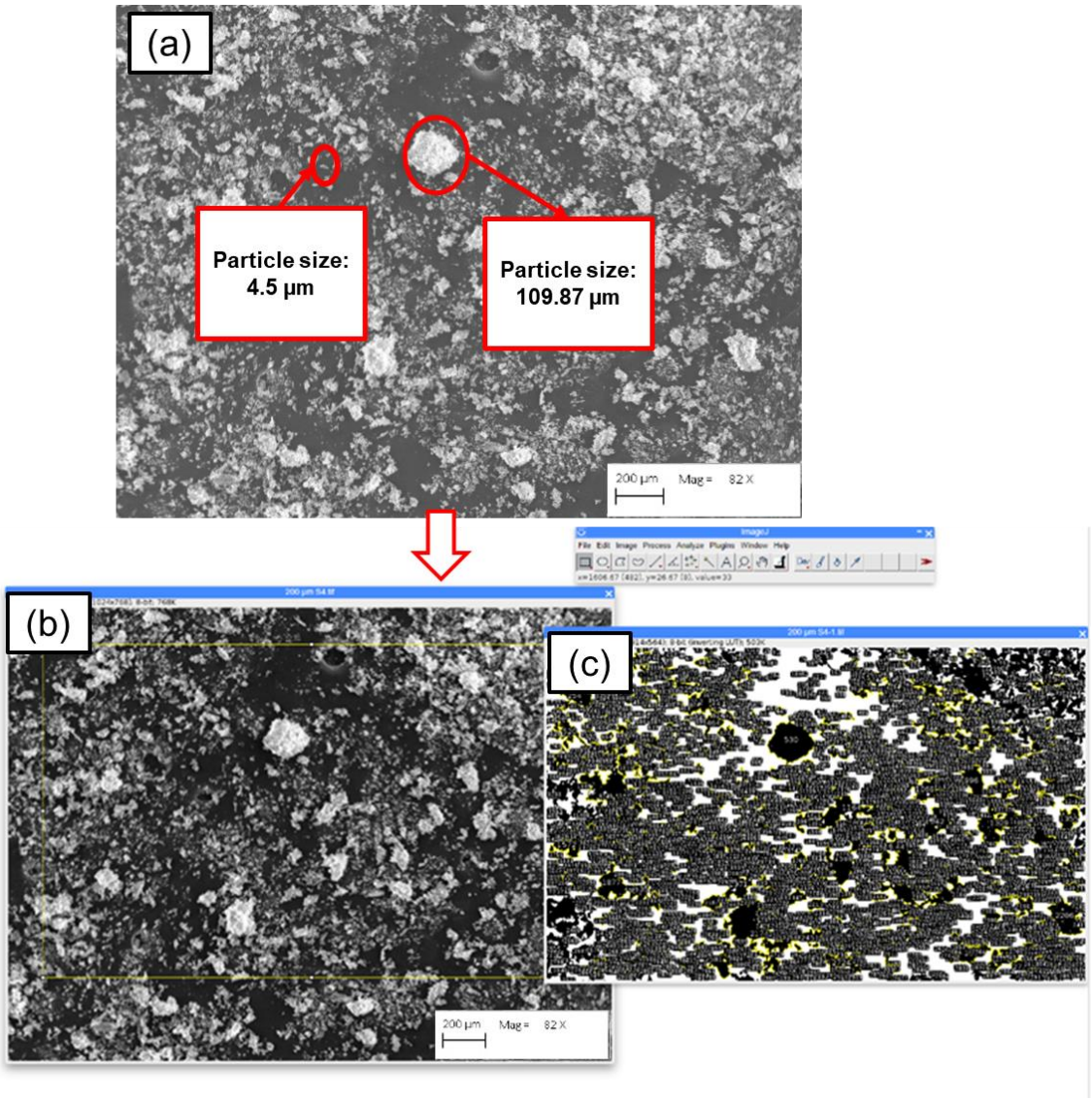

Figure 3.11 (a) SEM image of TNA pyrolysed at 800 ℃, (b) adjusted brightness and contrast of the SEM image of TNA-800 using ImageJ, (c) particle size count of TNA-800

Ensuring comparability was achieved by applying consistent thresholding to all images. Table *3.4* displays the particle count, minimum particle size, maximum particle size, and average particle size for TNA pyrolysed at the three temperatures. Figure *3.12*(a,b and c) display comprehensive particle size distributions for TNA pyrolysed at 600℃, 700℃, and 800℃, respectively.

As the pyrolysis temperature increased, a trend towards smaller particle sizes was observed. As detailed in Table *3.4*, the smallest particle size for TNA that was produced at 600℃ was 4.8 µm. The size reduced to 3.76 µm at 700℃ and further decreased to 2.62 µm at 800℃. The behaviour can be ascribed to the breakdown of organic substances at elevated temperatures, leading to the formation of smaller particles. At a temperature of 500℃, incomplete pyrolysis occurred, resulting

in certain particles maintaining their initial size and structure while undergoing partial changes. At a temperature of 600℃, a higher degree of conversion to ash occurred, leading to the formation of smaller and more evenly sized particles. At temperatures of 700℃ and 800℃, a more complete breakdown resulted in additional reduction in the size of the particles.

Although there was no clear correlation between temperature and particle count, the average particle size followed the expected trend. For instance, the TNA pyrolysed at 600℃ exhibited a greater number of particles compared to the TNA pyrolysed at 700℃, possibly attributable to the quantity of ash present in the sample. This suggests that the particle count has no substantial impact on the final average particle size.

Table 3.4: The minimum, maximum and average particle sizes of TNA produced at 3 different temperatures

Sample	Particle Count	Minimum Value (μm)	Maximum Value (μm)	Average Value (μm)
TNA	3612	4.80	171.55	9.16
TNA-700	2921	3.76	153.19	8.49
TNA-800	9783	2.62	109.86	6.30

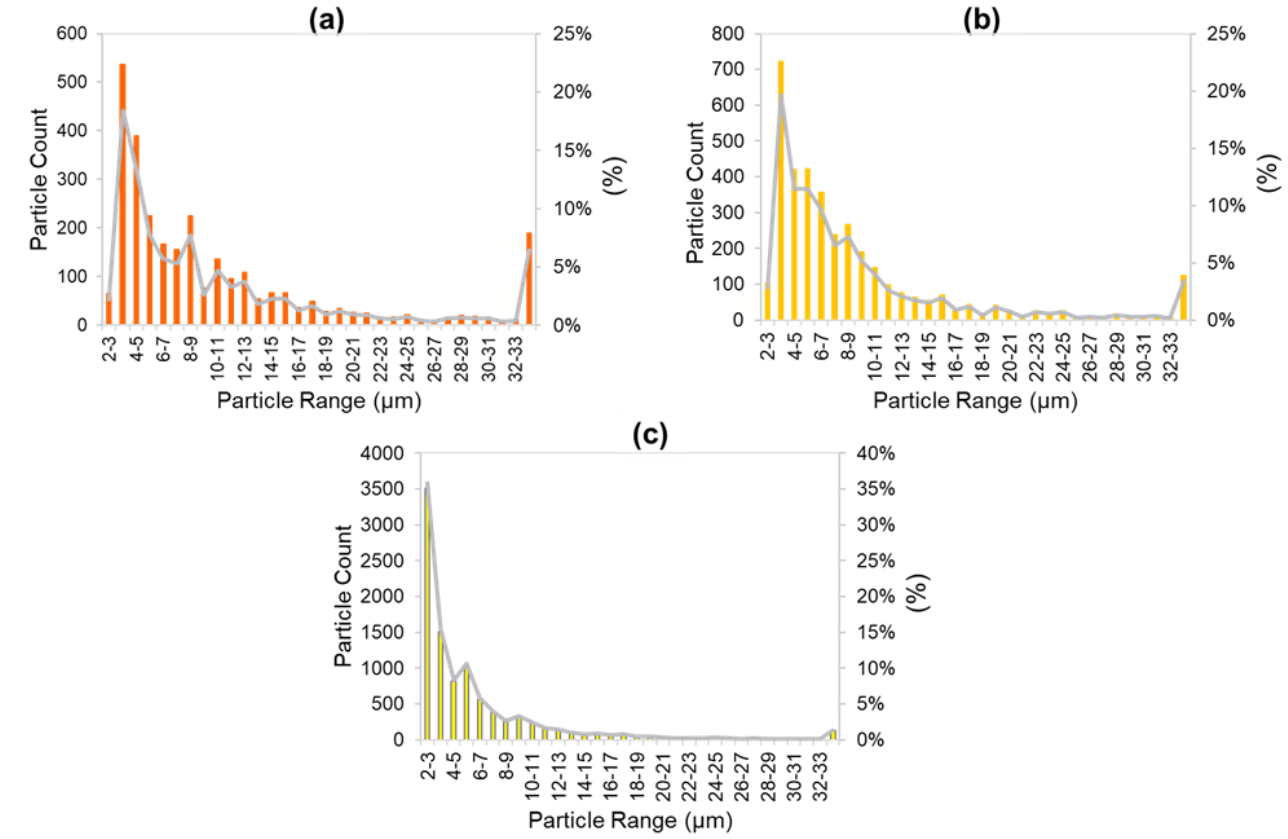

Figure 3.12 Particle size distribution using ImageJ method of (a) TNA pyrolysed at 600 ℃, (b) TNA pyrolysed at 700 ℃ and (c) TNA pyrolysed at 800 ℃

3.2.5 TNA Particle size distribution using laser diffraction

Laser diffraction was used to measure the particle size distribution of TNA pyrolysed at 600℃ and 800℃, in addition to the previously mentioned technique. The HORIBA LA-960 laser scattering particle size distribution analyser was used for this purpose. Each sample was tested three times to assure consistency. In order to avoid clumping, a dry dispersion technique (with air) was employed.

Laser diffraction is based on the notion that particles scatter light at angles that are inversely proportionate to their size when they are exposed to a laser beam. Particles of bigger size exhibit a greater intensity of light scattering at smaller angles, while particles of smaller size exhibit a lower intensity of light scattering at larger angles. Sensors positioned at different angles around the specimen measure the intensity of the scattered light. Subsequently, the collected data is subjected to analysis employing mathematical models, such as Mie theory, in order to determine the distribution of particle sizes. Usually, the findings are displayed as a volume distribution, which shows the proportion of the total volume that is made up of particles of various sizes. This technique is preferred due to its fast and precise readings, particularly for particles within the range of nanometres to millimetres.

The laser diffraction experiment findings are displayed in Figure *3.13*a and Figure *3.13*b for TNA pyrolysed at 600℃ and 800℃, respectively. The figures depict the proportion of volume occupied by particles of particular sizes. For the TNA-800 sample, a peak at 6.72 µm showed that particles of this size represented 11% of the sample volume. The particle size range measured ranged from 4.472 to 51.471 µm for TNA pyrolysed at 600℃, and from 3.905 to 44.938 µm for TNA pyrolysed at 800℃. It is worth mentioning that there were no particles larger than 63 µm found in either of the samples. This matches the size of the sieve employed (63 µm) and highlights the effectiveness of the dry dispersion approach in separating clumps of particles. This is a process that cannot be done with the ImageJ method.

The average particle size for TNA pyrolysed at 600℃ was 9.37 µm, while for the TNA pyrolysed at 800℃, it was 8.01 µm. The results align with those obtained using the ImageJ approach, which indicated average particle sizes of 9.16 µm for TNA pyrolysed at 600℃ and 6.3 µm for TNA pyrolysed at 800℃. The consistency in the results validates the use of ImageJ for particle size measurement, despite laser diffraction being a more widely recognized and accurate technique.

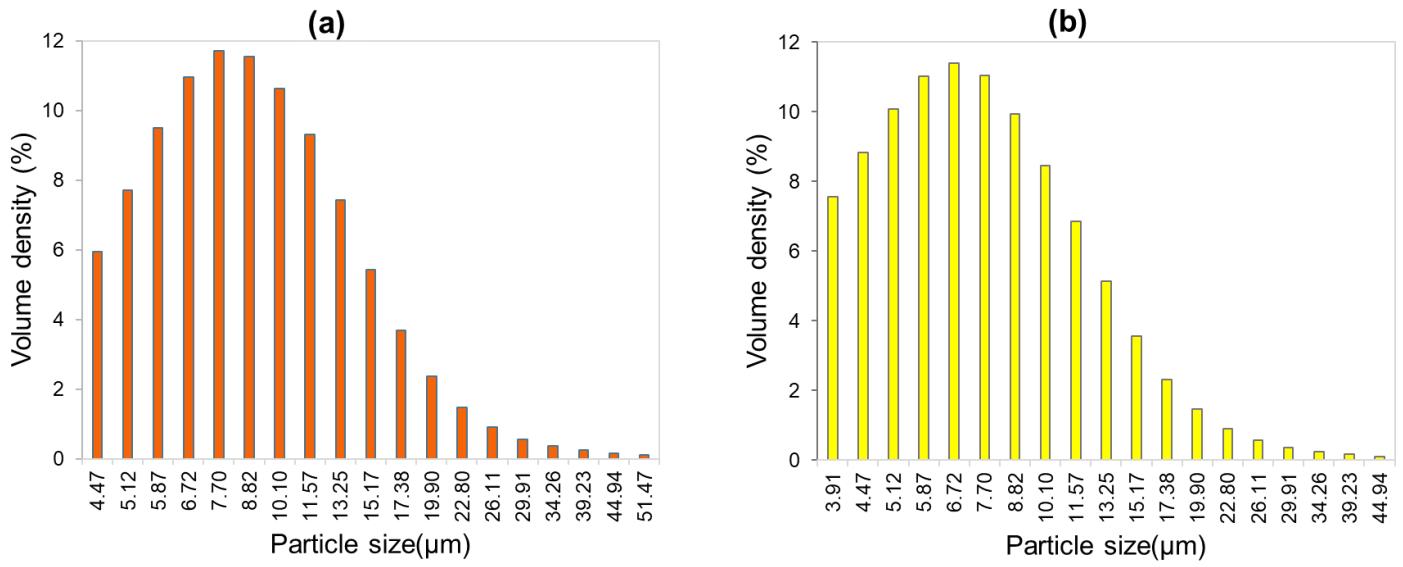

Figure 3.13 Particle size distribution using laser diffraction method of (a) TNA pyrolysed at 600 ℃ and (b) TNA pyrolysed at 800 ℃

3.2.6 Fibre size distribution using ImageJ

In order to ascertain the disparity in fibre length distribution across the natural fibres, six distinct sets of samples were randomly selected from various containers containing the sieved materials. For each sample, a picture was captured on one quarter of the sample holder pin, resulting in a total of 48 images. Then, ImageJ was used in conjunction with the captured SEM images based on its known scale with enhancing the quality and clarity of the images. This enabled the accurate measurement of the length of the observed fibres.

Figure *3.14* illustrates the distribution of fibres as a percentage over varied lengths ranging from 0.1 to 2 mm for both TNFm and TNFs. A total of 774 fibres were identified in the TNFm sample, with 67% of these fibres exhibiting a length less than 1 mm. In contrast, TNFs exhibited the presence of 116 fibres, all of which were found to have a length less than 0.3 mm, the remaining particles were seen in the form of dust (or crushed fibres). A notable disparity in the fibre length was seen between the two materials, only TNFm exhibited significant amount of fibres with an average length of 0.82 mm in contrast to TNFs that had an average length of 0.22 mm. The observed variation may be ascribed to the size of the sieve, indicating that a decrease in sieve size led to a reduction in both particle size and the number of long fibres.

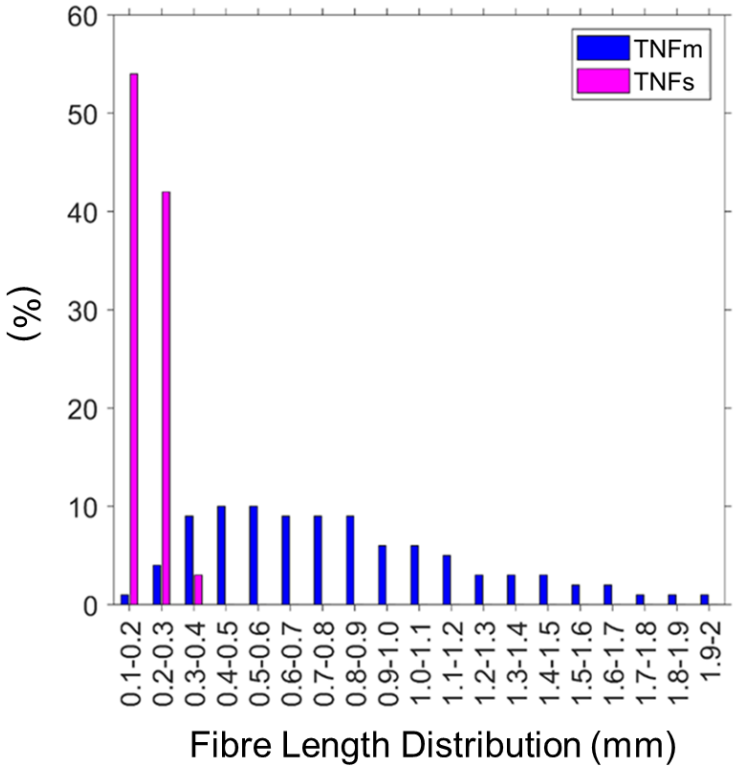

Figure 3.14 TNFm and TNFs fibre length distribution

3.2.7 Mercury Intrusion Porosimetry (MIP)

Mercury Intrusion Porosimetry (MIP) was employed to determine the pore size distribution of our samples utilising a micrometrics AutoPore V instrument located at MCA services, Cambridge (Range: 30 nm to 400 micrometres). The test is carried out by placing 1 g of material on a penetrometer (a cylindrical cell) containing mercury, which intrude from large to small pores with the gradual increase of pressure.

The data of cumulative intrusion volume per unit mass of sample at each pressure level is the output of the MIP tests. To relate these pressures to the pore sizes, the Washburn equation (3.2), which assumes that these pores are open cylinders, is used. The total volume of mercury that permeated the sample is equal to the sample's total pore volume. The porosity of the sample can be calculated by dividing the total pore volume by the total sample volume. Densities of the sample's bulk and skeletal are additional important outcomes of the MIP tests.

$$D = \frac{\kappa \cdot 4\gamma \cos \theta}{P} \tag{3.2}$$

Where D is the pore diameter, γ the surface tension between fluid and air, κ the shape factor, θ the angle of contact of fluid and wall interface and P the pressure of intrusion. Through using the MIP, the range of pore sizes of tree-based natural fibre, tree-based natural ash pyrolysed at

different temperatures, and previously studied fumed silica were observed. In addition of obtaining the values of average pore diameter, porosity, bulk density and skeletal density of all the materials.

I. Cumulative pore size distribution (V)

The cumulative volume of mercury intruded in the sample at each pressure was plotted respectively to its pore diameter. In order to mercury intrude on a pore, pressure must be applied, therefore the curve in Figure *3.15* must be read from right to left as the cumulative volume increases with smaller pore diameters. The higher the slope at specified pore diameter the higher the pore volume occupied by the pores, and the horizontal line shows the absence of the corresponding pore diameter in the sample. In Figure *3.15* it was observed that most of the pores of all pyrolysed TNA were above 2 µm and this may be attributable to the impact of mercury compression on ash. On the other hand, the TNFs sample showed higher slope at 1 µm similar whereas TNFm showed increasing volume until 0.2 µm and that can be attributed to the number of long fibres that can have small pores. Only fumed silica showed monotonically increasing volume across all pore diameters indicating the presence of all sizes of pores. FS were noticed to have higher porosity then all tested tree-based natural fibres and ash and that was observed by the difference of values of the cumulative intrusion volume.

It was observed that there was high variation in pores for all samples tested therefore the x-axis was converted to logarithmic scale.

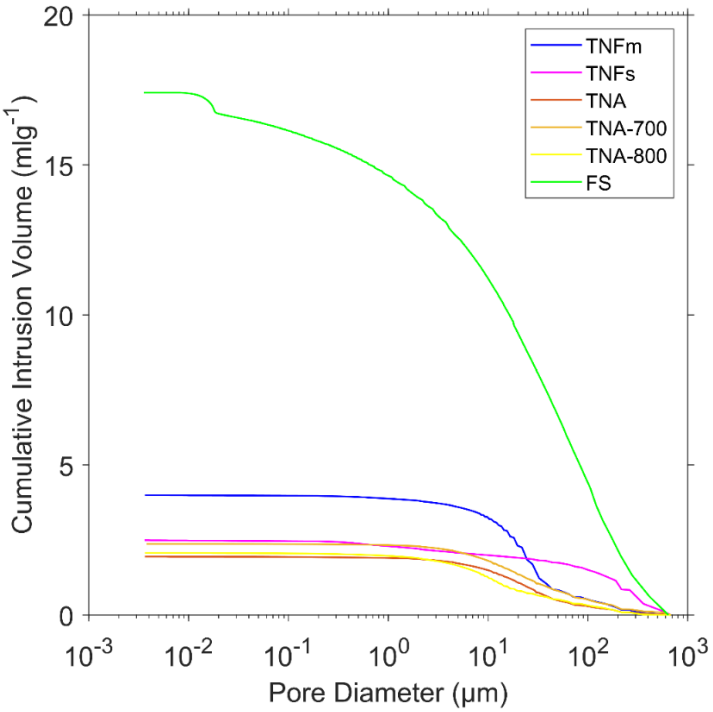

Figure 3.15 Cumulative intrusion volume of tree-based natural fibre samples compared to FS

II. Incremental pore size distribution (dV)

Figure *3.16* presents the deducting subsequent elements from the cumulative pore size data (dV1 = V2 - V1) that indicates the pore volume occupied by each pore diameter independently. TNF and TNA were found to have higher peak at higher pore diameter. Nevertheless, the peaks do not correspond to the sample's pore frequency. The volume occupied by one large pore may be more than that of several thousands of microscopic pores.

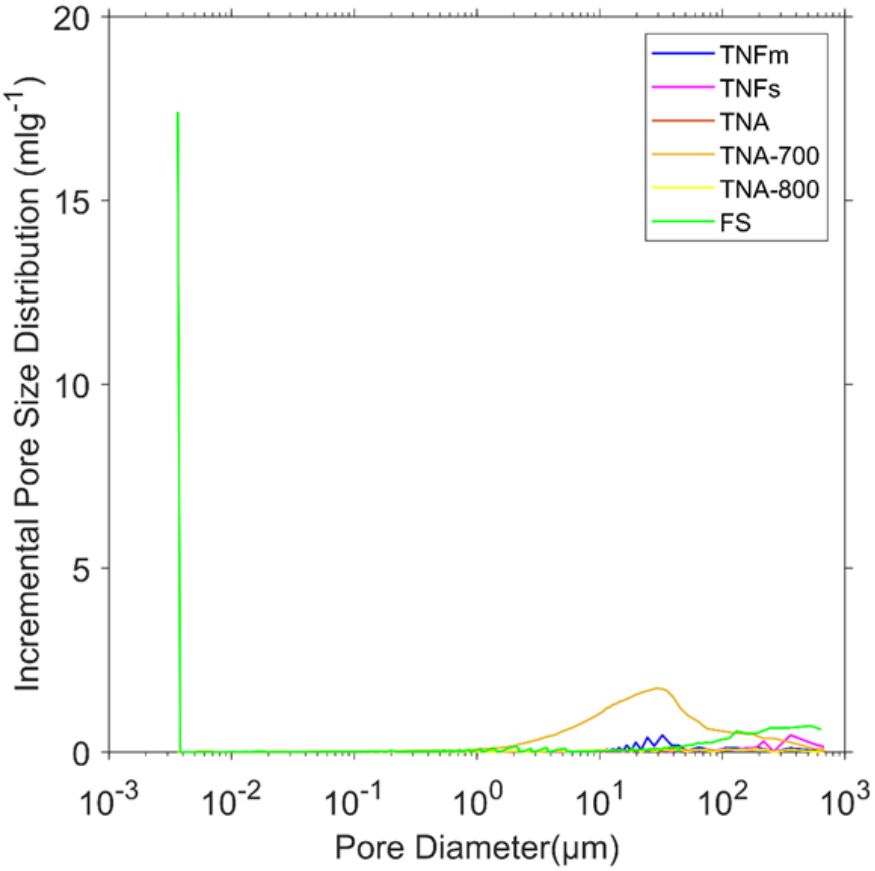

Figure 3.16 Incremental pore size distribution (dV) of all tested samples

III. Differential intrusion (dV/dD)

The following curve (Figure *3.17*) presents the differential intrusion of all materials using the following equation dV/dD= (V2-V1)/(D2-D1). This technique helps in observing if there are any pores below 0.1 μm. Figure *3.17* indicates that fumed silica has a peak at 0.01 μm. All the TNF cores do not show any peaks below 0.1 μm except for the tree-based natural ash pyrolysed at 700 ℃. The peaks of the curve should correspond to the peaks of the incremental pore size distribution. Yet, the difference between D2 and D1 was significantly smaller for small sized pores

than large sized pores, the peak only appeared for smaller pore sizes that were present in significant amount in the sample due to inhomogeneous data distribution.

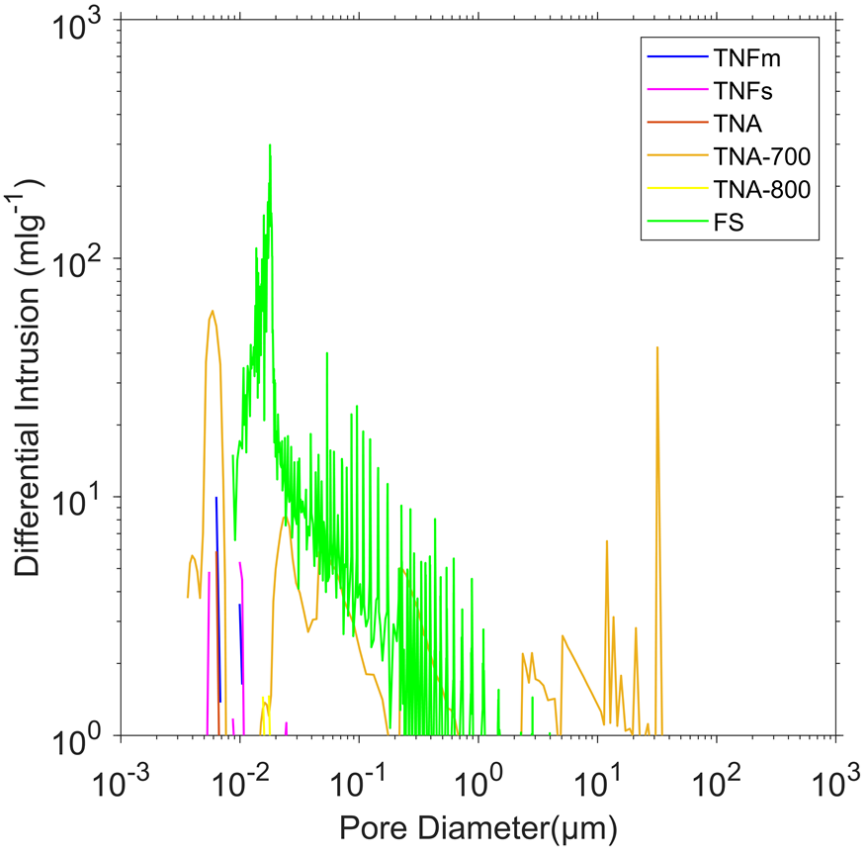

Figure 3.17 Differential intrusion (dV/dD) of all tested samples

IV. Log differential intrusion (dV/dlogD)

Figure *3.18* depicts the log differential intrusion, which is the smoother version of the incremental intrusion. First, the data is homogenised by interpolating the cumulative pore volume so that the difference between the logarithms of each successive pore size is the same. As with the incremental incursion volume curve, the peaks show the pore sizes which occupied the most volume. As predicted all the tree-based natural ash pores were larger than 2 μm with TNA pyrolysed at 700 ℃ to have the smallest pores between the ash. On the other hand, TNFm had one peak at larger pore sizes of 200 μm, while the second peak was observed at lower pore sizes of 0.3 μm. The bimodal distribution may be attributed to the significant variance in the sizes of both small and large fibres, which can result in the presence of both small and large pores. TNFs sample exhibited a distinct peak on the curve within the 10 to 40 μm range, indicating a higher concentration of pores within this size range. The observation may be explained on the basis of a lower quantity of fibres present in the sample compared to the larger number of particles. Only

Fumed silica has pores below 0.1 μm and that can be attributed to the small size of primary particles and the way they aggregate gave a result of FS having large volume of very small pores.

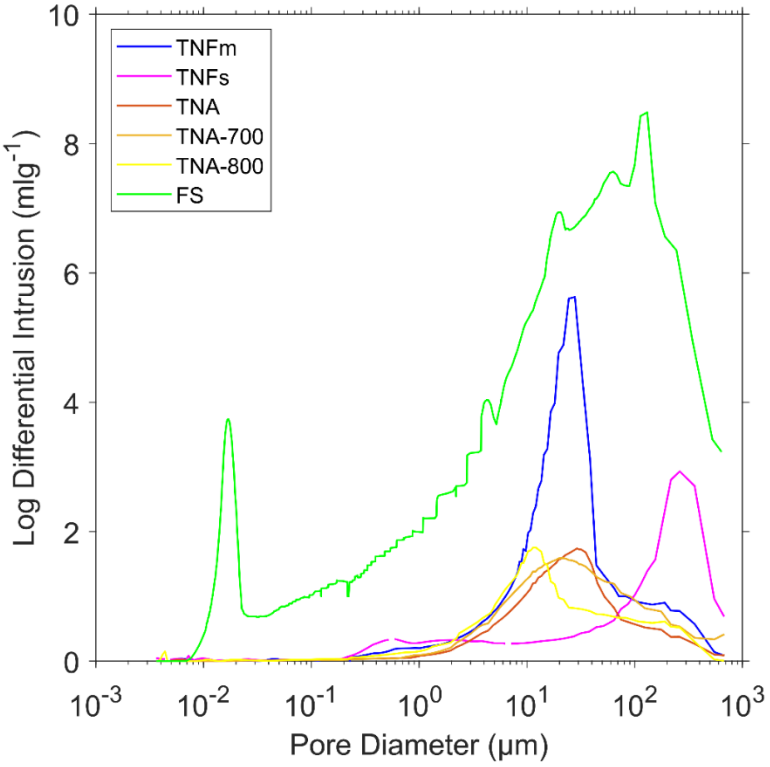

Figure 3.18 Log differential intrusion (dV/dlogD) of all tested samples

3.2.8 Pore sizes and porosity of Individual powders and fibres

The porosity (φ) of each sample which refers to the voids within the powdered and fibrous material within the addition of voids presented between individual particles, typically expressed as percentage of the total volume, was calculated using equation (3.3).

$$\varphi = \frac{V_P}{V_B} \tag{3.3}$$

where $\mathrm{V_P}$ is the pore volume and $\mathrm{V_B}$ the bulk volume of the sample.

The average pore diameter (D) was computed as a function of the total intrusion volume and the total pore area using equation (3.4).

$$D = \frac{4V}{A} \tag{3.4}$$

where V is the total pore volume and A the total pore area.

Table 3.5: Average pore diameter, porosity and bulk density comparison of individual samples using MIP technique

Sample	Total intrusion volume (V) x 10^{-6} ($m^3.g^{-1}$)	Total pore area (A) ($m^2.g^{-1}$)	Average pore diameter x 10^{-6} (m)	Porosity (%)	Bulk Density ($kg.m^{-3}$)
FS	17.41	264.24	0.26	91.54	52.60
TNFm	2.49	14.24	0.70	77.35	310.40
TNFs	3.99	8.05	1.98	84.93	212.60
TNA	2.37	3.90	2.43	84.34	356.10
TNA-700	1.95	3.98	1.96	82.83	425.60
TNA-800	2.07	4.94	1.68	82.79	400.10

FS exhibited the maximum porosity, measuring at 91.54%, in comparison to TNFm and TNFs, which had porosity values of 77.35% and 84.93%, respectively, as indicated by the data in Table *3.5*. The material properties, such as bulk density and particle size, may be responsible for the variations in porosity observed among the different samples. The results suggest that composites with a larger FS content would have a higher porosity, as it exhibited the largest intrusion volume and the lowest bulk density of 52.6 $kg.m^{-3}$ in comparison to TNF samples.

It was observed that the samples exhibit minor complex differences when pyrolysed at varying temperatures due to TNA. The average pore diameter and porosity of TNA pyrolysed at 600 ℃ were the largest among the tested samples. one possible explanation for these results is the discrepancy in particle sizes, with TNA having the largest particle size when pyrolysed at 600 ℃.

3.2.9 Effect of composites on pore size distribution

Upon the addition of FS to TNFm, TNFs and TNA, the small FS particles infiltrated the inter and intra-particle pores of TNF composites. As a result of the elevated proportion of FS (70 wt.%) in the samples, it was observed that composites FS_TNA1, FS-TNFm1 and FS-TNFs1 exhibited a consistent and gradual increase in volume across all pore diameters, like that of sample FS. In the case of FS-TNA3 (50 wt.% for each) gradual increase was observed in volume across all pore diameter but not as high as the previous samples, see Figure *3.19*a. For composite samples, the peaks seen in the curve at larger pore sizes may be attributed to the influence of mercury compression, whilst the peaks below 0.1 μm can be attributed to the pores of FS, see Figure *3.19*b.

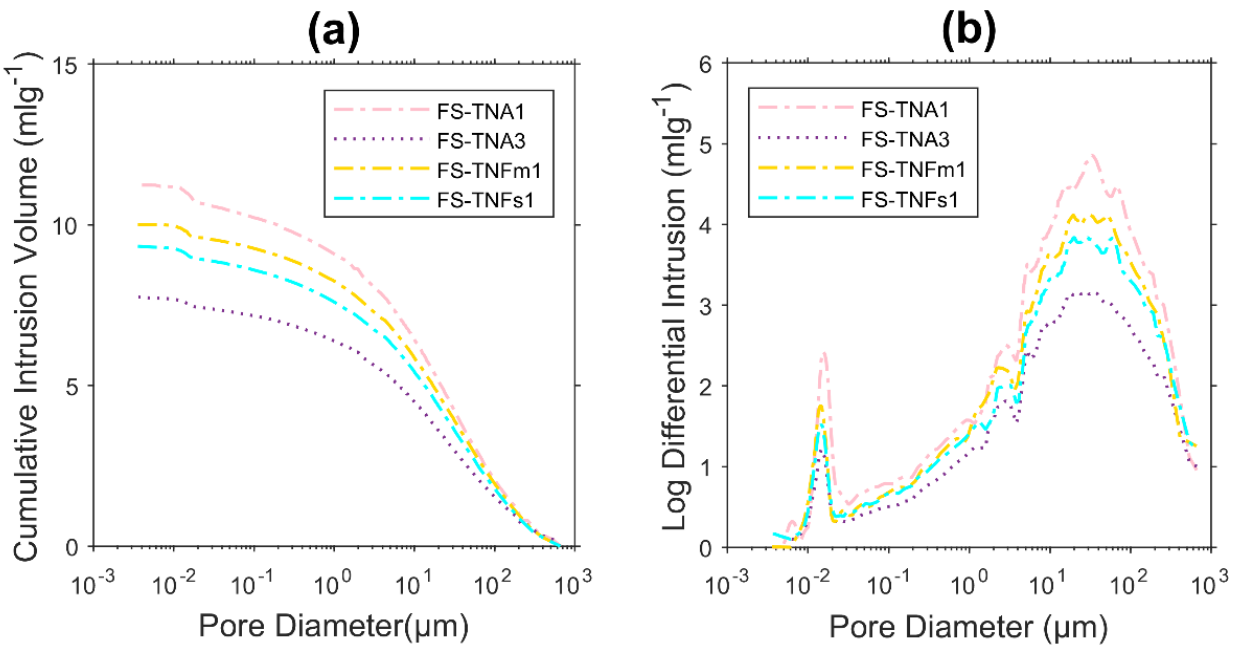

Figure 3.19 (a) The Cumulative intrusion and (b) the log differential intrusion for FS-TNA1, FS-TNA3, FS-TNFm1 and FS-TNFs1 measured using MIP technique

Table 3.6 Average pore diameter, porosity and bulk density comparison of composite samples using MIP technique

Sample	Total intrusion volume x 10^{-6} (m^3g^{-1})	Total pore area (m^2g^{-1})	Average pore diameter x 10^{-6} (m)	Porosity (%)	Bulk Density (kgm^{-3})
FS-TNA1	11.24	234.61	0.19	88.37	78.60
FS-TNA3	7.75	156.37	0.19	90.99	117.40
FS-TNFm1	10.01	170.74	0.23	88.27	88.20
FS-TNFs1	9.33	189.32	0.19	89.44	95.80

The results shown in Table *3.6* indicate that the total pore area and bulk density of the tree-based natural fibre samples are significantly increased and decreased, respectively, by the incorporation of fumed silica. The increased presence of microscopic particles from FS is the reason of this effect. For example, the average pore diameter of samples FS-TNA1 and FS-TNA3 was almost identical, despite the fact that FS-TNA3 contained only 50 wt.% FS, whereas FS-TNA1 contained 70 wt.%. Furthermore, the porosity of all samples increased, although they remained slightly below the original porosity of pure FS, which was 91.54%. The increase in porosity and the

distinctive characteristics of fumed silica contribute to the enhanced performance of VIP samples, enabling lower thermal conductivity even at higher pressures

3.2.10 Thermogravimetric analysis (TGA)

Thermogravimetric analysis (TGA) was conducted to ascertain the temperature threshold for drying tree-based natural fibres and to investigate the occurrence of any chemical degradation upon temperature elevation. The thermogravimetry curves were acquired using the thermogravimetric analyser (SDT Q600 V8.3) as the samples were subjected to a temperature increase from ambient conditions to 900 ℃ with a heating rate of 15 ℃/min. The analysis was performed at the Experimental Techniques Centre (ETC) at Brunel University.

The amount of moisture contained in the core material has a significant effect on the energy required to manufacture VIPs, as powders or fibres core containing more dampness would require more time and more pumping energy to evacuate to desired lower pressures. The drying process could pose challenges for various materials, particularly tree-based natural fibres. For example, when the temperature increased it was noticed that mass loss occurred due to chemical changes in addition to the loss of water vapour, see Figure *3.20*. Two different sizes of TNF were examined using thermogravimetry analysis. Both TNFm and TNFs exhibited an initial decline in weight prior to reaching a temperature of 200 ℃. The decline amounted to 9.4% and 9.1% for TNFm and TNFs respectively, primarily attributable to the complete evaporation of moisture. Furthermore, the process of hemicellulose degradation was seen to occur throughout the temperature range of 200-315 ℃ as also reported by other studies (Chen et al., 2022). The most significant weight decline was seen at a temperature of 342.3 ℃ for TNFm and 347.3 ℃ for TNFs, resulting in weight losses of 62.1% and 52.8% respectively. The reduction can be attributed to the disintegration of cellulose, which occurred throughout the temperature range of 315-400 ℃, similar to the findings of (Zhou et al., 2013). The phenomenon seen at a temperature above 440 ℃ can be attributed to the process of Lignin breakdown (Abdel-Hamid et al., 2013). The primary distinction in weight loss occurrence between TNFm and TNFs was due to the particle size distribution. TNFs had larger proportion of dust (or crushed fibres) content compared to TNFM. Conversely, it was shown that the composite samples (FS-TNFm1 and FS-TNFs1) exhibited reduced decreases in comparison to TNFm and TNFs, which was attributed to the presence of FS (70 wt.%). Materials used to form composites are nonreactive in nature (ceramic and natural fibres), hence the stability of individual materials would confirm the stability of composite materials. The findings of the thermogravimetric analysis provided valuable insights for this

investigation by elucidating the moisture content and determining the appropriate temperature at which these materials should be dried.

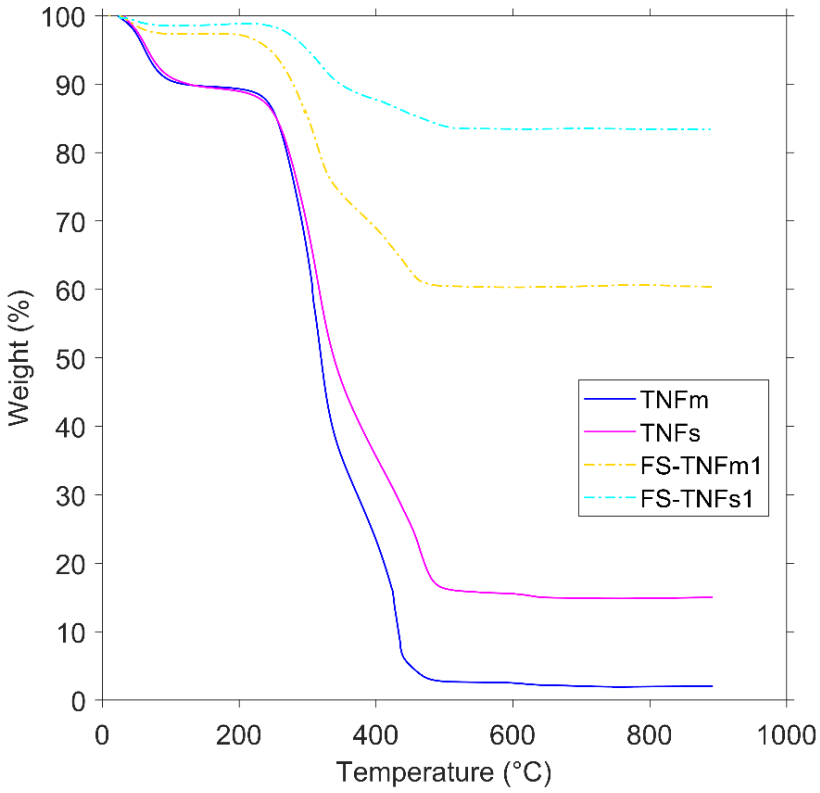

Figure 3.20 Investigated thermogravimetry curves of the TNFm, TNFs, FS-TNFm1 and FS-TNFs1

3.2.11 Fourier Transform Infrared (FTIR) spectroscopy

Fourier Transform Infrared (FTIR) spectroscopy is a method employed to acquire the infrared (IR) transmission spectrum of a material. The method involves the transmission of several polychromatic IR waves through the sample. The magnitude of the transmitted wave is detected and recorded as interferograms. Subsequently, a Fourier transform was employed on these interferograms to generate the infrared transmission spectrum of the sample. This approach is distinct from dispersive spectrometry, which involves transmitting multiple monochromatic waves through the sample and identifying the intensity variation of each transmitted wave. The FTIR analysis was conducted by combining the sample with an alkali halide such as potassium bromide (KBr) and compacting it into a pellet, following the ASTM E1252, 2013 standard, for powdered materials. The study employed quantitative FTIR spectroscopy, employing a Perkin Elmer One spectrophotometer equipped with a Specac ATR-FTIR. The attachment included a diamond crystal with a fixed angle of incidence of 45°. The equipment is located at the Experimental

Techniques Centre at Brunel University London. The following steps explain the process for the KBr pellet-based FTIR:

I. The KBr powder and the sample were subjected to oven drying at a temperature of 120℃ for the duration of one night.
II. The KBr and samples were left to cool in a desiccator.
III. The grinder was used to grind 100 mg of KBr. Subsequently, a further 0.8 mg of the sample was added and carefully grinded for a maximum duration of 30 seconds, due to the hygroscopic nature of KBr.
IV. The two components of the die body were assembled, and a single die pellet was inserted with its polished side facing upwards.
V. The KBr and sample mixture was placed in the die and uniformly distributed using the plunger. The plunger was extracted gradually to facilitate the entry of air into the die. Next, the second die pellet was inserted into the die with its polished side facing downwards.
VI. The plunger was put into the die, ensuring that the O-ring made contact with the upper surface of the die body.
VII. The die was positioned inside the hydraulic press was securely fastened onto the plunger. The die was subjected to vacuum using a rotary pump for a brief period. Subsequently, the valve on the press was sealed and pressured to 10 tonnes while maintaining the vacuum. It was left under pressure and vacuum for a duration of about 3 minutes.
VIII. The rotary pump was switched off, and the bleed screw of the hydraulic press was gradually opened to prevent a sudden decrease in pressure, which may potentially cause the sample disc to break.
IX. The die was removed from the hydraulic press, the base was detached, and the die was held in an inverted position. The die was positioned in an inverted manner on the piston of the hydraulic press, ensuring that the plunger does not dislodge from the lower part. The upper section of the die body was pressed downwards, causing the lower die pellet to be released from the bore.
X. The KBr located between the pellets was carefully removed to prevent any damage to the polished surfaces of the pellets.
XI. Using a little spatula, the compressed KBr disc was moved to the sample holder for IR measurement and promptly examined to prevent moisture absorption from the atmosphere.

KBr powder and the sample were dried in an oven for 120 ℃ for overnight.

The FTIR method was employed to obtain the Infrared transmission data within a spectral wavelength range of 2.5 to 20 μm at a temperature of 20 ℃. The spectral transmission was obtained by converting the independent variable from wavenumber to wavelength using the equation (3.5).

$$wavelength(\mu m) = \frac{1000}{wavelength\ (cm^{-1})} \quad (3.5)$$

The value of the spectral extinction coefficient e^* was determined by equation (3.6) (Wei et al., 2013).

$$e^* = -\frac{ln(\tau)A}{mP} \quad (3.6)$$

where τ is the transmission of the samples, m the total mass of the KBr pellet, P the percentage mass of the original base material in the pellet and A the cross-sectional area of the pellet.

Figure *3.21*a displays the spectral extinction for TNFm, TNFs, TNA, FS and EP. The study revealed that TNFm and TNFs exhibited comparable spectral extinction values across all wavelengths, despite differences in particle size. Additionally, it was noted that although TNFs contained dust particles more than TNFm, however its presence did not impact the results and that can be due to small portion presented in the sample and the method of preparation, as fibres needed to be grinded.

Figure *3.21*b displays same content as the previous figure, but covers a wavelength range of 2.5 to 7.5 μm. It was noted that both types of TNF and TNA exhibited a higher spectrum extinction coefficient in comparison to FS and EP, suggesting a reduced radiative leakage over the examined wavelength range. For instance, between 3.5 and 6 μm, the FS spectral extinction varied between 38.4 and 50.9 m^2kg^{-1}, whereas the TNFm and TNFs varied between 85.7 and 100.1 m^2kg^{-1} and 83.5 and 97.6 m^2kg^{-1}, respectively.

Figure *3.21*c shows the spectrum extinction coefficient of TNA at three distinct temperatures: 600, 700, and 800 ℃. While the chemical composition of all three materials was almost same, the extinction coefficient varied. Specifically, the TNA pyrolysed at 600℃ had a higher extinction coefficient compared to both the TNA pyrolysed at 700℃ and 800℃, across all wavelengths. The ash mostly comprises inorganic oxides, including SiO_2, CaO, and K_2O. Among these three components, TNA pyrolysed at 600 ℃ has the lowest percentage. These components often exhibit lower light absorption characteristics in comparison to organic residues, resulting in a reduced spectral extinction coefficient.

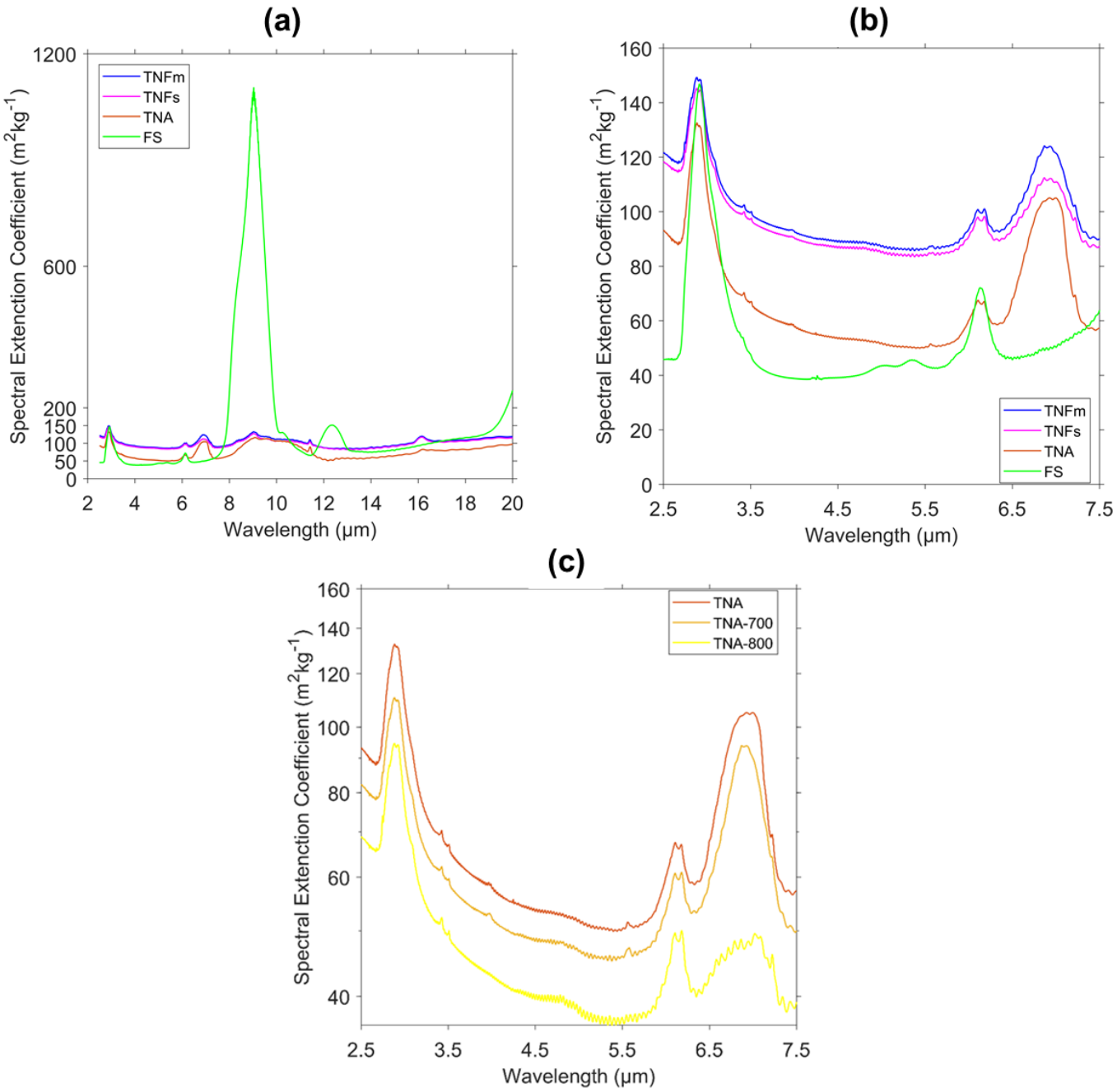

Figure 3.21 Spectral extinction coefficients derived from the transmission data for TNFm, TNFs, TNA and FS measured over (a) 2.5-20 μm, (b) 2.5-7.5 μm and (c) for TNA pyrolysed at different temperatures

3.2.12 Effect of composites on spectral extinction coefficient.

The Beer-Lambert law states that the absorbance of a particular sample is determined by the concentration and molar absorptivity of its distinct components. According to the provided law, each component absorbs its specific infrared (IR) wavelength, and this absorption is not influenced by the presence of other components.

The spectral extinction coefficient obtained from the transmission spectrum can be used as a measure of the molar absorptivity of the material, assuming that there is minimal scattering present (R. Caps et al., 1984). The spectral extinction coefficient of composite samples can be determined using equation (3.7) (Liu et al., 2017b; Wei et al., 2011).

$$e_T^* = \sum_i m_i \times e_i^* \tag{3.7}$$

where e_T^* is the total spectral extinction coefficient, m_i the mass fraction of the ith component in the composite and e_i^* the spectral extinction coefficient of the ith component.

An example of calculating the spectral extinction coefficient of FS-TNA1 (70% FS and 30% TNA) where $e_{FS-TNA1}^* = 0.7 \times e_{FS}^* + 0.3 \times e_{TNA1}^*$.

In order to verify the equation's accuracy, two samples, FS-TNA1 and FS-TNA3, were computed and subsequently examined. The results presented in Figure *3.22* exhibited a remarkably similar pattern in the spectral extinction coefficient of two distinct samples. This prompted the use of the the equation to compute the spectral coefficients of various composites.

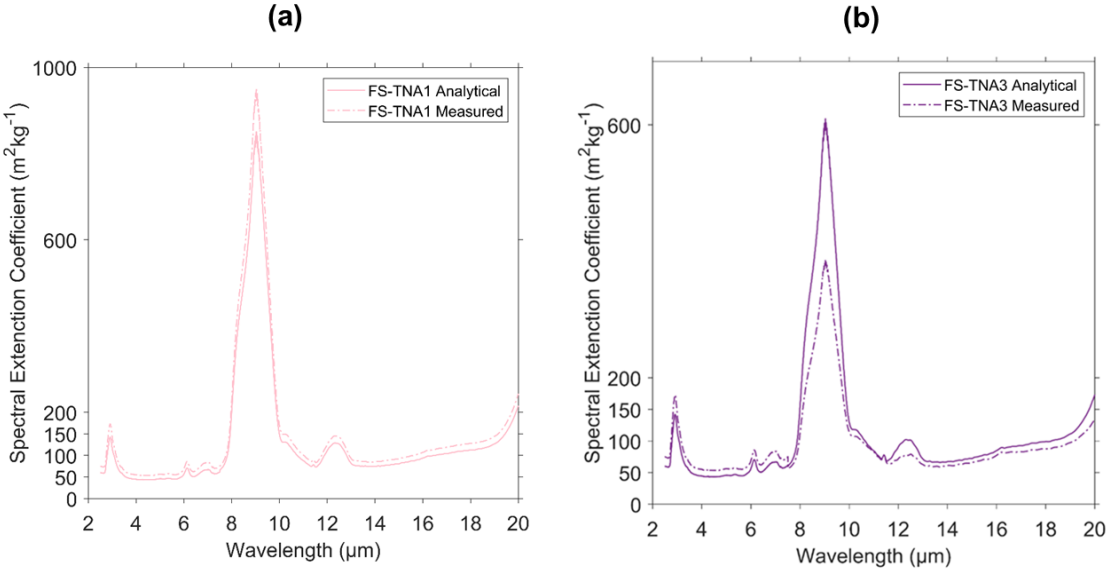

Figure 3.22 Spectral extinction coefficients comparison between analytical value and measured of (a) FS-TNA1 and (b) FS-TNA3

3.3 Rational for material selection

The selection of TNFm, TNFs, and TNA as candidate core materials was guided by their structural properties in relation to established literature benchmarks for high-performance VIP cores followed in section 2.3.6. Compared to traditional materials such as wood pulp (100–119 $kg.m^{-3}$), glass fibres (254 $kg.m^{-3}$), and wood fibre (91 $kg.m^{-3}$), the bulk densities of TNFm (310.6 $kg.m^{-3}$), TNFs (212.6 $kg.m^{-3}$) and TNA (356.1 $kg.m^{-3}$) were relatively high. However, when blended with fumed silica, the bulk densities significantly decreased to values between 78.6–95.8 $kg.m^{-3}$, closely aligning with FS and FS containing composites such as rice husk ash (52 $kg.m^{-3}$).

In terms of fibre dimensions, TNFm (180 µm diameter, 0.82 mm length) and TNFs (60 µm, 0.22 mm) were coarser than typical GF (17.5 µm, 3.4 mm) or bamboo fbre (17.5 µm, 0.96 mm), and closer to wood-pulp (45.6 µm, 1.45 mm). While larger diameters may lead to slightly increased radiative losses, the short fibre lengths promote tight packing and reduce solid conduction. The average pore sizes of raw TNFm (0.7 µm), TNFs (1.98 µm), and TNA (2.4 µm) were substantially reduced in the FS based composite, reaching 0.19–0.23 µm, thus becoming even lower than the FS benchmark value of 0.3 µm and well below materials like wood-pulp (45.4 µm) or wood fibre (112.8 µm), where gaseous conduction dominates at higher pressure.

Porosity also improved significantly upon blending. The raw materials exhibited porosity values between 77.3–84.9%, which is comparable to BF (75.7%) and WF (78%). After FS addition, the porosities increased to 88.2–89.4%, aligning well with fumed silica and sawdust composites (79.2%).

Overall, the modified composites demonstrate a microstructural profile highly comparable to state-of-the-art FS composites found in the literature. Combined with their low cost, waste origin, and lack of industrial competition, these materials offer an environmentally and economically viable pathway for alternative VIP core development. Figure 3.23 to Figure 3.27 present the pore diameter, porosity, fibre length, fibre diameter, and bulk density of previously studied core materials discussed in. Section 2.3.6, compared with materials investigated such as TNFm, TNFs, TNA, and their composites with fumed silica.

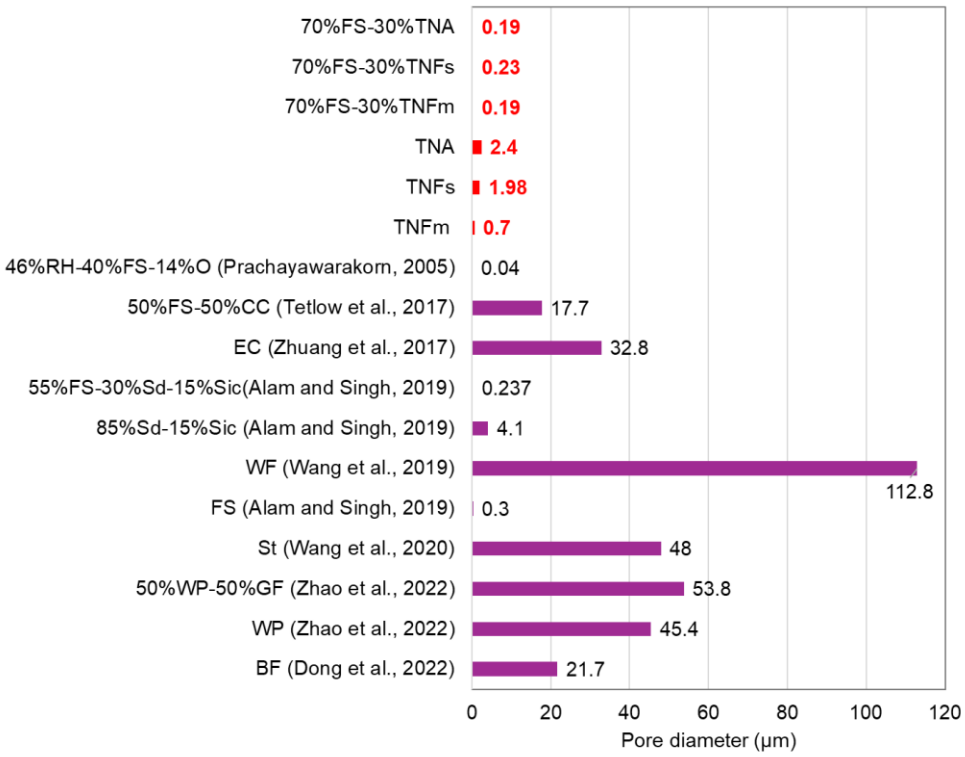

Figure 3.23 Pore diameter of VIP core materials from literature and materials investigated

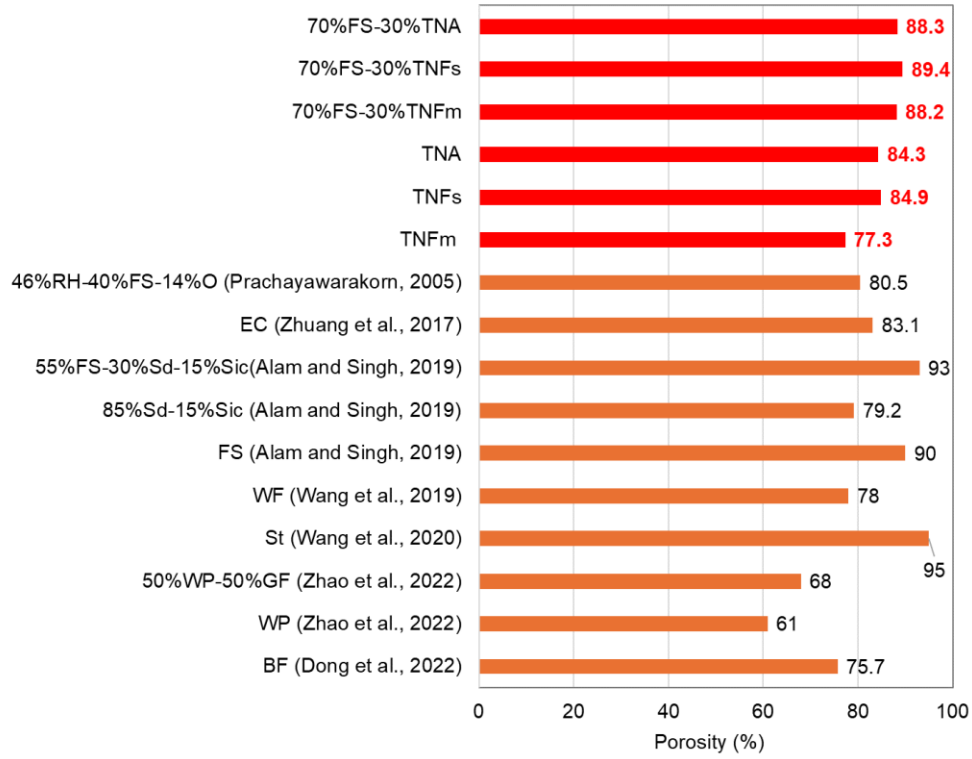

Figure 3.24 Porosity of VIP core materials from literature and materials investigated

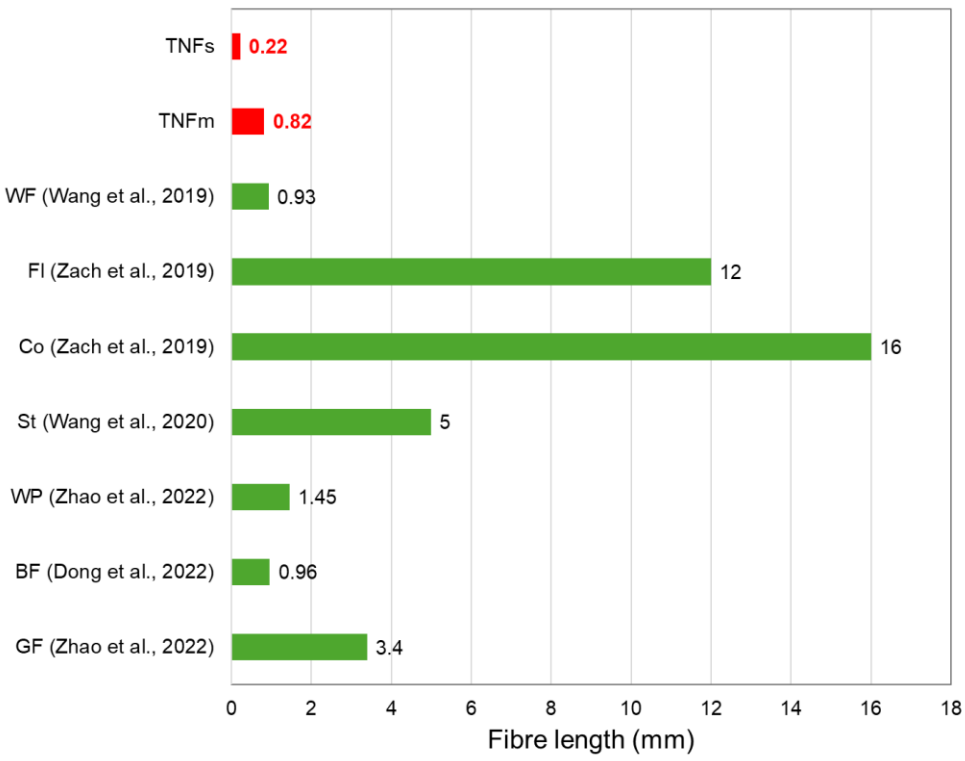

Figure 3.25 Fibre length of VIP core materials from literature and materials investigated

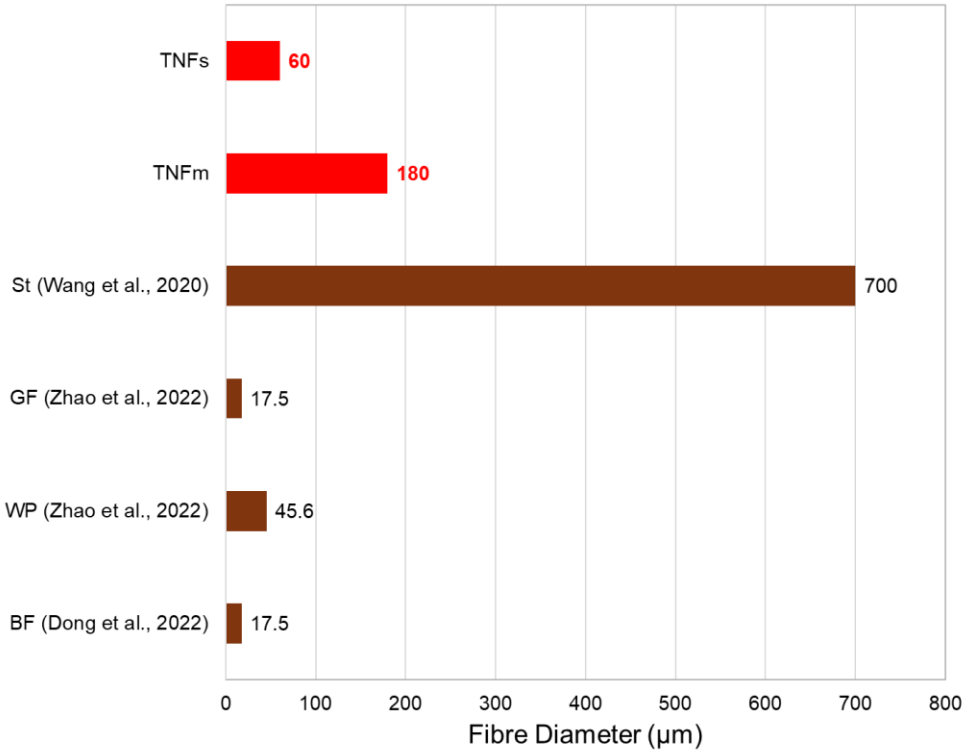

Figure 3.26 Fibre length of VIP core materials from literature and materials investigated

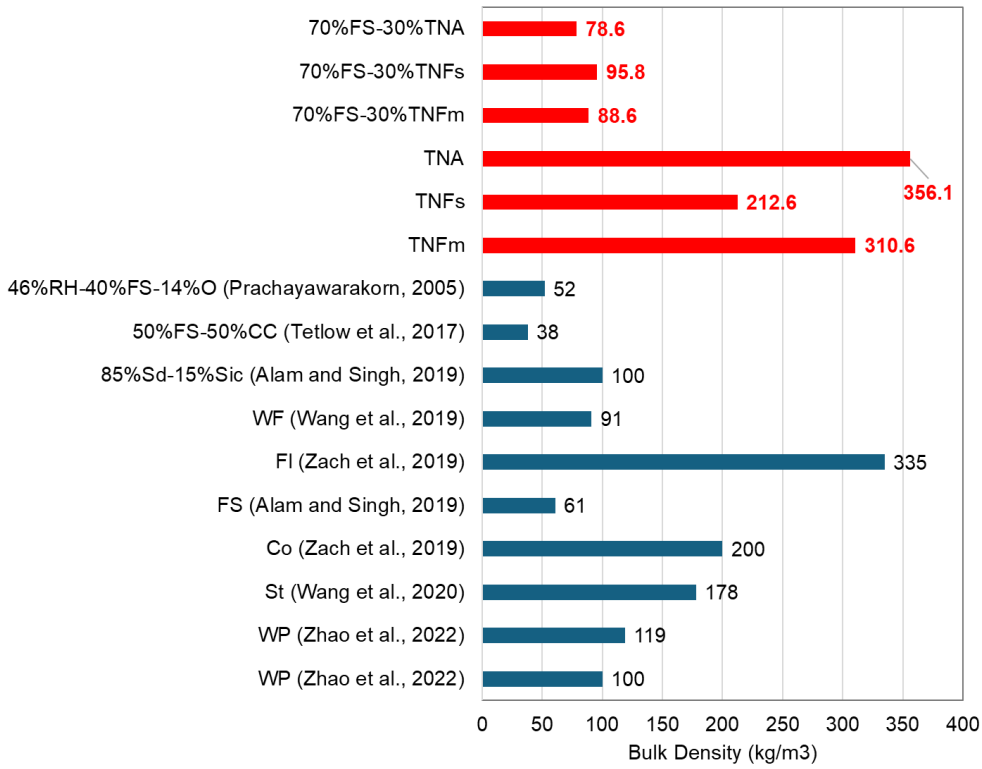

Figure 3.27 Bulk density of VIP core materials from literature and materials investigated

3.4 Manufacturing of VIPs

VIPs were manufactured at CSEF lab in Brunel University of London and the following describes the steps involved:

I. The mass of the core material was determined by multiplying the desired density by the intended volume. The mass of each composite sample was determined using the weight percentage. To ensure the preservation of materials during the development of VIPs, an additional 10% was included for each material respectively to their wt%.

II. The composites were mixed using a 3D mixer, as shown in Figure 3.28a, for a period of 10 minutes at a speed of 50 RPM. The composite's final mixture was placed in a little pan (The sample presented in the Figure 3.28b was FS-TNFs2).

III. The samples were placed in the oven shown in Figure 3.28c and dried overnight at a temperature of 120 ℃.

IV. A fleece was accurately cut according to the exact measurements of the core of the VIP (150 mm x 150 mm) and sealed on three sides. Similarly, the envelope was sealed at a temperature of 110 ℃, with three sides sealed and dimensions of 200 mm x 250 mm.

V. The dried core material was inserted into the fleece and the fourth side of the fleece was then sealed at a temperature of 115 ℃. This resulted in the core material taking on the appearance of a cushion, as depicted in Figure 3.28d.

VI. The loose core was positioned inside a steel die depicted in Figure 3.28e. The core was pressed to the desired thickness using the hydraulic press seen in Figure 3.28f for a minimum duration of 20 minutes. The core experienced a pressure of around 850 kPa, which varied depending on the material of the core.

VII. The core was transferred carefully into the prepared envelope, and the fourth side was vacuumed and sealed using the vacuum sealer depicted in Figure 3.28g to achieve the desired pressure.

The final appearance of the produced VIP was showcased in Figure 3.28h.

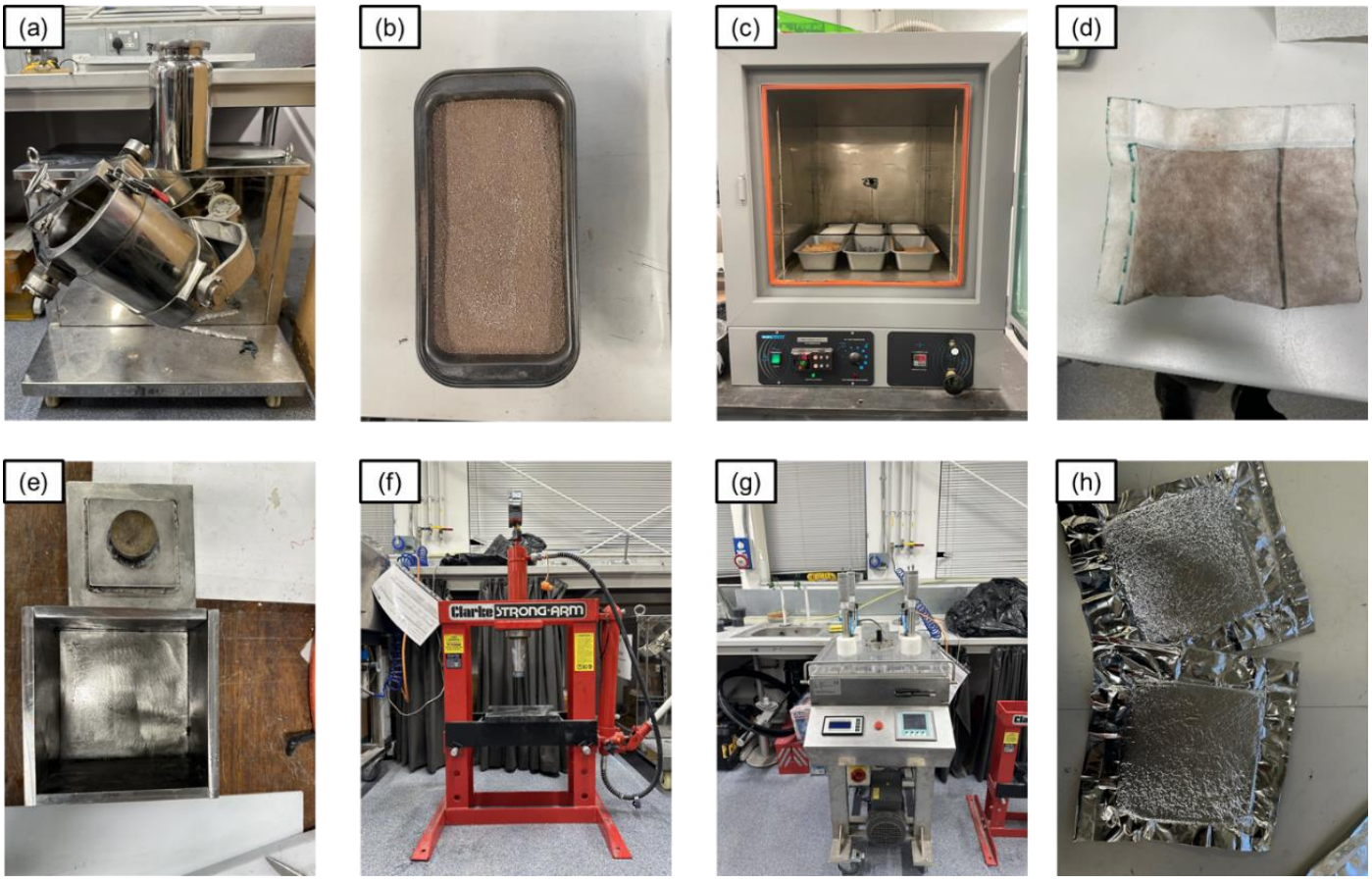

Figure 3.28 The procedure of manufacturing a VIP; (a) 3D mixer, (b) mixed loose core (EP-TNFs2), (c) oven used to dry the core, (d) core inside the fleece, (e) steel die, (f) hydraulic press, (g) vacuum sealer and (h) VIP product

3.4.1 VIP samples

Four categories of VIPs were created, and evaluated with the following objectives:

Thermal conductivity of new processed materials

To see the thermal performance of pure new processed cores (TNFm, TNFs and TNA) and compare it with already studied FS VIPs, see Table *3.7*. This can help in understanding the characteristics of pure material. These samples are used in the life cycle model.

Temperature and pressure effect of composites

To experimentally observe the effect of temperature (up to mean of 70 ℃) and pressure of composites of new processed cores with FS with varying proportion of their composites.

Thermal conductivity effect of composites

To observe the variation of thermal conductivity with varying proportion of their composites. The composites were made from using TNA with FS, TNFm with FS and TNFs with FS. These composites are used in the car painting booth modelling, economical assessment and life cycle assessment.

Ageing and environmental impact

To understand the effect of ageing on core material and climatic conditions at two different climatic conditions, see Table *3.8*. These results are used in the car painting booth model and then in the life cycle assessment in sections 6.5 and 6.6.

Table 3.7 Dimensions and physical details of the VIPs developed

Sample	Thickness (mm)	Density ($kg.m^{-3}$)
TNFm	15.71	492.70
TNFs	14.64	428.2
TNA	9.91	715.21
FS	13.59	222.58
FS-TNA	13.47	222.58
FS-TNA1	13.63	226.58
FS-TNA2	13.48	227.92
FS-TNA3	12.20	230.42
FS-TNA4	7.57	271.13
FS-TNA	13.47	222.58
FS-TNFm1	13.02	227.24
FS-TNFm2	11.70	255.67

FS-TNFm3	10.55	281.18
FS-TNFs1	11.48	257.89
FS-TNFs2	10.22	289.67

Table 3.8: VIP stored at two climate conditions for evaluating the effect of ageing

Storage Condition	Sample	Thickness (mm)	Density (kg.m^{-3})
20℃ and 40% RH	FS	13.47	222.58
	FS-TNFm1	13.02	227.24
	FS-TNFs1	11.48	257.89
	FS-TNA1	13.63	227.92
70℃ and 85% RH	FS	13.47	222.58
	FS-TNFm1	13.02	227.24
	FS-TNFs1	11.48	257.89
	FS-TNA1	13.63	227.92

3.5 Summary

In this chapter, material development, VIP production, characterisation methodologies and experimental techniques utilised to quantify various properties are provided in detail for TNFm, TNFs, TNA and FS and composite samples.

Material preparation

- 28% of the tree-based sheath waste was processed to TNFm, 11% was processed to TNFs while 4.27% of the total waste was pyrolysed to TNA.
- TNA was pyrolysed to three different temperatures 600, 700 and 800 ℃.

Particle size distribution (ImageJ and laser diffraction)

- In the case of TNA, As the pyrolysis temperature increased, a trend towards smaller particle sizes was observed. The smallest particle size for TNA that was pyrolysed at 600℃ was 4.8 µm. This size reduced to 3.76 µm at 700℃ and further decreased to 2.62 µm at 800℃. The behaviour can be ascribed to faster breakdown of organic substances at elevated temperatures, leading to the formation of smaller particles.
- The average particle size for TNA pyrolysed at 600℃ was 9.37 µm, while for the TNA pyrolysed at 800℃, it was 8.01 µm. The results align with those obtained using the

ImageJ approach, which indicated average particle sizes of 9.16 μm for TNA pyrolysed at 600℃ and 6.3 μm for TNA pyrolysed at 800℃. The consistency in the results validates the use of ImageJ for particle size measurement.

- TNFm exhibited significant amount of fibres with an average length of 0.82 mm in contrast to TNFs that had an average length of 0.22 mm. The observed variation may be ascribed to the size of the sieve, indicating that a decrease in sieve size led to a reduction in both particle size and the number of long fibres.

Mercury Intrusion Porosimetry

- The average pore diameter of all FS with tree-based natural fibres composites samples was found to be less than 0.26 μm, which can play a significant role in keeping the gaseous conductivity low even when the VIP pressure was is high.
- TNFs showed a higher pore size (1.95 μm) and porosity (84.93%) than TNFm.
- For TNA as the pyrolysis temperature increased the pore size of the ash decreased with TNA (600 ℃) having an average pore size of 2.43 μm and TNA 800 ℃ having an average pore size of 1.68 μm

Thermogravimetric analysis

- There is no decrease in the weight of the TNF samples after 600 ℃. Hence 600 ℃ and higher temperatures can be selected for pyrolysis process.
- The primary distinction in weight loss occurrence between TNFm and TNFs was due to the particle size distribution. TNFs had larger proportion of dust content compared to TNFm.

Fourier Transform Infrared spectroscopy

- The study revealed that TNFm and TNFs exhibited comparable spectral extinction values across all wavelengths, despite differences in particle size.
- It was noted that both types of TNF and TNA exhibited a higher spectrum extinction coefficient in comparison to FS in the range of 2.5 to 7.5 μm, suggesting a reduced radiative leakage over the examined wavelength range.
- The spectral extinction coefficient of composites can be measured by using weighted average of spectra of its components. where the analytical and measured values were exhibiting a remarkably similar pattern.

Thermal conductivity measurements

Fourteen different VIPs samples were manufactured and the results of thermal conductivity at different temperatures and pressures are presented in section 4.4 and 4.5.

CHAPTER 4: Thermal Conductivity Measurements

Experimental measurements were performed to measure the centre of panel thermal conductivities of three FS-TNFm composites, two FS-TNF composites and five FS-TNA composites, in comparison to pure FS VIP. The measurements were conducted at core pressures from 0.64 to 1000 mbar and mean temperatures between 20 ℃ and 70 ℃. The chapter examined the potential for reusability of core materials, as well as the ageing effects on these materials under two distinct climatic conditions: a temperature of 20℃ and 40% relative humidity, and a temperature of 70℃ and 75% relative humidity.

4.1 Testing of VIPs

The thermal conductivity of all the samples was measured using a heat flow metre (NETZSCH HFM 446 Lambda). The device consists of a stationary lower plate and a movable top plate located in an enclosed chamber. The maximum size of the samples that can be tested inside the chamber is 300 mm x 300 mm x 60 mm. The temperature range within which these two plates can vary is from 0 to 90 ℃. Furthermore, the plates have the capability to exert a pressure ranging from 0.1 kPa to 20 kPa on the sample. The mean testing temperature was determined by calculating the average of the temperature values from the two plates. There was one heat flux sensor placed at the centre, along with many thermocouples in each plate. A separate Chiller is linked to the HFM in order to achieve exact temperature regulation for the cooling plates, guaranteeing accurate, consistent and precise thermal conductivity measurements.

The testing procedure followed the guidelines of ISO 8301 and ASTM C518, which standardise the use of steady-state heat flow meter methods for measuring the thermal resistance of insulation materials. These standards are widely accepted in both industrial and research settings and are particularly suited for thin, planar materials such as VIPs.

The VIPs produced in this study had dimensions of 149.58 ± 3.85 mm × 149.11 ± 2.73 mm × 11.91 ± 1.89 mm. For placing the samples in the centre of the chamber where the heat flux sensors are located, two thin sheets of extended foam of size 300 mm x 300 mm were utilised. These sheets were chosen for their low thermal conductivity. The extended foam was blanked from the centre of a 150 mm x 150 mm hole in which VIP to be tested was inserted. The assembly was directly placed in the chamber. To ensure a firm contact between the plates and the samples, a pressure of 15 kPa was exerted. The samples underwent testing at average temperatures of 20, 40, 50, and 70 ℃, with a consistent temperature difference of 20 ℃ between the two plates.

The HFM method was selected over alternative approaches such as the guarded hot plate or transient plane source method due to its suitability for flat, thin samples with relatively low thermal conductivity. Furthermore, the method allows for controlled plate pressure, which is essential for ensuring proper surface contact and minimising interface resistance, particularly relevant in the case of vacuum insulation panels. Despite its advantages, the HFM method can be influenced by factors such as imperfect plate-sample contact, edge heat losses, and sample inhomogeneity. These limitations were addressed in this study by careful sample placement, pressure control, and the use of low-conductivity foam to minimise lateral heat transfer.

4.1.1 Calibration of HFM

The calibration of the heat flow metre often entails the measurement of the thermal conductivity of a known material. The study utilised a fibre glass board (SRM NIST 1450D), which is a standardised sample commonly used by NETZSCH. A calibration curve is plotted by comparing the observed thermal conductivity of the fibre glass board with the pre-existing value. In order to achieve precise calibration, it is necessary for the heat flux passing through the samples being measured to closely match the heat flux passing through the calibration sample. Given that the heat flux is directly proportional to the thermal conductivity of the sample, it can be deduced that the heat flux through the VIP sample in this scenario should be 4 to 7 times lower than that of the standard fibrous glass. In order to address this problem, the HFM underwent calibration using the calibration approach outlined in section 8.6 of ASTM C1667 – 15. Furthermore, the heat flux is directly proportional to both the temperature differential across the sample and the thickness of the sample. By adjusting either the temperature difference or the thickness of the sample during calibration, it is possible to make the heat flow through the vacuum insulation panel and the calibration sample similar, according to the updated calibration procedure. The study involved adjusting temperature differences. During the calibration process, a temperature difference of 5℃ was set, whereas during the measurement of the VIP, a temperature difference of 20 ℃ was set. This enabled the determination of the heat flow values through both the calibration sample and the measurement sample, which were located in close proximity to one other.

4.1.2 Uncertainty

The Heat Flow Meter (HFM) employed in this study was equipped with embedded thermocouples in each plate and a centrally located heat flux sensor, facilitating precise thermal characterisation of VIP samples. This configuration enabled the determination of the effective thermal conductivity at the core of the VIP using Fourier's law, as shown in equation (4.1). To quantify the measurement

uncertainty associated with the derived thermal conductivity values, the law of propagation of uncertainties was applied, as described in equation (4.2).

$$\lambda = \frac{q\Delta d}{\Delta T} \tag{4.1}$$

$$\left(\frac{\partial\lambda}{\lambda}\right)^2 = \left(\frac{\partial q}{q}\right)^2 + \left(\frac{\partial\Delta d}{\Delta d}\right)^2 + \left(\frac{\partial\Delta T}{\Delta T}\right)^2 \tag{4.2}$$

where λ is thermal conductivity value, q heat flux, d thickness of the VIP and ΔT difference in temperature. The underlying assumptions of the uncertainty analysis include that all variables are statistically independent and uncorrelated, that measurement errors follow a normal (Gaussian) distribution, and that the linearity of Fourier's law allows for the use of first-order Taylor series approximations in uncertainty propagation.

The thickness of the VIP was measured using a high-precision digital micrometre with a resolution of 0.001 mm, corresponding to a relative uncertainty of less than 0.1%. The temperature difference was measured using calibrated thermocouples with a minimum resolution of 0.1 K, resulting in a relative uncertainty below 1% under normal operating conditions. Given these small contributions, the dominant source of uncertainty in the thermal conductivity measurements was the heat flux sensor. According to the manufacturer's specifications for the HFM 446 Lambda, the heat flux measurement accuracy ranges from ±1% to ±3%, depending on surface contact conditions and calibration. Consequently, the overall uncertainty in the calculated thermal conductivity values was primarily governed by the heat flux measurement, with a maximum propagated uncertainty not exceeding ±3% in the worst-case scenario. Each sample was tested three times under consistent boundary conditions (as mentioned in the above two sections), and the reported thermal conductivity values represent the mean of these independent measurements, thereby improving statistical reliability and reducing the influence of random experimental error.

4.2 Gaseous conductivity of pure samples and composites

Heat in gases flows by convection and conduction. The intensity of conduction through gases is contingent upon the Knudsen number, which is determined by the ratio between the mean free path of gas molecules and the pore size. The gaseous conductivity (λ_g) of the several materials described in sections 3.3.8 and 3.3.9, was determined by equation (4.3).

$$\lambda_g = \frac{\lambda_{g0}}{1 + \left(\frac{0.32}{P\phi}\right)} \tag{4.3}$$

where λ_{g0} is the gaseous conductivity of free gas, ϕ the average pore size of the material, and P the gas pressure.

For FS, TNFm, TNFs, TNA and the composites of FS-TNFm1, FS-TNFs1, FS-TNA1, FS-TNA3 average pore size were measured, while the average pore sizes of the remaining samples was predicted without accounting for the migration of FS particles with or into NFs. The results presented in Figure 4.1a indicate that the gaseous conductivity of all samples at pressures below 1 mbar was insignificant. As the core pressure increased to 10 mbar the gaseous conductivity of the TNFs and TNA increased dramatically to 1.9 $mW.m^{-1}.K^{-1}$ and 2.3 $mW.m^{-1}.K^{-1}$, respectively. However, TNFm and FS had gaseous conductivity below 1.11 $mW.m^{-1}.K^{-1}$ even at 10 mbar. FS had the lowest with 0.26 $mW.m^{-1}.K^{-1}$. At 100 mbar, it was seen that FS had a small rise in gaseous conductivity (2.21 $mW.m^{-1}.K^{-1}$) when pressure raised. On the other hand, other samples had an increase in gaseous conductivities ranging from 5.84 $mW.m^{-1}.K^{-1}$ to 11.75 $mW.m^{-1}.K^{-1}$, at the same core pressure. Under atmospheric pressure (1000 mbar), all samples, except TNFm and FS, exhibited high gaseous conductivity values exceeding 25 $mW.m^{-1}.K^{-1}$. TNFm displayed a comparatively lower gaseous conductivity of 22.33 $mW.m^{-1}.K^{-1}$, while FS exhibited the lowest conductivity among all samples, measuring 14.68 $mW.m^{-1}.K^{-1}$. All this can be attributed to the difference in pore size of the different materials where it was expected that lower pore size would lead to a lower gaseous conductivity.

Theoretically, composites of FS with tree based natural fibres should be between the gaseous conductivity of FS and the tree based natural fibres but experimentally the results showed differently as presented Figure 4.1b. All composite samples with measured average pore size exhibited a lower gaseous conductivity compared to FS. This can be attributed to the intrusion of small particles of FS into the pores of the fibres in case of TNFm, TNFs and the creation of smaller cavities due to the aggregation of particles in FS and TNA samples.

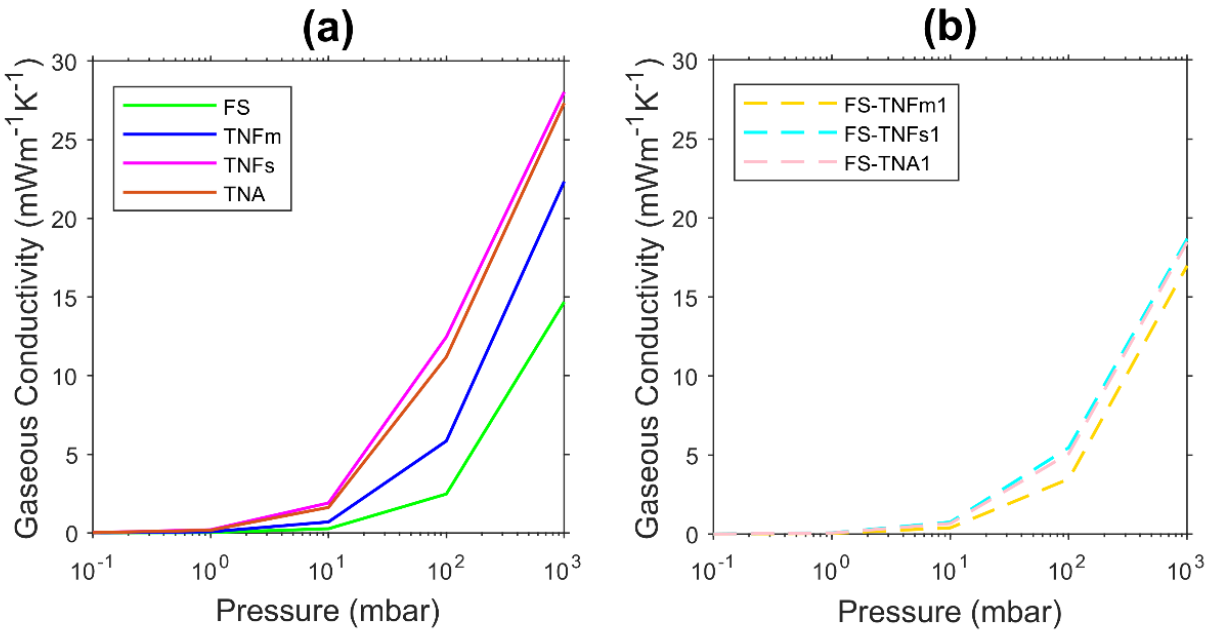

Figure 4.1 Gaseous conductivity derived from pore size measurements for (a) pure samples and (b) composite samples

4.3 Radiative conductivity

Figure *4.2* displays the radiative conductivity (λ_R) values of FS, TNFm, TNFs and TNA. λ_R of an optically thick medium was calculated using equation (4.4).

$$\lambda_R = \frac{16n^2\sigma T^3}{3E_R(T)} \tag{4.4}$$

where n is the refractive index, σ the Stephan Boltzmann constant (5.67 ×10^{-8} W.m^2.K^{-4}), T the mean temperature and E_R the Rosseland mean extinction coefficient.

The optical thickness (α) of a material was determined by multiplying the Rosseland mean mass specific extinction coefficient (e_R^*) with the density and thickness (th) of the VIP, as specified in equation (4.5) (Jalali et al., 2024).

$$\alpha = \rho \times e_R^* \times th \tag{4.5}$$

A material is said to be optically thick when its optical thickness is > 15. The Rosseland mean mass specific extinction coefficient value drops as temperature increases. At the maximum temperature investigated (70 ℃), α was determined using the equation (4.5) and presented in the Table *4.1*

Table 4.1: Values of calculated optical thickness of TNFm, TNFs, TNA and FS at 70 ℃

Sample	α at 70 ℃
TNFm	436.09
TNFs	430.78
TNA	441.63
FS	269.41

The Rosseland mean extinction coefficient was determined using equation (4.6) (Fricke et al., 2006).

$$E_R(T) = e_R^* \times \rho \quad (4.6)$$

The significant difference observed in Figure *4.2* between FS with TNFm, TNFs and TNA could be due to three primary parameters: the Rosseland mean mass specific extinction coefficient, the refractive index, and the density.

The findings presented in section 3.3.11 indicated that a FS composite containing a larger content of TNFm or TNFs exhibited a lower radiative conductivity. This was attributed to the increase in the spectral extinction coefficient and the increase in density of the VIP core. These changes ultimately led to an increase in the Rosseland mean extinction coefficient. Moreover, it was noted that TNFm exhibited a higher spectral extinction compared to TNFs and TNA, as illustrated in section 3.3.12. However, when considering radiative conductivity, it was observed that the samples TNA and TNFs had lower values compared to TNFm. The behaviour can be attributed to the difference in core density of the VIPs, samples containing TNFs exhibited a higher density compared to those containing TNFm. This may also indicate that the density of the core material had a greater impact on the radiative conductivity than both refractive index and spectral extinction coefficient.

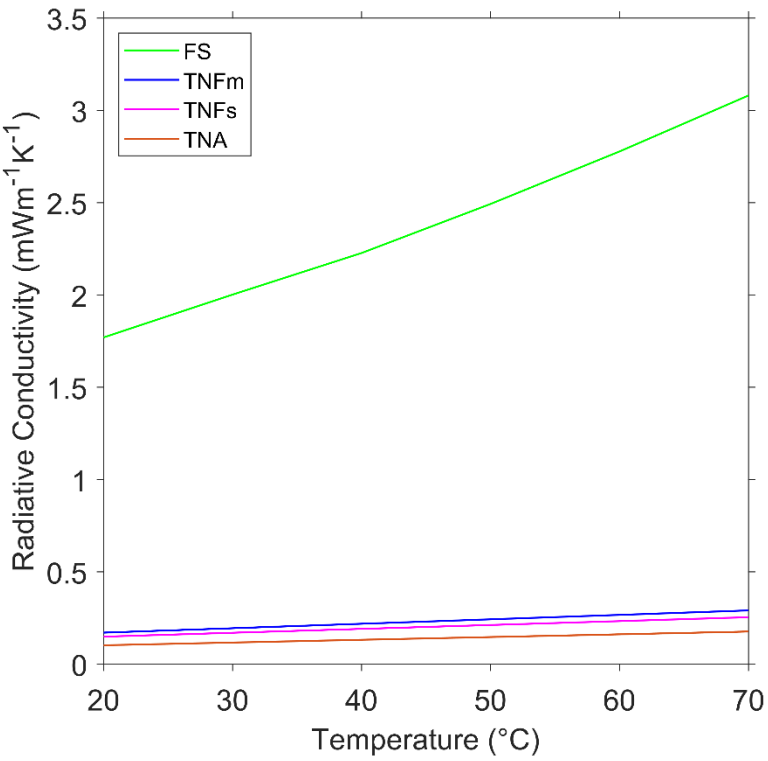

Figure 4.2 Radiative conductivity of pure materials at temperature ranging from 20 to 70 ℃

4.4 VIPs thermal conductivity measurements

4.4.1 Effect of temperature

Experimental measurements were conducted to determine the centre of panel thermal conductivities of FS, TNFm, and TNFs composite cores. The measurements were taken at core pressures ranging from 0.64 to 2.15 mbar, and mean temperatures ranging from 20 to 70 ℃. The main motivation of this study was to investigate the variation in thermal conductivity resulting from the addition of TNFm, TNFs and TNA in FS.

FS sample exhibited a thermal conductivity of 7.84 $mW.m^{-1}.K^{-1}$ at an average temperature of 20 ℃, see Figure *4.3* This value significantly increased as the temperature was increased, 11.58 $mW.m^{-1}.K^{-1}$ at 70 ℃. The observed rise of 47.7% in thermal conductivity for FS sample can be attributed to increase in radiative conductivity. It is worth noting that while fumed silica shows excellent performance in terms of low solid and gaseous conductivity due to its small pore size, particle size, high porosity, and low density, but it suffers from a lower thermal resistance against radiative heat transfer (Modest and Mazumder, 2021).

Increasing the mass ratio of TNFm to 50% (by mass), the thermal conductivity experienced a rise from 7.84 $mW.m^{-1}.K^{-1}$ to 8.27 $mW.m^{-1}.K^{-1}$ at a mean temperature of 20 ℃, as represented in Figure

4.3. The inclusion of fibres resulted in a 5% increase in the overall conductivity of the sample compared to the reference material (FS). The increase can be attributed to the net effect of a rise of in solid conductivity and a decrease of in radiative conductivity. It is worth noting that the density of FS-TNFm3 was much greater at 281.18 $kg.m^{-3}$ compared to pure fumed silica VIP which had a density of 222.50 $kg.m^{-3}$, see section 3.4.3. The observed distinction can be related to differences in physical characteristics where fumed silica is recognised for its fused spherical structure organised in branching chains, characterised by a very small particle size and high porosity. In contrast, TNFm exhibited bigger fibre-sized particles with differing lengths that were distinctly separated from one another and lower porosity as indicated in section 3.3.12. FS-TNFm3 was observed to have a lower rate of increase in thermal conductivity with rising temperature compared to FS. The curves for FS and FS-TNFm3 intersected at a temperature of 35 ℃ where they had the same thermal conductivity, see Figure *4.3*. As the temperature continued to rise, the thermal conductivity of FS-TNFm3 increased to a final value of 10.39 $mW.m^{-1}.K^{-1}$ lower than that of pure fumed silica. This phenomenon demonstrated a notable influence of temperature on radiative conductivity, and thus overall conductivity. Initially FS sample, which had a lower overall conductivity at 20 ℃ when solid conductivity had a greater impact, ended with a higher value at 70 ℃ as compared to composites due to a dramatic rise in radiative conductivity with temperature.

As previously said, the contribution of solid and gaseous conductivity outweighs radiative conductivity at ambient temperature. Due to a low core pressure (vacuum) in all samples, the influence of gaseous conductivity was minimal. The quantity of organic fibres was decreased in a gradual manner in order to obtain a VIP with highest thermal insulation properties. It was observed that the thermal conductivity value decreased considerably when 40 wt.% of TNFm (sample FS-TNFm2) was present to 7.19 $mWm^{-1}K^{-1}$, lower than that of samples FS and FS-TNFm3. Furthermore, this lower value persisted even at elevated temperature, leading to a 35.75% reduction in the overall thermal conductivity compared to that of FS at 70 ℃. In the same line of reasoning, it was observed that reducing the amount of TNFm in the composite sample to 30 wt.% (sample FS-TNFm1) resulted in a drop-in conductivity at both 20 ℃ and 70 ℃. Particularly the lowest conductivity values among the tree-based fibres samples tested in this study were recorded for FS-TNFm1 as 6.75 $mW.m^{-1}.K^{-1}$ and 8.28 $mW.m^{-1}.K^{-1}$ at 20 ℃ and 70 ℃, respectively. The results can be attributed to the significant influence of solid conductivity, which surpasses the radiative conductivity in the composite samples.

In the case of composites containing 30 wt.% TNFs (sample FS-TNFs1), it was seen that the density exhibited a significant increase, reaching a highest value of 257.9 $kg.m^{-3}$. The density of FS-TNFs1 surpassed that of the 40 wt.% TNFm, and continued to rise to 289.67 $kg.m^{-3}$ when 40 wt.% of TNFs (sample FS-TNFs2) was added. Despite the higher density of pure TNFm compared to TNFs, the observed discrepancy in the results can be attributed to the smaller size and lower quantity of fibres in TNFs, which therefore led to the presence of more separated dust particles.

This consequently created additional gaps within the core filling. The observed outcome led to a slight increase in the overall conductivity as compared to TNFm composites at an average temperature of 20 ℃, with FS-TNFs1 and FS-TNFs2 exhibiting values of 7.2 $mW.m^{-1}.K^{-1}$ and 7.65 $mW.m^{-1}.K^{-1}$, respectively, see Figure *4.3*.

In the context of TNA, composite samples (FS-TNA1, FS-TNA2, and FS-TNA3) exhibited reduced thermal conductivity compared to FS, attributable to the same reasons previously discussed for FS-TNFm and FS-TNFs samples.

The only difference in this case of FS-TNA3 was that when the mass ratio of TNA increased by 50% (by mass), its thermal conductivity measured 7.18 $mWm^{-1}K^{-1}$ and 8.32 $mWm^{-1}K^{-1}$ at 20 ℃ and 70 ℃, respectively which was still lower than that of FS across all mean temperatures.

An additional sample, labelled FS-TNA4, was prepared by increasing the mass ratio of TNA by 60%. FS-TNA4 sample exhibited a lower thermal conductivity than both FS and FS-TNFm3, with values ranging from 7.44 $mWm^{-1}K^{-1}$ to 8.96 $mWm^{-1}K^{-1}$ within the same temperature range. Notably, it had the highest density among all tested samples, measuring 381.92 $kg.m^{-3}$. The reason for this can be ascribed to the lower solid conductivity of TNA compared to TNFm and its lower radiative conductivity in comparison to FS.

To determine when radiative conductivity effect surpasses that of solid conductivity, one more sample was developed with 20 wt.% TNA (sample FS-TNA). FS-TNA exhibited lower thermal conductivity than FS, but higher thermal conductivity than FS-TNA1 at both 20 ℃ and 70 ℃, as illustrated in Figure *4.4*. The optimal composite of FS and TNA was identified when the mass ratio of TNA increased by 30%, yielding a thermal conductivity of 6.23 $mWm^{-1}K^{-1}$ at 20 ℃ and 7.41 $mWm^{-1}K^{-1}$ at 70 ℃, which was the lowest value among the eleven samples examined.

Samples of pure TNFm, TNFs, and TNA were removed from comparison because they failed to achieve the required density, exhibiting values between 428.2 $kg.m^{-3}$and 715.2 $kg.m^{-3}$. Their thermal conductivity values started from 19 $mWm^{-1}K^{-1}$at 20℃, making them incomparable to the FS or composites samples.

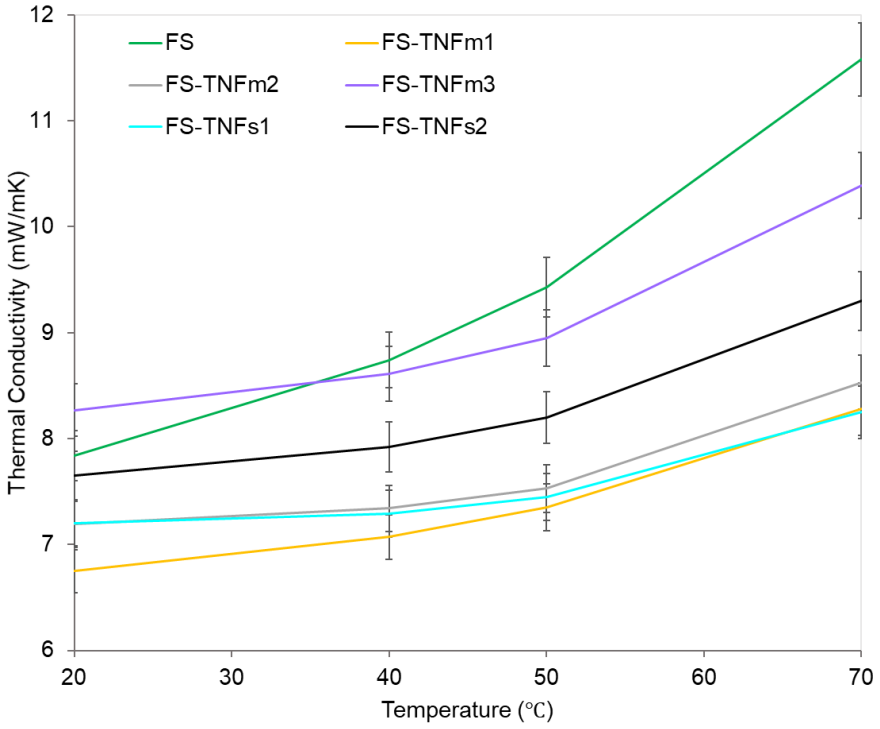

Figure 4.3 Thermal conductivity of FS, FS-TNFm composites and FS-TNFs composites at four mean temperatures (20,40,50 and 70 ℃)

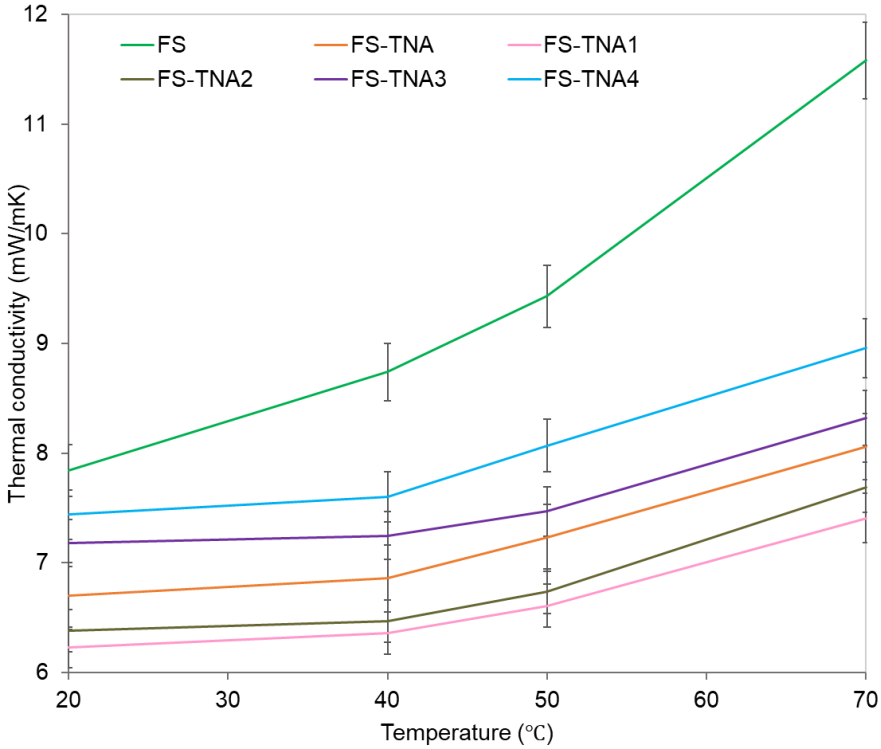

Figure 4.4 Thermal conductivity of FS and FS-TNA composites at four mean temperatures (20,40,50 and 70 ℃)

4.4.2 Effect of compaction

All FS, FS-TNFm1, FS-TNFs1, and FS-TNA1 samples were unsealed after a period of 6 months following production. The samples were stored at room temperature of 20 ℃ and relative humidity of 40%. According to Figure *4.5*, The thermal conductivity of all samples after remaking showed a slight increase which did not exceed 3% of the initial value (before breaking the VIPs). The effect of fibre compaction with fumed silica did not result in a noticeable increase. Therefore, the impact of reused fibres was minor when mixed with materials that do not alter their structure when compacted, such as fumed silica.

This work demonstrates that cores can be reused even when the VIPs have been long stored. Furthermore, compaction of the core material, caused during core shaping and vacuuming process, does not have any time-dependent impact on the sample as long if it is stored under controlled conditions. Meaning that the reprocessing methodology proposed in this work can reverse any changes in the core properties caused by damaged VIP barrier envelope, thus providing environmental and economic benefits.

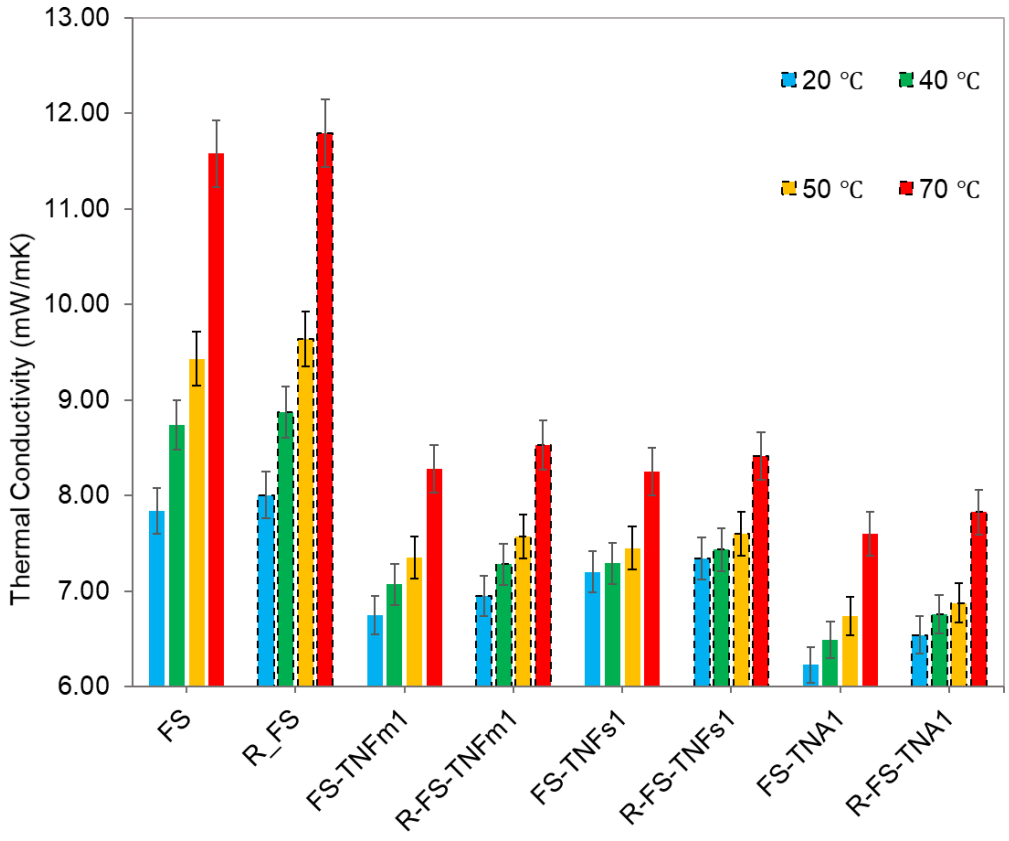

Figure 4.5 Comparison of thermal conductivity of initial core manufactured VIPs with reused core VIPs

4.5 VIP lifespan

4.5.1 VIPs thermal conductivity at different pressure

The thermal conductivity of the all composites excluding FS-TNA and FS-TNA4 was measured at different pressures and at temperature of 70 degrees. The aim was to vacuum the VIPs, starting at lowest pressure which was 0.1 mbar, at 10 mbar, at 100 mbar and to measure the thermal conductivity at atmospheric pressure.

As shown in Figure *4.6*, all tree-based composites exhibited lower thermal conductivity at low pressures (varying between 0.64 mbar and 2.88 mbar), which was due to the reasons explained in section 4.4.1. At the target 10 mbar, the thermal conductivity of all composite samples increased by a maximum of 2.24 $mW.m^{-1}.K^{-1}$ for FS-TNFs1 and a minimum of 0.49 $mW.m^{-1}.K^{-1}$ for FS-TNA3. The results at this pressure were challenging to compare since the sample pressures were not precisely 10 mbar; FS-TNFs1 exhibited a pressure of 14.2 mbar, while FS-TNA3 displayed 8.2 mbar, due to the limited control of the vacuum sealer used in this study.

For FS, the pressure was 10 mbar, and the rise was a minimum of 0.29 $mW.m^{-1}.K^{-1}$, which falls within the error margin of 3%. The result aligned with the predictions in section 4.2, where a minimal rise in thermal conductivity for FS and composites was predicted. It is noteworthy that, despite certain tree-based composites exhibiting pressures nearly 6 mbar greater than that of FS, all tree-based composite samples demonstrated lower thermal conductivity than the FS sample. The findings indicates that radiative conductivity exerted a more significant influence on overall thermal conductivity than gaseous conductivity at this pressure range (>20 mbar).

Similarly, at the target pressure of 100 mbar, comparison was also challenging as the pressure of the samples varied between 80.8 mbar to 195.8 mbar. All TNA composites exhibited lower thermal conductivity than FS at pressures ranging from 89 to 93.9 mbar. Furthermore, FS-TNFm1 and FS-TNFs1 demonstrated lower thermal conductivity at elevated pressures of 132.3 mbar and 155.1 mbar, respectively.

This phenomenon demonstrated that the radiative conductivity at elevated temperatures surpasses the influence of gaseous conductivity, and that small particles of FS intruded the pores of the fibres in the cases of TNFm and TNFs.

At atmospheric pressure it was easier to compare the samples where it was noticed that only FS-TNA1 and FS-TNA2 had lower thermal conductivity than that of FS with value of 23.4 $mW.m^{-1}.K^{-1}$, 23.9 $mW.m^{-1}.K^{-1}$ and 25 $mW.m^{-1}.K^{-1}$ respectively. Whereas FS-TNFm1 and FS-TNFs1 had higher thermal conductivity of 26.2 $mW.m^{-1}.K^{-1}$ and 25.5 $mW.m^{-1}.K^{-1}$. The findings

indicated that gaseous conductivity at atmospheric pressure surpassed the effect of radiative conductivity. In addition, the higher solid conductivity of TNF relative to FS resulted in FS-TNFm3 exhibiting a thermal conductivity 2.6 $mW.m^{-1}.K^{-1}$ greater than that of FS-TNFm1. The effect of solid conductivity on TNA was minimal, with a measured increase of 1.6 $mW.m^{-1}.K^{-1}$.

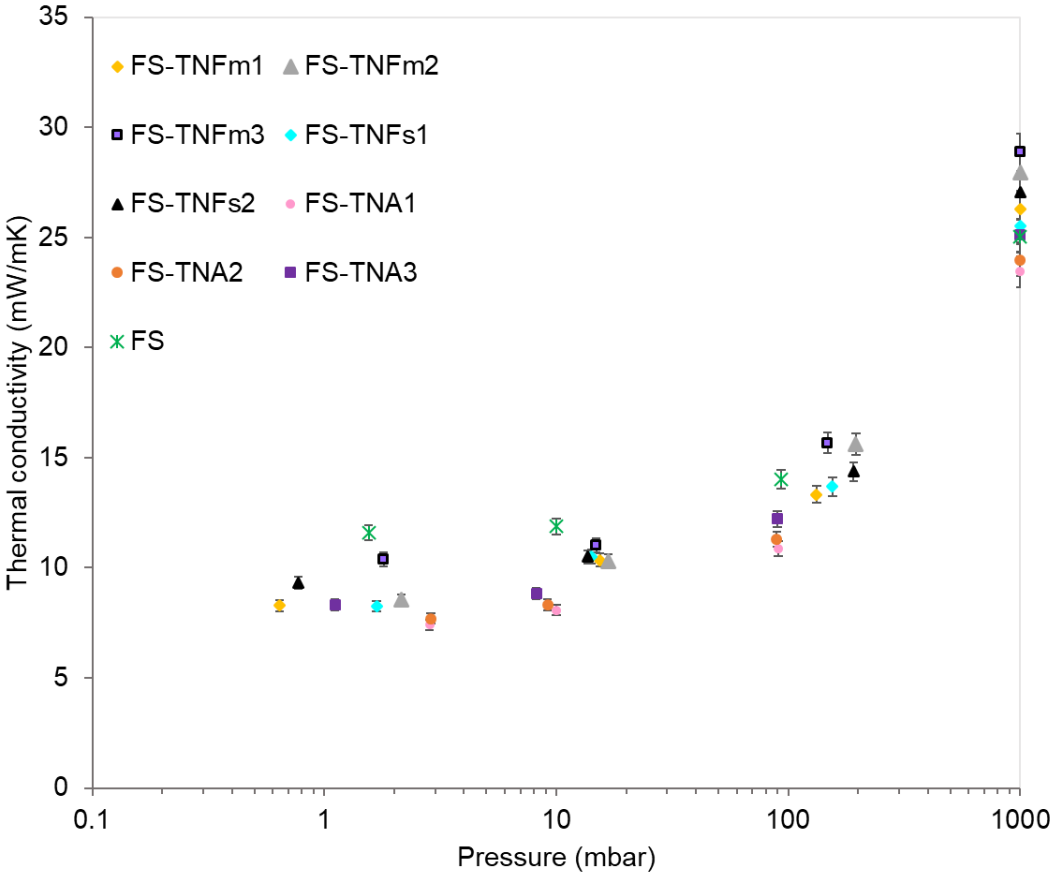

Figure 4.6 Measured thermal conductivity of nine manufactured VIPs at different pressures at mean temperature of 70 ℃

4.5.2 Effect of ageing

The thermal conductivity of VIP increases over time due the progressive increase in internal air pressure and moisture. The primary factors contributing to this increase are the envelope material and the core material utilised. For example, materials such as FS are hydrophobic that resist moisture absorption, whereas materials like TNF are hydrophilic due to their natural properties, allowing them to absorb moisture, particularly when exposed to variations in temperature and humidity.

The ageing performance was a crucial aspect of this study, aimed at identifying which component or core material contributes to a greater increase under varying environmental conditions. Additionally, the results were utilised to forecast the impact of variations in VIP performance on

the operation of a car painting booth over 10 years. The thermal conductivity of eight VIPs, containing 70% FS and different compositions of 30% TNFm, 30% TNFs, and 30% TNA, was assessed under various climatic conditions. All VIPs utilised identical envelope materials, which were sealed under pressure ranging from 0.64 to 2.84 mbar to minimise the impact of variations in thermal conductivity only on the differences in core materials and climatic changes.

The VIPs were measured post-manufacturing, after 7 days, 30 days, and then monthly for an entire year. Equation (4.7) was employed to forecast the increase of thermal conductivity over a decade:

$$r = \frac{\lambda(t)-\lambda 0}{t} \quad (4.7)$$

where r is the rate of increase of thermal conductivity, $\lambda(t)$ the thermal conductivity when measured at different days, $\lambda 0$ the thermal conductivity measured after manufacturing and t the time.

The rate of increase was employed to estimate the time needed for the VIP's thermal conductivity to rise by 5 $mW.m^{-1}.K^{-1}$, a standard that would significantly affect the performance of the car painting booth model, or by 17 $mW.m^{-1}.K^{-1}$ in the case of envelope failure, indicating the maximum difference between measured VIPs sealed at low pressure and atmospheric pressure.

4.5.2.A Room temperature

The first batch of VIPs was stored under controlled room conditions with an average temperature of 20 ℃ and an average relative humidity of 40%. Figure *4.7* illustrates the variation in thermal conductivity of these four VIPs at a mean temperature of 70 ℃. No envelope failure was observed for all measured VIPs, as the thermal conductivity did not rise by 17 $mW.m^{-1}.K^{-1}$ for either of the measured VIPs, which would signify an envelope breach. The findings indicated that the variation in thermal conductivity was only due to changes in the core materials rather than the stability of the envelope.

As predicted, samples containing TNF materials exhibited a significant increase in overall conductivity over time. The reason behind it was ascribed to outgassing where materials like TNF, consisting of cellulose, hemicellulose, and lignin tend to retain residual moisture due to their hydrophilic properties. Despite the proper drying of the TNF composite cores prior VIP manufacturing, some moisture likely persisted in the larger pores of these fibres, especially during the handling phases between drying and vacuum sealing. The trapped moisture can gradually evaporate under elevated temperature conditions, resulting in outgassing and an increase in thermal conductivity.

On the other hand, the pyrolysis of TNA at high temperature (600 ℃), resulted in the decomposition of components like cellulose and hemicellulose into substances such as CaO, Na_2O, and P_2O_5. These chemical compounds are recognised for their hygroscopic properties, enabling them to attract and retain moisture even under low environmental conditions. The presence of these compounds (approximately 18%) is linked to the gradual increase of thermal conductivity over time. However, the overall conductivity increase rate for TNA samples was inferior to that of TNF samples, indicating that VIPs with TNA may possess a longer lifespan under comparable storage conditions.

Table 4.2: Time required for the tested VIPs to increase by 5 $mW.m^{-1}.K^{-1}$ and 17 $mW.m^{-1}.K^{-1}$ at low storage conditions

Sample ID	Time (years) to increase by	
	5 $mW.m^{-1}.K^{-1}$	17 $mW.m^{-1}.K^{-1}$
FS	17.2	58.6
FS-TNFm1	3.5	12.1
FS-TNFs1	4.2	14.2
FS-TNA1	10.4	35.4

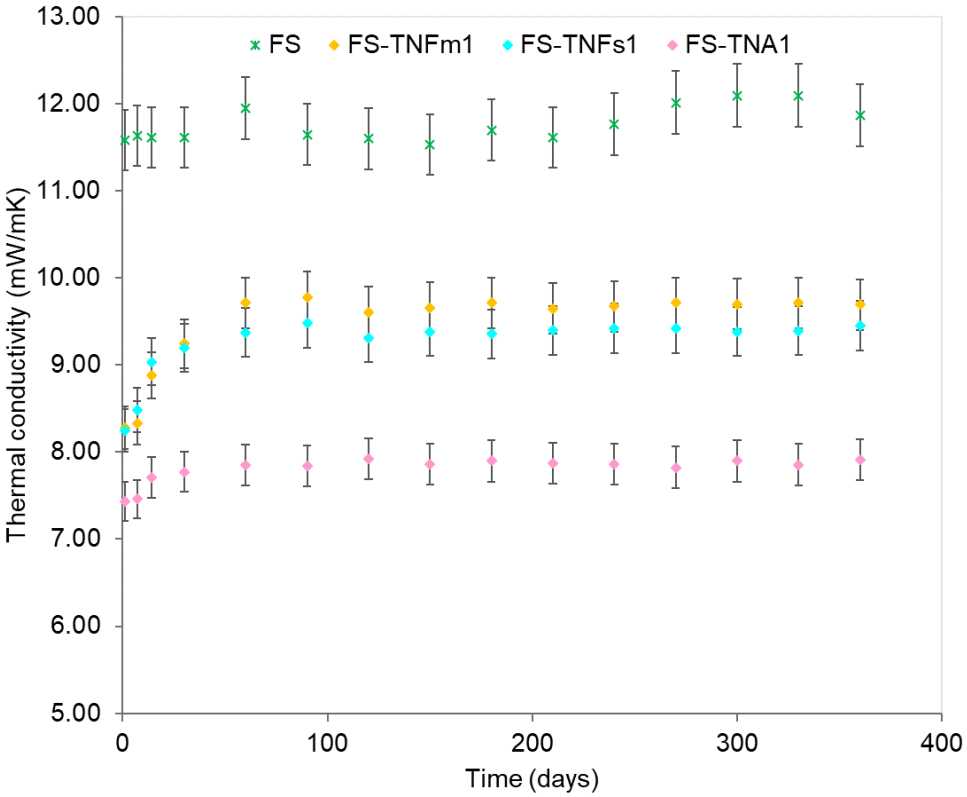

Figure 4.7 Ageing thermal conductivity of three composites VIPs and FS VIP under storing conditions of 20 ℃ and 40 % RH

4.5.2.B High humidity, temperature conditions

The second batch of VIPs was stored under more severe climatic conditions, with a temperature of 70 ℃ and relative humidity of 75%. Figure *4.8* illustrates the variation in thermal conductivity of these four VIPs at a mean temperature of 70 ℃. The study showed that all tested VIPs lost their vacuum after 330 days, a phenomenon attributed to harsh climatic conditions, which did not occur in the previous test performed under lower storage conditions.

The disparity in thermal conductivity enhancement was significant between lower and higher storage conditions for all samples, except for that of FS. For example, FS-TNFm1 sample exhibited an increase of nearly 12% of overall thermal conductivity under lower climatic conditions after 30 days, while a 27% increase was observed under higher climatic conditions. The accelerated rate of increase is due to the rise of outgassing effects at higher temperatures. The accelerated rate highlights the significance of core material stability in more harsher climate conditions.

The envelope utilised in this study was considered unsuitable for prolonged use in applications like a car painting booth, particularly under conditions of elevated temperature and humidity. It was unjust to evaluate the ageing of various core materials based on envelope failure, particularly since materials such as FS exhibit a significantly lower variance due to their higher thermal conductivity post manufacturing. The study aimed to focus on the impact of core material ageing by calculating the rate of increase just before the envelope got damaged (330 days). The results were more realistic with this approach, since different envelopes with greater moisture resistance may be utilised in real-life scenarios.

Table *4.3* displayed the years for the four measured samples to increase by 5 $mW.m^{-1}.K^{-1}$ and 17 $mW.m^{-1}.K^{-1}$. It was observed that 5.7 years of operation are needed for the FS VIP to reach an increase of $mW.m^{-1}.K^{-1}$ in the car painting booth, while the FS-TNA1 samples require 4.6 years for the same increase. Furthermore, the loss of vacuum for these two samples necessitates 19.4 years for FS and 15.5 years for FS-TNA1, both exceeding the operational lifespan of the car painting booth. For the TNF composites, it was observed that during the initial two years, these samples would experience an increase of 5 $mW.m^{-1}.K^{-1}$. In addition, after approximately six years, the FS-TNFm1 VIP would lose its vacuum, while the FS-TNFs1 would lose its vacuum after 6.6 years. Therefore, the car painting booth model would operate for four years with VIPs losing their vacuum in the case of FS-TNFm1, and for three years in the case of FS-TNFs1.

Table 4.3: Time required for the tested VIPs to increase by 5 $mW.m^{-1}.K^{-1}$ and 17 $mW.m^{-1}.K^{-1}$ at 70 ℃ and 75 % RH

Sample ID	Time (years) to increase by	
	5 $mW.m^{-1}.K^{-1}$	17 $mW.m^{-1}.K^{-1}$
FS	5.7	19.4
FS-TNFm1	1.7	5.9
FS-TNFs1	1.9	6.6
FS-TNA1	4.6	15.5

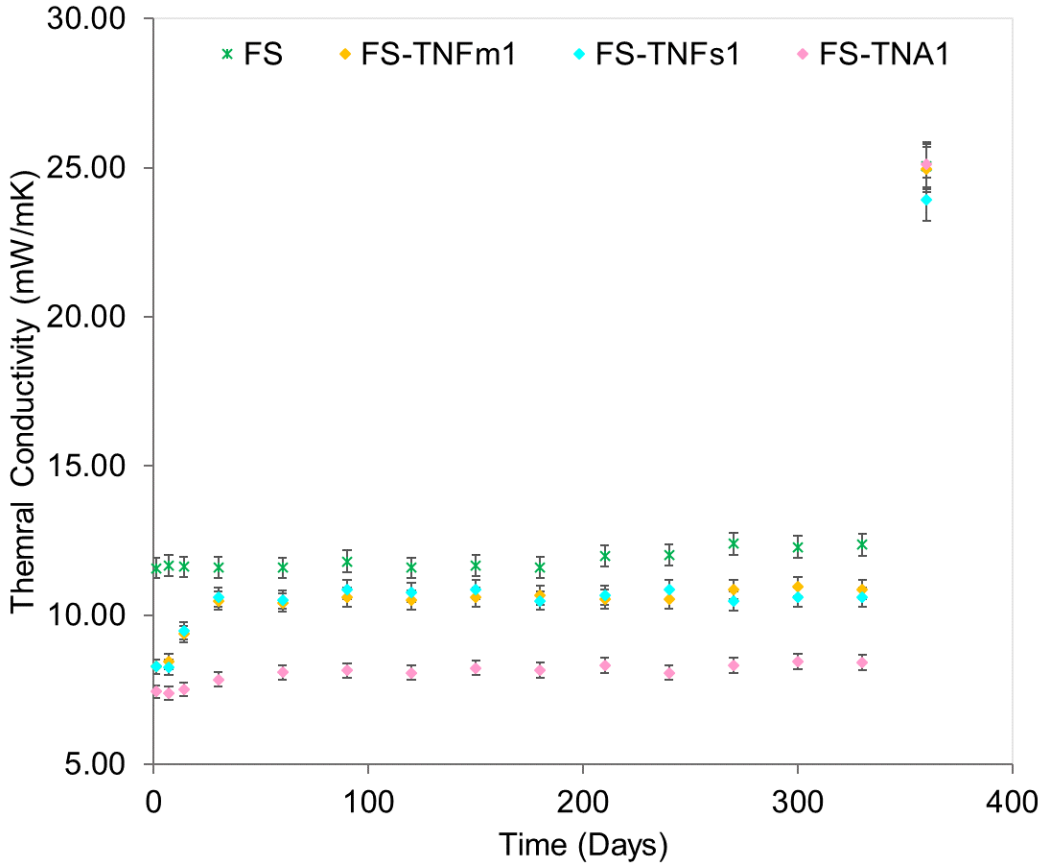

Figure 4.8 Ageing thermal conductivity of three composites VIPs and FS VIP under storing conditions of 70 ℃ and 75 % RH

4.6 Summary

Experimental measurements were performed to measure the centre of panel thermal conductivities of three FS-TNFm composites, two FS-TNF composites and five FS-TNA composites, in comparison to pure FS VIP. The main results are outlined as follows:

- The experimental analysis revealed that the inclusion of TNFm, TNFs, and TNA in FS decreased the thermal conductivity of the VIP.
- FS-TNFm1(30 wt.% TNFm) showed the lower thermal conductivity of 6.75 and 8.28 $mW.m^{-1}.K^{-1}$at 20 and 70 ℃ among all FS-TNFm composites.
- FS-TNFs1 (30 wt.% TNFs) showed the lowest values of 7.2 and 8.25 $mWm^{-1}K^{-1}$ at 20 and 70 ℃ among all FS-TNFs composites.
- FS-TNA1 (30 wt.% TNA) showed the lowest thermal conductivity among all composites studied with a value of 6.23 and 7.41 $mW.m^{-1}.K^{-1}$at 20 and 70 ℃.
- At atmospheric pressure it was noticed that only FS-TNA1 and FS-TNA2 (60 wt.% FS and 40 wt.% TNA) had lower thermal conductivity than that of FS with value of 23.4 $mW.m^{-1}.K^{-1}$, 23.9 $mW.m^{-1}.K^{-1}$ and 25 $mW.m^{-1}.K^{-1}$,respectively. Whereas samples such as FS-TNFm1 and FS-TNFs1 had higher thermal conductivity of 26.2 $mW.m^{-1}.K^{-1}$ and 25.5 $mW.m^{-1}.K^{-1}$. The findings indicated that the effect of gaseous conductivity at atmospheric pressure surpassed the effect of radiative conductivity.
- The best three composite samples of each material (FS-TNFm1, FS-TNFs1, and FS-TNA1) along with FS were unsealed after a period of 6 months following production where they been kept at room temperature of 20 ℃ and a RH of 40%. The thermal conductivity of all samples after remaking showed a slight increase which did not exceed 3% of the initial value (before breaking the VIPs), suggesting the possibility of reusing the cores.

CHAPTER 5: Life Cycle Assessment

VIPs are known for enhancing energy efficiency of appliances and processes in different sectors including buildings, transport, industry and commercial, and reducing CO_2 emissions. However, a key concern is whether if the environmental impacts associated with VIPs over their full life cycle outweigh the environmental benefits they provide in use. If so, is there any room for improvement in the different stages of the VIP life cycle to assist end users in selecting different materials or processes for producing a greener VIP?

The primary goal of Life Cycle Assessment (LCA) is described in two sections in this chapter. The study begins by examining the cradle to gate environmental impacts of extracting and processing fumed silica and tree-based natural fibres. The second phase covered the cradle to cradle life of car painting booth VIPs, including raw material extraction, production, use, and disposal.

This study provided explanations of the functional units used, as well as the system boundaries and limitations of the work. In addition, a comprehensive data collection on material extraction, processing and its associated energy consumption for different core materials (TNFm, TNFs, and TNA) was performed.

Subsequently, a comprehensive analysis was conducted on two methodologies, namely Cumulative Energy Demand (CED) and EN15804 + A2 (European standard), along with their corresponding impact categories. The analysis focused on the substances that are the primary contributors to these impacts, as well as the relationship between electricity usage in the UK and these impacts. To ensure accuracy, the results were adjusted to reflect the most recent data from the International Energy Agency (IEA) in their latest file from 2022.

The following includes the novel aspects of the LCA performed in this study:

(i) Analysis of the life cycle impacts, including climate change, acidification, land use, and both non-renewable and renewable energy, associated with various core materials used in VIPs.

(ii) Detailed comprehension of the influence of resources such as oil and natural gas on the overall outcomes, as well as the potential effects of changes in CED on climate change, which is an impact category outlined in the EN 15804 + A2 standard.

(iii) Critical investigations to demystify the "black box" approach commonly seen in LCA studies, in which the use of tools like SimaPro without fully understanding how the database could impact the outcomes. It has been shown that tools like SimaPro are not accountable for the final outcomes; they merely serve as a means to provide

approximate estimations of how a product or service could impact the environment. It is concluded that these tools should be used judiciously and exclusively by experts who have deep knowledge of the methodologies and data at hand.

5.1 Goal and scope definition

The LCA study was divided into two main sections. The initial section examines and compares the environmental impacts of extracting and processing different core materials, such as fumed silica and tree-based natural fibres (cradle to gate). The second stage expands the evaluation to include the whole life cycle of VIPs that are specifically designed for use in the car painting booth (cradle to cradle). Key stages such as the extraction of raw materials, their preparation, production, usage, and disposal at the end of their life were examined. A mixed-method approach is employed to specifically target the scientific community. It aims to showcase several ways and methodologies for assessing environmental impact, utilising SimaPro. It explains how different inputs can impact the interpreted outcomes to prevent the misleading conclusions. Furthermore, this LCA aims to inform industrial stakeholders about the primary factors that contribute in the increase of environmental impacts during the extraction of raw materials and the manufacturing of VIPs. The study also emphasised the environmental consequences of substituting the fumed silica core with natural fibres derived from trees, as well as the potential advantages of reusing the core material. The following details the scope of the work:

5.1.1 Functional unit

Two functional units were used to accommodate the extensive scope of VIP output. It includes not only the process of combining the VIP components, but also important processes that involved obtaining the raw materials and transporting them to the manufacturing facilities. The first functional unit was determined by considering the load capacity of the truck used for transporting raw materials from the extraction site to the manufacturing site, which was 6.2 tonnes. The second functional unit was defined as the production of 1 m^2 of VIP with 25 mm thickness, based on the standard size of VIPs available commercially.

5.1.2 System boundaries

The life cycle stages of construction materials such as insulations have previously been defined in the European standards (Pargana et al., 2014). According to these regulations, the system boundaries are typically categorised as:

I. Cradle to gate: This stage focuses on the product phase (A1-A3)
II. Cradle to grave: This approach encompasses the entire lifecycle of a product, starting from its production and transportation to the site, followed by its usage, maintenance, and ultimately, its final disposal (A1-C4).
III. Cradle to cradle: This stage expands on the concept of the cradle to grave approach by considering the potential for materials to be recycled, recovered, or reused.

In order to achieve more precise and realistic outcomes, it is crucial to comprehend the genuine environmental consequences of processing the core material, which serves as the primary component of VIPs. To meet the goals of the LCA and ensure transparency and traceability, several steps were divided into many parts, as outlined in Table *5.1*.

Table 5.1: LCA boundaries and life cycle stages of VIP

LCA boundaries	Life cycle stages	Life cycle stage and description
Cradle to gate	Product stage (A1-A3)	A1.1 Raw material extraction A1.2 Packing of raw material A2 Transport to manufacture A3.1 Raw material processing A3.2 Packing and transport of processed core materials A3.3 Manufacturing of VIPs A4. Packing and transport the manufactured VIPs to the CPB
Cradle to cradle Cradle to grave	Usage stage- data related to the operation of CPB (B1-B7)	B1 Installation of VIPs in the CPB B6 Operational energy use of the CPB
	End of life stage (C1-C4)	C2.1 Transport to disposal site C2.2 Transport back to VIP manufacture C4 Disposal
	Benefits beyond the system boundary (D)	Potential reuse of the core material

The initial phase of this life cycle assessment involved analysing the environmental effects of different core materials. It is common knowledge that the final core materials, which are readily available for purchase, require processing before they can be used. Some of these materials can be obtained from waste, such as tree-based natural fibres, and undergo various phases of processing to become usable as core materials. Additionally, there are different material that are not obtained from waste but still require processing in order to be utilised as the central material for VIPs. The boundaries were partitioned:

- A1.1: Raw material extraction

  In this stage for TNF the main focus was on the quantity of tree waste material utilised. For fumed silica the amount of silicon tetrachloride ($SiCl_4$) required was considered.

- A1.2: Packing of raw material

  The weight of the carton boxes was determined by considering the density of the raw tree-based natural fibres and the assumed size of the carton box. The calculation used the mass-density-volume relationship, where the density of the raw tree-based natural fibres was 1200 $kg.m^{-3}$. Regarding silicon tetrachloride, the situation was different because it is a volatile liquid. Therefore, it was chosen that typical Intermediate Bulk Containers (IBCs)(Kurasov, 2009) with a capacity of 1000 litres and dimensions of 1.2 x 1 x 1.2 m^3 would be employed. The density of $SiCL_4$ was estimated to be 1480 $kg.m^{-3}$ (Jóvári et al., 2001).

- A2: Transport to manufacturing facility

  The packed raw materials were transported to the manufacturing facility, where they underwent processing to core materials for VIPs. The quantity of these materials was determined by considering the size of the truck, which served as the initial functional unit. It included considering the capacity size of the truck, the size of the folding boxes for TNF and the size of the IBCs for silicon tetrachloride.

- A3.1: Raw material processing

  The raw material processing of TNF into TNFm, TNFs, and TNA, as well as the transformation of $SiCL_4$ into FS was considered.

- A3.2: Packing and transport of processed core materials

  TNFm, TNFs, and TNA were packaged in carton, while FS and TNA were kept in bulk bags. After being packed, these materials were delivered to VIP manufacturing facility, marking the completion of the initial LCA phase. A1.1 to A3.2 encompassed the entire

process from extracting raw materials to reaching the VIP manufacturing gate (cradle to gate of the first LCA).

- A3.3: Manufacturing of VIPs

  In this step, the environmental impact of producing a single VIP with a size of 1 m² (second functional unit) was analysed. The assessment included the environmental impacts of the core materials, which were evaluated in the first phase of the LCA, as well as other components and manufacturing methods specified in section 5.3.1.K.

- A4: Packing and transport the manufactured VIPs to the CPB

  The packaging and transport of produced VIPs to the car painting booth for installation and use are examined in this section. A1.1 to A4 concludes the first part of the second LCA study, covering the environmental impact from VIP manufacturing to the car painting booth (cradle to gate).

- B1: Installation of VIPs in the CPB

  The installation of VIPs in the car painting booth was considered in this step. The installation process included the use of glue to facilitate the installation, provide proper stability, and maximise insulation performance. Human activity was not considered in this study.

- B6: Operational energy use of the CPB

  The energy use of the car painting booth when VIPs were used as a replacement for conventional insulation (EPS) is considered in this section. Excluded from consideration were maintenance (B2), repair (B3), replacement (B4), refurbishment (B5), and water consumption (B7), as VIPs are presumed to be free from the need for maintenance or repair and did not involve the use of water.

- C2.1: Transport to disposal site

  After 10 years of operation in CPB the VIPs were transported to a designated disposal site. Demolition (C1) was excluded, as it did not include any removal activities. This was the initial scenario of the second LCA study, in which it was expected that all components of the VIPs, including the core materials, would be disposed of at the end of their life cycle.

- C2.2: Transport back to VIP manufacture

  The transport of only the used core materials back to the VIP manufacturing facility, where it would be reused in the production of new VIPs was considered in this section. In this second scenario, all additional components were expected to be recycled rather than disposed of or sent to landfills.

- C4: Disposal

  This section specifically examined the disposal of all VIP components, with a specific focus on the environmental effects of landfilling various core elements. The second part of the second LCA study was concluded after this phase, covering all aspects except C2.2 (cradle to grave).

- D: Potential reuse of the core material

  The last stage evaluates the beneficial consequences of reusing VIP core materials, encompassing the advantages and impacts of further usage in the new life cycle. The phase concluded the third component of the second LCA study, excluding C2.1 and C4 (cradle to cradle), see Figure *5.1*.

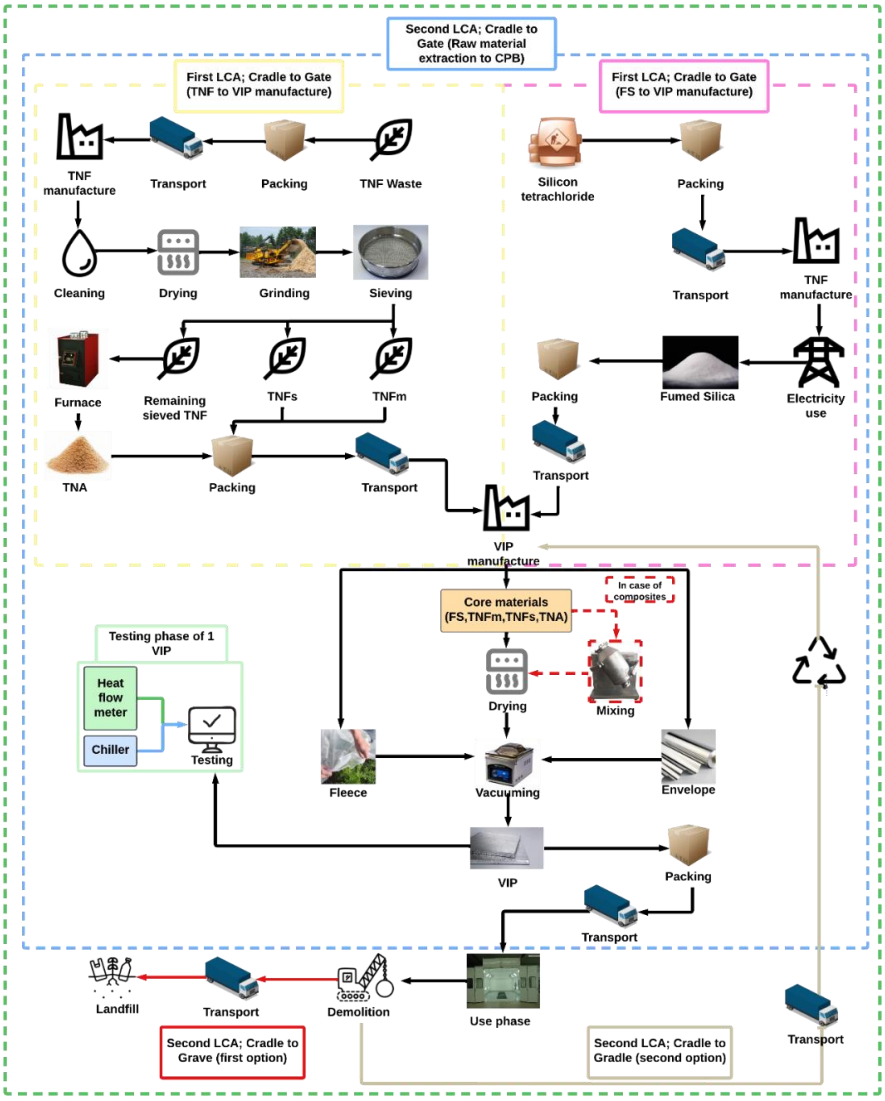

Figure 5.1 All LCA phases for vacuum insulation panel including cradle to gate, cradle to grave and cradle to cradle.

To align the LCA with the dual objectives of (1) evaluating the environmental impact of raw material selection and processing, and (2) assessing the real-world lifecycle implications of using VIPs in high-temperature industrial applications, two complementary system boundary approaches were adopted. The cradle-to-gate boundary was selected for the first stage to isolate and quantify the upstream environmental burdens associated with alternative core materials, enabling direct comparison of their material-level impacts. The cradle-to-cradle boundary, used in the second stage, was chosen to reflect the complete lifecycle performance of VIPs in the context of an industrial setting, specifically, a car painting booth. This approach accounts for potential material reuse and captures downstream benefits beyond the conventional end-of-life scenario. Excluding cradle-to-cradle considerations would underestimate the environmental advantages of recyclable or reusable core materials, thereby weakening the relevance of the findings for circular economy strategies. These boundary selections were therefore made to ensure both methodological rigour and alignment with the LCA goals.

5.1.3 LCA approaches

Attributional LCA (ALCA) using either the Cut-off or APOS models was employed, in which VIPs with fumed silica and tree-based fibres core materials were compared. Using the cut-off model, this analysis would specifically assess and compare the immediate effects of manufacturing, utilising, and disposing VIPs with different core materials. The focus would be on the current situation, without considering any benefits from recyclability. The APOS approach allocates the environmental impacts equally, considering the shared responsibility of the processes involved in producing VIPs. A more detailed understanding of the impacts of various stages and materials on the overall environmental burden could be offered. An analysis would be conducted to evaluate the potential effects on environmental issues such as land usage, carbon sequestration, and agricultural practices resulting from the increased demand for tree-based fibres and decreased demand for fumed silica. To completely compare the environmental consequences of the different core materials for vacuum insulation panels, it is necessary to choose the suitable LCA approach and system model that align with the specific research topics, which in this case would be cut-off and APOS. The consequential approach has been excluded as this study emphasised on identifying the environmental impacts directly linked to the VIP life cycle and solely offers a static analysis of these impacts based on the current supply chain and technology.

5.1.4 Assumptions of the study

To ensure methodological transparency, consistency, and replicability, several assumptions were made during the definition of system boundaries and life cycle inventory modelling. These assumptions were required to model the VIP system in a simplified, yet representative, manner, in accordance with ISO 14040 and ISO 14044 standards. All assumptions were applied uniformly across the comparative scenarios to maintain consistency and avoid introducing bias.

First, all background inventory data, including resource extraction, energy inputs, transportation, emissions, and end-of-life treatment, were sourced from the Ecoinvent v3.8 database using SimaPro. European average datasets were employed in all cases, reflecting the geographic context of the supply chains under consideration. This assumption ensures consistency in energy mix, transport emissions, and industrial infrastructure data, while avoiding regional variability that could confound comparative interpretation.

Second, the useful life span of VIPs installed in the car painting booth (CPB) was assumed to be 10 years, based on typical industrial maintenance intervals and durability specifications from manufacturers. This figure was used across all scenarios to normalise environmental impacts over a consistent time horizon, thereby enabling fair comparison between core material configurations.

Third, the installation stage (B1) was modelled as a one-time event with negligible environmental impact. The process involves manual placement of panels and the use of polyurethane adhesive in small quantities (approximately 30 g per panel), which was deemed too minor to significantly affect overall life cycle results. No energy or water consumption, nor heavy equipment usage, was associated with installation. Human labour was excluded in accordance with standard practice in attributional LCA unless labour-related impacts are significant.

The maintenance (B2), repair (B3), replacement (B4), and refurbishment (B5) phases were excluded from the use stage. VIPs are sealed, non-mechanical components designed to function continuously without the need for maintenance or replacement over their service life. No empirical data or manufacturer guidance indicated any material degradation requiring intervention within the 10-year operational window. Water consumption (B7) was also excluded, as the insulation system is not exposed to water during operation.

Transport distances for raw material acquisition, intermediate processing, and delivery of final products were uniformly set to 200 km for each stage. This distance reflects average road transportation ranges within European logistics networks for building and thermal insulation

materials. For all transport processes, EURO 6 diesel trucks were assumed as the standard vehicle class. Volumetric constraints were considered based on packaging dimensions (such as Intermediate Bulk Containers for $SiCl_4$: 1.2 m × 1.0 m × 1.2 m, 1000 L capacity; and carton boxes for TNF with estimated density of 1200 $kg \cdot m^{-3}$).

In modelling end-of-life, two scenarios were defined. In the disposal scenario, it was assumed that all VIP components were transported 200 km to a landfill site and processed via conventional waste streams (C2.1, C4). In the reuse scenario, only the core material was returned to the manufacturing facility over a distance of 200 km, where it was assumed to be mechanically reintegrated into a new VIP product without thermal or chemical reprocessing. The remainder of the VIP components were assumed to be recycled, consistent with current European waste management practices for composite building materials.

The selected Attributional LCA (ALCA) framework applied both the Cut-off and APOS allocation models. The Cut-off approach was employed to highlight the direct environmental impacts of production and disposal without attributing environmental credit for material recovery. The APOS model, in contrast, distributed environmental burdens proportionally across product systems based on economic value, capturing shared responsibility across the supply chain. The Consequential LCA approach was excluded, as the aim of this study was not to assess system-wide market dynamics or long-term policy effects, but to compare current core material options within an operationally constrained system.

These assumptions were designed to balance scientific rigour, data availability, and realistic modelling of the VIP life cycle, ensuring comparability across alternative core materials and alignment with the defined LCA objectives. Sensitivity analysis (Section 6.4) was conducted to evaluate the influence of key modelling assumptions, including the choice of attributional LCA approach (Cut-off vs. APOS) and the impact of using updated energy-related data sourced from the IEA with non-updated datasets provided within the SimaPro database.

5.1.5 Limitations and uncertainties of the study

The limitations and uncertainties of the study are outlined as:

I. Assessment of the quality and accuracy of inventory data

The data on the production of VIPs and the processing of TNF were gathered from multiple sources, including laboratory experiments conducted at Brunel University and secondary data (from literature). Given that TNF has not been commercialised, it was hypothesised that utilising commercial equipment with greater power and capacity would yield more accurate outcomes. The

energy data for converting silica tetrachloride to fumed silica, which is readily available for purchase, was obtained from published literature. To produce VIPs, the data were scaled up by expanding the equipment and methodology employed in the laboratory to match the level of industrial production. The utilisation of these data sources would introduce a level of uncertainty due to the fact that the laboratory scale data does not accurately reflect the details of large-scale industrial processes.

II. Assumptions and simplification

In order to maintain consistency and avoid distorting the results, it was assumed that the journey distances for both the transport of silicon tetrachloride to fumed silica manufacture and the transportation from fumed silica manufacture to VIP manufacture were the same. The approach was similar to the transportation of TNF from raw material to TNF manufacture and from TNF manufacture to VIP manufacture. Regarding landfilling, it was assumed that only TNF would have an environmental influence due to the degradation of the cellulosic fibres. On the other hand, fumed silica would just occupy the land area based on its density and quantity, as there is no literature available explaining the negative environmental impact of fumed silica when it is disposed of in a landfill. The secondary materials, such as envelopes or fleece, were obtained from the SimaPro database, which may introduce further inaccuracies. These assumptions can add uncertainty that can influence the overall LCA outcomes.

III. Ecoinvent database constraints

The background data for the LCI models were obtained from Ecoinvent, utilising various methodologies like cut-off and APOS. The availability of datasets for these approaches was constrained, either due to outdated data such as the IEA data for electricity production in the year 2016. A modification was implemented to the outcomes and revised to the year 2022. The constraint and change can also introduce uncertainty.

IV. Reliability of LCIA methodologies

The life cycle impact assessment of core materials and VIPs, along with the benefits of reusing core materials, was carried out using SimaPro. The assessment of the environmental impact was conducted using Cumulative Energy Demand (CED), which incorporates 6 impact categories, and the EN 15804 + A2 standard, which encompasses 13 impact categories. Only the significant impacts resulting from these two methods were considered in the final LCA impact. Any impacts that have minimal effect or those unrelated to the specific application (producing VIP) were excluded. However, variations in LCA methods could result in uncertainties in the final impact assessment.

5.2 Life cycle inventory analysis

Fumed silica was bought from commercial suppliers, but the processing of tree-based natural fibres and the manufacturing of the VIP were conducted in Brunel lab. It is crucial to note that the manufacturing processes adopted followed similar procedures as those used by VIP manufacture industry. Understandably, the quantity of materials used in VIP production differs significantly in both cases. Misleading results can occur when assessing the environmental impact of the work due to these differences. In addition, the process of scaling up TNF has not yet been implemented by VIP manufactures. It was necessary to utilise secondary data in a way comparable with the laboratory-based work, but using industrial equipment that had greater capacity and power. This was done to obtain more realistic results. The process for fumed silica was followed and assumed based on previous research (Resalati et al., 2021).

5.2.1 Sieving of TNF

The VIBRO sifter machine from Dahan Machinery was utilised to sieve the tree-based natural fibres (Dahan Machinery, 2023). The capacity of the VIBRO machine ranges from 100 to 3300 $kg.h^{-1}$, and a power range of 0.18 to 2.2 kW. The duration for the process of separating TNF into TNFm and TNFs was 5 minutes. Assuming that VIBRO was functioning at its highest efficiency, the amount of energy needed to obtain TNFm and TNFs can be calculated using equation (5.1).

$$E_{Ms} = (P_{Ms} \times T_s) \times N \quad (5.1)$$

where $\mathrm{E_{Ms}}$ is the energy consumption at maximum capacity, $\mathrm{P_{Ms}}$ the maximum power for the VIBRO machine, $\mathrm{T_s}$ the time required to sieve TNFm and TNFs and N is the number of times needed to run the sieving machine.

The two fibre diameters utilised in this work were TNFm (with a sieve size of 250 μm) and TNFs (with a sieve size of 125 μm). During the sieving process, 28% of the TNF was retained by the 125 μm sieve and 11% passed through Therefore, in order to acquire 1 tonne of TNFm or TNFs, the sieve machine must be operated on multiple cycles. For the production of 1 tonne of TNFm, a total of 3571.42 kg of TNF must be sieved. In contrast, to obtain 1 tonne of TNFs, a larger quantity of 9090.90 kg of TNF was required. In this scenario, there are two alternatives: either utilise the sieving machine at its maximum capacity many times, or employ the sieving machine by combining its maximum and minimum capacities. The equation (5.1) was rewritten in the following way as shown in equation (5.2).

$$E_{Ts} = E_{Ms} + (P_{ns} \times T_s) \quad (5.2)$$

where $\mathrm{E_{Ts}}$ is the sum of energy consumption at maximum capacity and needed capacity based on the quantity of materials, and $\mathrm{P_{ns}}$ the power for the VIBRO depending on the needed material to be sieved. For instance, if a production requirement of 1000 kg of TNFm necessitates the sieving of 3571.42 kg of TNF, and the machine could only sieve 3300 kg in one run, leaving 271.42 kg remaining, then instead of sieving another 3300 kg at full capacity, only the remaining 271.42 kg would be sieved at a lower power rate of approximately 0.3 kW, see Table *5.2*.

Table 5.2: Energy consumption of TNFm and TNFs at 5 different scenarios

Case	TNF (kg)	TNFm		TNFs	
		TNFm (kg)	E_{Ts} (kWh)	TNFs (kg)	E_{Ts} (kWh)
1	3300	924	0.18	363	0.18
2	6600	1848	0.36	726	0.36
3	3571.42	1000	0.21	392.85	0.21
4	9900	2772	0.54	1089	0.54
5	9090.9	2545.45	0.50	1000	0.50

Note: Case 1- sieving machine maximum capacity; Case 2- to produce 1 tonne of TNFm at maximum capacity of the sieving machine. (equation (5.1)); Case 3- to produce exactly 1 tonne of TNFm without using maximum capacity more than once. (Equation (5.2)); Case 4- to produce 1 tonne of TNFs at maximum capacity of the sieving machine. (equation (5.1); Case 5- to produce exactly 1 tonne of TNFs without using maximum capacity more than once. (Equation (5.2))

5.2.2 Grinding of TNF

The HL/5/22/25 grinder from Scanhugger was utilised for the purpose of grinding tree-derived natural fibres(Scanhugger, 2022). The machine's capacity ranges from 2000 to 12000 kg.h^{-1}, while its power ranges from 90 to 110 kW. The energy required was determined by equation (5.3) and the results were presented in Table *5.3*. To determine the duration needed to grind TNF equation (5.4) was used.

$$E_g = P_g \times T_g \quad (5.3)$$

where E_g is the energy consumption of the grinder, P_g the power of the HL/5/22/25 grinder and T_g the time required to grind TNF.

$$T_g = \frac{Total\ weight}{Machine\ capacity} \quad (5.4)$$

Table 5.3: Energy consumption of the grinding machine of raw TNF

Case	Maximum capacity		Minimum capacity	
	T_g (min)	E_g (kWh)	T_g (min)	E_g (kWh)
1	16.5	30.25	99	148.5
2	33	60.5	198	297
3	17.86	32.74	107.14	160.71
4	49.5	90.75	297	445.5
5	45.45	83.33	272.73	409.1
6	60	110	360	540
7	10	18.3	60	90

Note: Case 1 to 5 similar to Table 5.2; Case 6 - to grind 12 tonnes of materials at maximum and minimum capacity of HL/5/22/25 grinder; Case 7 - to grind 2 tonnes of materials at maximum and minimum capacity of HL/5/22/25 grinder

5.2.3 Pyrolysis of TNF

The furnace can be utilised for two distinct processes: either to combust the residual sieved TNF particles that were retained at a mesh size bigger than 250 µm, resulting in the complete utilisation of TNF waste and the manufacture of TNFm, TNFs, and TNA; or to directly combust the TNF without sieving, resulting in the production of only TNA. The selected furnace model was Model N (4000/85 HA) with a heating temperature of 850 ℃ and a heating power of 90 kW, as stated by Nabertherm (Nabertherm, 2021). In order to determine the capacity of the furnace, it was crucial to know the density of TNF and the internal dimensions of the furnace. The capacity was calculated using mass-density-volume relationship. The decision was made to use bigger inner dimensions (1500 x 2200 x 1200 mm^3). The density of the sieved TNF was assumed to be 400 $kg.m^{-3}$, which is higher than the measured density of TNFm (310.40 $kg.m^{-3}$). The density of the non-sieved TNF was obtained from literature and was found to be 900-1200 $kg.m^{-3}$ (Awad et al., 2021). The highest capacity for processing sieved TNF was 1584 kg, while the maximum capacity for processing non-sieved TNF was 3564 kg assuming that density of non-sieved TNF was 1200 $kg.m^{-3}$ and the density of sieved TNF was 400 $kg.m^{-3}$. The energy consumption associated with the conversion of TNF to TNA was determined using the following equation (5.5).

$$E_f = (P_f \times T_f) \times N \quad (5.5)$$

where E_f is the energy consumption, P_f the power of furnace, T_f the time required for pyrolysis TNF to TNA as discussed in section 3.1.2.

However, in an effort to minimise energy usage, TNF were pyrolysed at a lower temperature of 600 ℃ for 180 minutes. The heating power in this scenario would be 63.5 kW, calculated using the formula: ($Power\ at\ 600\ ℃ = 90\ kW \times \frac{600℃}{850℃}$) and the results are presented in Table *5.4*.

Table 5.4: Comparison of energy consumption between sieved and non-sieved TNF to TNA

Case	Sieved			Non-Sieved		
	TNF (kg)	E_f (kWh)	TNA (kg)	TNF (kg)	E_f (kWh)	TNA (kg)
1	2013	381.2	141	3300	190.6	231
2	4063	571.8	284	6660	381.2	466
3	2179	381.2	152	3571	190.6	250
4	6039	762.4	423	9900	571.8	693
5	5545	762.4	388	9091	571.8	636
6	7320	952.9	512	12000	762.4	840
7	1220	190.6	85	2000	190.6	140
8	2013	381.2	141	3300	190.6	231
9	4063	571.8	284	6660	381.2	466

Note: Case 1 to case 7 similar to Table 5.3; Case 8- Pyrolisis of TNA based on the capacity of the furnace using sieved TNF; Case 9- Pyrolysis of TNA based on the capacity of the furnace using non-sieved TNF

When converting TNF to TNA, 7% of the original weight was obtained. Meaning that to produce 1 tonne of TNA, 14.2857 tonnes of TNF must be pyrolysied (assuming it was not sieved). However, in the alternative scenario where TNF was sieved the leftover unused TNF determine the precise amount of material required, the equation (5.6) was utilised:

$$TNA = (TNF - TNFm - TNFs) \times 7\% \quad (5.6)$$

To pyrolyse 1 tonne of TNA, an initial amount of 23.4 tonnes of TNF was required. Out of this, 6.6 tonnes was sieved into TNFm, 2.6 tonnes was sieved into TNFs, and the remaining 14.2 tonnes was pyrolysed into TNA, see Table *5.5*.

Table 5.5: Comparison of energy consumption between sieved and non-sieved TNF to TNA considering two new cases

Case	Sieved			Non-Sieved		
	TNF (kg)	E_f (kWh)	TNA (kg)	TNF (kg)	E_f (kWh)	TNA (kg)
10	14285	1715.3	1000	23400	1334.1	1638
11	8714	1143.5	610	14285	952.9	1000

Note: Case 10 – to produce exactly 1000 TNA using sieved TNF; Case 11 – to produce exactly 1000 TNA using non-sieved TNF

5.2.4 Drying of TNF

To initiate the drying process, the KTR 22500 model was selected. It has an inner capacity of 22.5 m^3 and operates at a heating temperature of 260 ℃, with a heating power of 108 kW. Upon examination of this study, it was observed that the oven had an extra capacity, resulting in a significant amount of unused space throughout both the core material and raw material drying stages. The additional space has the potential to distort the obtained results. Consequently, a compact oven with reduced heating capacity was used. The selected model is the KTR 12300, which has an inner volume of 12.25 m^3 and operates at a heating temperature of 260 ℃ with a heating power of 90 kW (Nabertherm, 2021). The energy usage for drying the raw material was determined using the equation (5.7).

$$E_{OR} = (P_{OR} \times T_{OR}) \times N \quad (5.7)$$

where E_{OR} is the energy consumption, P_{OR} the power of the oven, T_{OR} the time required to dry the raw material.

The conventional method for drying the untreated TNF after cleaning involved subjecting them to a temperature of 60 ℃ for a duration of 24 hours. However, in an effort to minimise energy usage, the cleaned raw TNF were instead dried at a higher temperature of 120 ℃ for a shorter period of 4 hours, as determined by the TGA results in section 3.2.10. The heating power in this scenario would be 41.5 kW, calculated using the formula: $(Power\ at\ 120\ ℃ = 90\ kW \times \frac{120℃}{260℃})$ and the results are presented in Table *5.6*.

Table 5.6: Energy consumed during drying TNF

Case	TNF (kg)	E_{OR} (kWh)	
		Full capacity	Needed capacity
1	3300	166	49.7
2	6600	166	99.4
3	3571.4	166	53.8
4	9900	166	149.1
5	9090.9	166	136.9
6	2000	166	30.1
7	12000	332	180.7
8	1584	166	23.8
9	3564	166	53.7
10	23419.2	498	352.6
11	14285.7	332	215.1

5.2.5 Total energy consumption of core material

Once the energy consumption of the sieve machine, grinder, and oven has been obtained, the total energy consumed in the production of TNFm, TNFs, and TNA was calculated. The processing of TNFm and TNFs involved a single method, which included drying the TNF after cleaning, grinding the dried TNF, and then sieving it at various mesh sizes. There are two methods for the pyrolysis of the TNA. The first involved taking the remaining grinded TNF and then using furnace for pyrolysis, named Complete Cycle pyrolysis (CC). The second method was to immediately grind the TNF without cleaning it, and then using furnace for pyrolysis, named Direct pyrolysis (D). Equations (5.8),(5.9) and (5.10) representing the overall energy consumption are shown below:

$$E_{(TNFm)t} = E_{(TNFs)t} = E_{Ts} + E_g + E_{OR} \quad (5.8)$$

$$E_{(TNA)tc} = E_{Ts} + E_g + E_{OR} + E_f \quad (5.9)$$

$$E_{(TNA)td} = E_g + E_f \quad (5.10)$$

where, $E_{(TNFm)t}$ is the total energy consumption of processing TNFm, $E_{(TNFs)t}$ the total energy consumption of processing TNFs, $E_{(TNA)tc}$ the total energy consumption of the pyrolysis of TNA (CC) and $E_{(TNA)td}$ the total energy consumption of the pyrolysis of TNA (D), see Table *5.7*.

Table 5.7: Total energy consumption of producing 1 tonne of TNFm, TNFs and TNA (complete cycle and direct pyrolysis)

Production of 1 tonne	Raw TNF (kg)	E_{Ts} (kWh)	E_g (kWh)	E_{OR} (kWh)	E_f (kWh)	Total energy consumed (kWh)
TNFm	3571.4	0.2	32.7	53.8	0	86.8
TNFs	9090.9	0.5	83.3	136.9	0	220.7
TNA (CC)	23419.2	1.28	214.7	352.6	2702.9	3271.5
TNA (D)	14285.7	0	130.9	215.1	1201.3	1547.4

5.2.6 Packing of raw materials

Two distinct packaging methods were employed for the storage of raw materials. For TNF waste standard folding carton cardboard were utilised with dimensions of 0.6 x 0.4 x 0.4 m^3 (LxWxH) each weighing 0.5 kg. TNF was measured to have a density of 1200 $kg.m^{-3}$, which means any carton stored 115.2 kg of TNF. The maximum weight allowed for the vehicle was 6200kg. Assuming that the weight of the empty boxes was neglected, the number of boxes that can be loaded based on weight was 53.8, which was rounded to 53. In order to verify that the predictions were well within the vehicle's volume capacity, it was also assumed that the conventional truck had an internal volume of 33 m^3. The total volume of the 53 boxes was 5.1 m^3 (calculated by multiplying the number of boxes by the volume of each box). This volume comfortably fits within the capacity of the normal truck. The total weight of TNF amounted to 6105.6 kg, while the overall weight of the truck's load reached 6121.5 kg These measurements were determined using the calculations outlined in equation (5.11).

$$Weight_{\ Total} = N_{boxes} \times (Weight_{\ boxes} + Weight_{\ TNF}) \quad (5.11)$$

Regarding silicon tetrachloride, the packaging cannot be same to TNF because it was a volatile liquid. Thus, it was assumed that standard IBCs with a volume of 1000 litres and dimensions of 1.2 x 1 x 1.2 m^3 would be used, weighing 60 kg each. The density of $SiCL_4$ was estimated to be 1480 $kg.m^{-3}$ (Blonk et al., 2023). The total weight of the filled IBCs was 1549 kg, including the weight of 1000 litres of $SiCL_4$ and the weight of the IBCs. The weight of $SiCL_4$ and containers was determined using the identical methods employed for measuring the weight of TNF in the truck. The findings are presented in Table *5.8*.

Table 5.8: Overview of TNF waste and silicon tetrachloride packaging and material data

	TNF waste	Silicon tetrachloride
Number of packages	53	4
Total weight of packages (kg)	27.5	240
Total volume of packages (m^3)	5.1	5.76
Total weight of material (kg)	6105.6	5920
Total weight of filled packages (kg)	6132.1	6160

5.2.7 Total energy consumption of core materials based on the 1st FU

The products TNFm, TNFs, and TNA were all obtained from the same raw material, designated as TNF. The study provided a detailed comparison of the energy consumption and total quantity of materials derived from an initial 6105.2 kg of TNF, as shown in Table *5.9*.

Table 5.9: Total energy consumption of producing TNFm, TNFs and TNA (complete cycle and direct pyrolysis) based on the 1st FU

Process	TNF (kg)	TNFm		TNFs		TNA	
		(kg)	(kWh)	(kg)	(kWh)	(kg)	(kWh)
CC	6105.2	1709.5	222.7	671.6	222.7	260.7	830.2
D		0	0	0	0	427.4	460.9

The findings indicated that during the entire cycle, 6105.2 kg of TNF were converted into 1709.5 kg of TNFm, with an energy usage of 222.7 kWh. Using an equivalent amount of energy, 671.6 kg of TNFs was processed, resulting in 3724.2 kg of materials that were unsuited for this study's application (VIP core). The sieved TNF underwent pyrolysis in the industrial furnace, resulting in the production of 260.7 kg of new core material known as TNA. The procedure required an energy usage of 830.2 kWh. In the case of TNA, it was essential to consider adding the energy consumed during the cleaning to sieving process (222.7 kWh) to the energy consumed in the furnace (607.5 kWh). In contrast, the direct process does not involve the production of TNFm and TNFs. The process required only the grinding of 6105.2 kg of TNF (equivalent to 55.96 kWh) and the subsequent pyrolysis of the ground TNF in an industrial furnace to generate TNA (equivalent to 405 kWh). The furnace energy consumption was lower in the direct pyrolysis compared to the complete cycle, despite the higher amount of TNF. The difference can be attributed to the change in material density. It is important to note that sieved TNF had lower

density compared to non-sieved TNF. Meaning that more material can be loaded into the chamber of the furnace, resulting in reduced usage time for the furnace. In the direct pyrolysis, a total of 427.4 kg of TNA was pyrolysed, requiring an energy expenditure of 460.9 kWh.

Conversely, fumed silica was generated through the reaction of vaporised silicon tetrachloride with hydrogen in a high-temperature reactor. The reaction yields silicon dioxide (SiO_2) and hydrochloric acid (HCl), with the silicon dioxide being obtained as a fine, porous powder. According to Resalati (2021) the production of 1 tonne of FS required the use of 2700 kg of $SiCl_4$ and an energy input of 16.5 GJ. In this study, the values were adjusted according to the initial amount of $SiCl_4$ that was loaded into the truck. It was estimated that 5920 kg of $SiCl_4$ produced roughly 2.19 tonnes of FS, with an energy consumption of 10044.4 kWh.

5.2.8 Packing core materials

A truck with a load capacity of 6.2 tonnes and an internal space of 33 m^3 would be utilised to deliver the newly processed material from the production site to the VIP manufacturing facility. During the manufacturing process, three materials - TNFm, TNFs, and TNA - would be carried simultaneously from the TNF manufacture to the VIP manufacture. However, FS would be transported from a separate manufacture, but the distance travelled was deemed to be the same in order to ensure accurate comparison. The TNFm and TNFs products were enclosed in folding carton cardboard measuring 0.6 x 0.4 x 0.4 m^3 and weighing 0.5 kg. The TNA and FS were enclosed in polyethylene bags measuring 0.4 x 0.4 x 0.2 m^3 and weighing 0.5 kg. Table *5.10* provides the required volume, number of cartons or bags, and total weight for each material based on their densities and production quantities.

Table 5.10: Properties and packaging data for TNFm, TNFs, TNA, and FS materials

	TNFm	TNFs	TNA (CC)	FS
Density ($kg.m^{-3}$)	310.4	212.6	356.1	52.6
Amount processed (kg)	1709.5	671.6	260.7	2190
Volume of the materials (m^3)	5.51	3.16	0.73	41.63
Number of carton/bags	58	33	23	1301
Total volume (m^3)	5.57	3.17	0.74	41.63
Total weight (kg)	1738.5	688.1	272.2	2840.5
Total volume/ truck (m^3)		9.48		41.63
Total weight/ truck (kg)		2698.8		2840.5

It is worth noting that the materials produced by the TNF manufacturer were well within the truck's capacity in terms of both volume and weight. Meaning that it was possible to transport all the materials in one trip while adhering to the truck's weight restrictions. However, although FS falls within the truck's load capacity, its low density prevented the transportation of the entire processed amount in one trip. The total volume of FS was 41.63 m^3, which exceeded the truck's internal volume limit of 33 m^3. Consequently, a maximum of 1735.8 kg can be delivered in a single trip, leaving 454.2 kg to be transferred in a subsequent trip. In reality, manufacturing more VIPs can have a greater environmental impact due to the increased need for fumed silica core. However, the target was to produce 128 VIPs (the number of VIPs required to be installed in one car painting booth) weighing a maximum of 640 kg. Therefore, the impact of the remaining FS core would not play a significant role. The only change to be considered here was the reduction in the number of polyethylene bags to 1031 bags, considering the transportation of the first batch of FS within the truck's full volume.

5.2.9 Total energy consumption of core materials based on the 2nd FU

The data displayed in the Table *5.9* above do not accurately reflect the actual difference in energy consumption among the processed materials. The study only provided information on the energy consumption based on the FU. For a comprehensive analysis of energy consumption for each processed material, a standard VIP size measuring 1 m^2 and 25 mm in thickness was selected for this study. The density of this VIP was estimated to be 200 $kg.m^{-3}$. Indicating that the core material necessitated a mass of 5 kg. Table *5.11* presents the actual energy consumed (E_{core}) of various core materials for a single standard VIP.

Table 5.11: the actual energy consumed of various core materials for a single standard VIP.

Core material	E_{core} (kWh)
TNFm	0.65
TNFs	1.66
TNA (CC)	15.92
TNA (D)	5.39
FS	22.93

The data in Table *5.11* indicated that when converting TNF to TNFm and TNFs, the energy consumption for both was 222.7 kWh. However, when comparing the energy consumption for the same standard core VIP, the production of TNFs consumed 2.5 times more energy than TNFm. The difference resulted from the fact that the production of TNFm exceeded that of TNFs by a factor of 2.5 during the process of sieving TNF into TNFm and TNFs. Therefore, to generate an

equivalent quantity of TNFs as TNFm, it would necessitate an additional amount of raw materials, resulting of greater equipment usage and subsequently higher energy consumption (as detailed Table *5.7*). Regarding TNA, it was shown that the density of the materials significantly influenced energy usage. As previously stated, the density of the sieved TNF was greater than that of the non-sieved TNF, resulting in increased utilisation of the furnace for the pyrolysis of TNA. Despite the increase in furnace capacity, energy consumption would still be 2.5 times higher in the case of sieved TNF. The only benefit in using the complete cycle when producing TNA was the production of TNFm and TNFs. However, if the end users are only interested with TNA material, then the direct procedure would result in reduced energy use. It is important to understand that the selection of parameters has a substantial impact on the outcomes when evaluating the energy usage of core materials for standard VIPs.

5.2.10 Total water usage

The cleaning process was another factor in this proposed model as it determines the appropriate amount of water required to convert TNF into TNFm, TNFs, and TNA. The cleaning procedure comprises three crucial steps: an initial shake and brush, followed by soaking and a light rinse. The study aimed to quantify the amount of water needed to clean 6105.2kg of TNF from accumulated particles. The soaking stage was estimated to require 5 litres of water per kilogramme of TNF, whereas the rinse step was estimated to require 2 litres of water per kilogramme of TNF. No water was needed for the shaking and brushing steps. In order to input the water value of 1 kg of TNF into SimaPro, it was necessary to convert the volume of water used, which was 7 litres, to cubic metres. The conversion resulted in a value of 0.007 m^3. When scaled up to 6105.2 kg, the cleaning procedure requires a total volume of 42.73 m^3. The quantity of water ensured that the TNF were thoroughly cleaned of any collected dust and prepared for subsequent procedures.

5.2.11 Total energy consumption for VIP cores

The production of VIPs entails multiple sequential procedures, including the drying of the core materials to minimise moisture content, the compression of the core using a hydraulic press, the evacuation of the core material to the desired pressure level (about 0.1 mbar) through vacuuming, and the blending of composites using a 3D mixer. Furthermore, VIP underwent thermal conductivity testing utilising a heat flow meter equipped with a chiller. Aside from the manufacturing and testing phases, the production of VIPs also required the use of additional components, such as the envelope and fleece. The following illustrated the energy required to produce one standard VIP and the quantity of envelope and fleece materials needed. The figures

were multiplied by 128, according to the number of VIPs needed for installation in the car painting booth.

The core material was dried using the same oven model that was used for drying the raw materials. The identical equation (5.12) was employed and the energy consumption results for 1 core and 128 cores were displayed in Table *5.12*.

$$E_{OR} = (P_{OC} \times T_{OC}) \times N \quad (5.12)$$

where E_{OC} is the energy consumption, P_{OC} the power of the oven, T_{OC} the time required to dry the raw material.

Table 5.12: Difference in energy consumption for drying 1 core and 128 cores

Core material	Density (kg.m^{-3})	Maximum capacity of core material (kg)	E_{OC} for 5 kg of core material (kWh)	E_{OC} for 128 VIP (kWh)
TNFm	310.4	1901.2	0.22	27.9
TNFs	212.6	1302.2	0.32	40.7
TNA	356.1	2181.1	0.19	24.3
FS	52.6	322.2	2.57	329.0
EP	33.0	202.1	4.10	524.3
FS-TNFm1	88.2	540.2	1.53	196.2
FS-TNFs1	95.8	586.8	1.41	180.6
FS-TNA1	78.6	481.4	1.72	220.1

The study also involved the analysis of composites using a process that resembled the one used for individual materials. However, an additional step was required to prepare the core material: blending the composites using a mixer. The PNA Conical Screw Mixer, which has a strong resemblance to the large-scale mixer utilised by VIP manufacturers, was used (PNA CONICAL SCREW MIXER, n.d.). The mixer was configured with a working volume of 6 m³ and a power rating of 22 kW. The process of mixing operated for 10 minutes. Based on the densities listed in Table *5.12*, the mixer has to be used multiple times in order to obtain a total of 640 kg of materials for 128 VIPs. It was assumed that the mixer would operate twice at maximum capacity. The mixer's energy consumption is described by equation (5.13), and the findings are presented in Table *5.13*.

$$E_{Mx} = (P_{Mx} \times T_{Mx}) \times N \quad (5.13)$$

where E_{Mx} is the energy consumption, P_{Mx} the power of the mixer, T_{Mx} the time required to mix the composites.

Table 5.13: Energy consumption of the mixer for different VIP composites

Core material	Density ($kg.m^{-3}$)	Maximum capacity of core material (kg)	E_{Mx} for 5 kg of core material (kWh)	E_{Mx} for 128 VIP (kWh)
FS-TNFm1	88.2	529.2	0.035	4.43
FS-TNFs1	95.8	574.8	0.032	4.08
FS-TNA1	78.6	471.6	0.039	4.98

The vacuuming and testing of the VIPs were conducted using a uniform method for all samples. Each piece of equipment was used once for manufacturing each VIP. For the purpose of testing, only one VIP was examined, under the assumption that the remaining VIPs would have identical characteristics. The Heat Flow Meter (NETZSCH HFM 446 Lambda) with a power output of 1.15 kW and the chiller from JULABO with a power output of 0.69 kW were utilised. Every VIP underwent testing at four distinct average temperatures, with each individual test lasting for a duration of 30 minutes. The vacuum sealer required 10 minutes to achieve the desired pressure and had a power of 2.4 kW. Equations (5.14),(5.15) and (5.16) showed the calculations for the energy consumption of vacuuming, testing and total energy consumption for producing 1 VIP. Table *5.14* displays the total energy use for producing VIPs with various core materials and the overall energy usage for all produced VIPs required for a single car painting booth.

$$E_V = P_V \times T_V \tag{5.14}$$

$$E_{Test} = (P_{HFM} \times T_{HFM}) + (P_{ch} \times T_{ch}) \tag{5.15}$$

$$E_{VIP} = E_{core} + E_V + E_{OC} + E_{Test} + E_{Mx} \tag{5.16}$$

Table 5.14: Total energy consumption based on the 2nd FU

Core material	E_{core} (kWh)	E_V (kWh)	E_{OC} (kWh)	E_{Test} (kWh)	E_{Mx} (kWh)	E_{VIP} for 1 VIP (kWh)	E_{VIP} for 1 CPB (kWh)
TNFm	0.7	0.4	0.22	0.92	0.000	2.2	280.0
TNFs	1.7	0.4	0.32	0.92	0.000	3.3	422.1
TNA	15.9	0.4	0.19	0.92	0.000	17.4	2231.0
FS	22.9	0.4	2.57	0.92	0.000	26.8	3433.0
FS-TNFm1	16.2	0.4	4.10	0.92	0.035	5.4	693.3
FS-TNFs1	16.5	0.4	1.53	0.92	0.032	19.1	2449.1
FS-TNA1	20.8	0.4	1.41	0.92	0.039	23.9	3060.0

5.2.12 Packing of VIPs

The combined weight of the 128 VIPs is 640 kg, with each VIP weighing 5 kg. The total space occupied by the VIPs is 3.2 m^3, with each VIP having dimensions of 1x1x0.025 m^3. The boxes utilised for packaging the TNF are not suitable for accommodating the VIP, hence a larger folding carton with dimensions of 1.1 x 1.1 x 0.2 m^3 was selected. A total of 32 boxes, each capable of holding 4 VIPs, were utilised. Additionally, each box weighed 0.5 kg. The overall weight of the packed boxes is the combined weight of the 128 VIPs, which amounts to 640 kg, along with the additional weight of the empty boxes, which is 16 kg. Considering that the weight of the packed VIP and the volume to be loaded were comfortably within the truck's maximum capacity limit.

5.3 Life cycle impact assessment

Once the model for manufacturing VIPs with various cores has been designed and the required functional units and system boundaries have been defined, it was crucial to choose the right impact categories. The SimaPro database, as described in the database manual methods (SimaPro database manual Methods library, 2024) offered a variety of impact methods for calculating the relevant impact categories of interest. The impact assessment techniques consist the following steps:

5.3.1 Characterisation

In this stage, known to as midpoint, the substances were multiplied by a characterisation factor to quantify their contribution to a certain effect category. As an example, in the context of climate change, carbon dioxide has a characterisation value of 1, but dinitrogen monoxide has a characterisation factor of 273. Indicating that the release of dinitrogen monoxide would result in an equivalent climate impact as emitting 273 kg of CO_2. Specific characterisation criteria are facilitated by the use of sub-compartments and regionalisation, such as at the country or continent level

5.3.2 Damage assessment

Also known as endpoint, this stage consolidates various indicators of impact categories into a single damage category. Certain techniques incorporate damage assessment directly during the characterisation phase. In the process of damage assessment, it is possible to combine all impacts that share the same unit of assessment.

5.3.3 Normalisation

Impact category indicator data can sometimes be compared using a reference or normal value, which involves dividing these impact categories by the reference value. The selection of these

references is unrestricted. Typically, normalisation is employed in LCA to assist users in establishing a benchmark for comparing the LCA studied against something that readers can easily comprehend.

5.3.4 Weighting

Weighting is a typical subsequent step to normalisation, where the outcomes of impact category indicators are multiplied by weighting factors. The addition of these additional values is the final stage in the LCA, resulting in a single score. These individual scores can be used to compare two or more products/services based on their overall environmental impact, which is often measured in a single score, expressed in point (pt).

Only the characterisation stage was considered, which determined the direct effect of the substance on the impact category without converting these impacts into potential damage or normalising the outcomes for wider comparison. The study focused on analysing the direct environmental impact of manufacturing VIPs or key materials by examining specific impact categories such as acidification or global warming potential. The methodology simplified the LCA process and eliminated the complexity of damage assessment, normalisation, and weighting, while ensuring the transparency and traceability of data.

5.4 Categorisation of methods

SimaPro contains six distinct categories of methodologies. The European methods are mainly employed for studies conducted in Europe and are centred on the European context. Global methods are comprehensive LCIA methods that have a global scope. Methods that were devised in North America are referred to as North American methods. In addition, single-issue methods are concentrated on a single metric or environmental impact area, with the exception of water-focused methods. Only water-related impacts are evaluated by water footprint methodologies. Superseded methods are outdated and no longer supported by PRé, and their use is discouraged. The energy consumed in the refining of the core material and the development of VIPs was evaluated using the Cumulative Energy Demand (CED) method and the EN15804 + A2 method in this study, as the work was conducted in the United Kingdom.

5.4.1 Cumulative Energy Demand (CED)

The cumulative energy demand (CED) is designed to evaluate the total energy consumption of a product or service over its entire life cycle, which encompasses both direct and indirect energy consumption associated with the use of basic materials (Hischier et al., 2010). The methodology was established in the early 1970s following the initial oil crisis and has maintained a long-

standing tradition in energy analysis. The impact categories are divided into two primary categories: the non-renewable category, which encompasses the sum of fossil, nuclear, and biomass, and the renewable category, which includes the sum of biomass, water, wind, and solar. The equations (5.17),(5.18),(5.19),(5.20),(5.21) and (5.22) present each of these impact categories specifically for various substances.

$$NR_T = NR_F + NR_N + NR_B \quad (5.17)$$

$$R_T = R_B + R_{Wa} + R_{Wi,S} \quad (5.18)$$

$$NR_F = S_{C,b} + S_{C,h} + S_{G,m} + S_{G,n} + S_O + S_P \quad (5.19)$$

$$NR_T = S_{C,b} + S_{C,h} + S_{G,m} + S_{G,n} + S_O + S_P + S_U + S_{E,1} \quad (5.20)$$

$$R_{Wi,S} = S_{E,k} + S_{E,g} + S_{E,so} \quad (5.21)$$

$$R_T = S_{E,2} + S_{E,p} + S_{E,k} + S_{E,g} + S_{E,so} \quad (5.22)$$

Where NR_T is the total non-renewable energy consumed, R_T the total renewable energy consumed, NR_F, NR_N and NR_B are the non-renewable energy consumed from fossil, nuclear and biomass, respectively. while R_B ,$R_{Wa}$and $R_{Wi,S}$ are the renewable energy consumed from biomass, water and wind, solar and geothermal, respectively. $S_{C,b}$, $S_{C,h}$, $S_{G,m}$,$S_{G,n}$,S_O , S_P, S_U , $S_{E,1}$,$S_{E,2}$,$S_{E,p}$,$S_{E,k}$,$S_{E,g}$ and $S_{E,so}$ are the substance from coal-brown, coal-hard, gas-mine-of gas, gas-natural, oil-crude, peat, uranium, energy-gross calorific value in biomass that are not replenished on a human timescale, energy-gross calorific value in biomass that are replenished on a human timescale, energy-potential (in hydropower reservoir), energy-kinetic (in wind), energy-geothermal and energy-solar, respectively.

Throughout this thesis, the term "energy consumption" has been used to describe the actual energy used during specific processes, such as core material processing and the operation of the car painting booth which will be discussed in later sections and chapters. The reason for this choice lies in the nature of the analysis, which focuses on quantifying the real UK energy utilised in these processes.

Table *5.15* presents the impact of category findings when 1 MJ of electricity was inputted into the SimaPro software using the cut-off approach and analysed using the Cumulative Energy Demand (CED) method. The dataset illustrated the transfer of 1 MJ of electricity at a high voltage level inside the United Kingdom. It included the processes of electricity generation, transmission losses, and direct emissions. However, it does not account for losses that occur during voltage transformation or accidental emissions. The specific substances and their individual contributions to their corresponding impact categories are outlined in Table *5.16*.

Table 5.15: Different impact categories of CED method

Impact category	Unit	Total	%
Non-renewable, fossil	MJ	1.29	46
Non-renewable, nuclear	MJ	0.97	34
Non-renewable, biomass	MJ	2.02E-05	1E-03
Renewable, biomass	MJ	0.20	7
Renewable, wind, solar, geothe	MJ	0.32	11
Renewable, water	MJ	0.03	1
Total	MJ	2.82	100

Table 5.16:Different substances related to the impact categories of CED method

Substances	Unit	Total	%
Coal, brown	MJ	0.0069	0.5
Coal, hard	MJ	0.1267	9.8
Gas, mine, off-gas, process, coal mining/m3	MJ	0.0024	0.2
Gas, natural/m3	MJ	1.1022	85.4
Oil, crude	MJ	0.0518	4.1
Peat	MJ	0.0011	8E-02
Uranium	MJ	0.9670	100.0
Energy, gross calorific value, in biomass, primary forest	MJ	2.02E-05	100.0
Energy, gross calorific value, in biomass	MJ	0.2075	100.0
Energy, geothermal, converted	MJ	0.0001	4E-02
Energy, kinetic (in wind), converted	MJ	0.2377	75.1
Energy, solar, converted	MJ	0.0789	24.9
Energy, potential (in hydropower reservoir), converted	MJ	0.0333	100.0

The non-renewable fossil fuel was identified as the primary source, accounting for 46% of the overall energy use. The impact was categorised into six parts, revealing that the majority of power produced in the UK is derived from natural gas, accounting for 85.36% of the non-renewable fossil fuel sources. Peat was found to be a little source to non-renewable fossil fuels, accounting for

only 0.08%. Uranium was the sole substance in the model and hence made a 100% contribution to the non-renewable nuclear energy. When discussing the modelling of electricity mixes and technology mix in an energy market, it was crucial to comprehend the methodology used for modelling these mixes. According to Ecoinvent (Bo Weidema, 2003) the attributional systems model was built around the 2016 data from the International Energy Agency (IEA). This data includes information on power mixes for 142 countries, including the United Kingdom, which represented the whole world electricity generation. In contrast, the consequence system model incorporates the projected composition of the future electrical market in 40 countries, including the UK. This model covered 76.5% of global energy output and was based on forecasts from authoritative sources such as the European Commission and the IEA (2016). This raises important questions:

- How the data from the IEA are compared with the Ecoinvent database.
- How may SimaPro software be utilised to evaluate the environmental consequences of global or country-specific developments, such as those occurring in the UK?
- How might variations in outcomes effect the actual environmental impact of a product?

Upon analysing the IEA collected data, it was seen that the primary sources of energy generation in the year 2016 and according to the most recent data provided in 2022 are displayed in Table *5.17*, together with their respective contributions to the total electricity generation.

Table 5.17: Difference in electricity generation sources in the UK between 2016 and 2022

Electricity generation sources in UK	Value (GWh) year 2016	% Year 2016	Value (GWh) year 2022	% Year 2022
COAL	31435	9.3	7066	2.2
OIL	1890	0.6	2097	0.7
GAS	143356	42.5	125300	38.7
NUCLEAR	71726	21.3	47723	14.7
HYDRO	8329	2.5	7307	2.3
TIDE	0	0	9	2.8E-03
BIOFULES	27325	8.1	30666	9.5
WASTE	5628	1.7	9655	2.9
WIND	37159	11.0	80162	24.8
SOLAR	10395	3.1	13920	4.3
Total SOLAR, WIND	47554	14.1	94082	29.1
Total	337243		323905	

Table *5.17* revealed a significant shift in electricity generation sources in the UK between 2016 and 2022. Notably, the contribution of coal to the overall electricity generation decreased from 9.3% in 2016 to 2.2% in 2022. Conversely, the combined use of solar and wind power increased from 14.1% to 29.1% in 2022. It is widely recognised that the UK is actively pursuing a strategy to achieve net zero emissions by 2050(mikeinlondon, 2021). When striving for more precise outcomes, it was crucial to adjust to the ongoing changes. This was because the data in Ecoinvent, when employing the attributional technique, may not yield realistic results. Therefore, it was necessary to modify the contribution of energy generation sources in this case. However, it was crucial to note that Table *5.17* highlights the presence of certain sources in the SimaPro results that are not found in the IEA database. One such example was peat, which can influence the results and alter the environmental footprint of the product under study. There are several reasons that can be attributed to these modifications, such as data processing and harmonisation. The IEA provides raw statistical data, which may not be directly linked with the categories used in the Ecoinvent database. Another reason might be the temporal mismatches arise because Ecoinvent utilises data that was generally three years older than the database's release year. The 2016 IEA data utilised by Ecoinvent may have undergone distinct processing methods or been revised in following years. In addition to those reasons, the Ecoinvent database incorporates regional data adjustments, such as including peat in its UK dataset based on supplementary sources not included in the IEA's primary reporting. These adjustments highlight the differences in methodology, as Ecoinvent aimed to provide comprehensive LCA data and may incorporated additional sources to better align with these LCA models.

This study involved extracting and modifying data from 1 MJ obtained from SimaPro. The adjustments were made using the most recent data released by the IEA in 2022. The modifications included excluding data related to peat, reducing the quantity of coal used, increasing the utilisation of wind and solar energy, and eliminating both renewable and non-renewable biomass. The outcomes of the alternative methodology were displayed in Table *5.18* and Table *5.19*.These newly obtained results are subsequently utilised in the study.

Table 5.18:New values of the impact category based on the IEA (2022)- Cut-off approach

Impact category/ *Substances*	SimaPro Value (MJ)	New Value based on IEA in 2022 (MJ)
Non-renewable, fossil	1.29	1.24
COAL	0.13	0.06
GAS	1.11	1.15
OIL	0.05	0.02
Peat	1.05E-03	-
Non-renewable, nuclear	0.97	0.44
Non-renewable, biomass	2.02E-05	-
Renewable, biomass	0.21	-
Renewable, wind, solar, geothe	0.32	0.87
Renewable, water	0.03	0.07
TOTAL	2.82	2.61

Table 5.19: New values of the impact category based on the IEA (2022)- APOS approach

Impact category/ *Substances*	SimaPro Value (MJ)	New Value based on IEA in 2022 (MJ)
Non-renewable, fossil	1.44	1.32
COAL	0.25	0.07
GAS	1.12	1.23
OIL	0.07	0.02
Peat	1.19 E-03	-
Non-renewable, nuclear	1.04	0.47
Non-renewable, biomass	4.03E-05	-
Renewable, biomass	0.19	-
Renewable, wind, solar, geothe	0.27	0.92
Renewable, water	0.03	0.07
TOTAL	2.98	2.78

5.4.2 EN15804 + A2

The EN 15804+A2 standard is a specific impact assessment methodology designed specifically for the construction industry. It establishes Product Category Rules (PCRs) for construction products and services guaranteeing the comparability of Environmental Product Declarations (EPDs) within the sector (EPD, 2024). The A2 amendment, implemented in 2019, aligns the

standard with the methodology of the Environmental Footprint (EF) 3.0, as stated by the European Commission.

Both the EN 15804+A2 and EF 3.0 methodologies have similarities, especially in how they incorporate compatible adaptations with data libraries like those available in SimaPro. Nevertheless, the only significant distinctions between the two methods, notably in the characterisation factors employed for particular impact categories, such as climate change and climate change-biogenic. The EN 15804+A2 standard includes 27 impact categories, as shown in Table *5.20*.

Table 5.20: Different impact categories of EN 15804+A2 method

Impact category	Unit
Acidification	mol H+ eq
Climate change	kg CO_2 eq
Climate change - Biogenic	kg CO_2 eq
Climate change - Fossil	kg CO_2 eq
Climate change - Land use and LU change	kg CO_2 eq
Ecotoxicity, freshwater - part 1 and 2	CTUe
Ecotoxicity, freshwater - inorganics	CTUe
Ecotoxicity, freshwater - organics - p.1 and 2	CTUe
Particulate matter	disease inc.
Eutrophication, marine	kg N eq
Eutrophication, freshwater	kg P eq
Eutrophication, terrestrial	mol N eq
Human toxicity, cancer (inorganic & organic)	CTUh
Human toxicity, non-cancer (inorganic & organic)	CTUh
Ionising radiation	kBq U-235 eq
Land use	Pt
Ozone depletion	kg CFC11 eq
Photochemical ozone formation	kg NMVOC eq
Resource use, fossils	MJ
Resource use, minerals and metals	kg Sb eq
Water use	m3 depriv.

The focus was on the impact categories of climate change, acidification, human toxicity, land use, ozone depletion, photochemical ozone formation and water use. Certain impact categories are further subdivided into subcategories such as climate change and human toxicity, and their equations (5.23) and (5.24) are presented as follows.

$$CC = CC_B + CC_F + CC_L \quad (5.23)$$

$$HT = HT_{Ci} + HT_{Co} + HT_{NCi} + HT_{NCo} \quad (5.24)$$

where the overall climate change, denoted as CC is the combined effect of three factors: climate change associated with fossil fuels CC_F, climate change associated with biogenic sources CC_B and climate change associated with land use CC_L. HT is the total human toxicity which is the sum of human toxicity cancer, both organic HT_{Co} and inorganic HT_{Ci}, and the human toxicity non-cancer, both organic HT_{NCo} and inorganic HT_{NCi}.

The SimaPro database for climate change impact assessment identified 42 compounds that contribute to this specific category. Among them, carbon dioxide emitted by fossil fuels is the most significant, accounting for 86% of the results(SimaPro database manual Methods library, 2020). The remaining 41 substances are a combination of methane emitted by fossil fuels and carbon dioxide produced by biogenic sources. In the case of acidification, six substances were responsible for this environmental impact. The majority, 93%, consisted of a combination of sulphur dioxide and nitrogen oxides. The remaining 7% was divided among the other four substances, with ammonia being the highest among them, followed by nitrogen monoxide, sulphur oxides, and sulphur trioxide. The modification in the CED would influence the impact categories of the EN 15804 + A2. The reduction of various energy sources in the CED would have diverse effects on the environmental impacts of EN 15804 + A2, depending on their specific features and the context in which they are utilised. Below is a comprehensive analysis of these effects:

A. Non-renewable fossil
    - Climate change-fossil: It directly decreases since it assesses the effect of greenhouse gas emissions from fossil fuels.
    - Climate change-land use and LU change: Reducing the utilisation of fossil fuels results in decreased extraction of fuel, which in turn frequently leads to modifications in land use. Nevertheless, this study did not consider these alterations due to complexity and lack

of data. Like water use, land use impact, and ozone depletion, the reduction of fossil fuel may also lead to a decrease in these factors.

- Acidification: The decrease is expected as a result of the reduction in emissions of SO_2 and NO_x from the combustion of fossil fuels.

B. Non-renewable nuclear
   - Climate change: Minor effect, as nuclear energy has low direct greenhouse gas emissions. This also applies to ozone depletion.
   - Acidification: Due to the minimal impact, no alterations were considered essential since nuclear energy shows low levels of SO_2 and NOx.

C. Non-renewable biomass
   - Climate change-biogenic: When removing non-renewable biomass in CED, the impact of climate change caused by biogenic factors was deemed insignificant, as biomass emits biogenic CO_2.

D. Renewable biomass, wind, solar and water
   - Climate change: Renewable energy sources do not emit greenhouse gases directly. Nevertheless, the production procedures of these technologies can result in environmental effects, mostly linked to the utilisation of fossil fuels. The effects mentioned were not examined in this specific case, and hence no alterations were considered.
   - Land use: The land use can be influenced by the expansion of renewable energy sources, particularly if these alternative energy sources need larger land areas.

A comparison analysis was conducted using SimaPro using the EN 15804 + A2 methodology to modify the estimates of these consequences for a 1 MJ energy input. The CO_2 emissions resulting from the use of fossil fuels were divided by the non-renewable fossil fuel results obtained using the CED approach. The factors are displayed in Table *5.21* and subsequently multiplied by the updated values derived from the IEA data in the year 2022. A similar approach for the acidification was carried out and the findings were documented in

Table *5.22* and

Table *5.23*. The revised impact values for the 1 MJ of electricity have been compiled in

Table *5.24* and was be utilised for this study.

Table 5.21:CO_2 emissions and non-renewable fossil factors across different assessment approaches

Approaches	CO_2, fossil	Non-renewable fossil	Factor
Cut-off	0.08	1.29	0.06
APOS	0.08	1.44	0.06

Table 5.22:NOx emissions and non-renewable fossil factors across different assessment approaches

Approaches	NOx, Acidification	Non-renewable fossil	Factor
Cut-off	1.08E-04	1.29	8.36E-05
APOS	1.14E-04	1.44	7.94E-05

Table 5.23:SO_2 emissions and non-renewable fossil factors across different assessment approaches

Approaches	SO_2, Acidification	Non-renewable fossil	Factor
Cut-off	1.56E-04	1.29	1.21E-04
APOS	1.76E-04	1.44	1.22E-04

Table 5.24:Difference between the amended values and the SimaPro values for acidification and climate changes with different system approaches

Impact category	Cut-off		APOS	
	SimPro Value	New Value	SimPro Value	New Value
Acidification	2.87E-04	2.76E-04	3.11E-04	2.87E-04
Climate change	8.42E-02	4.88E-02	9.97E-02	6.64E-02

5.4.3 Additional changes in the system model

5.4.3.A Transportation

Transportation played a significant role in this study, encompassing seven different aspects. The transportation of silicon tetrachloride to the fumed silica manufacture, the transport of TNF waste to the TNF manufacture, and the transportation of processed TNF and FS to the VIP manufacture in the first LCA study (cradle to the gate) were considered. In addition, the second LCA study focused on the transportation of VIPs from the VIP manufacturing facility to the car painting booth. It also investigated several transportation scenarios at the end-of-life stage. The

scenarios involved either transporting used VIPs to a landfill (cradle to grave, first option) or returning them to the VIP manufacturing site for reuse (cradle to cradle, second option).

SimaPro offers three choices for road transport: small trucks (less than 10 tonnes) with an average load capacity of 3 tonnes, medium-sized vehicles (10-20 tonnes) with an average load capacity of 6.2 tonnes and large trucks (above 20 tonnes) with an average load capacity of 24 tonnes. The study examined various vehicles, including the Atego 818 and Eurocargo 120E18, which have different emission standards ranging from EURO1 to EURO5. Each truck was evaluated based on its overall weight, load capacity, and fuel consumption under both full and empty load conditions. The values in Table *5.25* were derived from the study by Blonk et al. (2023), which presents empirically measured fuel consumption ranges for commercial freight vehicles operating under varied loading conditions and road types. This source was selected due to its high data resolution, inclusion of both loaded and empty states, and relevance to European transport contexts. While SimaPro provides pre-modelled emission factors for trucks based on tonne-kilometre (tkm), it lacks flexibility in directly adjusting for fuel consumption variation by road type or load status. Therefore, using real-world fuel consumption data allowed for a more granular and representative estimation of transport-related emissions. This approach ensures that fuel usage is not treated as linearly dependent on distance alone, but also accounts for the physical behaviour of trucks under realistic driving conditions, which is particularly important when modelling end-of-life transportation in cradle-to-cradle systems.

Table 5.25: Fuel consumption when fully loaded and empty for different sized trucks

Size of the truck	Fuel consumption (l/km)	
	When fully loaded	When empty
Small	0.18	0.13
Medium	0.26	0.19
Large	0.39	0.28

The calculation of total fuel consumption was determined by categorising roads into three types. In 2010, trucks spent the least amount of time in urban areas, accounting for 17.5% of the total time. Additionally, 22.1% of the distance covered was on country roads, while the majority, 60.4%, was on highways. The emission factor for fuel was based on the Intergovernmental Panel on Climate Change (IPCC) guidelines, which stated that the emission of CO_2 per litre of fuel was 2.64 (IPCC, 2023).

When utilising the EN15804 + A2 method on SimaPro to input 1 tkm for each type of three sized truck, the climate change findings are as follows: 0.31 kg CO_2 eq for small trucks, 0.22 kg CO_2 eq for medium trucks, and 0.085 kg CO_2 eq for large trucks. There was a total of 35 distinct substances assessed for this impact category, with carbon dioxide accounting for 86% of the overall contribution. The carbon dioxide readings were 0.27 kg CO_2, 0.19 kg CO_2, and 0.073 kg CO_2, respectively. The method for calculating the emission per tkm was determined using the equation (5.25).

$$Emission\ per\ tkm = \frac{Fuel\ consumption\ \times Emission\ of\ fuel}{Load} \quad (5.25)$$

The emissions resulting from the combustion of fuels and the wear and tear of roads were determined based on the findings of Klein (2018) in Netherlands. Controlling fuel usage and distance separately in SimaPro was challenging due to the truck's input being only in tonne-kilometre. Furthermore, SimaPro only provided particular load factors (%LF), representing the percentage of the truck's load capacity that was occupied. These load factors were limited to 20%, 50%, 80%, and 100%. Furthermore, the SimaPro model for trucks now includes only up to EURO5 emission standard. However, the European Commission has recently proposed a new emission standard for road vehicles, known as EURO7, on November 9th, 2022 (European Comission, 2022). In SimaPro, it was observed that increasing the tkm value results in a linear increase in emissions. However, this relationship does not adequately reflect real-world conditions. Given the limits and uncertainty, it was necessary to develop a customised method to accurately evaluate the environmental impact. According to equation (5.25), all the components remain unchanged, except for the overall fuel consumption which increases with distance. However, the fuel consumption per unit distance remains consistent. Hence, the emissions per tonne-kilometre (tkm) were calculated using equation (5.25), whereas the total fuel consumption was determined using modified assumptions.

To overcome the limitations of the fixed truck profiles available in SimaPro (which are restricted to EURO 1–5 engines and limited load factor resolution), a more recent truck model was selected to estimate real-world fuel consumption. The selected model truck was the Mercedes Benz Actros L equipped with a EURO VI engine, 7.7 L in size, boasting a total power output of 175 kW, and a load capacity of 6.2 tonnes (Mercedes-Benz, 2023). This choice reflects the current European transport fleet and ensures that the emission modelling remains aligned with present-day policy and technology standards.

The fuel consumption of this vehicle ranges from 25 to 35 litres per 100 km, depending on factors such as road conditions and the amount of load it carries. The truck was estimated to consume 35 litres per 100 km when driving in urban areas, 30 litres on country roads, and 25 litres on highways when carrying a load. When the vehicle was empty, it was projected to consume 25 litres per 100 km on all three types of roads. The distance covered from the source of the raw material to the manufacturing facility where the raw materials are processed was 200 miles. The same distance was also accounted for from the manufacturing facility where the raw material was processed to the VIP manufacturing facility. The assumed distance from the VIP manufacturing facility to the car painting booth was 500 miles, while the distance to carry the used VIP to the landfill or back to the manufacturing facility was also 200 miles. The overall fuel use would be 224.14 litres (190.52 kg, assuming a diesel density of 0.85 g/ml (Osman and Stefaniu, 2023) for every 500 miles travelled when fully loaded. When the vehicle is loaded, the fuel usage covered by the 200 miles distance would be 89.66 litres (76.21 kg), and when it is empty on the return trip, the fuel usage would be 201.17 litres (170.99 kg) per 500 miles and 80.47 litres (68.39 kg) per 200 miles. The newly introduced impact categories, specifically climate change and acidification, are displayed in Table *5.26*.

Table 5.26: The new impact categories based on the load of the truck of different materials

Truck loading different materials	Load (tonnes)	Emission per tkm (kg CO_2 eq)	Climate change (kg CO_2 eq)	Acidification (mol H+ eq)
Silicon tetrachloride	5.92	1.46	59.82	0.43
TNF waste	6.15	1.41	59.77	0.43
TNF processed	2.64	3.27	61.64	0.43
FS	2.19	3.95	62.31	0.43
VIPs	0.64	13.52	159.43	1.07

5.4.3.B Land use

The Land use impact category utilising EN15804+ A2 was excluded because of its intricate nature and lack of assurance. The only assumption used was to calculate the emissions of gases, such as CO_2 and CH_4, during the degradation of TNF, based on its chemical composition. Additionally, the area of land required for the disposal of materials, such as FS, was determined based on the quantity and density of the material. The findings are presented in chapter 6.

5.4.3.C Biological decomposition of TNF

TNF mostly contains cellulose, hemicellulose and lignin. The degradation of these molecules occurs primarily through anaerobic microbial degradation over time (Barlaz, 2006). The decomposition of cellulose and hemicellulose takes place according to the equations (5.26) and (5.27) respectively.

$$(C_6H_{10}O_5)n + nH_2O \rightarrow 3nCO_2 + 3nCH_4 \quad (5.26)$$

$$(C_5H_8O_4)n + nH_2O \rightarrow 2.5nCO_2 + 2.5nCH_4 \quad (5.27)$$

One kg of sample would be decomposed to 491 g of carbon dioxide and 178.8 g of methane which was due to the decomposition of cellulose and hemicellulose. Lignin is more resistant unlike cellulose or hemicellulose towards degradation. It decomposes very slowly but eventually forms humic substances and landfill gases.

5.5 Cradle to gate results

The first part of this LCA study involved the processing of TNFm, TNFs, and TNA derived from tree-based waste, while the second part focused on the processing of FS from silicon tetrachloride. Both segments were categorised under cradle to gate, utilising the primary functional unit defined by the truck's maximum load capacity, which was set at 6.2 tonnes.

The third part extended the cradle to gate analysis, incorporating the findings from both the first and second parts, along with the manufacturing process of the VIP. This stage was drawn up based on a new functional unit, defined as the standard dimensions of the VIP (1 m^2 x 0.025 m). A cut-off approach was employed to conduct a thorough analysis of two methodologies: Cumulative Energy Demand (CED) and EN15804 + A2 (European standard), along with their respective impact categories.

5.5.1 Cradle to gate (TNF) 1st FU

The process begins with the packaging of tree-based fibre waste, considered to be the raw material prior to the processing of TNFm, TNFs, and TNA. Based on the calculation in section 5.3.7 it was estimated that 53 boxes, each weighing 0.5 kg, were required, resulting an overall truck load of 6121.5 kg, which was within the truck's maximum load capacity of 6200 kg. The procedure involved transporting the packaged raw material to the TNF manufacturing facility, located 500 miles away, where the TNF waste was subjected to grinding, drying, and sieving to produce TNFm and TNFs. As explained in section 3.1.1, 28% of the TNF waste was converted to TNFm (1709.6 kg out of 6105.6 kg), while 11% was converted to TNFs (671.6 kg out of 6150.6

kg). The remaining 61% of the sieved TNF underwent pyrolysis in an industrial furnace to form TNA (CC), representing 4.27% of the original TNF raw material (260.7 kg out of 6105.6 kg).

During TNA pyrolysis, degassing occurred, emitting carbon dioxide (491 g) and methane (178.8 g) per kilogramme of TNF, as described in section 5.4.3.C. The pyrolysis stage exclusively focused on carbon dioxide emissions, as methane is generally captured for alternative applications instead of being emitted into the atmosphere. This would result in a rise of the climate change impact regarding the pyrolysis of TNA. In addition, a direct pyrolysis for TNA has been assessed in case where the end user only required TNA, utilising only a grinder and furnace, without the need for sieving and drying. For TNA (D), the entire 6105.6 kg was utilised to produce 427.4 kg of TNA through direct pyrolysis.

Figure *5.2* illustrates the environmental effects of acidification, climate change, non-renewable energy, and renewable energy concerning the processing of TNFm, TNFs, TNA (CC), and TNA (D). Impacts are presented as percentages, in relation to the maximum value for each category; for instance, the acidification value during the pyrolysis of TNA (CC) in the furnace was 1.41 mol H+ eq (100%), whereas the acidification value for TNA (D) was 0.91 mol H+ eq (64%). The results indicated that among all TNF samples, the highest energy consumption during TNA (CC) pyrolysis was attributed to the furnace, which consumed 7639.9 MJ for the complete cycle, followed by 5093.3 MJ for direct TNA pyrolysis. Despite the increased material usage in TNA (D), its lower energy consumption compared to TNA (CC) can be attributed to the disparity in density; sieved TNF exhibited a lower density than non-sieved TNF, resulting in longer furnace operation for TNA (CC). The third highest energy consumption was associated with the drying of raw TNF, necessary for all samples except TNA (D), amounting to 1567.1 MJ. This was followed by grinding, utilised in all four samples, which consumed 527.8 MJ. Sieving exhibited the lowest energy consumption at 5.2 MJ.

The energy values were derived from the most recent IEA data (2022) for 1 MJ of electricity in the UK, with 64.1% sourced from non-renewable origins and 35.9% from renewable sources. The effects of climate change and acidification were directly linked to the consumption of non-renewable energy, with 73.8% of this energy derived from fossil fuels, resulting in CO_2 emissions. Hence, this implied that greater energy consumption correlates with increased climate change and acidification impacts. It was evident in all cases represented in Figure *5.2*, with the exception of the furnace applications for TNA (CC) and TNA (D). The difference can be ascribed to the degassing effect of TNF, wherein TNA (D) exhibited a 30% reduction in energy consumption compared to TNA (CC), yet climate change impact was 26.83% greater than that of TNA (D)

knowing that TNA (CC) utilised 1.6 times less material than TNA (D). The impact of TNF degassing surpassed the carbon dioxide emissions from fossil fuels utilised in TNA pyrolysis.

Packaging materials differed based on the specifications outlined in Chapter 5. Energy consumption data for the production of each packaging type was obtained from the ecoinvent library. Fertiliser packaging for TNA (D) and TNA (CC) necessitated 1.8 MJ per kilogramme, comprising 96% from non-renewable and 4% from renewable energy sources. The second category of packaging, folding boxboard carton, was utilised for raw materials, TNFm, and TNFs, necessitating 29.7 MJ per kilogramme, with 78% derived from non-renewable sources and 22% from renewable sources. The packaging of raw material and TNF exhibited a greater environmental impact than TNA packaging due to elevated energy demands.

For the remaining part of the study, TNA (CC) was selected as it achieves a complete pyrolysis utilising 100% tree-based waste. All processed tree materials were packaged and transported from the tree-based manufacturing facility to the VIP manufacturing site at once.

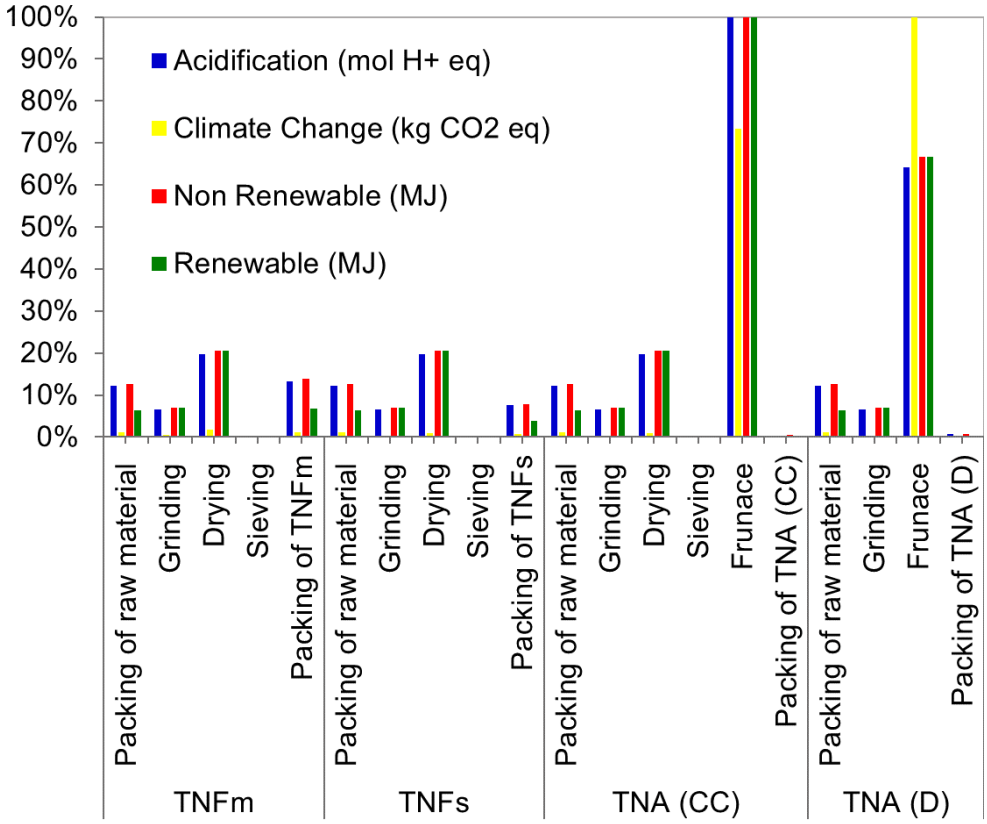

Figure 5.2.LCIA results for the production of TNFm, TNFs, TNA (CC) and TNA (D)

5.5.2 Cradle to gate (FS) 1st FU

In the context of FS production, silicon tetrachloride was selected as primary raw material, with data obtained from the ecoinvent library. The electricity utilised in the production of $SiCl_4$ was presumed to be modelled according to the Rest-of-World (RoW) framework.

For precision the electricity value was converted using UK-specific energy parameters, as it was presumed that this LCA was conducted in the UK. The results indicated that the production of 1 kg of $SiCl_4$ consumed 14.2 MJ, of which 10.4 MJ was derived from non-renewable sources and 3.8 MJ from renewable sources. The packaging of $SiCl_4$ differed from that of TNF and TNA due to $SiCl_4$ being a volatile liquid. According to section 5.2.6, the maximum quantity of $SiCl_4$ transported to the FS manufacturing facility was 5920 kg, with the IBC weight being 240 kg. The $SiCl_4$ was converted into FS, yielding a total mass of 2840.5 kg of FS, with an energy consumption of 94700 MJ. The findings of the comparison between TNF and FS are illustrated in Figure *5.3*. Based on the first FU (6200 kg maximum truck capacity) the results for the impact category showed that:

I. **Non-Renewable energy:** The production of $SiCl_4$ exhibited the highest energy consumption from non-renewable sources, amounting to 61973.5 MJ, followed by the production of FS at 60748.5 MJ. The transportation of materials from the extraction site to the processing facility and from the processing facility to the VIP manufacturing site consumed 8009.9 MJ, primarily due to diesel usage, as detailed in section 5.4.3.A. The processing of all TNF materials (TNFmm, TNFs, and TNA (CC)) consumed 6245.5 MJ, which was 19.6 times lower than both $SiCL_4$ and FS non-renewable impact. The packaging of $SiCl_4$ exhibited a significantly higher electricity consumption from non-renewable sources, totalling 7750.19 MJ, even surpassing the total energy required for processing TNF materials. The packaging of TNF processed material necessitated 1079.7 MJ, distributed as 62.6% for TNFm, 35.6% for TNFs, and 1.8% for TNA. The difference can be attributed not only to the higher energy consumption associated with the production of folding carton boxes compared to fertiliser bags, but also to the quantity of material contained within the packages. The quantity of bags required for FS exceeded that for TNA by 1278 bags, leading to an additional 895.4 MJ for non-renewable impact.
II. **Renewable energy:** The production of FS consumed the highest amount at 33990.2 MJ, surpassing the production of $SiCl_4$, which consumed 22168.5 MJ. The discrepancy arises from the assumption that the FS was produced using the UK grid power (2022 data). However, the $SiCl_4$ data sourced from the ecoinvent database indicated 26.4% of its

production used renewable power with FS using 36% of it. The processing of TNF material exhibited the third highest renewable impact, primarily due to the UK grid electricity utilised by the furnace, which accounted for 78% of the total value of 3494.5 MJ. The transportation of the materials had a minimal renewable impact (or highest negative environmental impact) due to the use of diesel fuelled lorries, which consumed 26.92 MJ.

III. **Climate Change:** As predicted, increased utilisation of non-renewable energy resulted in a greater impact on climate change, primarily attributable to CO_2 emissions from the combustion of fossil fuels. The maximum values were for the production of $SiCl_4$ and FS, at 3024 kg CO_2 eq and 2964.5 kg CO_2 eq, respectively. This was applicable to all processes depicted in Figure *5.3*, except for TNF processing. While the non-renewable value associated with TNF processing was lower than that of transport, the climate change impact was significantly greater for TNF processing. The climate change value for transport was 450.65 kg CO_2 eq, whereas the value for TNF processing was 2028.5 kg CO_2 eq, primarily attributed to the operation of the furnace, which emitted CO_2 as a result of material degradation, accounting for 77.8% of the total value.

IV. **Acidification:** Similar to the climate change impact the acidification impact also increased with the increase of usage of non-renewable energy as more SO2 and NOx were emitted with combustion of fossil fuels. The degradation of TNF material did not directly cause acidification; the primary influence was associated with electricity consumption, especially from non-renewable sources. The findings indicated that $SiCl_4$ production exhibited the most significant acidification effect, measuring 17.1 mol H+ eq, while the minimal value was recorded in the packing of TNF waste, with a value of 9.2×10^{-4} mol H+ eq.

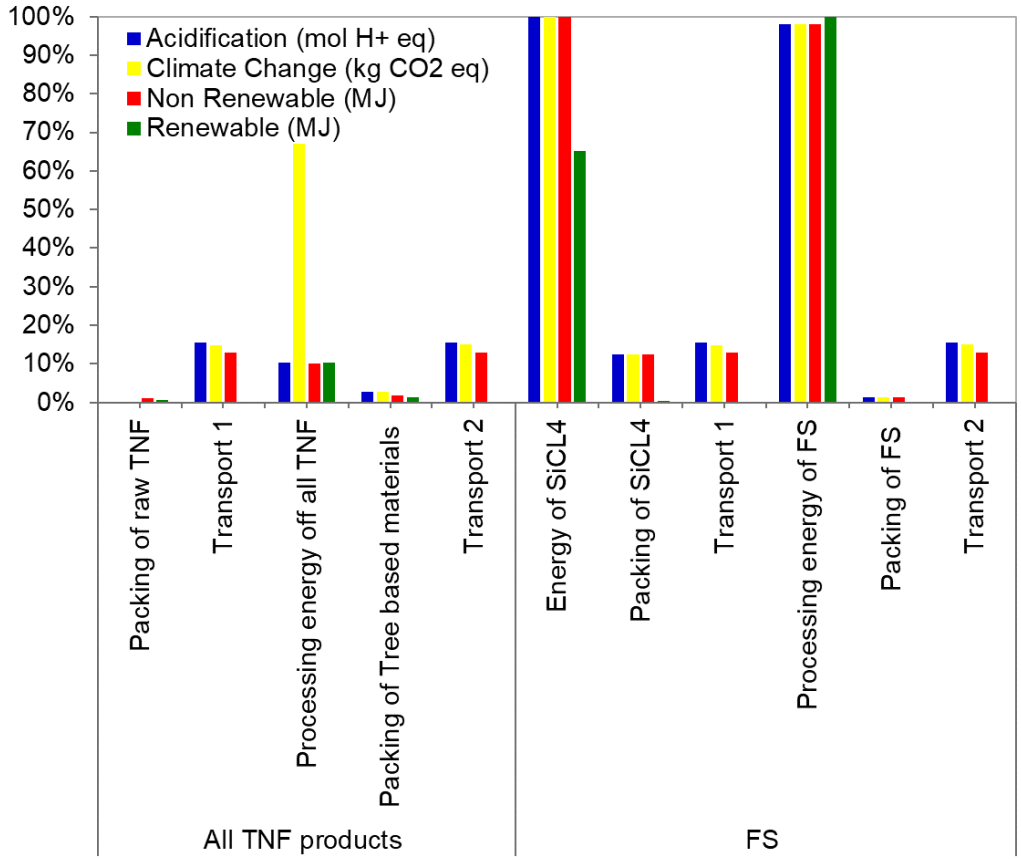

Figure 5.3 LCIA results comparing the production of all TNF products with the production of FS

5.5.3 Cradle to gate 2nd FU

The primary objective of the study was to assess the environmental impact of various core materials utilised for VIPs; consequently, a second FU unit was employed, featuring a VIP core dimension of 1 m by 1 m with a thickness of 25 mm. Each VIP created for this study was designed with a core density of 200 $kg.m^{-3}$, equivalent to 5 kg of material per VIP. Although the second FU was originally assigned as the only metric, the first FU was integrated for better precision. Based on the results obtained from section 5.5.2 the new values for one core material are presented in Table *5.27* and Figure *5.4*.

Table 5.27: LCIA results of the core energy production of TNFm, TNFs, TNA and FS

	TNFm	TNFs	TNA	FS
Acidification (mol H+ eq)	0.02	0.04	0.10	0.07
Climate Change (kg CO_2 eq)	2.68	6.83	49.60	18.44
Non-Renewable (MJ)	56.06	139.92	439.25	377.90
Renewable (MJ)	5.59	12.66	71.36	149.07

The study revealed that the non-renewable impact for the processing of FS, including $SiCl_4$ production, amounted to 316.4 MJ per 5 kg of FS, the highest among all materials studied. The packing of raw material ($SiCl_4$) and the packing of FS based on the second FU cumulatively amounted to 20.3 MJ, with the packing of raw material constituting 87.3% of this total value. The cumulative value for transport 1 (from the extraction site to FS manufacture) and transport 2 (from FS manufacture to VIP manufacture) was 41.4 MJ, representing a 10.7% contribution to the total value of 377.9 MJ presented in Table *5.27*.

Conversely, TNA's non-renewable impact was inferior to that of FS, recorded at 119.8 MJ. However, the addition of both transport 1 and 2 resulted in a combined non-renewable value of 308 MJ, constituting 70.2% of the total value of 439.5 MJ presented in Table *5.27*, thereby yielding a greater total non-renewable impact for TNA compared to FS. The rationale was based on the fact that the FS truck contained 1735.8 kg of FS, whereas the TNA truck held only 260.7 kg of TNA, thereby highlighting the significance of transportation in this case study and highlighting the value of the initial functional unit employed. In the absence of the initial FU, the results would suggest that the energy consumption for producing 5 kg of FS would exceed that of TNA in terms of non-renewable source utilised. In reality, FS's energy consumption for transportation per unit of material was lower than that of TNA, resulting in decreased total non-renewable impact. The same approach was applied to TNFm and TNFs, as larger amount of TNFm was processed and transported, led to a reduced overall non-renewable energy impact.

In the context of renewable energy impact, it was demonstrated that FS exhibited the highest value of 149 MJ, with 148.5 MJ derived from the production of $SiCl_4$ in addition to the production of FS. Despite TNA's higher need for energy in transportation, the minimal dependence of diesel production on renewable sources limited TNA's total renewable energy utilisation to 1.04 MJ, which was the highest among the four materials studied.

TNA exhibited the highest value of 48.6 kg of CO_2 eq per 5 kg, attributed to elevated energy consumption from non-renewable energy sources (fossil fuels) and the CO_2 degassing that occurred during the pyrolysis of TNA. TNFm exhibited the minimal climate change impact, recording a value of 2.7 kg of CO_2 eq per 5 kg. The acidification per core of VIP was minimal, with the highest value for TNA at 0.09 mol H+ eq and the lowest for TNFm at 0.01 mol H+ eq.

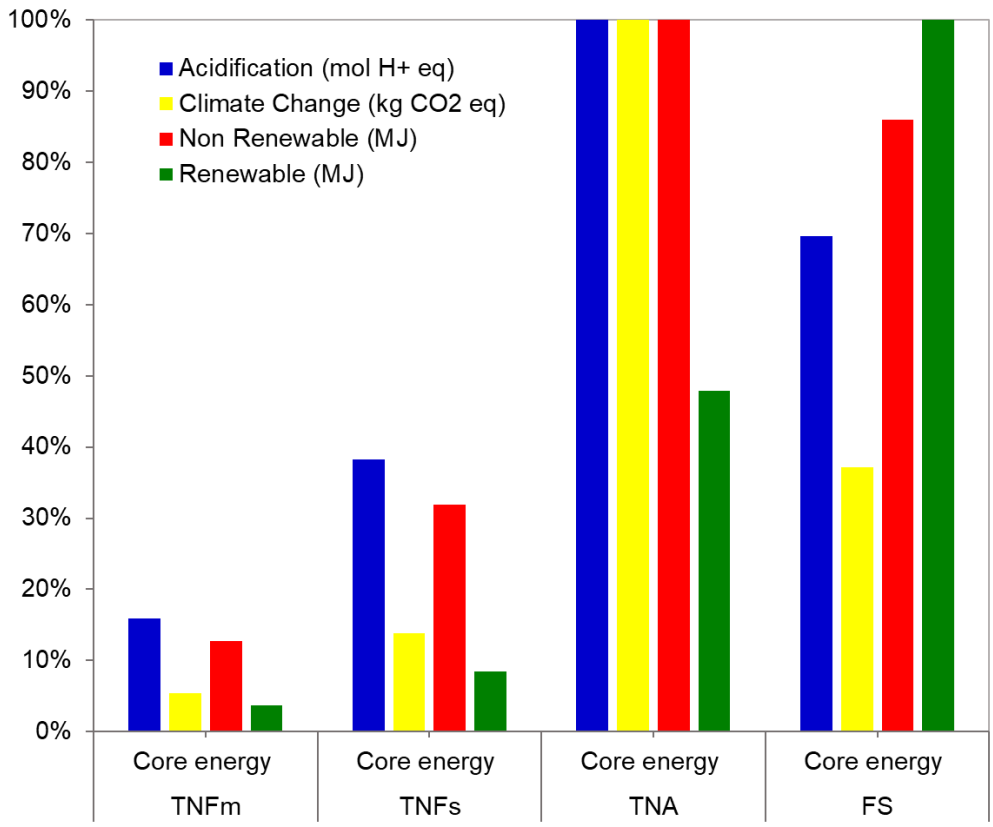

Figure 5.4LCIA results of the core energy production of TNFm, TNFs, TNA and FS

The preparation of the core material was not the only energy-intensive aspect of VIP manufacturing, as VIPs also comprised additional components like the envelope barrier and fleece to secure the core, along with numerous steps including core mixing, vacuuming, drying, and thermal performance testing. Table *5.28* outlines the various impact categories associated with the components and processes involved in the manufacturing of the FS-TNA1 VIP, comprising 30% TNA and 70% FS. Further core material findings are provided in the Appendix 3.

Table 5.28: LCIA results of the energy production of FS-TNA1 VIP

	Core	Mixing	Drying	Vacuuming	Testing	Envelope	Fleece
Acidification (mol H+ eq)	0.0754	0.0001	0.0029	0.0007	0.0015	0.0125	0.0007
Climate Change (Kg CO_2 eq)	27.79	0.01	0.51	0.12	0.27	2.22	0.13
Non-Renewable (MJ)	396.31	0.21	10.40	2.42	5.56	45.40	2.57
Renewable (MJ)	125.76	0.03	5.82	1.35	3.11	10.25	0.12

The results in Table *5.28* indicated that the primary contributor to the environment in the manufacturing process of a VIP was the preparation of the core material, accounting for 85.6% of the total value in the case of FS-TNA1. For the other studied VIPs, the values ranged from a minimum of 49.5% (in the case of TNFm VIP) to a maximum of 88.5% (in the case of TNA VIP). FS core contributed within 84.1% to the environment in the process of VIP production.

The envelope for the VIP was presumed to be aluminium foil and selected from the ecoinvient library. The electricity utilised in the envelope's production was presumed to be representative of Global (GLO), which averaged data from 43 countries (accounting for 95% of global GDP) and incorporated over 150 smaller nations categorised into five 'Rest of the World' groups by continent (SimaPro database manual Methods library, 2020).Transportation was included, and product losses during transit were deemed negligible. To ensure accuracy, the electricity value was adjusted according to UK energy consumption. The findings indicated that the production of 54 g of aluminium foil (the weight for a 1 m² VIP) required 45.4 MJ from non-renewable sources, ranking as the second highest after core processing. The fleece component, obtained from ecoinvent as nonwoven polypropylene fabric, was similarly modelled for GLO. It necessitated low non-renewable energy, utilising merely 2.6 MJ for the production of 30 g used per VIP.

The drying of the core prior to vacuuming the VIP constituted the third highest energy consumption, significantly influenced by the material's density before compression. As stated in chapter 5, the oven possessed an internal volume of 6.125 m³, necessitating the segregation of certain materials, such as FS, for drying, as the total weight of 640 kg of FS exceeded the oven's capacity, resulting in increased energy consumption. In this instance, FS-TNA required two drying cycle, resulting in a total of 10.4 MJ for each VIP core. The testing of VIP post manufacturing exhibited a total non-renewable impact of 5.6 MJ, owing to the utilisation of HFM and chiller, both of which were necessary for assessing the thermal conductivity of the VIP. Only one test was

necessary during the manufacturing process of 128 VIPs, as it was presumed that the remaining 127 VIPs would exhibit similar thermal conductivity. The vacuuming and mixing processes for each VIP core demonstrated the minimal non-renewable energy impact at 2.42 MJ and 0.21 MJ, respectively.

5.6 Core materials cost

In order to accurately evaluate insulation materials, it is crucial to carefully assess factors such as thermal conductivity, density, and the costs associated with both the material itself and its manufacturing process (Roberts et al., 2015). The current market value of TNF is £0.024 per kilogramme. The cost of the processed fibres (TNF_p) was calculated by considering the time it takes for the sieving process and the current average electricity cost in the United Kingdom. The material cost for TNA (TNA_p) was estimated and calculated accordingly, see equation (5.28). The cost associated with each core material, including the off the shelf prices of EPS (Business Analytiq, 2024) and FS (Alam et al., 2014) are outlined in Table *5.29*.

$$TNF_p = TNA_p = \sum \frac{(E \times e) + (RM \times Ca_{max})}{Ca_{max}} \tag{5.28}$$

where E is the energy consumption of each process (kWh), e average price of electricity (£0.34 per kWh), RM the raw material price (£.kg^{-1}) and Ca_{max} the total amount of material filled at maximum capacity of each process (kg).

Table 5.29: Core material cost of tree-based core materials, FS and EPS

Material	Material cost (£kg^{-1})
TNFm	0.14
TNFs	0.27
TNA (CC)	0.71
TNA (D)	0.45
FS	6.00
EPS	1.70

The study revealed that the cost of FS was significantly higher by approximately 43 times than that of TNFm, 22 times in case of TNFs and 8 times in case of TNA (CC). The core material cost was calculated using the equation (5.29) (Alam et al., 2014).

$$C_{core} = m_{FS} \times C_{FS} + m_{TNF1} \times C_{TNF1} + m_{TNF1} \times C_{TNF2} + m_{TNA} \times C_{TNA} \quad (5.29)$$

where C_{core} is the core cost per unit mass (£kg^{-1}); m_{FS}, m_{TNF1}, m_{TNF1}, m_{TNA} the masses of FS, TNFm, TNFs and TNA in 1 kg of the core material respectively; and C_{FS}, C_{TNF1}, C_{TNF2}, $C_{TNA}$the costs per unit mass for FS, TNFm,TNFs and TNA respectively.

The replacement of FS with TNF or TNA can clearly result in a substantial reduction in the cost of the core material, as shown in Table *5.30*. Increasing the content of TNFm to 30% led to a proportional reduction of 29.3% in the cost of the core material. Similarly, a 30% increase in TNFs content resulted in a 28.6% decrease in core price, while an increase in TNA led to a 26.5% decrease.

Table 5.30: Price of composites (FS-TNFm1, FS-TNs1 and FS-TNA1)

Core Material	Cost of core material (£kg^{-1})
FS-TNFm1	4.24
FS-TNFs1	4.28
FS-TNA1	4.41

5.7 Summary

The significance of selecting appropriate LCA approaches and methods, along with their rationale, was discussed in depth:

Data collection and calculations

- The energy consumption for grinding in order to produce 1 tonne of material was 32.7 kWh, 83.3 kWh, 214.7 kWh and 130.9 kWh for TNFm, TNFs, TNA when producing at complete cycle and TNA in direct pyrolysis.
- When it comes to TNA the direct pyrolysis required 14285.7 kg less by 1.6 times the amount of raw TNF needed to process TNA at complete cycle.

- The energy consumed in the direct pyrolisis was 1201.3 kWh while the energy for the complete cycle was more than double the energy consumed with 2702.9 kWh due to the high difference in densities.
- The energy consumption for grinding in order to produce 1 tonne of material was 53.8 kWh, 136.9 kWh, 352.6 kWh and 215.1 kWh for TNFm, TNFs, TNA(CC) and TNA(D).
- In the case of raw material packing 4.5% of the weight was lost in case of silicon tetrachloride while less than 1% of the weight was lost in the case of TNF.
- Although TNFm and TNFs had same energy consumption in the production process but the amount of material produced was larger in case of TNFm which means when comparing with the 2nd FU the overall energy consumption for TNFm was lower than that of TNFs.

Changes in the model

- The total energy consumption reduced from 2.82 to 2.61 MJ in the case of cut-off and reduced from 2.98 MJ to 2.78 MJ in the case of APOS.
- The most affected impact categories in EN15804+A2 by the changes in CED where the climate change in fossil and the acidification. At 1MJ of electricity use in the UK the new values of acidification and climate changes decreased by values ranging from 3.8% to 42.1% in the case of allocation.
- Transportation played a significant role in this study, encompassing seven different aspects. Given the limits and uncertainty, it was necessary to develop a customised method to accurately evaluate the environmental impact.
- The only assumption used was to calculate the emissions of gases, such as CO_2 and CH_4, during the degradation of TNF, based on its chemical composition. Additionally, the area of land required for the disposal of materials, such as FS, was determined based on the quantity and density of the material.

CHAPTER 6: An Example Application of the Developed VIP Materials

The three optimal core materials for each composite were selected (FS-TNFm1, FS-TNFs1 and FS-TNA1), along with the FS VIP, to serve as alternative insulation to the commonly utilised EPS in the Car Painting Booth (CPB). This selection aimed to evaluate the total energy consumption of the CPB over a decade of operation, considering the ageing effect of the VIPs.

Furthermore, the results of the CPB were utilised to evaluate a Life Cycle Assessment (LCA) of the VIPs (cradle to cradle), encompassing the extraction of core materials, production of VIPs, and transportation. Two LCA methodologies, cut-off and APOS, were employed utilising two environmental impact evaluation techniques: Cumulative Energy Demand (CED) and EN15804 + A2. Impact categories were analysed and adjusted based on electricity consumption in the UK.

The potential for reusing core material was experimentally evaluated, and its environmental impact was studied. Additionally, the cost per R-value of all manufactured VIPs at 20 ℃ and 70 ℃ was calculated.

6.1 Car Painting Booth (CPB)

Car painting booths, which are specialised environments, are utilised to attain a superior paint finish. It serves the purpose of containing and eliminating any excess paint and vapour that is produced during the spraying process. Booths are categorised based on the direction of the airflow, which can be classified into three main types: cross-draft, downdraft, and semi-downdraft. Cross-draft, also referred to as tunnel booths, are the most common type of booths used in painting operations. They are distinguished by their horizontal air flow that moves parallel to the floor. While, the downdraft booths provide a more advanced method for painting. This type of booth is ideal for high-quality paint jobs due to its design, which facilitates a downward flow of air from the ceiling to the floor, passing over the car or vehicle being painted. Furthermore, Semi-downdraft is a hybrid painting booth which combines both cross-draft and downdraft models. This system achieves a balance between the high cost of a downdraft setup and the more affordable option of a cross-draft setup. The cross-draft booth was selected for this study because it is the most commonly utilised booth and is more cost-effective compared to other models.

6.1.1 Model Geometry and materials

A COMSOL Multiphysics based three-dimensional finite element model of a cross-draft CPB was developed as shown in Figure *6.1*a. The booth consisted of a ceiling, a floor, and four structural. The dimensions of the booth were determined based on the standard size commonly found in the

market as well as the dimensions chosen for the car, see Table *6.1*. In addition, four sensors were positioned above the steel car to control the heating of the enclosed chamber, presented in Figure *6.1*b.

The walls were insulated using different insulation materials, primarily Expanded Polystyrene (EPS) known for their widely use in CPB and VIPs, with varying thicknesses (25 and 75 mm) and different core materials such as FS-TNFm1, FS-TNFs1, FS-TNA1 and FS.

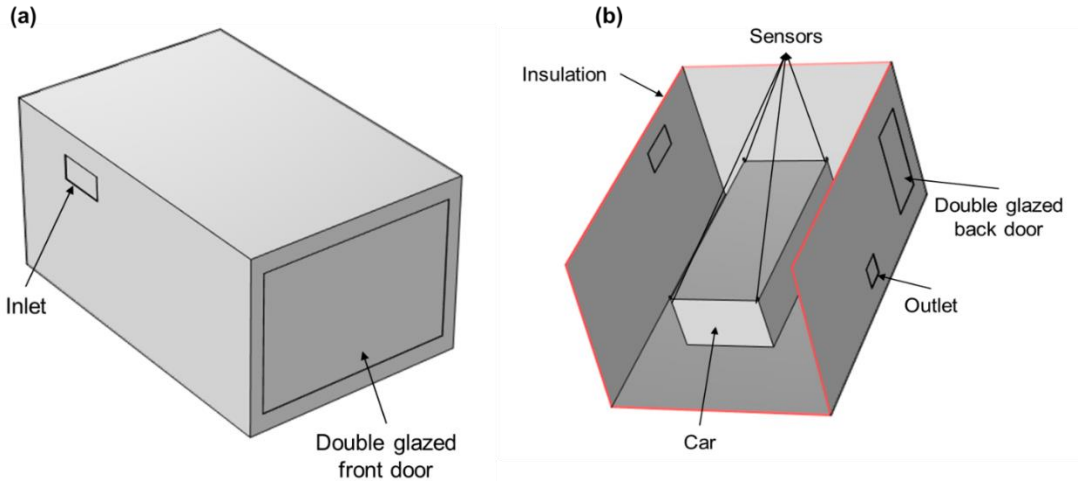

Figure 6.1 (a) Three-dimensional view and (b) internal view of the CPB studied

Table 6.1:Geometric parameters of the CPB components

Description	Value	Unit
Wall length	6.9	m
Wall width	4.5	m
Wall height	3.5	m
Insulation thickness	25	mm
Inlet area	0.5	m^2
Outlet area	0.25	m^2
Double-glazed glass front door area	9.6	m^2
Double-glazed glass back door area	2	m^2
Car length	4.5	m
Car width	1.8	m
Car height	1.2	m
Sensor volume	27	cm^3

6.1.2 Physics

The car painting booth model developed in COMSOL Multiphysics integrates multiple physical phenomena to precisely simulate the environmental conditions encountered during the painting process. The primary domains of physics encompassed in this context are turbulent flow, heat transfer in both solids and fluids, and surface-to-surface radiation.

6.1.2.A Turbulent flow (k-ω)

Fluid dynamics relies on a full understanding of flow regimes to effectively model and predict fluid behaviour. As flow of air in the car painting booth is in turbulent regime and there are obstacles in the booth. This results in the development of turbulent conditions within the booth. Furthermore, achieving a consistent air temperature within the painting booth is essential for optimising temperature uniformity as there is more intermixing in fluid flows.

Two widely used turbulent models are the k-omega ($k-\omega$) and k-epsilon ($k-\varepsilon$) models (Launder, 1995). Both models utilise a two-equation approach, employing transport equations for turbulent kinetic energy (k) and ω, which is also referred to as the specific dissipation rate or ε, which stands for the turbulent dissipation rate. However, the $k-\omega$ model was chosen because it provides various benefits, including improved accuracy near walls (Driver and Seegmiller, 1985). In a painting booth, the flow near walls or car surfaces has a significant impact on the overall fluid dynamics. The $k-\varepsilon$ model is not able to accurately capture the effects near the wall due to the high Reynold (Re) number flows. Moreover, the $k-\omega$ model demonstrates greater efficiency in flows with lower Re numbers and exhibits increased stability and reduced sensitivity to the complex geometry of the painting booth, as compared to the $k-\varepsilon$ model leading to more reliable and durable simulations.

6.1.2.B Heat Transfer in solids and fluids

In order to comprehend the temperature distribution and energy consumption during the operation of the car painting booth, it was crucial to simulate the thermal environment during the drying process. To accurately simulate the thermal environment, three main mechanisms of heat transfer were considered: conduction within the solid components of the booth (such as walls and car parts), convection within the fluid (air) domain and radiation among all indoor solid surfaces. The heat transfer phenomena in solids and fluids are described by equation (6.1) and equation (6.2).

$$\rho C_p \frac{\partial T}{\partial t} + \rho C_p u.\nabla T + \nabla.q = Q \quad (6.1)$$

$$q = -k\nabla T \quad (6.2)$$

where ρ is the material density, C_p the material specific heat, u the velocity field, T the temperature field, t the time, q the heat flux, Q the heat energy and k thermal conductivity.

6.1.2.C Surface to surface radiation

In order to accurately simulate heat transfer during the paint drying and curing process in the car paint booth, the COMSOL model incorporated diffuse surface to surface radiation to account for radiative heat transfer. The method considers the transfer of thermal radiation between all surfaces inside the booth. Diffuse surfaces uniformly reflect radiative intensity in all directions, which is essential for ensuring a consistent distribution of temperature. Equation (6.3) represents the radiative heat balance at surfaces. It quantifies the amount of heat that is emitted from a surface through radiation. If the irradiance exceeds the blackbody emissive power, the surface is deemed to absorb more radiation than it emits, resulting in a net heat flux into the surfaces. On the other hand, when the amount of irradiance is lower than the surface, it emits more radiation than it absorbs, resulting in a net heat flux out of the surface.

$$-n \cdot q = \epsilon\big(G - e_b(T)\big) \quad (6.3)$$

where n is the normal vector to the surface, q the heat flux, ϵ the emissivity, G the irradiance, $e_b(T)$ is the blackbody hemispherical total emissive power.

6.1.3 Boundary and initial conditions and assumptions and their justification

6.1.3.A Temperature control

The lifespan of car painting booths generally ranges from 10 to 20 years, depending on the quality of the booth and the maintenance practices used. For the study, it was assumed that the CPB would function for a duration of 10 years. During this time frame, it is expected that the thermal conductivity of insulation materials such as EPS or VIPs undergo alterations, potentially leading to significant impacts on energy consumption, heat loss, and subsequently, CO_2 emissions. Furthermore, external weather conditions have a crucial impact, as they can affect the initial temperature at which the CPB is set. It was assumed that the booth would start its operation at the ambient temperature of its surroundings. In the UK, the climate is defined by four distinct seasons: spring (March, April, May) with an average temperature of 11℃, summer (June, July, August) with 18.3℃, autumn (September, October, November) with 13.2℃, and winter (December, January, February) with 6.8℃. The seasonal averages were calculated using the

London climate data (BBC Weather, 2023). The 2021 Intergovernmental Panel on Climate Change (IPCC) report predicts that global temperatures could rise by approximately 0.1℃ to 0.3 ℃ every ten years, depending on the level of greenhouse gas emissions in the future (IPCC, 2021). Nevertheless, since the CPB is projected to function for only a duration of 10 years in this study, no modifications were made to the booth's set temperature in accordance with these predictions.

The model begins by regulating the air flow inlet of the car painting booth, where air enters the booth at a presumed velocity of 0.4 m/s (Goyer, 1995). The selected inlet velocity guarantees a uniform distribution of air within the cavity, directly influencing the mass flow rate, which is crucial for achieving adequate heat transfer within the booth. moreover, a heating system with a power rating of 20 kW was utilised to control the temperature of the incoming air. The heating system was responsible for increasing the temperature of the incoming air until the booth reached the desired temperature (T_{set}) of 70 ℃ and it was based on the time required to dry and cure the paint.

6.1.3.B Sensor mechanism

For improved temperature regulation, four sensors sized 3 x 3 x 3 cm^3 were carefully placed above the car within the CPB. The purpose of these sensors was to monitor the temperature within the booth. Once the average temperature of these sensors reaches 70 ℃, the system automatically stops the flow of hot air. The technique was crucial for assessing the energy efficiency of different insulation types used for the CPB. The inlet air temperature was determined using the energy balance equation. Equation (6.4) ensures that the heating system operates efficiently by maintaining the paint application process and only supplying heat when needed.

$$T_{in} = T_{out} + \left(\frac{P_{heater} \cdot step1(T_C)}{\dot{m} \cdot C_p}\right) \quad (6.4)$$

where, T_{in} is the inlet temperature of the air, T_{out} the outlet temperature, P_{heater} the heater power, $\dot{m}$ the mass flow rate of the air and C_p the average specific heat capacity of the air within the system, outlet and T_C the sensor temperature.

C_p was determined by considering the conditions at the outlet, which accurately represents the temperature state of the air as it exits the system. The calculation of this mean value was crucial in determining the amount of energy that was transported by the air. The function $step1(T_C)$ serves as a binary control that turns on or off the heater depending on the temperature reading from the

employed sensors. When T_C is lower than the T_{set}, the function has a value of 1, indicating that the heater is activated and energy is consumed. Once T_C reaches or surpasses T_{set}, the function value becomes equal to 0, causing the heater to turn off and no energy consumption to occur. The incorporation of this boundary condition and temperature control guarantees a more effective energy system for the car painting booth.

This study did not consider any potential leakage of air and heat through door gaskets.

6.2 Factors affecting the energy consumption of CPB

This section examines the energy consumption of CPB utilising various types of insulation, such as EPS and VIPs with different core materials (FS-TNFm1, FS-TNFs1, FS-TNA1, and FS). All VIPs possessed a uniform thickness of 25 mm, and the comparison primarily involved EPS of the same thickness, alongside a comparison with EPS at 75 mm. The CPB was modelled to function for 10 years in the UK across four distinct seasons (spring, fall, summer, and winter), considering only the degradation of various core materials of VIPs as outlined in section 4.5.2.B. The model was set up to run for four hours (240 minutes), with a target temperature of 70 ℃, as outlined in chapter 4. Initially, hot air enters the booth, and when the average temperature of the four sensors depicted in Figure 6.2 reaches 70 ℃, the inflow of hot air ceases, allowing only air to circulate within the booth. Once the average temperature of the sensors decreases below 70 ℃, hot air re-enters the booth to raise the temperature. The primary output of the model was the energy consumption during the booth's operation as well as the heat loss. A transient heat transfer model was employed in this study to accurately capture the temporal evolution of the thermal conditions within the CPB during each drying and curing cycle. Although the system parameters such as airflow velocity and heater power remained constant, the booth initiates each cycle from ambient temperature, which varies seasonally. Consequently, the total energy consumption must account not only for maintaining thermal conditions but also for the energy required to heat the internal air volume and surrounding surfaces. A steady-state model would neglect this energy associated with the thermal mass, thereby underestimating both heat-up time and actual consumption. The transient approach adopted herein enables the dynamic interaction between temperature, insulation performance, and operational cycles to be fully resolved over time, providing a more accurate representation of real-world CPB operation. The results were calculated using trapezoidal integration of the energy consumption curve. The following reasons significantly contributed to energy consumption:

I. **Ambient Temperature:** The climate in the UK is characterised by four distinct seasons: Spring (March, April, May) with an average temperature of 11℃; Summer (June, July, August) with 18.3℃; Autumn (September, October, November) with 13.2℃; and Winter (December, January, February) with 6.8℃, as detailed in section 6.1.3.A. The booth's initial value was chosen to correspond with the ambient temperature. For instance, with FS-TNFm1 VIP, the duration for the booth to reach 70 ℃ was recorded as 103 minutes in summer, 115.2 minutes in fall, 119 minutes in spring, and 130 minutes in winter. The operational time for drying and curing a car in a booth is reduced by 27 minutes in summer compared to winter, resulting in a 21.25% decrease in energy consumption between the two seasons. The energy consumption of CPB during the summer was 148.8 MJ, 167.4 MJ in the autumn, 173.12 MJ in the winter, and 188.9 MJ in the winter. The results of FS-TNFm1 at varying temperatures are illustrated in Figure 6.2. Energy consumption reductions ranging from 21.25% to 21.5% were observed across all VIP core materials and EPS.

II. **Thermal Conductivity:** The thermal conductivity significantly influenced energy consumption; lower thermal conductivity results in allowing the booth to reach 70 ℃ faster thereby reducing energy consumption. The thermal conductivity of VIPs with different cores changes with increasing temperature. As expected, CPB insulated with FS-TNA1 VIP exhibited the quickest time to reach 70 ℃, whereas EPS that had the highest thermal conductivity required the longest time to reach 70 ℃ inside the booth. For example, in winter at an ambient temperature of 6.3 ℃, the FS-TNA1 VIP required 129.3 minutes to attain 70 ℃ inside the booth, whereas the EPS required 167.8 minutes, which was 38.5 minutes longer than the CPB insulated with FS-TNA1 VIP, as illustrated in Figure 6.2. The substitution of EPS with FS-TNA1 VIP resulted in a decrease in energy consumption from 249.9 MJ to 188.2 MJ, representing an approximate reduction of 24.7% in a single cycle within the CPB. In comparing the various cores of VIPs, it was observed that the disparity between the lowest thermal conductivity value, FS_TNA1 (7.41 $mW.m^{-1}.K^{-1}$ at 70 ℃), and the highest thermal conductivity value, FS VIP (11.58 $mW.m^{-1}.K^{-1}$ at 70 ℃), resulted in a 1.9% decrease in energy consumption and a time variance of 2.8 minutes to attain 70℃ and a total energy consumption decrease of 11.6 MJ.

   For tree-based core materials, the variations in energy consumption were minimal, with FS-TNFm1 and FS-TNFs1 exhibiting only 0.4% and 0.6% greater energy usage relative to FS-TNA1. The influence of insulation on pre-heating was important, as FS-TNFm1

exhibited marginally lower thermal conductivity than FS-TNFs1 up to 50℃, yet slightly higher at 70℃, resulting in a minor decrease of 0.3 MJ in energy consumption per cycle. The reduction in energy consumption among VIPs with varying cores was minimal, attributable to a thermal conductivity difference of 3.94 $mW.m^{-1}.K^{-1}$ between the highest (FS) and lowest (FS-TNA1) values, resulting in a 1.9% reduction. Conversely, a significant reduction of 24.7% was observed between EPS and VIP insulation.

III. **Insulation thickness:** The thickness of the insulation significantly influenced energy consumption. The EPS utilised in the CPB originally had a thickness of 75 mm; however, this study employed VIPs with a thickness of 25 mm, as it was one of the functional units considered in the life cycle assessment. However, a comparison between 75 mm EPS and 25 mm VIPs was still important. The study demonstrated that, during winter, CPB insulated with a 75 mm EPS exhibited the quickest time to attain 70 ℃ inside the booth, achieving this in 126.3 minutes, which is 3 minutes faster than CPB insulated with FS-TNA1, as illustrated in Figure 6.3. Yet, the total energy consumption of CPB insulated with 75 mm EPS amounted to 189.4 MJ, exceeding that of FS-TNA1, FS-TNFm1, and FS-TNFs1, but lower than that of CPB insulated FS VIP (191.8 MJ). This can be ascribed to the increased thermal dissipation during the 70 minutes operational phase following hitting a temperature of 70 ℃, with EPS exhibiting a higher rate of heat loss compared to VIPs at about 59%, see Figure 6.4. Thermal conductivity significantly impacts energy consumption over time compared to insulation thickness, as the thermal resistance of EPS was inferior to that of VIPs.

IV. **Ageing:** The study did not account for the ageing of EPS, whereas ageing was considered for VIPs with various core materials. The ageing of VIPs significantly affected the performance of the car painting booth. As outlined in section 4.5.2.B, the thermal conductivity of VIPs increased over time, particularly when subjected to elevated temperatures (up to 70 ℃). As mentioned previously, the disparity of 3.94 $mW.m^{-1}.K^{-1}$ (between FS VIP and FS-TNA1 VIP) was determined to have a small effect on energy consumption, approximately 1.9%. The study investigated the energy consumption of VIPs under three conditions: when sealed at low pressure, when thermal conductivity increased by 5 $mW.m^{-1}.K^{-1}$, and when VIPs completely lost their vacuum. For instance, with FS-TNFm1 during winter, the duration to attain 70℃ was 130 minutes, accompanied by an energy consumption of 188.9 MJ when sealed under low pressure, see Figure 6.5. With an increase in thermal conductivity of 5 $mW.m^{-1}.K^{-1}$, the duration to attain 70℃

extended by 5 minutes, and energy consumption escalated to 196.8 MJ. In the event that the VIP entirely lost its vacuum, the duration increased by 14.6 minutes (from initial value), and energy consumption escalated by 7.21% to 212.11 MJ. Over a decade, FS VIPs demonstrated superior vacuum retention compared to FS-TNFm1, which loses its vacuum after six years. In this case, CPBs insulated with FS-TNFm1 would consume more energy than those insulated with FS, despite FS-TNFm1 exhibiting lower energy consumption within the first year of CPB operation.

All findings regarding the VIP core materials, ambient temperatures, and variations in thermal conductivity are fully outlined in the Appendix 1 and 2.

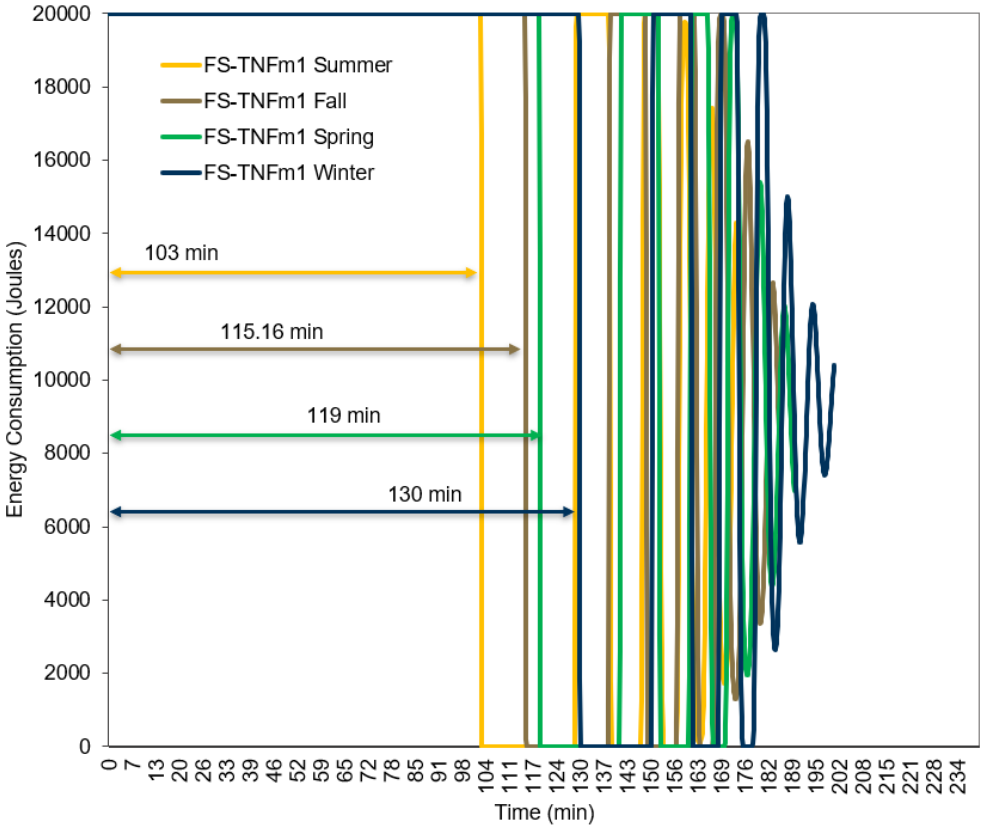

Figure 6.2 Energy consumption of CPB insulated with FS-TNFm1 VIPs over four distinct seasons

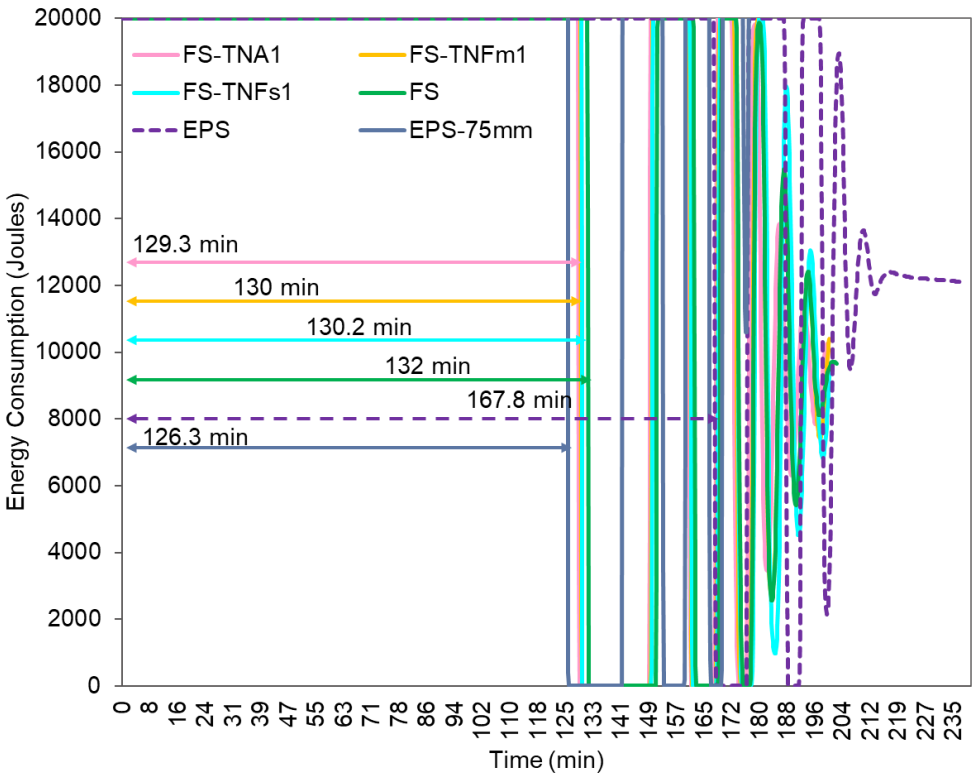

Figure 6.3 Energy consumption of the CPB with four different VIPs (25 mm) compared to EPS (25 mm and 75 mm)

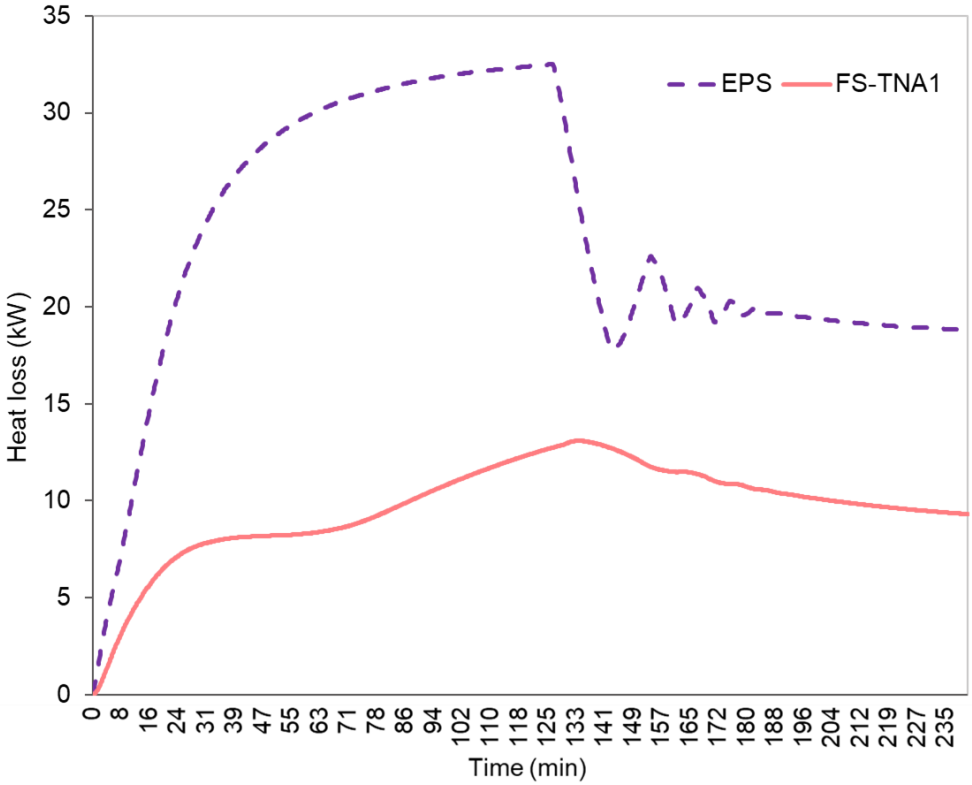

Figure 6.4 Heat loss comparison of two CPBs insulated with FS-TNA1 VIP and EPS VIP

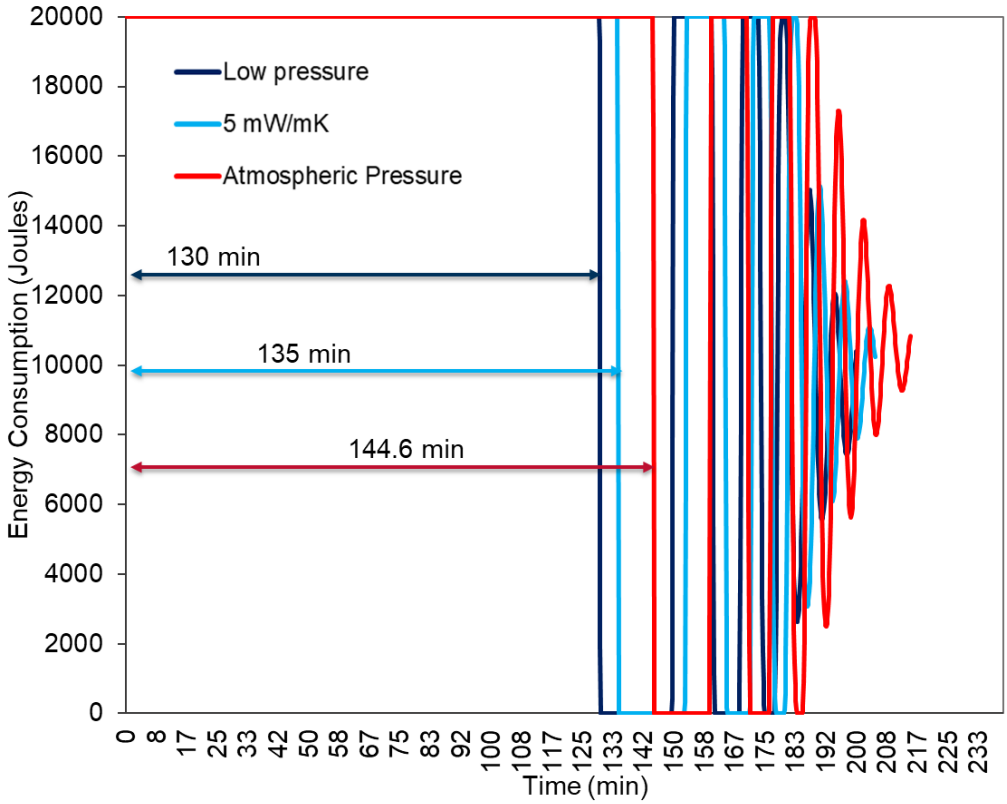

Figure 6.5 Energy consumption of CPB insulated by Fs-TNFm1 VIP at three different sealing pressures

6.3 Energy consumption of CPB over 10 years

The average duration of a single curing and drying cycle within one CPB, alongside the cumulative energy consumption of a CPB over one year of operation (252 working days) is outlined in this section. Furthermore, it examines the energy consumption over a decade for CPBs with various insulation types, considering the ageing effects of VIPs with different core materials. All findings are summarised in Table *6.2*.

Table 6.2: Average time required for one cycle of drying and curing and total energy consumption of CPB insulated with different VIP core and EPS over 1 year and 10 years

	VIP				EPS
	FS	Fs-TNFm1	FS-TNFs1	FS-TNA1	
Average time for one curing and drying cycle (min)	190	194	193	189	216
Total energy consumption of CPB in the 1st year (GJ)	43.3	42.7	42.8	42.5	55.1
Total energy consumption of CPB over 10 years (GJ)	440	454	451	434	551

The average duration of a single curing and drying cycle was determined from the results in Table *6.2*, considering the ageing effect of the VIP with various cores, while no ageing effect was considered for EPS. For CPB insulated with FS VIP, it was estimated that during the initial six years, the thermal conductivity would remain constant and the average drying and curing duration across four distinct climates estimated was 188.5 minutes. As the thermal conductivity increased by 5 $mW.m^{-1}.K^{-1}$ with the remaining four years of operation, the drying and curing time escalated by 2.2%, ending in an average of 193 minutes. For the CPB insulated with FS-TNA1, the thermal conductivity was constant over a period of five years, resulting in an average drying and curing time of 186.2 minutes, which was three minutes shorter than that of FS. Over the next five years of operation, the thermal conductivity increased by 5 $mW.m^{-1}.K^{-1}$ leading to the drying and curing time for CPB insulated with FS-TNA1 to rose up to 190.8 minutes which was only elevated by 1 minute in the comparison of CPB insulated with FS VIP sealed at low pressure.

In the case of tree-based fibre insulation (FS-TNFm1 and FS-TNFs1), thermal conductivity increased by 5 $mW.m^{-1}.K^{-1}$ after two years, with FS-TNFm1 losing its vacuum after six years and FS-TNFs1 after seven years. The average curing and drying times were 194 minutes for FS-TNFm1 and 193 minutes for FS-TNFs1, exceeding those of FS and FS-TNA1, yet lower than that of EPS, which averaged 216 minutes.

During the initial year, the energy consumption of the CPB was only affected by variations in ambient temperature and discrepancies in the thermal conductivity of various insulation materials. FS-TNA1 exhibited the lowest energy consumption at 42.5 GJ over 252 days of operation in CPB, followed by FS-TNFm1 of 42.7 GJ, FS-TNFs1 of 42.8 GJ, FS of 43.3 GJ, and EPS of 55.1 GJ. After a decade of operation CPBs insulated with FS VIP was determined to be lower by 14 GJ compared to FS-TNFm1 and 11 GJ compared to FS-TNFs1 due to the increase in thermal conductivity of FS-TNFm1 and FS-TNFs1 which exceeded the thermal conductivity of FS after two years of operations.

CPB insulated with FS-TNA1 exhibited the lowest thermal performance among all insulation materials examined. Although CPB insulated with FS VIP operated for a year at a lower thermal conductivity (in its sixth year, FS exhibited a thermal conductivity of 11.58 $mW.m^{-1}.K^{-1}$, while FS-TNA1 had a thermal conductivity of 12.4 $mW.m^{-1}.K^{-1}$), this advantage was insufficient for CPB insulated with FS to outperform FS-TNA1 over the 10 years of operation. CPB insulated with EPS exhibited heightened energy consumption, exceeding CPB insulated with FS-TNFm1 by 17.6% and FS-TNA1 by 21.2%. These findings demonstrated that thermal conductivity was the most

significant factor affecting the energy consumption of the CPB compared to all other studied factors.

The total energy consumption values reported in Table 6.2 are based on a set of standardised boundary conditions and modelling assumptions outlined in Sections 6.1 and 6.2. All CPBs were assumed to operate for 10 years, with 252 working days per year, and a set-point curing/drying temperature of 70 °C. Seasonal ambient temperatures in the UK were incorporated, and a consistent insulation thickness of 25 mm was used for all VIPs and EPS to ensure comparability. Thermal ageing of VIPs was modelled by assuming an increase of 5 $mW \cdot m^{-1} \cdot K^{-1}$ in thermal conductivity at specific intervals (2, 5, or 6 years, depending on the core material), while EPS ageing was not considered. All other system parameters, including heating power, airflow velocity, and thermal control logic, were held constant across simulations.

Nevertheless, several limitations should be acknowledged. First, the thermal ageing profile was assumed linear, whereas actual degradation in vacuum performance may occur in a nonlinear or sudden manner. Second, the effects of mechanical damage, poor installation, or air leakage, which could significantly impact long-term energy performance, were not included. Third, the exclusion of EPS ageing introduces a bias in favour of EPS for long-term comparison. Lastly, the simulations did not account for variability in booth operation, such as partial load conditions, off-days, or maintenance downtimes, which could alter the cumulative energy demand over time. Despite these limitations, the comparative results provide a robust foundation for evaluating insulation performance under controlled, equivalent conditions.

6.4 Sensitivity analysis

To verify the accuracy and reliability of the car painting both model, two sensitivity analyses were performed. The first study concentrated on mesh size, whereas the second investigated the impact of time step selection. Due to the significance of accurate temperature data recording in the model, especially from the small sensors located within the booth, the mesh size of the sensors was determined to be finer than that of the overall CPB. The decision was made because the sensors, being considerably smaller than the booth, necessitate a higher resolution mesh to accurately capture localised thermal gradients. A free tetrahedral mesh was utilised, with the sensor mesh consistently one size smaller than that of the CPB. Five mesh configurations were evaluated: Coarser + Coarse (25,186 elements), Coarse + Normal (45,059 elements), Normal + Fine (95,251 elements), Fine + Finer (265,482 elements), and Finer + Extra Fine (1,897,645

elements). An EPS insulation with a thickness of 25 mm was utilised at an ambient temperature of 6.3 ℃ for all varying mesh sizes.

The findings in Figure 6.6 revealed that the energy consumption for the largest mesh was 255.27 MJ, whereas the energy consumption using the smallest mesh was 249.36 MJ, resulting in a difference of approximately 2.3%. As anticipated, finer meshes offered more precise energy consumption estimates, accurately reflecting intricate thermal gradients, particularly in regions with complex geometries. Nonetheless, the mesh 3 (Normal + Fine) showed results that were approximately 0.2% superior to those obtained from the finest mesh (Finer + Extra Fine). Mesh 3 provides an optimal equilibrium between computational efficiency and precision, with energy consumption variations staying within acceptable thresholds relative to the coarser meshes. Thus, the Normal mesh for the CPB and the Fine mesh for the sensors were identified as the optimal configuration for the model.

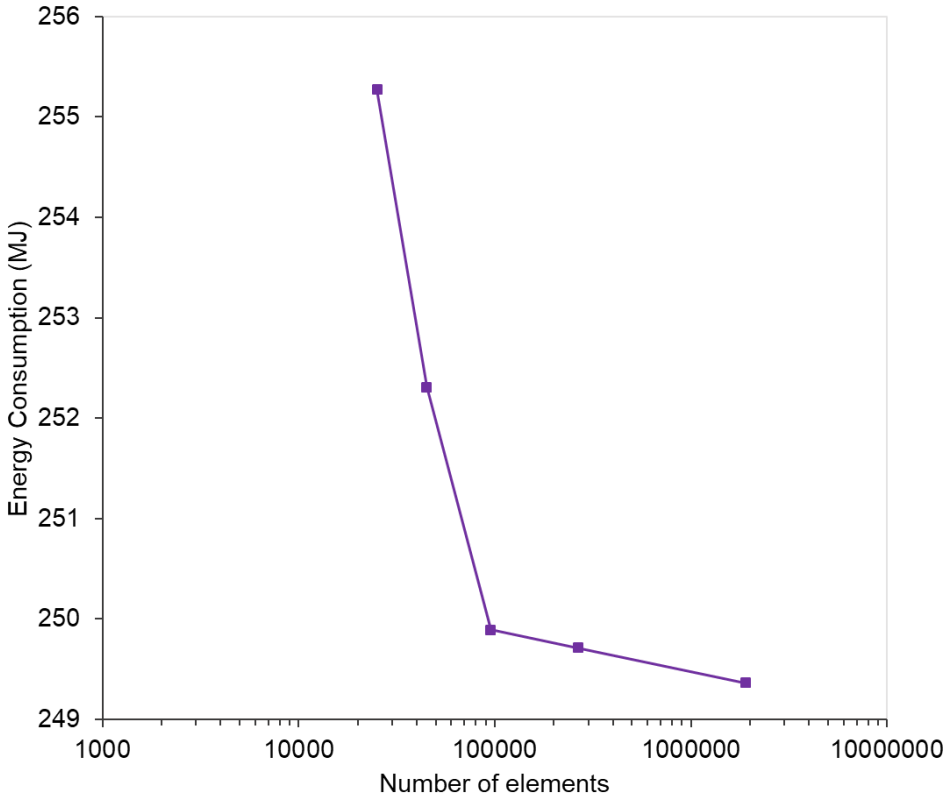

Figure 6.6 Mesh independence study for CPB insulated with EPS (25 mm) at 6.3 ℃ using 5 different mesh scenarios

In the second sensitivity analysis, four distinct time steps of 5, 10, 15, and 20 seconds were selected to investigate their effect on the energy consumption of the CPB. The identical EPS with a thickness of 25 mm at an ambient temperature of 6.3 ℃ was selected.

Table 6.3: Total energy consumption of CPB insulated with 25 mm EPS at different time steps

Time Step (s)	Operational Time (s)	Total Energy Consumption (MJ)
5	14265	249.61
10	14270	249.89
15	14270	250.13
20	14270	250.21

The results displayed in Table *6.3* indicated that the operational duration for CPB was identical across all selected time steps, with the exception of the 5-second time step, which recorded a total operational time of 14,265 seconds, representing a reduction of 5 seconds. However, regarding total energy consumption, a minor variation not exceeding 0.6 MJ was observed between the shortest time step (5 s) and the longest time step (20 s). Utilising a smaller time step, such as 5 seconds, facilitates a more detailed monitoring of temperature variations within the booth, thereby enhancing the accuracy and precision of the simulation. However, in this case, a larger time step exhibited minimal errors in energy consumption estimates. A 10-second time step was selected as it offered an optimal equilibrium between accuracy, computational efficiency, and simulation duration.

6.5 Economic assessment of VIPs

When evaluating insulation, it is essential to consider factors such as thermal conductivity, density, thickness of insulation (th) and cost (both raw material and processing). The determination of the amount of the optimum amount TNFm, TNFs and TNA with FS not only consider the cost of the material which was discussed in section 5.6, but also incorporates thermal resistance (R-value) as a key performance parameter, as presented in Table *6.4* for tree-based core composites with FS composites. The R-value, defined as the reciprocal of the thermal transmittance (U-value), is calculated using equation (6.5).

$$R = \frac{1}{U} = \frac{th}{\lambda_{\mathrm{T}}} \tag{6.5}$$

Table 6.4: Core material cost, thickness, overall conductivity and thermal resistance of all VIPs manufactured at 20 ℃ and 70 ℃.

Samples	C_{core} (£.kg^{-1})	th (m)	λ_T (mW.m^{-1}·K^{-1})		R (m^2.K.W^{-1})	
			At 20 ℃	At 70 ℃	At 20 ℃	At 70 ℃
FS	6.00	0.014	7.84	11.58	1.73	1.17
FS-TNFm1	4.24	0.013	6.75	8.28	1.93	1.57
FS-TNFm2	3.66	0.012	7.19	8.53	1.63	1.37
FS-TNFm3	3.07	0.011	8.27	10.39	1.28	1.02
FS-TNFs1	4.28	0.011	7.2	8.25	1.59	1.39
FS-TNFs2	3.71	0.01	7.65	8.61	1.34	1.09
FS-TNA	4.94	0.014	6.7	8.06	2.01	1.67
FS-TNA1	4.41	0.014	6.23	7.41	2.19	1.84
FS-TNA2	3.88	0.014	6.38	7.69	2.11	1.75
FS-TNA3	3.36	0.012	7.18	8.32	1.70	1.47
FS-TNA4	2.83	0.008	7.44	8.69	1.02	0.87

An alternative approach was employed in this study to compare economic performance of various VIP core composites. The findings reveal that FS, owing to its higher material cost, exhibited the highest cost per R-value among the insulation materials examined, see Figure 6.7. At temperatures of 20 ℃ and 70 ℃, FS exhibited cost values of £3.47 kg⁻¹ per R-value and £5.13 kg⁻¹ per R-value, respectively. The VIP cost reduced to £2.20 kg⁻¹ per R-value when the TNF content was elevated to 30% (sample FS-TNFm1), while it was £2.69 kg⁻¹ per R-value for sample FS-TNFs1 and £2.02 kg⁻¹ per R-value for FS-TNA1 at a temperature of 20℃. Upon increasing the content to 40% of the tree-based core, it was observed that only FS-TNA2 exhibited a lower cost of £1.84 kg⁻¹ per R-value and £2.22 kg⁻¹ per R-value, representing the lowest values among FS composites, whereas FS-TNFm2 and FS-TNFs2 demonstrated higher cost values than the 30% content. The outcome is ascribed to the minimal difference in thermal conductivity upon increasing the TNA content to 40%, in contrast to the nearly 10% decrease in core price, which had a more significant influence compared to the performance of the VIP. The cost value consistently increased with the addition of tree-based core content, reaching a maximum studied value of £ 3.25 kg⁻¹ per R-value for FS-TNA4 (60% of TNA), £3.01 kg⁻¹ per R-value for FS-TNFm3

(50% of TNFm), and £3.25 kg^{-1} per R-value for FS-TNFs2 (40% of TNFs), all of which were determined to be lower to the value of FS at 70 ℃.

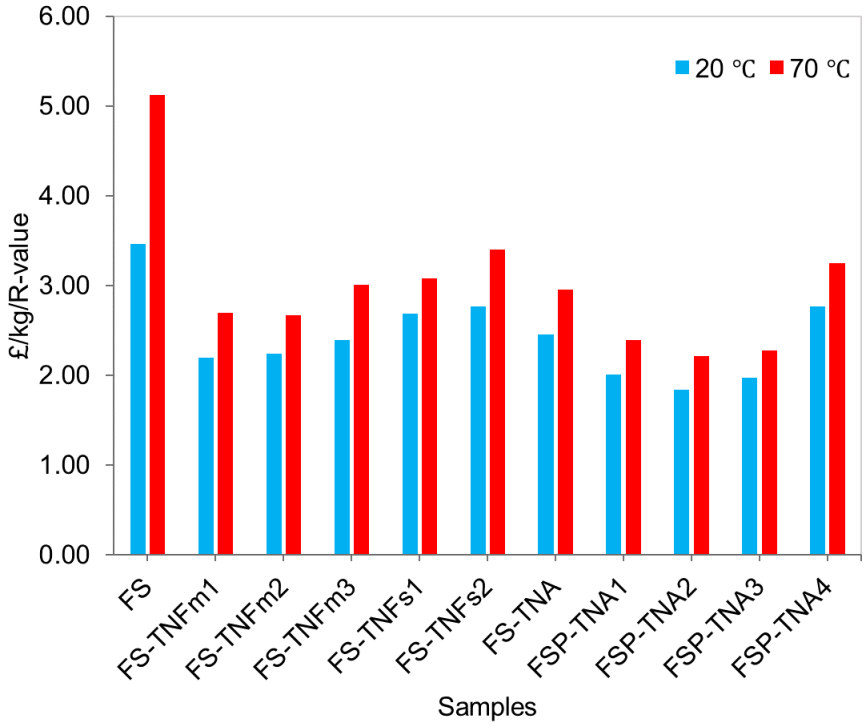

Figure 6.7 Cost per R-value of all manufactured VIPs at 20 ℃ and 70 ℃

6.6 Interpretation of the LCA results

The cradle to gate phase includes the results presented in section 5.5.3, in addition to the packing of VIPs and their transportation from the VIP manufacturing site to the CPB location, based on the second functional unit defined as the standard dimensions of the VIP (1 m^2 x 0.025 m).

The second part represented the cradle to grave analysis, which involved the operational phase within the car painting booth, including the application of adhesive to secure the VIPs to the booth's walls. It also covered the transportation from the VIP manufacturing facility to the CPB location and subsequently to the disposal site. Additionally, factors such as material degradation and impact assessment related to land use, were incorporated into this study.

The third and final stage involved a cradle to cradle analysis that assessed the reuse potential of VIP core materials, emphasising the related energy savings, as well as the transportation from the CPB site back to the VIP manufacture.

This study employed a cut-off approach to conduct a thorough analysis of two methodologies: Cumulative Energy Demand (CED) and EN15804 + A2 (European standard), along with their

respective impact categories. The impact categories were carefully analysed and compared utilising data acquired from SimaPro. The analysis concentrated on the substances that predominantly contribute to these effects, along with the correlation between electricity consumption in the UK and these effects. The results were modified to align with the most current and accurate data from the International Energy Agency (IEA) in their latest 2022 report. The results were subsequently compared with APOS approach, as well as with the unmodified SimaPro results.

6.6.1 Cradle to gate

All produced VIPs with various core materials were adequately packaged in 32 carton boxes as outlined in section 5.2.8. All VIPs were of identical dimensions despite differing core materials, resulting in an equivalent contribution of the folding boxes for each of the 128 VIPs prepared. The total energy consumption for manufacturing these boxes was 476.14 MJ, with approximately 78% derived from non-renewable energy sources.

Additionally, these VIPs were transported to the CPB installation site, covering a distance of 500 miles, resulting in a total fuel consumption of 224.14 litres. The transport of these VIPs contributed between 20.7% to 54.8% of the total combined non-renewable and renewable impact. For instance, the cumulative impact of the 128 manufactured VIPs, encompassing both non-renewable and renewable sources, amounted to 96,841.4 MJ, as detailed in Table 6.5. Of this total, the transport contribution was 20,092.59 MJ, representing 20.7% of the overall impact. In contrast, TNFm VIPs demonstrated a total energy impact of 36,680.9 MJ, with transportation accounting for 54.8% of this amount.

The increase impact of transportation resulted in a rise in climate change for every 128 VIPs transported to the CPB location, where only non-renewable impact directly contributed to this increase in climate change. In the case of TNFm VIP, it was observed that the transportation accounted for 62% of the total climate change impact associated with the extraction, processing, and manufacturing of 128 TNFm VIPs, whereas it constituted 29% for FS VIPs. The findings underscore the significance of transporting such products and the distance travelled, as greater distances from the VIP manufacturer to the installation site can result in an increase of over 50% in climate change impact.

Increasing the production of VIPs, optimising truck load capacity, and selecting storage facilities in closer to the installation site can significantly mitigate the impact on climate change. An alternative solution is the utilisation of electric trucks, as fuel consumption has been a primary

contributor to the increment of climate change impact. Figure 6.8 illustrates the contribution of 128 VIPs composed of seven distinct core materials across four different impact factors from the cradle to gate stage.

Table 6.5: Contribution of four core materials to the four environmental impacts (cradle to gate approach)

	FS	TNFm	TNFs	TNA
Acidification (mol H+ eq)	19.9	10.5	13.2	20.8
Climate Change (kg CO_2 eq)	3893.8	1821.4	2355.9	7826.3
Non-Renewable (MJ)	75777.1	34197.7	45009.0	83223.8
Renewable (MJ)	21064.3	2483.3	3432.2	10889.8

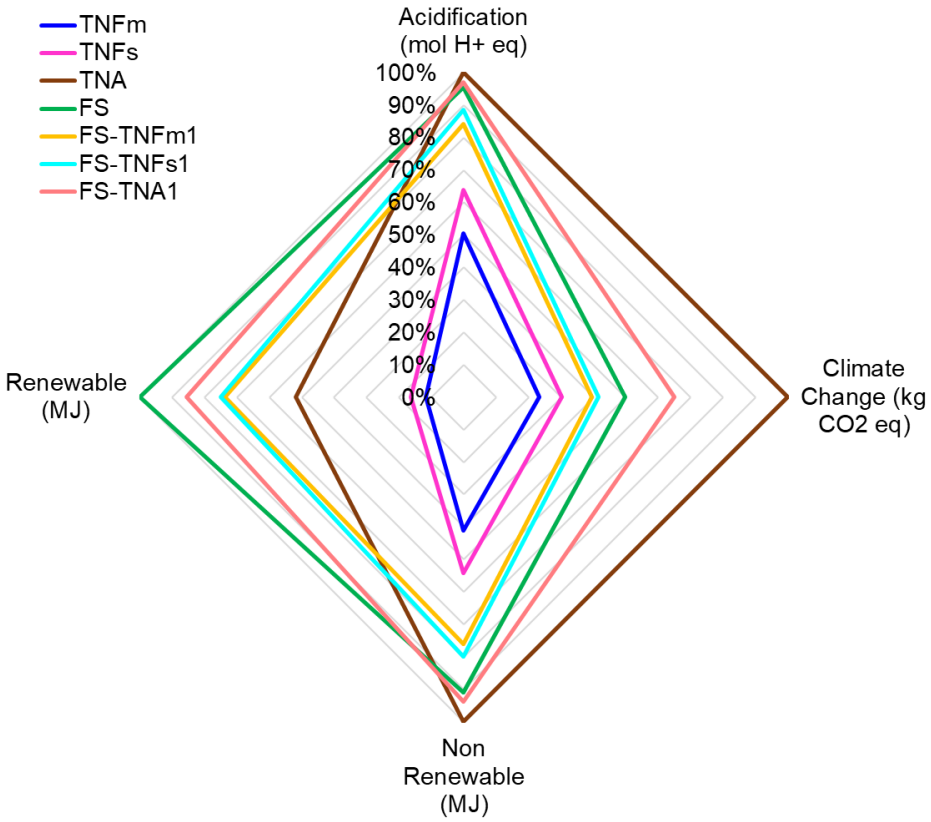

Figure 6.8. Contribution of seven core materials to the four environmental impacts (cradle to gate approach)

6.6.2 Cradle to grave

In the usage phase of the VIPs, only installation of VIPs and the operation energy use of the CPB was considered. The installation of VIPs consisted on using 200 g of polyurethane adhesive for each VIP to provide proper stability, and maximise insulation performance. Considering no damage to the VIPs and no human activity was involved, the VIPs were removed from the CPB

after 10 years of operations and were transported to the landfill site to be disposed. The distance covered to transport the used VIPs to the landfill site was assumed to be 500 miles.

No electricity consumption was accounted for in the demolition of the VIPs at either the CPB site or the landfill site, as it was presumed that the VIPs were cut and subsequently divided into core, fleece and envelope components. The only electricity consumption accounted for in the disposal process of the cores was to the production of bags for fertilisers, in which all cores would be packaged and compressed for landfilling. The number of bags was determined by the material density: 381 bags were needed for 128 VIPs, 65 for TNFm, 95 for TNFs, 57 for TNA, 227 for FS-TNFm1, 209 for FS-TNFs1, and 255 for FS-TNA1. The data for disposing of the fleece and envelope was obtained from the SimaPro database due to limited primary data, indicating a minimal environmental impact, with a total combined energy consumption of 0.2 MJ for all 128 VIPs, encompassing both non-renewable and renewable resources. Consequently, it was excluded from the calculations.

An additional impact category, land use, was incorporated in the cradle to grave analysis, as these materials were landfilled and occupied land space. The land use was determined according to the material's density. The most extensive area occupied was by FS core, measuring 12.7 m^3, while the least was by TNA core, measuring 1.8 m^3, for the 128 VIPs utilised in one CPB. Figure 6.9 illustrates the effects of polyurethane adhesive, landfill transportation, and VIP disposal.

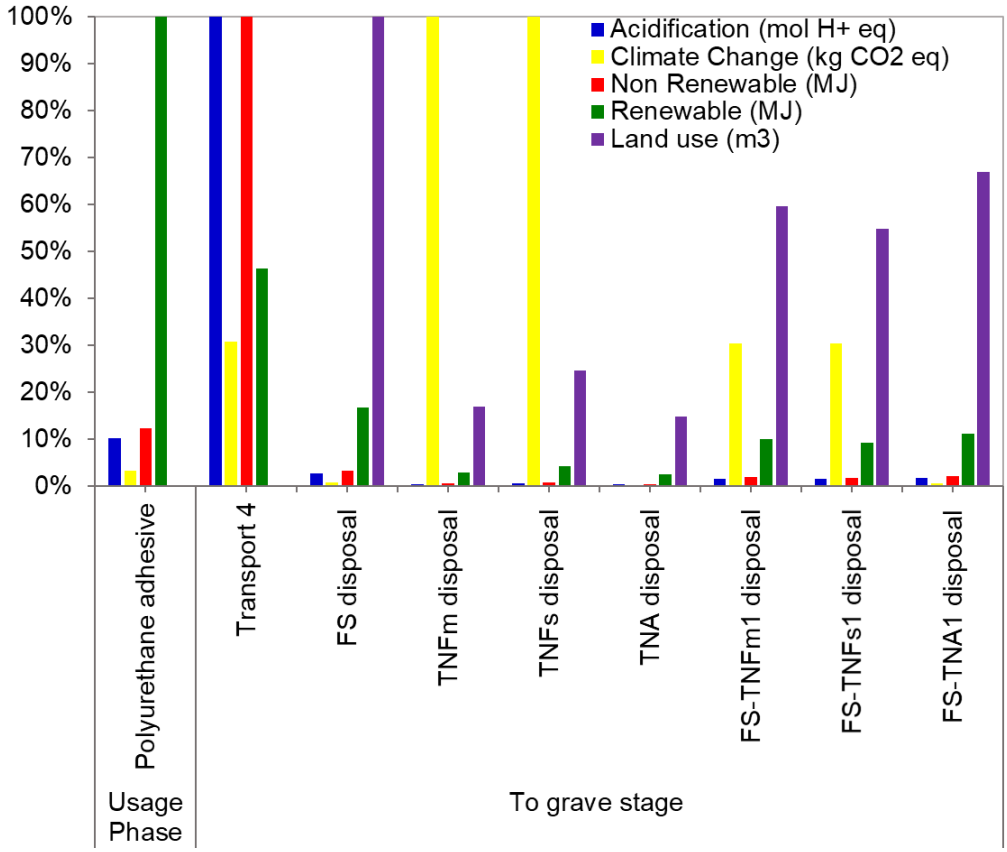

Figure 6.9 LCIA results of the usage phase and the disposal of seven different core materials of VIPs

Figure 6.10 exhibited a comparable pattern to the cradle and gate results in the majority of cases, where TNFm and TNFs demonstrated the lowest energy consumption, indicating minimal renewable and non-renewable impact categories. Conversely, TNA VIP displayed the largest non-renewable resource utilisation throughout its entire production lifecycle until the grave stage, alongside the highest climate change impact, determined at 9087.77 kg CO_2 eq. However, unlike other materials, the disposal of TNF materials resulted in degradation, emitting both carbon dioxide and methane into the atmosphere, with no assumption of capture or repurposing for either gas. The degassing resulted in an increase of climate change impact by 3673.6 kg CO_2 eq for both TNFm and TNFs core disposed, representing the highest contribution to climate change throughout the entire life cycle of these materials, accounting for 54% and 50% of the total climate change value, respectively. The findings highlight the significant impact of material degradation on climate change, indicating that TNF waste should be utilised for industrial applications instead of being dumped and ignored.

Although FS VIPs exhibit the highest total energy consumption, their environmental impact regarding climate change was the lowest among all materials, attributable to their greater dependence on renewable energy sources and the absence of degradation emissions. Thus, from a cradle to grave perspective, FS VIPs were recognised as the more environmentally sustainable option, demonstrating the minimal environmental impact among the analysed samples. Operational energy consumption was omitted from the cradle to grave evaluation to isolate and highlight the environmental consequences of raw material degradation.

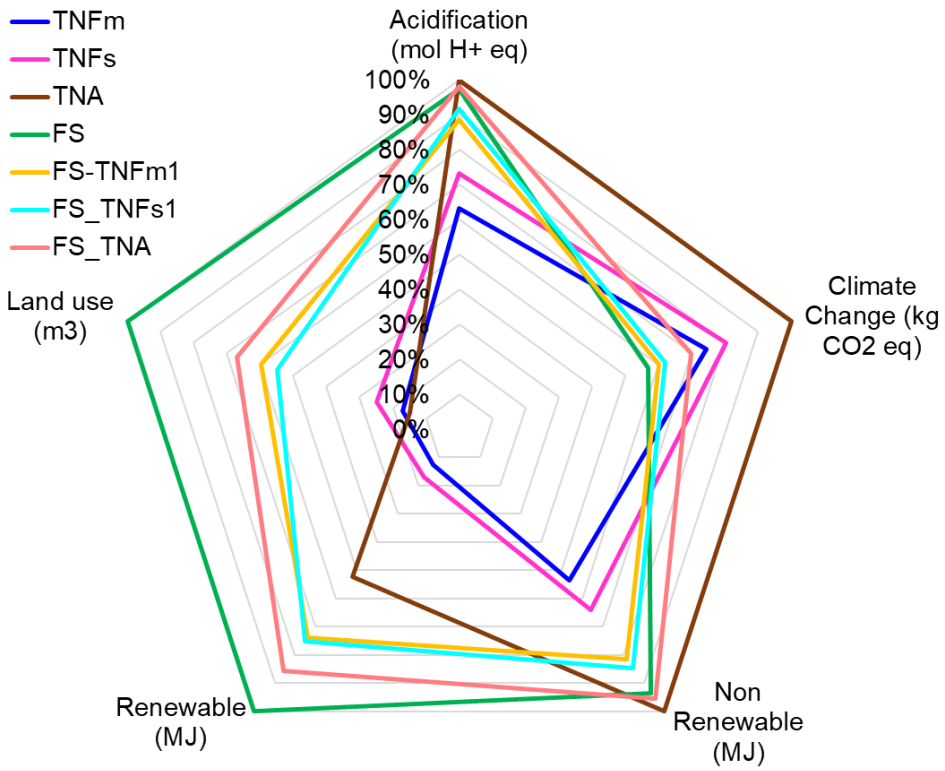

Figure 6.10 Contribution of seven core materials to the five environmental impacts (cradle to grave approach)

6.6.3 Cradle to cradle

During the cradle to cradle phase, it was essential to illustrate the real-life scenario in which energy consumption during the operational phase was significant. Consequently, VIPs with TNFm cores, TNFs, or TNA were excluded from the study, as their thermal conductivity was not assessed due to the difficulty of creating a 100% VIP with these cores. The only rationale for assuming their feasibility in earlier stages was to utilise them as a reference in the cradle to cradle phase. Moreover, the impact of land use was overlooked as no materials were disposed of. The modifications from cradle to gate and cradle to cradle involved the utilisation of polyethylene adhesive and the transportation from the CPB site to the VIP manufacturing facility, where the VIPs undergo processing for a second run. The modifications resulted in an increase in the overall renewable impact, non-renewable impact, acidification impact, and climate change impact by 212.8 MJ, 22483.3 MJ, 7.3 mol H+ eq, and 1256.6 kg of CO_2 eq, respectively, for all manufactured VIPs with various cores utilised for one CPB. The embodied energy throughout the entire life cycle of the VIPs, from raw material extraction to the reuse phase, including the energy consumed during the use phase was assessed in this part of the study. The outcomes of the various impacts analysed for the FS VIP and the composites during the cradle to cradle phase are displayed in Table 6.6 and Figure 6.11.

Table 6.6: Contribution of four core materials to the four environmental impacts (cradle to cradle approach)

	FS	FS-TNFm1	FS_TNFs1	FS_TNA
Acidification (mol H+ eq)	148.5	150.0	150.1	147.2
Climate Change (kg CO_2 eq)	26615.4	26499.2	26510.5	27507.7
Non-Renewable (MJ)	837218.1	848439.4	846621.7	829564.1
Renewable (MJ)	434741.5	442425.2	439878.1	426156.6

It was observed that although the TNA composite VIP exhibited a greater non-renewable and renewable impact than the TNFm composite VIP due to elevated electricity consumption during TNA production, as detailed in section 6.6.1, the overall non-renewable and renewable impact for the TNA composite was lower in the cradle to cradle phase. The reduction in electricity consumption during the operational phase of the CPB over ten years resulted in a savings of 19,990.5 MJ when utilising TNA VIP composite instead of TNFm composite VIP, which consequently decreased the total non-renewable and renewable impact by 35,143.9 MJ. Nonetheless, these savings were inadequate to diminish the climate change impact of TNA

composites below that of TNFm composites. In the cradle to gate stage, TNA composites exhibited a climate impact of 1,983.9 kg CO_2 eq greater than that of TNFm composites, which decreased to 1,009.5 kg CO_2 eq during the cradle to cradle phase. The processing method of TNA would continue to exert a greater environmental impact despite the substantial operational advantages it provides over the ten-year period in the CPB.

Among all evaluated samples, FS-TNFm1 exhibited the minimal impact on climate change, despite having the highest non-renewable and renewable impacts. For FS VIPs, the embodied energy was lower than that of FS-TNFm1, leading to a reduction of 18,904.9 MJ in both non-renewable and renewable impacts, although the climate change impact was only 116.2 kg CO_2 eq higher.

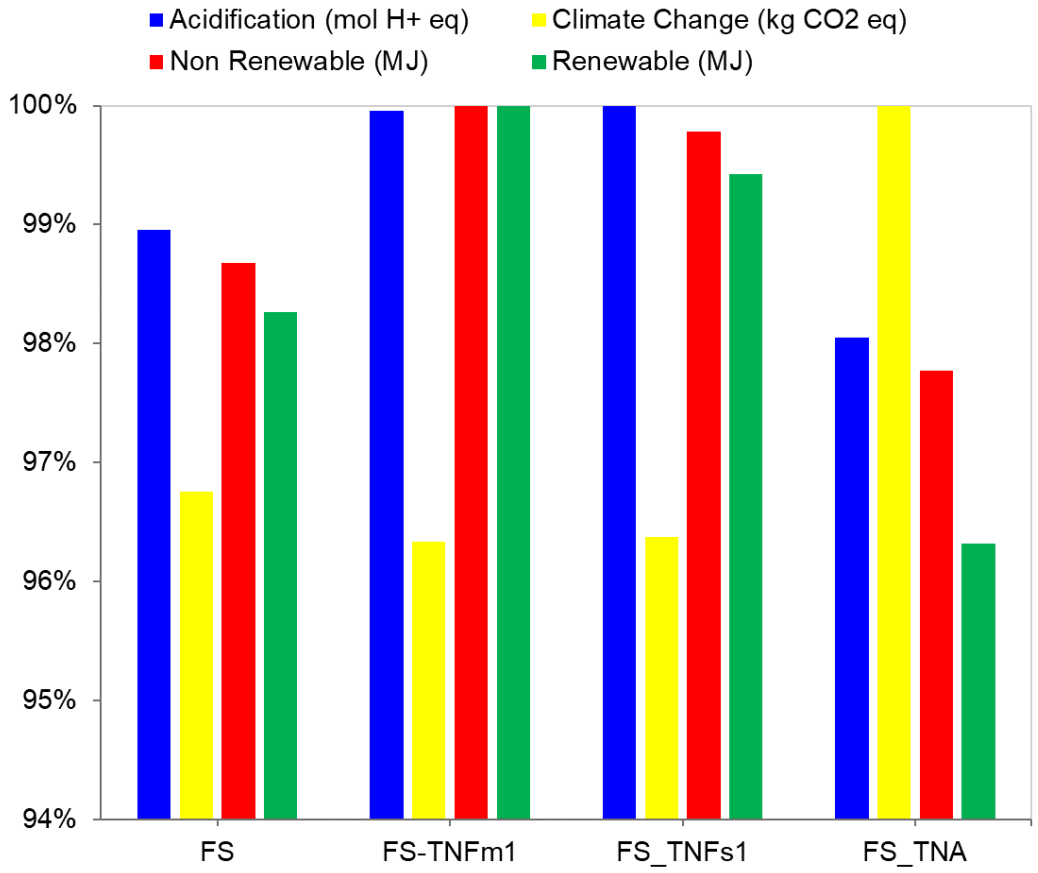

Figure 6.11 Contribution of four core materials to the four environmental impacts (cradle to cradle approach)

Given these diverse outcomes, it was difficult to ascertain the most sustainable VIP based exclusively on operational usage, core cost, and environmental impacts. Consequently, a normalisation study was essential as direct comparisons of raw values (i.e., MJ, kg CO_2 eq, mol H+ eq, and cost) could yield misleading conclusions. To accurately compare materials regarding all environmental impacts (Non-Renewable + renewable, climate change, acidification) alongside the initial core cost, normalisation was implemented by representing each impact as a fraction relative to the highest (worst-performing) impact within each category. The outcomes of various environmental impacts associated with distinct core materials from cradle to cradle, along with the initial costs of these materials, are illustrated in Table 6.7, while the normalisation of only environmental impact compared to total impacts is depicted in Figure 6.12.

Table 6.7: Results of various environmental impacts associated with distinct core materials (cradle to cradle, Cut-off) along with the initial costs of these materials

	FS	FS-TNFm1	FS_TNFs1	FS_TNA1
Acidification (mol H+ eq)	148.5	150.0	150.1	147.2
Climate Change (kg CO_2 eq)	26615.4	26499.2	26510.5	27507.7
Renewable + Non-Renewable (MJ)	1271959.6	1290864.6	1286499.8	1255720.6
Core Cost (£)	3840.0	2713.6	2739.2	2822.4

The results in Table 6.7 indicated that FS-TNFm1 exhibited the highest acidification value, surpassing the lowest value (FS-TNA1) by 1.9%, and the highest renewable plus non-renewable value, exceeding the lowest value (FS-TNA1) by 2.7%. Conversely, FS-TNA1 demonstrated the highest climate change impact, exceeding the lowest value (FS-TNFm1) by 3.7%. Additionally, the core cost of the FS sample (128 VIPs for one CPB) was the highest, exceeding the lowest value (FS-TNFm1) by 29.3%. When solely evaluating environmental impacts (acidification, climate change, renewable and non-renewable resources), FS was regarded as the "Green core" sought after for replacement. However, if the objective encompasses environmental considerations alongside core costs, then the FS-TNFm1 composite represents the optimal combination of all impacts, succeeded by FS-TNFs2, FS-TNA1, and finally FS core.

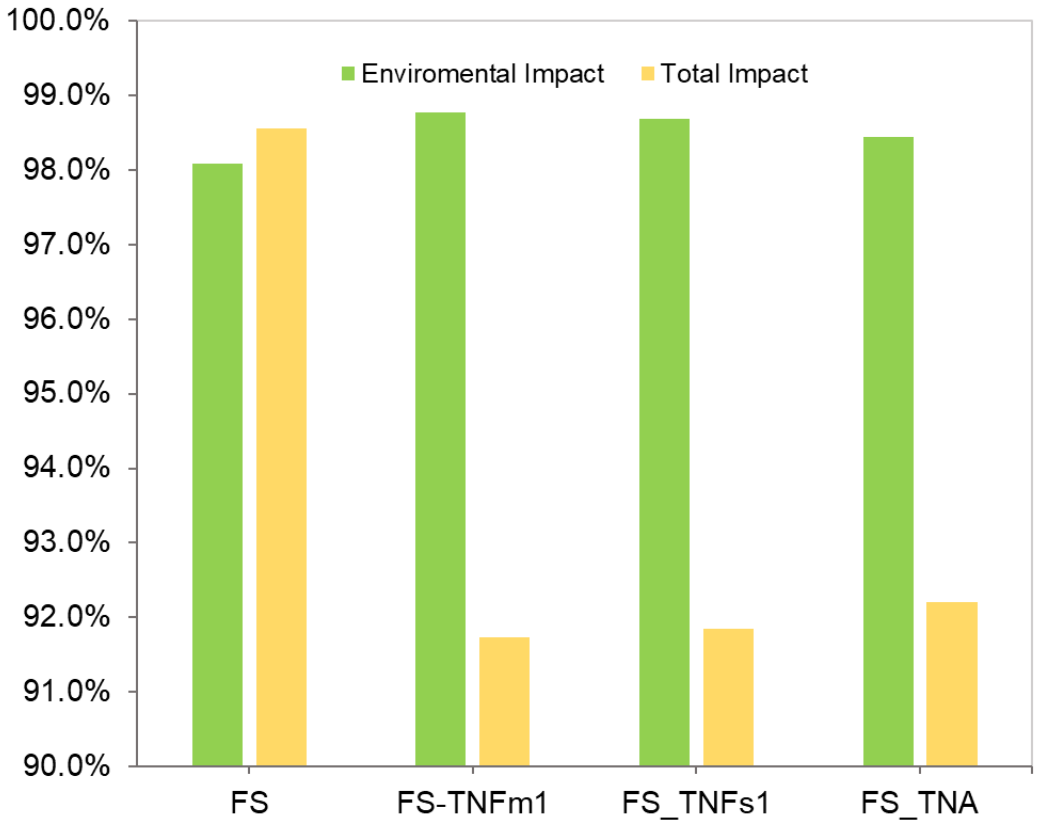

Figure 6.12 Environmental impact and total impact of four different VIP cores using Cut-off approach

6.6.4 Potential reuse of core material

According to section 4.4.2, core materials such as FS-TNFm1, FS-TNFs1, and FS-TNA1 exhibit the possibility for reuse as core materials in new VIPs following their initial usage. This phase exclusively addressed the transportation of utilised core materials from the automobile painting booth (usage phase) to the VIP manufacturing facilities, where these cores undergo exactly the same cradle to gate process outlined in section 6.6.3.

Figure 6.13 illustrates a comparison between FS and FS-TNFm1, highlighting the difference between the previously stated cradle to gate and the new cradle to gate that accounts the reuse phase. The findings indicated that in the case of FS all environmental impacts decreased by 64%, with the exception of the renewable impact, which dropped by 91% owing to the significantly higher non-renewable impact of transportation compared to the renewable impact. The reductions for FS-TNFm1 and FS-TNFs1 were 57% and 59% for all impacts, and 88% for the renewable impact, respectively. FS-TNA1 experienced the most significant decrease in the context of climate change, with a reduction of 74%, attributed to material deterioration during the initial preparation phase.

This highlighted the environmental advantages of utilising core materials like FS and TNA, despite their greater energy demands during initial preparation and increased CO_2 emissions compared to TNFm and TNFs. Incorporating reusability into the life cycle of the cores established a more sustainable production model across several cycles by reducing overall energy demand, lowering carbon footprint, and lowering the environmental burden associated with the materials. FS and TNA have greater stability over time, facilitating a continuous reuse loop, in contrast to TNF, which is susceptible to degradation due to its organic composition.

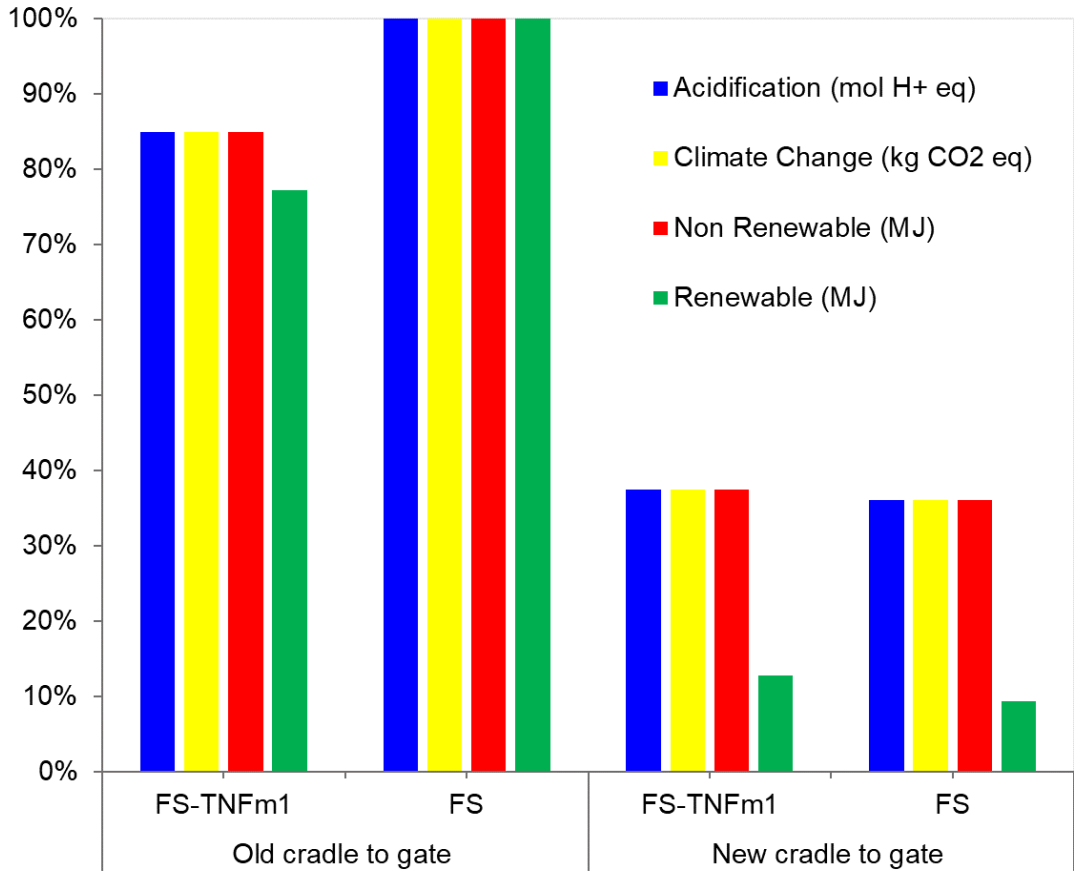

Figure 6.13 LCIA results comparing the initial cradle to gate with the new cradle to gate after reusing of cores

6.6.5 Results comparison and sensitivity analysis

All results detailed in the section 6.6.4 demonstrated the life cycle assessment from cradle to cradle of various composites of VIPs, employing the cut-off approach based on the modified data from the IEA for the year 2022. The investigation required to emphasise the significance of utilising current data, choosing the suitable LCA methodology, and comprehending how these choices affect final environmental effect assessments. The results detailed in section 6.6.4 were compared with those from Simapro without data adjustments and with the APOS approach, where data was modified in accordance with the same scope of work:

I. New and SimaPro results: The results in Table 6.8 indicated that the pattern remained similar when compared to the new data from IEA 2022, wherein FS-TNA had the most significant climate change impact due to material deterioration during combustion in the furnace. FS-TNFm1 exhibited the highest acidification impact and the most significant non-renewable and renewable impacts, attributable to the elevated energy consumption during the automobile painting booth operation over the decade. However, upon examining each impact separately, it was observed that the non-renewable impact rose by 24% for all VIPs, while the renewable impact diminished by 69%. Which resulted in an almost 43% increase in the impact of climate change and a 4% rise in acidification. The values were derived from the initial modifications in section 5.4.2, which involved the elimination of outdated generic data in SimaPro and its substitution with current UK data, including the removal of peat, a reduction in coal consumption, and an increase in the use of renewable resources, thereby reflecting the actual changes occurring in the UK in alignment with the targets set for 2050. The updated results did not mislead end users in selecting the best core material among those investigated; however, they may lead to incorrect conclusions that obscure the real benefits or the more accurate environmental implications of these products. The detailed results of LCA using SimaPro data is presented in Appendix 5.

II. Cut-off and APOS: In comparing several approaches, the results exhibited a distinct pattern compared to the SimaPro outcomes. Both the cut-off and the APOS approaches indicated that FS-TNFm1 exhibited the highest environmental consequences for acidification, non-renewable impact, and renewable impact, whereas FS-TNA shown the lowest, attributable to the previously mentioned reasons, see Table 6.9 and Figure 6.14. In terms of climate change impact, the APOS technique indicated that FS VIP had the greatest impact value, whilst the cut-off approach yielded the lowest. It is important to note that in the APOS methodology, if these wastes are left unused, degassing would occur over time. The emissions from tree-

based natural fibres were carbon dioxide and methane per kilogramme of material, as detailed in section 5.4.3.C. The utilisation of tree-based natural fibres results in an environmental advantage where this effect would be regarded as negative (-) in the calculations. Given that TNA necessitated the highest quantity of TNF waste and that CPB with FS-TNA VIP exhibited the lowest energy use, this resulted in reduced electricity usage and enhanced waste utilisation, hence reducing the influence on climate change. The detailed results of LCA using APOS approach is presented in Appendix 4.

Table 6.8: SimaPro results of various environmental impacts associated with distinct core materials (cradle to cradle, Cut-off) along with the initial costs of these materials

	FS	FS-TNFm1	FS_TNFs1	FS_TNA1
Acidification (mol H+ eq)	154.1	158.3	158.4	153.0
Climate Change (kg CO_2 eq)	46576.2	46301.3	46328.7	47235.3
Non-Renewable (MJ)	1103532.0	1119995.8	1116526.4	1091122.5
Renewable (MJ)	257603.8	262559.6	261090.8	252827.6

Table 6.9: Results of various environmental impacts associated with distinct core materials (cradle to cradle, APOS) along with the initial costs of these materials

	FS	FS-TNFm1	FS_TNFs1	FS_TNA1
Acidification (mol H+ eq)	149.1	151.0	151.1	147.9
Climate Change (kg CO_2 eq)	28351.2	28012.9	28081.9	28210.8
Non-Renewable (MJ)	885822.4	898430.3	896291.0	877627.8
Renewable (MJ)	457833.4	465937.6	463249.6	448812.4

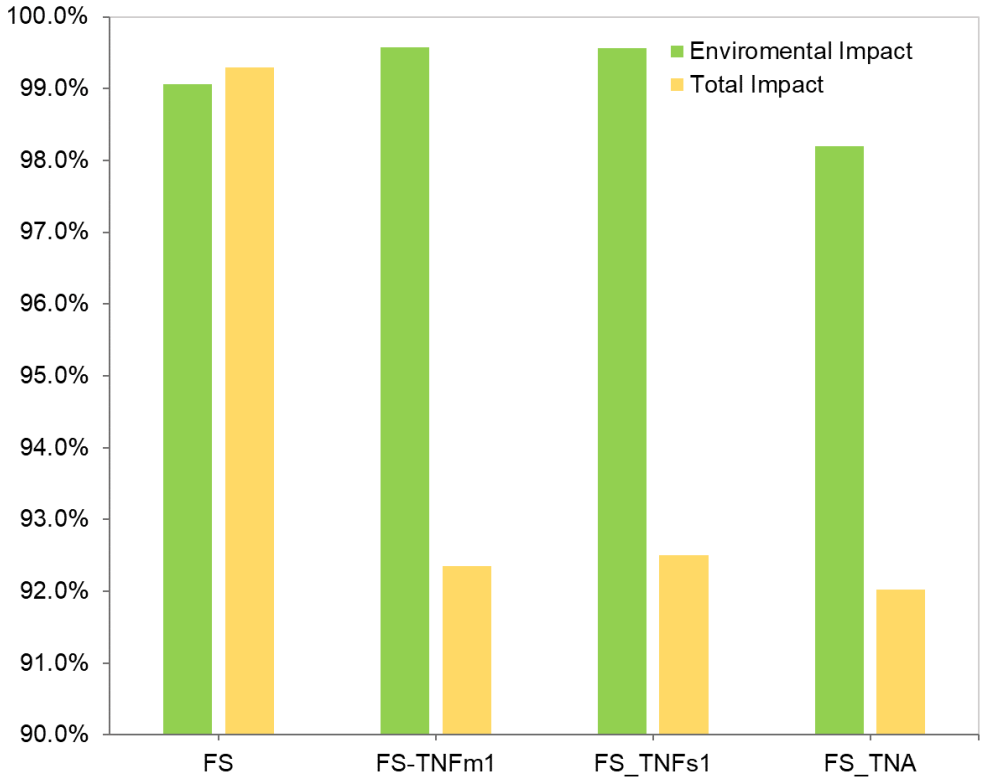

Figure 6.14 Environmental impact and total impact of four different VIP cores using APOS approach

6.7 Predicted LCA of VIPs in 2050

By 2050, the UK aims to achieve a net-zero emissions target, with its energy grid expected to operate entirely on renewable energy sources. Understanding the environmental impacts of different core materials and the associated processes used in the production of VIPs, particularly their embodied energy is critical, especially when considering energy consumption in the car painting booth over a decade. Transportation impacts were excluded from this analysis, as it is assumed that by 2050, lorries will operate with zero-carbon solutions such as batteries or hydrogen. Both cut-off and APOS approaches were considered in this part. Since all energy consumed in the UK in 2050 would be derived from renewable sources, no climate change impacts were assumed, except for the degradation of natural fibre materials.

In accordance with the prior discussions in section 6.6.1, the energy consumption in the production process of FS was deemed the highest in both the cut-off and APOS approaches, with values of 119537.5 MJ and 126865.5 MJ for 128 VIPs, respectively. Subsequently, FS-TNA1, FS-TNFs1, and FS-TNFm1 were identified as having lower energy consumption in their production compared to FS, according to both cut-off and APOS approaches, as illustrated in Table 6.10.

Table 6.10: Climate change, renewable energy impacts and embodied energy of four core materials using both cut-off and APOS approaches

Approach	Environmental impacts	VIP Samples			
		FS	FS-TNFm1	FS-TNFs1	FS-TNA1
Cut-off	Climate Change (kg CO_2 eq)	0.0	0.0	0.0	1149.3
	Renewable energy for the production of VIPs (MJ)	119537.5	101501.1	105028.2	118732.3
	Embodied energy (MJ)	1271959.6	1290864.6	1286499.8	1255720.6
APOS	Climate Change (kg CO_2 eq)	0.0	-3940.9	-10031.5	-15763.8
	Renewable energy for the production of VIPs (MJ)	126865.5	107723.4	111466.7	126010.9
	Embodied energy (MJ)	1343655.9	1364367.9	1359540.6	1326440.3

Regarding climate change impact, the production of FS VIPs resulted in zero CO_2 emissions since only renewable energy was used. However, for the TNF products, the degradation of the material was considered. Using the cut-off approach, where the producer is fully responsible for waste management and no credit is given for recyclable components, it was assumed that 1,149.3 kg of CO_2 would be emitted when the TNF were pyrolysed in a furnace to produce TNA, assuming that methane emissions were captured (based on the calculations of 192 kg of TNF waste). In contrast, the APOS approach considers the interdependence of processes and allocates environmental impacts based on each process's contribution to the overall system. As a result, FS-TNA1 showed the highest environmental benefit, as more TNF waste was used in the production of TNA. Specifically, 2,742.9 kg of TNF was required to produce 192 kg (30% of the total 640 kg used for 128 VIPs) of TNA, followed by TNFs, which required 1,745.5 kg and then TNFm, which required 685.71 kg.

When considering the embodied energy over a decade, including the usage phase of the CPB, TNFm exhibited the highest energy consumption, followed by FS-TNFs1, FS and FS-TNA1, respectively, in both the APOS and cut-off approaches, as presented in Table 6.10.

In line with the UK's net-zero target for 2050, the APOS approach emerges as the more environmentally favourable model by emphasising the benefits of waste utilisation. Among the core materials studied, FS-TNA1 demonstrated the lowest environmental impact (positive) when considering both production and usage phases, see Figure 6.15.

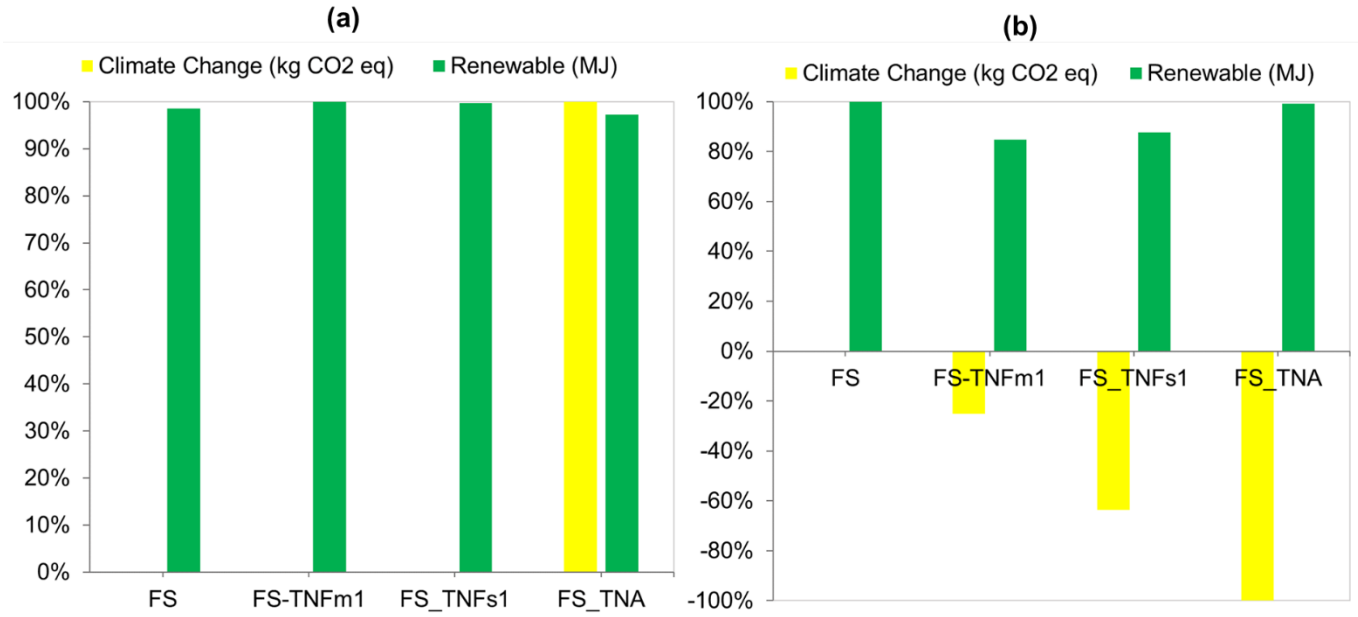

Figure 6.15 Comparison of climate change and renewable impacts of four different core materials VIPs in year 2050 using both (a) cut-off and (b) APOS approaches

6.8 Summary

The main results of the Car Painting Booth (CPB), the environmental impacts of the full life cycle of VIPs used in the CPB and the cost per thermal resistance are outlined as follows

- CPB insulated with FS-TNA1 consumed the least energy at 42.5 GJ over 252 days, followed by FS-TNFm1 at 42.7 GJ, FS-TNFs1 at 42.8 GJ, FS at 43.3 GJ, and EPS at 55.1 GJ over one year.
- The thermal conductivity of FS-TNFm1 and FS-TNFs1 exceeded that of FS after two years of operations.
- After a decade of operation CPBs insulated with FS VIP was determined to be lower by 14 GJ compared to FS-TNFm1 and 11 GJ compared to FS-TNFs1.
- The lowest energy consumption was 434 GJ for FS-TNA1, and the highest was 551 GJ for EPS over a decade.
- In the cradle to cradle cut-off approach, FS-TNFm1 and FS-TNFs1 had the highest non-renewable impact (848 GJ and 846 GJ, respectively), while FS was 837 GJ and FS-TNA1 was the lowest (829 GJ).
- CPB insulated with FS-TNA used the least energy over 10 years. TNA pyrolysis in initial material processing prevented these savings from reducing FS-TNA VIP climate change impact below TNFm composites and FS. Where, FS was considered the "Green core" for

replacement when only considered acidification, climate change, renewable and non-renewable impacts, using the cut-off approach.

- The utilisation of tree-based natural fibres resulted in an environmental advantage where this effect would be regarded as negative (-) in the calculations. Consequently, FS to have the highest (negative) environmental impact when using APOS approach.
- Since CPB with FS-TNA VIP used the least energy and TNA used the most TNF waste, this reduced electricity usage and improved waste utilisation, reducing climate change.
- In comparison to the SimaPro data, a similar pattern was observed, with non-renewable impact increasing by 24% and renewable impact decreasing by 69% for all VIPs studied.
- In line with the UK's net-zero target for 2050, the APOS approach emerges as the more environmentally favourable model by emphasising the benefits of waste utilisation. Among the core materials studied, FS-TNA1 demonstrated the lowest environmental impact (positive) when considering both production and usage phases.
- Reusing core materials like FS and FS-TNA reduced climate change impact by up to 74%, while FS-TNFm1 and FS-TNFs1 reduced by 57% and 59%, respectively, despite higher energy consumption.
- FS proved to be the least cost-effective, with values of £3.47 and £5.13kg^{-1} per R-value at 20°C and 70°C, respectively, surpassing FS-TNFm1 (£2.20 and £2.70 kg^{-1} per R-value), FS-TNFs1 (£2.69 and £3.07 kg^{-1} per R-value), and FS-TNA1 (£2.02 and £2.39 kg^{-1} per R-value) at 20°C and 70°C, respectively.

CHAPTER 7: Conclusions and Future Directions

7.1 Conclusions

The current investigation involved the experimental thermophysical, environmental and economical characterisation of three novel core materials obtained from tree based natural fibre waste. The objective was to manufacture and test VIPs made of the optimised tree based natural fibres, ash and their composites containing an optimum proportion of fumed silica. Further, COMSOL Multiphysics based system scale model for a typical car painting booth (up to 70 ℃) using the VIPs manufactured was developed. The findings were used to perform a comprehensive LCA from 'cradle to gate' to 'cradle to cradle' basis to assist end users in selecting best materials and processes for producing a greener VIP.

7.1.1 Material development and characterisation

Out of the tree-based sheath waste, 28% was processed to TNFm, 11% was processed to TNFs while the remaining 61% of tree sheath was pyrolysed into TNA (at three different temperatures 600 ℃, 700 ℃ and 800 ℃) in order to optimally utilise the raw material. Ten composite samples were produced, each including different combinations of FS with TNA, TNFm, or TNFs using a three-dimensional mixer at 50 RPM for a duration of 10 minutes to attain a comprehensive and uniform blend.

The SEM images and fibre length distribution demonstrated a notable disparity in the fibre length between the two materials, only TNFm exhibited significant number of fibres with an average length of 0.82 mm in contrast to TNFs that had an average length of 0.22 mm. For the particle size distribution in the case of TNA, as the pyrolysis temperature increased, a trend towards smaller particle sizes was observed. The smallest particle size for TNA that was pyrolysed at 600℃ was 4.8 μm. This size reduced to 3.76 μm at 700℃ and further decreased to 2.62 μm at 800℃. This behaviour can be ascribed to faster breakdown of organic substances at elevated temperatures, leading to the formation of smaller particles.

The MIP results demonstrated that FS had the lowest average pore diameter of 0.26 μm and the highest porosity of 91.54%, compared to TNFm with an average pore diameter of 0.7 μm and a porosity of 77.35%, TNFs with an average pore diameter of 1.98 μm and a porosity of 84.93%, and TNA with an average pore diameter of 2.43 μm and a porosity of 84.34%. In the case of composites, the porosity of all samples increased but remained lower than that of FS, while the average pore size decreased, becoming smaller than that of pure FS. FS-TNFm1 had an average pore diameter of 0.23 μm and a porosity of 88.27%, FS-TNFs1 had 0.19 μm and 89.44%, and

FS-TNA had 0.19 μm and 88.37%. This increase in porosity, along with the distinctive characteristics of fumed silica, contributes to the enhanced performance of VIP composite samples, allowing for lower gaseous conductivity even under higher internal pressures.

The thermogravimetric measurement indicated that TNF breakdown started at 600 ℃, suggesting that temperatures of 600 ℃ and above are suitable for the pyrolysis process. In addition, the primary distinction in weight loss occurrence between TNFm and TNFs was due to the particle size distribution. TNFs had larger proportion of dust (or crushed fibres) content compared to TNFm.

The FTIR showed that both TNF and TNA exhibited a higher spectrum extinction coefficient in comparison to FS in the wavelength range of 2.5 to 7.5 μm, suggesting a potentially reduced radiative heat exchanged through insulation over this range.

7.1.2 Thermal conductivity measurements

Experimental measurements were conducted to determine the centre of panel thermal conductivities three FS-TNFm composites, two FS-TNFs composites and five FS-TNA composites in comparison to pure FS VIP. The measurements were taken at core pressures ranging from 0.64 to 1000 mbar, and mean temperatures ranging from 20 ℃ to 70 ℃.

At low pressure (0.64 to 2.15 mbar) thermal conductivity of pure FS VIP and FS-TNFm3 (50 wt.% FS and 50 wt.% TNFm) intersected at a temperature of 35 ℃ where they had the same value. As the temperature continued to rise, the thermal conductivity of FS-TNFm3 increased to a final value of 10.39 $mWm^{-1}K^{-1}$ lower than that of pure fumed silica which was 11.58 $mW.m^{-1}.K^{-1}$. This phenomenon demonstrated a notable influence of temperature on radiative conductivity, and thus overall conductivity. Initially FS sample had a lower overall conductivity at 20 ℃ of value of 7.84 $mW.m^{-1}.K^{-1}$ where solid conductivity had a greater impact, but ended with a higher value at 70 ℃ as compared to composites due to a dramatic rise in radiative conductivity with temperature. All other composites demonstrated lower overall conductivity than FS across all temperatures assessed.

FS-TNFm1 (70 wt.% FS and 30 wt.% TNFm) achieved lower thermal conductivity of 6.75 $mW.m^{-1}.K^{-1}$ and 8.28 $mW.m^{-1}.K^{-1}$at 20 and 70 ℃ among all FS-TNFm composites.FS-TNFs1 (70 wt.% FS and 30 wt.% TNFs) showed the lower thermal conductivity of 7.2 and 8.25 $mWm^{-1}K^{-1}$ at 20 and 70 ℃, respectively, among all FS-TNFs composites. FS-TNA1 (70 wt.% FS and 30 wt.% TNA) showed the lowest thermal conductivity among all composites studied with a value of 6.23 $mW.m^{-1}.K^{-1}$and 7.41 $mW.m^{-1}.K^{-1}$at 20 and 70 ℃, respectively.

At atmospheric pressure and a mean temperature of 70 ℃, it was noticed that only FS-TNA1 and FS-TNA2 (60 wt.% FS and 40 wt.% TNA) had thermal conductivity of 23.4 $mW.m^{-1}.K^{-1}$, 23.9 $mW.m^{-1}.K^{-1}$, respectively, lower than FS (25 $mW.m^{-1}.K^{-1}$). Composite samples with larger pore sizes, FS-TNFm1 and FS-TNFs1 had higher thermal conductivity of 26.2 $mW.m^{-1}.K^{-1}$ and 25.5 $mW.m^{-1}.K^{-1}$, respectively. This indicated that the effect of gaseous conductivity at atmospheric pressure surpassed the effect of radiative conductivity.

VIPs made of the best three composite samples each of FS-TNFm1, FS-TNFs1, FS-TNA1 and FS were unsealed after 6 months of VIP manufacture. During this period these were stored at room temperature of 20 ℃ and a RH of 40%. The thermal conductivity of all samples after remaking showed a slight increase which did not exceed 3% of the initial value (before breaking the VIPs), suggesting the possibility of reusing the cores.

7.1.3 System level performance, economic and environmental assessments of the developed cores

The energy consumed over a decade by a Car painting Booth (CPB) insulated with the VIPs made of three best composites and FS developed was numerically predicted. The increase of thermal conductivity with time of VIPs with different core materials was accounted for and the results were compared with EPS which was the commonly used insulation in CPBs. The results indicated FS-TNA1 exhibited the lowest energy consumption at 42.5 GJ over 252 days of operation in CPB, followed by FS-TNFm1 of 42.7 GJ, FS-TNFs1 of 42.8 GJ, FS of 43.3 GJ, and EPS of 55.1 GJ over the same period of operation. The thermal conductivity of FS-TNFm1 and FS-TNFs1 exceeded that of FS after two years of operations. After a decade of operation CPBs insulated with FS VIP was determined to be lower by 14 GJ compared to FS-TNFm1 and 11 GJ compared to FS-TNFs1. Whereas FS-TNA1 remained to have the lowest energy consumption of 434 GJ and EPS remained to have the highest energy consumption with 551 GJ.

Thermal resistance (R-Value) and material costs are considered when determining the appropriate quantities of TNFm, TNFs, and TNA with FS. Sample FS proved to be the most cost-effective, with values of £3.47 and £5.13kg^{-1} per R-value at 20°C and 70°C, respectively, surpassing FS-TNFm1 (£2.20 and £2.70 kg^{-1} per R-value), FS-TNFs1 (£2.69 and £3.07 kg^{-1} per R-value), and FS-TNA1 (£2.02 and £2.39 kg^{-1} per R-value) at 20°C and 70°C, respectively.

The LCA study initially examined the environmental impacts of extracting and processing FS and TNF materials on cradle to gate approach assuming a functional unit of the load capacity of 6.2 tonnes of a standard lorry used for transporting raw materials. The second stage expanded the

evaluation to include the whole life cycle of VIPs that are specifically designed for use in the car painting booth (cradle to cradle) using 1 m^2 of VIP with 25 mm thickness as a new functional unit. Cumulative Energy Demand (CED) and EN15804 + A2 (European standard) techniques and impact categories were analysed using UK's current energy mix. The results were updated to adopt the International Energy Agency (IEA)'s 2022 file. The cradle to gate analysis showed that the processing of all TNF materials consumed 6245.5 MJ, which was 19.6 times lower than $SiCL_4$ (raw material used to produce FS) and FS's non-renewable impact. Material transportation consumed 8009.9 MJ, primarily due to diesel usage which was 1.3 times higher TNF materials production. Transport climate impact was 450.65 kg CO_2 eq, and TNF processing was 2028.5 kg CO_2 eq, primarily attributed to the operation of the furnace (in the case of TNA pyrolysis), which emitted CO_2 as a result of material degradation, accounting for 77.8% of the total value.

In the cradle to cradle cut-off approach, FS-TNFm1 and FS-TNFs1 had the highest non-renewable impact among the VIPs (848 GJ and 846 GJ, respectively) with FS (837 GJ) and FS-TNA1 (829 GJ) performing slightly better. CPB insulated with FS-TNA consumed the lowest amount of energy during its 10-year operation. Due to the pyrolysis process in initial manufacture stages, these savings were insufficient to reduce TNA composites' climate change impact below that of TNFm composites. Based on the cut-off approach, FS is pronounced a "Green core" among all materials studied based on environmental implications (acidification, climate change, renewable and non-renewable resources).

The APOS technique showed that FS VIP had the highest climate change impact, whereas the cut-off approach provided the lowest impact for FS VIP. This is because TNF waste degrades over time, if left unused. The utilisation of tree-based natural fibres results in an environmental advantage where this effect would be regarded as negative (-) during calculations. Since TNA used the most TNF waste and CPB with FS-TNA VIP used the least power, this means a lower climate change impact for FS-TNA VIPs.

In comparison to the SimaPro data, a similar pattern was observed, with non-renewable impact increasing by 24% and renewable impact decreasing by 69% for all VIPs studied.

In line with the UK's net-zero target for 2050, the APOS approach emerges as the more environmentally favourable model by emphasising the benefits of waste utilisation. Among the core materials studied, FS-TNA1 demonstrated the lowest environmental impact (positive) when considering both production and usage phases, see Figure 6.15.

Reuse core materials like FS and FS-TNA lowered climate change impact by up to 74%, with FS-TNFm1 and 57%-59% with FS-TNFs1 despite greater energy needs in the case of the later. FS and TNA were found to be physically and chemically stable and maintained their thermal conductivity or underwent lower degradation on reuse. This was not the case with TNF, which degraded over time.

7.2 Future directions

To further expand upon the findings of this study, several critical areas are suggested for future investigation:

I. Identification and assessment of new cost effective and environmentally friendly materials sourced from different tree-based waste as potential core materials for VIPs withs specific attention on their thermal performance at high-temperature applications (up to 70 ℃).
II. Full characterisation of post-compacted cores, as opposed to pre-compacted cores. Methods such as mercury intrusion porosimetry or nitrogen adsorption or any alternative methods should be explored to evaluate the impact of compaction on pore size and particle distribution within the core.
III. Characterisation and experimental investigation of TNA as an opacifier for VIP core materials in high-temperature applications (up to 500 ℃) to substitute costly and environmentally unfavourable opacifiers such as carbon black or silicon carbide.
IV. Collection of reliable primary data for a more accurate, comprehensive and realistic cradle to cradle life cycle assessment of VIPs including envelope and fleece materials.
V. Conduction of a dynamic LCA to predict future alterations in accordance with the UK's net zero objectives, while examining the environmental and economic advantages of VIPs and comparing them with the consequential methodology employed in SimaPro.

References

Abdel-Hamid, A.M., Solbiati, J.O., Cann, I.K.O., 2013. Insights into Lignin Degradation and its Potential Industrial Applications. pp. 1–28. https://doi.org/10.1016/B978-0-12-407679-2.00001-6

Alam, M., Singh, H., 2019. Sawdust based core material for eco-friendly Vacuum Insulation Panels (VIPs).

Alam, M., Singh, H., Brunner, S., Naziris, C., 2014. Experimental characterisation and evaluation of the thermo-physical properties of expanded perlite - Fumed silica composite for effective vacuum insulation panel (VIP) core. Energy Build 69, 442–450. https://doi.org/10.1016/j.enbuild.2013.11.027

Alam, M., Singh, H., Limbachiya, M.C., 2011. Vacuum insulation panels (vips) for building construction industry - a review of the contemporary developments and future directions. Appl Energy 88, 3592–3602. https://doi.org/10.1016/j.apenergy.2011.04.040

Al-Sallal, K.A., 2003. Comparison between polystyrene and fiberglass roof insulation in warm and cold climates, Renewable Energy.

Awad, S., Zhou, Y., Katsou, E., Li, Y., Fan, M., 2021. A Critical Review on Date Palm Tree (Phoenix dactylifera L.) Fibres and Their Uses in Bio-composites. Waste Biomass Valorization 12, 2853–2887. https://doi.org/10.1007/s12649-020-01105-2

Barlaz, M.A., 2006. Forest products decomposition in municipal solid waste landfills, in: Waste Management. pp. 321–333. https://doi.org/10.1016/j.wasman.2005.11.002

Barthel, H., Rosch, L., Weis, J., 1996. Fumed Silica-Production, Properties, and Applications.

BBC Weather, 2023. Weather Forecast for London UK [WWW Document]. URL https://www.bbc.co.uk/weather (accessed 12.23.24).

Beikircher, T., Demharter, M., 2013. Heat transport in evacuated perlite powders for super-insulated long-term storages up to 300 °c. J Heat Transfer 135. https://doi.org/10.1115/1.4023351

BEIS, 2022. UK-nationally-determined-contribution.

Blonk, H., Tyszler, M., Van Paassen, M., Braconi, N., Draijer, N., Van Rijn, J., 2023. Agri-footprint 6 and Agri-footprint FLAG Methodology Report Part 2: Description of Data About us Title Agri-footprint 6 and Agri-footprint FLAG Methodology Report.

Bo Weidema, 2003. Market information in life cycle assessment.

Božiček, D., Peterková, J., Zach, J., Košir, M., 2024. Vacuum insulation panels: An overview of research literature with an emphasis on environmental and economic studies for building applications. Renewable and Sustainable Energy Reviews 189, 113849. https://doi.org/10.1016/j.rser.2023.113849

Business Analytiq, 2024. Expandable Polystyrene (EPS) price index [WWW Document]. URL https://businessanalytiq.com/procurementanalytics/index/expandable-polystyrene-eps-price-index/#google_vignette (accessed 10.21.22).

Caps, R., Fricke, J., 2000. Thermal Conductivity of Opacified Powder Filler Materials for Vacuum Insulations 1, International Journal of Thermophysics.

Caps, Roland, Fricke, J., Reiss, H., 1984. Improving the extinction properties of an evacuated high-temperature powder insulation, in: European Conference on Thermophysical Properties. 8. pp. 225–232.

Caps, R., Trunzer, A., Büttner, D., Fricke, J., Reiss, H., 1984. Spectral transmission and reflection properties of high temperature insulation materials. Int J Heat Mass Transf 27, 1865–1872. https://doi.org/10.1016/0017-9310(84)90168-6

Chang, B., Zhong, L., Akinc, M., 2016. Low cost composites for vacuum insulation core material. Vacuum 131, 120–126. https://doi.org/10.1016/j.vacuum.2016.05.027

Changes to Approved Document L 2021 (England), 2022.

Chen, Z., Wang, Y., Cheng, H., Zhou, H., 2022. Hemicellulose degradation: An overlooked issue in acidic deep eutectic solvents pretreatment of lignocellulosic biomass. Ind Crops Prod 187, 115335. https://doi.org/10.1016/j.indcrop.2022.115335

Dahan Machinery, 2023. VIBRO SIFTER MACHINE [WWW Document]. URL https://www.sieving.net/Vibro-Sifter.html (accessed 6.20.23).

Danish EPA, 2003. Market information in life cycle assessment Bo Weidema 2.-0 LCA consultants.

De Masi, R.F., Gigante, A., Vanoli, G.P., 2021. Are nZEB design solutions environmental sustainable? Sensitive analysis for building envelope configurations and photovoltaic integration in different climates. Journal of Building Engineering 39. https://doi.org/10.1016/j.jobe.2021.102292

DEFRA, 2023. Single-use plastics bans and restrictions [WWW Document].

DESNZ, 2024. Clean Power 2030 Action Plan: A new era of clean electricity.

Dong, X., Zhang, Q., Lan, Y., Zeng, Q., Fan, M., Chen, L., Zhao, W., 2022. Preparation and characterization of vacuum insulation panels with hybrid composite core materials of bamboo and glass fiber. Ind Crops Prod 188, 115691. https://doi.org/10.1016/j.indcrop.2022.115691

Driver, D.M., Seegmiller, H.L., 1985. Features of a reattaching turbulent shear layer in divergent channelflow. AIAA Journal 23, 163–171. https://doi.org/10.2514/3.8890

EPBD, 2019. Energy Performance of Buildings Directive. Second Cost Optimal Assessment for the United Kingdom.

EPD, 2024. Programme: The International EPD ® System, www.environdec.com Programme operator: EPD International AB → Cradle to Gate with C and D and optional modules.

European Comission, 2022. Euro 7 Impact Assessment Study.

Evonik Industries, 2006. Invented to improve® AEROSIL® for Adhesives and Sealants.

Finnveden, G., Hauschild, M.Z., Ekvall, T., Guinée, J., Heijungs, R., Hellweg, S., Koehler, A., Pennington, D., Suh, S., 2009. Recent developments in Life Cycle Assessment. J Environ Manage 91, 1–21. https://doi.org/10.1016/j.jenvman.2009.06.018

Fricke, J., Lu, X., Wang, P., Buttner, D., Heinemann, U., 1992. Optimization of monolithic silica aerogel insulants, Muss Transfrr.

Fricke, J., Schwab, H., Heinemann, U., 2006. Vacuum insulation panels - Exciting thermal properties and most challenging applications. Int J Thermophys 27, 1123–1139. https://doi.org/10.1007/s10765-006-0106-6

Goyer, N., 1995. Performance of painting booths equipped with down-draft ventilation. Am Ind Hyg Assoc J 56, 258–265. https://doi.org/10.1080/15428119591017097

HBS, 2021. HM Government – Heat and Buildings Strategy.

Hischier, R., Weidema, B., Althaus, H.-J., Bauer, C., Doka, G., Dones, R., Frischknecht, R., Hellweg, S., Humbert, S., Jungbluth, N., Köllner, T., Loerincik, Y., Margni, M., Nemecek, T., 2010. Swiss Centre for Life Cycle Inventories Implementation of Life Cycle Impact Assessment Methods.

Intini, F., Kühtz, S., 2011. Recycling in buildings: An LCA case study of a thermal insulation panel made of polyester fiber, recycled from post-consumer PET bottles. International Journal of Life Cycle Assessment 16, 306–315. https://doi.org/10.1007/s11367-011-0267-9

IPCC, 2023. The Earth's Energy Budget, Climate Feedbacks and Climate Sensitivity, in: Climate Change 2021 – The Physical Science Basis. Cambridge University Press, pp. 923–1054. https://doi.org/10.1017/9781009157896.009

IPCC, 2021. Climate Change 2021: The Physical Science Basis .

Jalali, M.R., Kaushik, D., Verma, S., Singh, H., 2024. A coupled model of finite element method and Mie theory for heat transfer inside expanded perlite vacuum insulation panels (VIPs) at high temperatures. Int J Heat Mass Transf 219. https://doi.org/10.1016/j.ijheatmasstransfer.2023.124885

Jason Palmer, Ian Cooper, 2012. United Kingdom housing energy fact file.

Jóvári, P., Mészáros, G., Pusztai, L., Sváb, E., 2001. The structure of liquid tetrachlorides CCl4, SiCl4, GeCl4, TiCl4, VCl4, and SnCl4. J Chem Phys 114, 8082–8090. https://doi.org/10.1063/1.1355998

Kallel, H., Doumouro, J., Krachmalnicoff, V., De Wilde, Y., Joulain, K., 2019. Thermal emission from a single glass fiber. J Quant Spectrosc Radiat Transf 236. https://doi.org/10.1016/j.jqsrt.2019.106598

Kan, A., Yuan, Y., Zhu, W., Cao, D., 2020. Aging Model by Permeation of Moist Air on Service Life of Vacuum Insulation Panels (VIPs) with Fibrous Glass Core. ES Energy & Environment. https://doi.org/10.30919/esee8c716

Karami, P., Al-Ayish, N., Gudmundsson, K., 2015. A comparative study of the environmental impact of Swedish residential buildings with vacuum insulation panels. Energy Build 109, 183–194. https://doi.org/10.1016/j.enbuild.2015.10.031

Kim, J., Lee, J.H., Song, T.H., 2012. Vacuum insulation properties of phenolic foam. Int J Heat Mass Transf 55, 5343–5349. https://doi.org/10.1016/j.ijheatmasstransfer.2012.05.051

Klein, J., 2018. Methods for calculating the emissions of transport in the Netherlands 2018 Task Force on Transportation of the Dutch Pollutant Release and Transfer Register.

König, J., Nemanič, V., Žumer, M., Petersen, R.R., Østergaard, M.B., Yue, Y., Suvorov, D., 2019. Evaluation of the contributions to the effective thermal conductivity of an open-porous-type foamed glass. Constr Build Mater 214, 337–343. https://doi.org/10.1016/j.conbuildmat.2019.04.109

Kriker, A., Bali, A., Debicki, G., Bouziane, M., Chabannet, M., 2008. Durability of date palm fibres and their use as reinforcement in hot dry climates. Cem Concr Compos 30, 639–648. https://doi.org/10.1016/j.cemconcomp.2007.11.006

Kuhn, J., Korder, S., Arduini-Schuster, M.C., Caps, R., Fricke, J., 1993. Infrared-optical transmission and reflection measurements on loose powders. Review of Scientific Instruments 64, 2523–2530. https://doi.org/10.1063/1.1143914

Kurasov, A., 2009. Strategies for Entering the Russian Tank Container and Liquid Bulk Transportation Market.

Kwon, J.-S., Jang, C.H., Jung, H., Song, T.-H., 2009. Effective thermal conductivity of various filling materials for vacuum insulation panels. Int J Heat Mass Transf 52, 5525–5532. https://doi.org/10.1016/j.ijheatmasstransfer.2009.06.029

Launder, B.E., 1995. Turbulence Modelling for CFD . By D. C. W <scp>ILCOX</scp> . DCW Industries Inc., 1993. 460pp. $75. J Fluid Mech 289, 406–407. https://doi.org/10.1017/S0022112095211388

Li, B., Yuan, X., Liao, J., Mao, B., Huang, H., Wang, X., 2019. Fabrication and characterization of a novel high-temperature vacuum insulation composites with SiC nanowire core material. Mater Res Express 6. https://doi.org/10.1088/2053-1591/ab1872

Liu, H., Xia, X., Xie, X., Ai, Q., Li, D., 2017a. Experiment and identification of thermal conductivity and extinction coefficient of silica aerogel composite. International Journal of Thermal Sciences 121, 192–203. https://doi.org/10.1016/j.ijthermalsci.2017.07.014

Liu, H., Xia, X., Xie, X., Ai, Q., Li, D., 2017b. Experiment and identification of thermal conductivity and extinction coefficient of silica aerogel composite. International Journal of Thermal Sciences 121, 192–203. https://doi.org/10.1016/j.ijthermalsci.2017.07.014

Mercedes-Benz, 2023. Truck Euro VI Transmissions. [WWW Document]. URL https://www.mercedes-benz-trucks.com/gb/en/trucks/eactros-600.html (accessed 3.15.23).

mikeinlondon, 2021. Net Zero Strategy: Build Back Greener.

Modest, M.F., Mazumder, S., 2021. Radiative heat transfer. Academic press.

Nabertherm, 2021. THERMAL PROCESS TECHNOLOGY 1 FURNACES AND HEAT TREATMENT PLANTS FOR PROCESSES UNDER AIR Made in Germany.

Nemanič, V., Zajec, B., Žumer, M., Figar, N., Kavšek, M., Mihelič, I., 2014. Synthesis and characterization of melamine-formaldehyde rigid foams for vacuum thermal insulation. Appl Energy 114, 320–326. https://doi.org/10.1016/j.apenergy.2013.09.071

Osman, S., Stefaniu, A., 2023. Density, Viscosity, and Distillation Temperatures of Binary Blends of Diesel Fuel Mixed with Oxygenated Components at Different Temperatures. Sustainability 15, 15460. https://doi.org/10.3390/su152115460

Pargana, N., Pinheiro, M.D., Silvestre, J.D., de Brito, J., 2014. Comparative environmental life cycle assessment of thermal insulation materials of buildings. Energy Build 82, 466–481. https://doi.org/10.1016/j.enbuild.2014.05.057

PNA CONICAL SCREW MIXER, n.d.

Prachayawarakorn, J., 2005. Effect of recycling on properties of rice husk-filled-polypropylene Characterization and Properties of High Amylose Mung Bean Starch Biodegradable Films Cross-linked with Malic Acid or Succinic Acid View project, Article in Songklanakarin Journal of Science and Technology.

Ramli Sulong, N.H., Mustapa, S.A.S., Abdul Rashid, M.K., 2019. Application of expanded polystyrene (EPS) in buildings and constructions: A review. J Appl Polym Sci. https://doi.org/10.1002/app.47529

Rao, P.P., Gopinath, A., 2013. Energy savings in automotive paint ovens: A new concept of shroud on the carriers. Journal of Manufacturing Science and Engineering, Transactions of the ASME 135, 1–9. https://doi.org/10.1115/1.4024537

Reiss, H., 1988. Radiative Transfer in Nontransparent, Dispersed Media. Springer Berlin Heidelberg, Berlin, Heidelberg. https://doi.org/10.1007/BFb0108658

Renato Sarc, Roland Pomberger, Magdalena Prommegger, Stefan Eferdinger, 2013. Recycling of Cooling and Freezing Appliances Containing Vacuum Insulation Panels (VIPs).

Resalati, S., Okoroafor, T., Henshall, P., Simões, N., Gonçalves, M., Alam, M., 2021. Comparative life cycle assessment of different vacuum insulation panel core materials using a cradle to gate approach. Build Environ 188. https://doi.org/10.1016/j.buildenv.2020.107501

Roberts, B.C., Webber, M.E., Ezekoye, O.A., 2015. Development of a multi-objective optimization tool for selecting thermal insulation materials in sustainable designs. Energy Build 105, 358–367. https://doi.org/10.1016/j.enbuild.2015.07.063

Rottmann, M., Beikircher, T., 2022. Pressure dependent effective thermal conductivity of pure and SiC-opacified expanded perlite between 293 K and 1073 K. International Journal of Thermal Sciences 179. https://doi.org/10.1016/j.ijthermalsci.2022.107652

Scanhugger, 2022. Scanhugger HL 5/22/25.

Schrijvers, D.L., Loubet, P., Sonnemann, G., 2016. Developing a systematic framework for consistent allocation in LCA. Int J Life Cycle Assess 21, 976–993. https://doi.org/10.1007/s11367-016-1063-3

Schwab, H., Heinemann, U., Beck, A., Ebert, H.P., Fricke, J., 2005. Dependence of thermal conductivity on water content in vacuum insulation panels with fumed silica kernels. Journal of Thermal Envelope and Building Science 28, 319–326. https://doi.org/10.1177/1097196305051792

SimaPro database manual Methods library, 2024.

SimaPro database manual Methods library, 2020.

Simmler, H., Brunner, S., 2005. Vacuum insulation panels for building application. Energy Build 37, 1122–1131. https://doi.org/10.1016/j.enbuild.2005.06.015

Singh, H., Geisler, M., Menzel, F., 2015. Experimental investigations into thermal transport phenomena in vacuum insulation panels (VIPs) using fumed silica cores. Energy Build 107, 76–83. https://doi.org/10.1016/j.enbuild.2015.08.004

SMMT, 2024. AUTOMOTIVE SUSTAINABILITY REPORT 2023 DATA.

Sonnemann, G., Vigon, B., Rack, M., Valdivia, S., 2013. Global guidance principles for life cycle assessment databases: Development of training material and other implementation activities on the publication. International Journal of Life Cycle Assessment 18, 1169–1172. https://doi.org/10.1007/s11367-013-0563-7

Swimm, K., Reichenauer, G., Vidi, S., Ebert, H.P., 2009. Gas pressure dependence of the heat transport in porous solids with pores smaller than 10μm. Int J Thermophys 30, 1329–1342. https://doi.org/10.1007/s10765-009-0617-z

Tenpierik, M., Cauberg, H., 2007. Analytical Models for Calculating Thermal Bridge Effects Caused by Thin High Barrier Envelopes around Vacuum Insulation Panels. J Build Phys 30, 185–215. https://doi.org/10.1177/1744259107073160

Tetlow, D., De Simon, L., Liew, S.Y., Hewakandamby, B., Mack, D., Thielemans, W., Riffat, S., 2017. Cellulosic-crystals as a fumed-silica substitute in vacuum insulated panel technology used in building construction and retrofit applications. Energy Build 156, 187–196. https://doi.org/10.1016/j.enbuild.2017.08.058

Thiessen, S., Knabben, Fernando Testoni, Melo, Claudio, Gonã, J.M., Knabben, Fernando T, Melo, Cláudio, Gonçalves, J.M., 2016. Purdue e-Pubs An Experimental Study on the Use of Vaccum Insulation Panels in Household Refrigerators An Experimental Study on the Use of Vacuum Insulation Panels in Household Refrigerators.

Tillman, A.-M., 2000. Significance of decision-making for LCA methodology. Environ Impact Assess Rev 20, 113–123. https://doi.org/10.1016/S0195-9255(99)00035-9

Väntsi, O., Kärki, T., 2014. Mineral wool waste in Europe: A review of mineral wool waste quantity, quality, and current recycling methods. J Mater Cycles Waste Manag. https://doi.org/10.1007/s10163-013-0170-5

Verma, S., Singh, H., 2022. Predicting the conductive heat transfer through evacuated perlite based vacuum insulation panels. International Journal of Thermal Sciences 171. https://doi.org/10.1016/j.ijthermalsci.2021.107245

Verma, S., Singh, H., 2020. Vacuum insulation panels for refrigerators. International Journal of Refrigeration 112, 215–228. https://doi.org/10.1016/j.ijrefrig.2019.12.007

Verma, S., Singh, H., 2019a. Vacuum insulation in cold chain equipment: A review, in: Energy Procedia. Elsevier Ltd, pp. 232–241. https://doi.org/10.1016/j.egypro.2019.02.086

Verma, S., Singh, H., 2019b. Why and which insulation materials for refrigerators!, in: Refrigeration Science and Technology. International Institute of Refrigeration, pp. 1848–1854. https://doi.org/10.18462/iir.icr.2019.1874

Wang, B., Li, Z., Qi, X., Chen, N., Zeng, Q., Dai, D., Fan, M., Rao, J., 2019a. Thermal insulation properties of green vacuum insulation panel using wood fiber as core material. Bioresources 14, 3339–3351. https://doi.org/10.15376/biores.14.2.3339-3351

Wang, B., Li, Z., Qi, X., Chen, N., Zeng, Q., Dai, D., Fan, M., Rao, J., 2019b. Thermal Insulation Properties of Green Vacuum Insulation Panel Using Wood Fiber as Core Material.

Wang, L., Yang, Y., Chen, Zhaofeng, Hong, Y., Chen, Zhou, Wu, J., 2020. Preparation and characterization of a type of green vacuum insulation panel prepared with straw core material. Materials 13, 1–16. https://doi.org/10.3390/ma13204604

Wang, X., Walliman, N., Ogden, R., Kendrick, C., 2007. VIP and their applications in buildings: a review. Proceedings of the Institution of Civil Engineers - Construction Materials 160, 145–153. https://doi.org/10.1680/coma.2007.160.4.145

Wei, G., Liu, Y., Zhang, X., Du, X., 2013. Radiative heat transfer study on silica aerogel and its composite insulation materials. J Non Cryst Solids 362, 231–236. https://doi.org/10.1016/j.jnoncrysol.2012.11.041

Wei, G., Liu, Y., Zhang, X., Yu, F., Du, X., 2011. Thermal conductivities study on silica aerogel and its composite insulation materials. Int J Heat Mass Transf 54, 2355–2366. https://doi.org/10.1016/j.ijheatmasstransfer.2011.02.026

Zach, J., Peterková, J., Dufek, Z., Sekavčnik, T., 2019. Development of vacuum insulating panels (VIP) with non-traditional core materials. Energy Build 199, 12–19. https://doi.org/10.1016/j.enbuild.2019.06.026

Zhao, J.J., Duan, Y.Y., Wang, X.D., Wang, B.X., 2012. Effects of solid-gas coupling and pore and particle microstructures on the effective gaseous thermal conductivity in aerogels. Journal of Nanoparticle Research 14. https://doi.org/10.1007/s11051-012-1024-0

Zhao, W., Yan, W., Zhang, Z., Gao, H., Zeng, Q., Du, G., Fan, M., 2022. Development and performance evaluation of wood-pulp/glass fibre hybrid composites as core materials for vacuum insulation panels. J Clean Prod 357. https://doi.org/10.1016/j.jclepro.2022.131957

Zhou, H., Long, Y., Meng, A., Li, Q., Zhang, Y., 2013. The pyrolysis simulation of five biomass species by hemi-cellulose, cellulose and lignin based on thermogravimetric curves. Thermochim Acta 566, 36–43. https://doi.org/10.1016/j.tca.2013.04.040

Zhuang, J., Ghaffar, S.H., Fan, M., Corker, J., 2017. Restructure of expanded cork with fumed silica as novel core materials for vacuum insulation panels. Compos B Eng 127, 215–221. https://doi.org/10.1016/j.compositesb.2017.06.019

Zhuk, P., 2018. Lifecycle assessment of vacuum heat-insulation, in: IOP Conference Series: Materials Science and Engineering. Institute of Physics Publishing. https://doi.org/10.1088/1757-899X/365/3/032012

Appendices

Appendix 1: Energy consumption at different climatic conditions

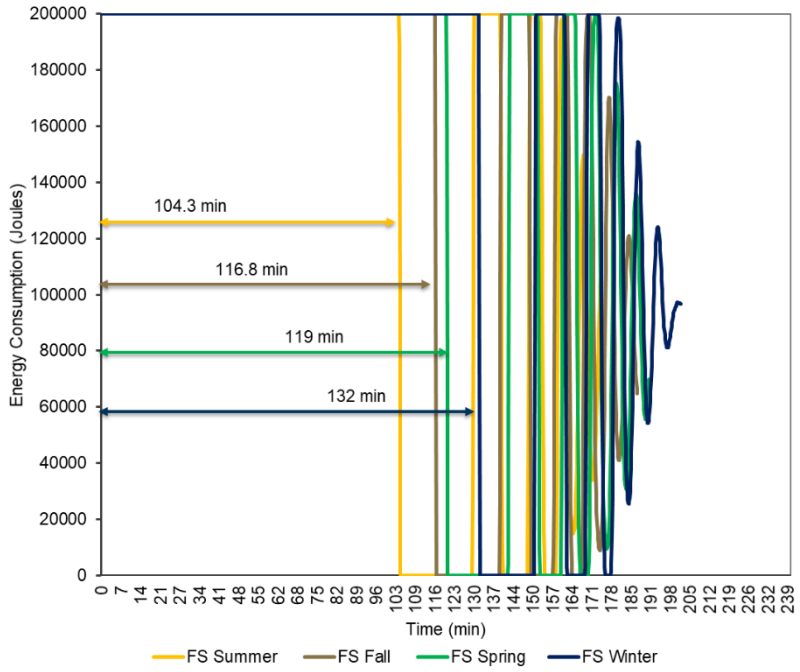

Figure A1.1 Energy consumption of CPB insulated with FS VIPs over four distinct seasons

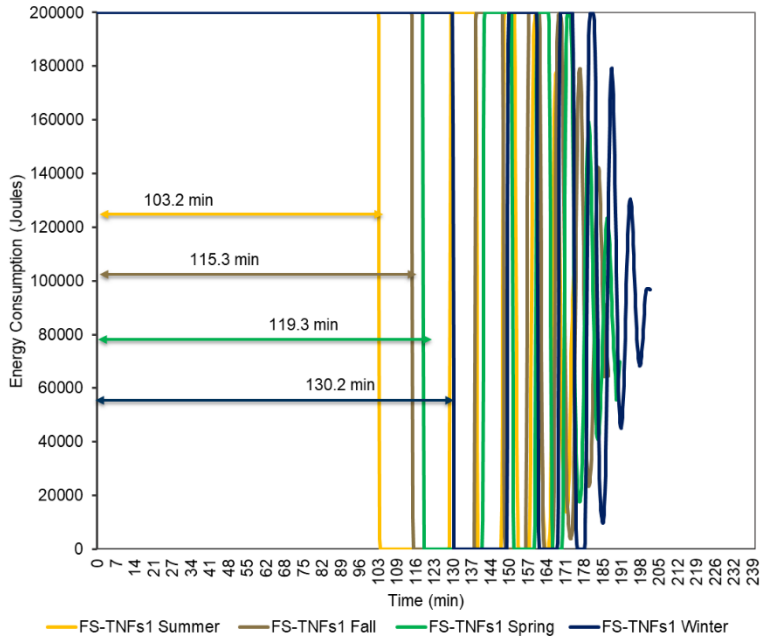

Figure A1.2 Energy consumption of CPB insulated with FS-TNFs1 VIPs over four distinct seasons

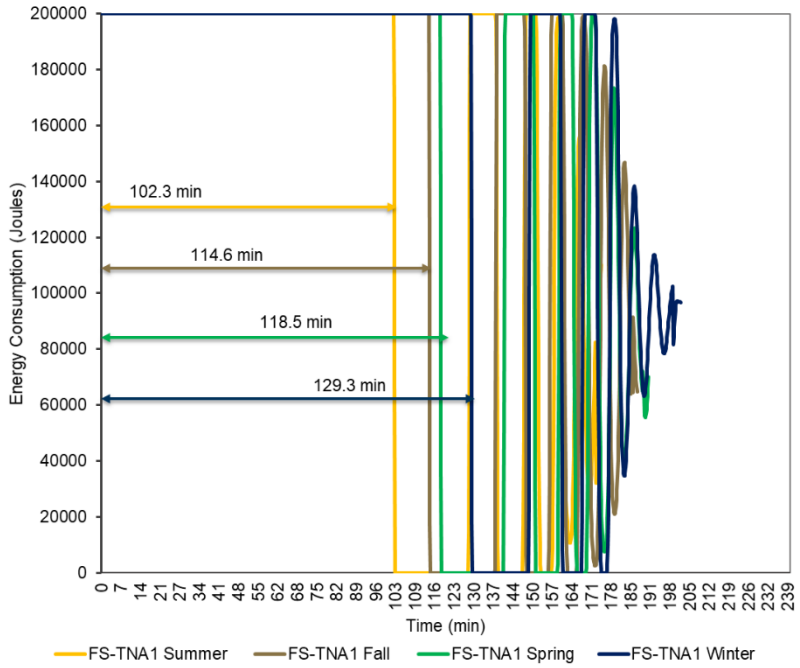

Figure A1.3 Energy consumption of CPB insulated with FS-TNA1 VIPs over four distinct seasons

Appendix 2: Energy consumption with variant thermal conductivity

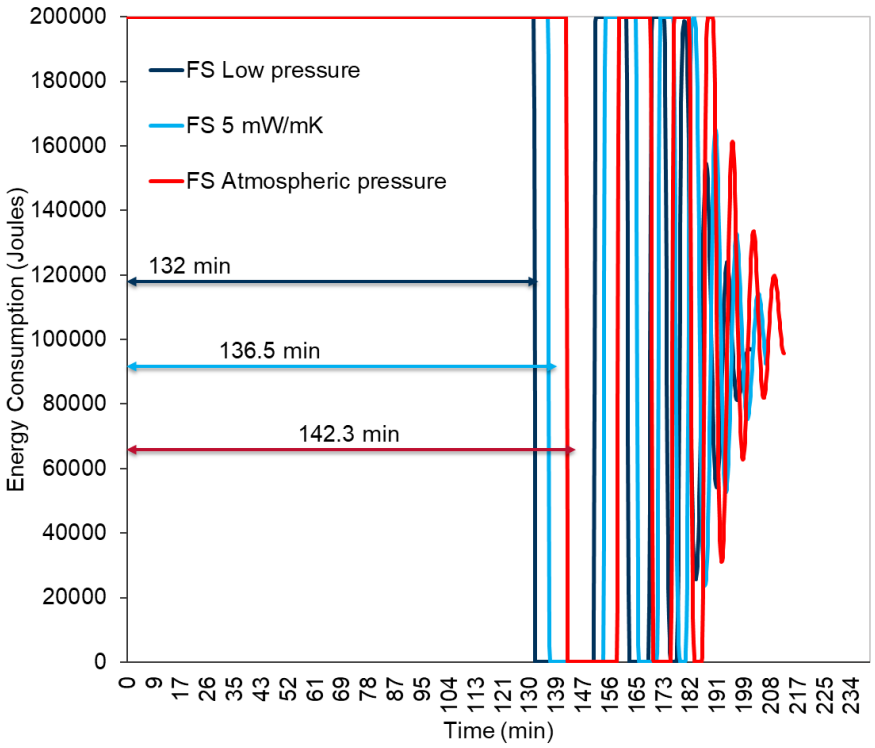

Figure A2.1 Energy consumption of CPB insulated by FS VIP at three different sealing pressures

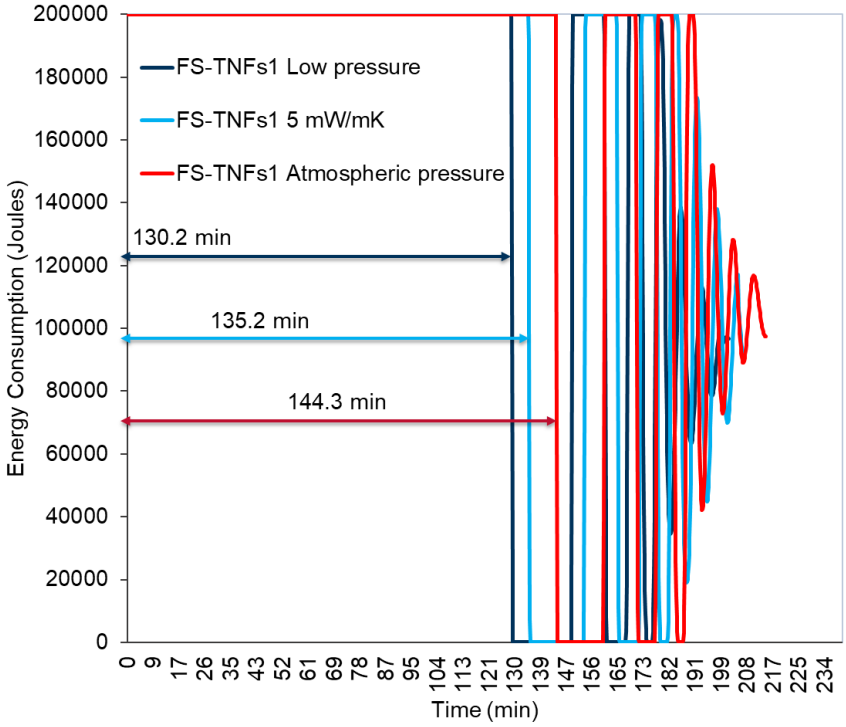

Figure A2.2 Energy consumption of CPB insulated by FS-TNFs1 VIP at three different sealing pressures

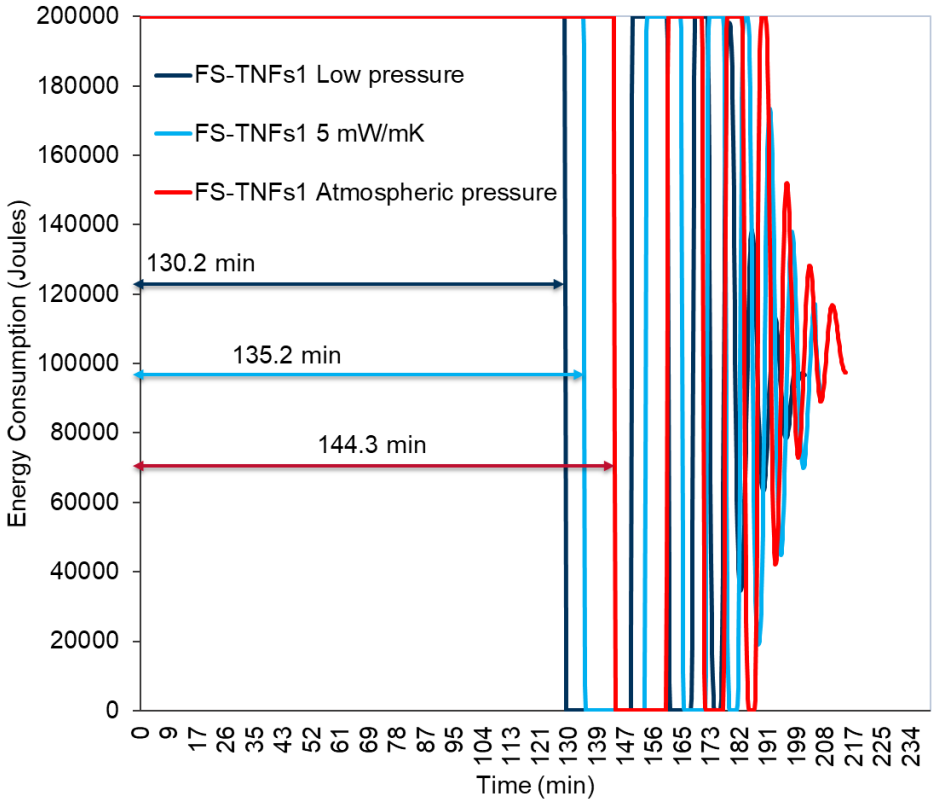

Figure A2.3 Energy consumption of CPB insulated by FS-TNA1 VIP at three different sealing pressures

Appendix 3: LCA results using Cut-off approach

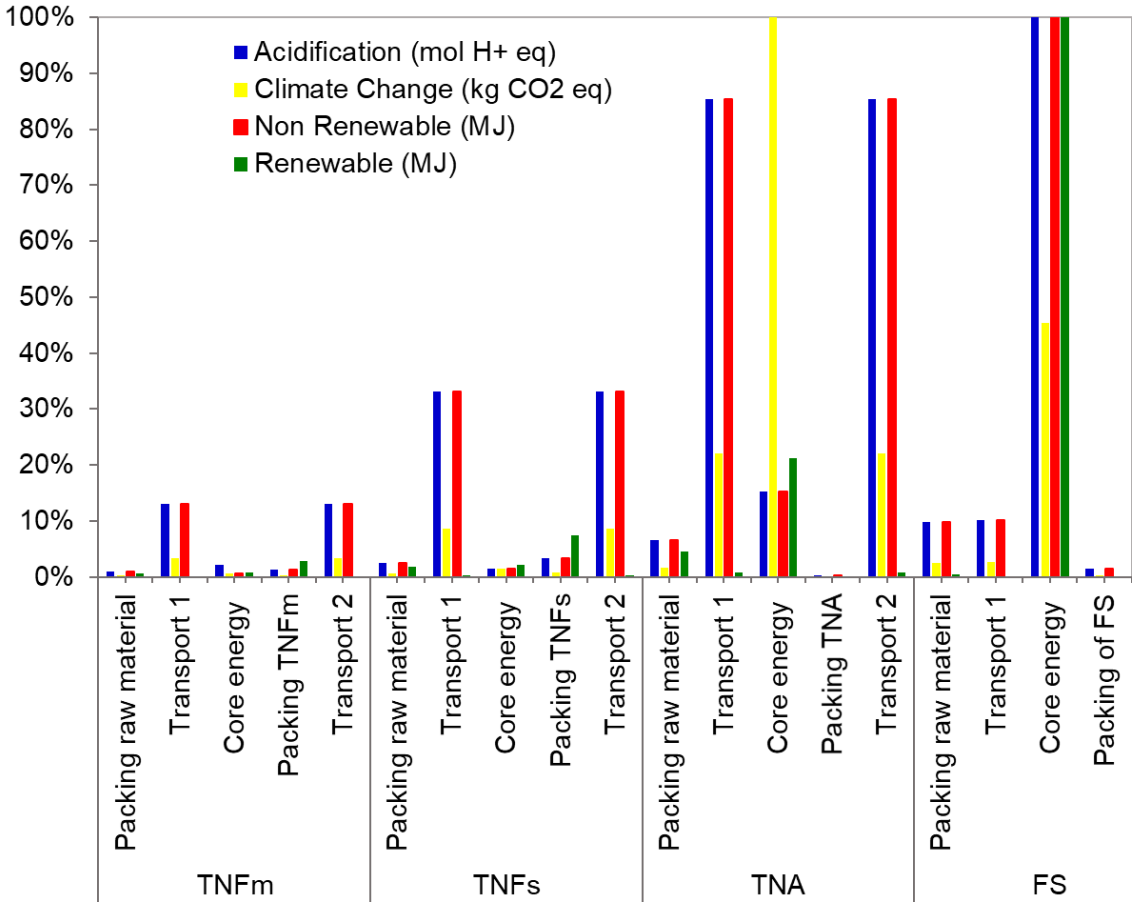

Figure A3.1 LCIA results for the production of TNFm, TNFs, TNA and FS

Table A3.1: Results of TNFm including transportation and packaging

	Packing raw material	Transport 1	Core energy	Packing TNFm	Transport 2
Acidification (mol H+ eq)	0.0005	0.0065	0.0011	0.0007	0.0065
Climate Change (kg CO_2 eq)	0.09	1.14	0.19	0.12	1.14
Non-Renewable (MJ)	1.81	23.43	1.09	2.37	23.43
Renewable (MJ)	0.50	0.08	0.61	2.11	0.08

Table A3.2: Results of TNFs including transportation and packaging

	Packing raw material	Transport 1	Core energy	Packing TNFs	Transport 2
Acidification (mol H+ eq)	0.001	0.016	0.001	0.002	0.016
Climate Change (kg CO_2 eq)	0.22	2.91	0.49	0.29	2.91
Non-Renewable (MJ)	4.60	59.64	2.79	6.03	59.63
Renewable (MJ)	1.28	0.20	1.56	5.37	0.20

Table A3.3: Results of TNA including transportation and packaging

	Packing raw material	Transport 1	Core energy	Packing TNA	Transport 2
Acidification (mol H+ eq)	0.0033	0.0424	0.0075	0.0001	0.0424
Climate Change (kg CO_2 eq)	0.58	7.50	34.01	0.02	7.50
Non-Renewable (MJ)	11.84	153.62	27.33	0.38	153.62
Renewable (MJ)	3.29	0.52	15.29	0.01	0.52

Table A3.4: Results of FS including transportation and packaging

	Packing raw material	Transport 1	Core energy	Packing of FS	Transport 2
Acidification (mol H+ eq)	0.005	0.005	0.050	0.001	0.006
Climate Change (kg CO_2 eq)	0.86	0.89	15.44	0.13	1.13
Non-Renewable (MJ)	17.67	18.27	179.85	2.58	23.07
Renewable (MJ)	0.37	0.06	72.11	0.10	0.08

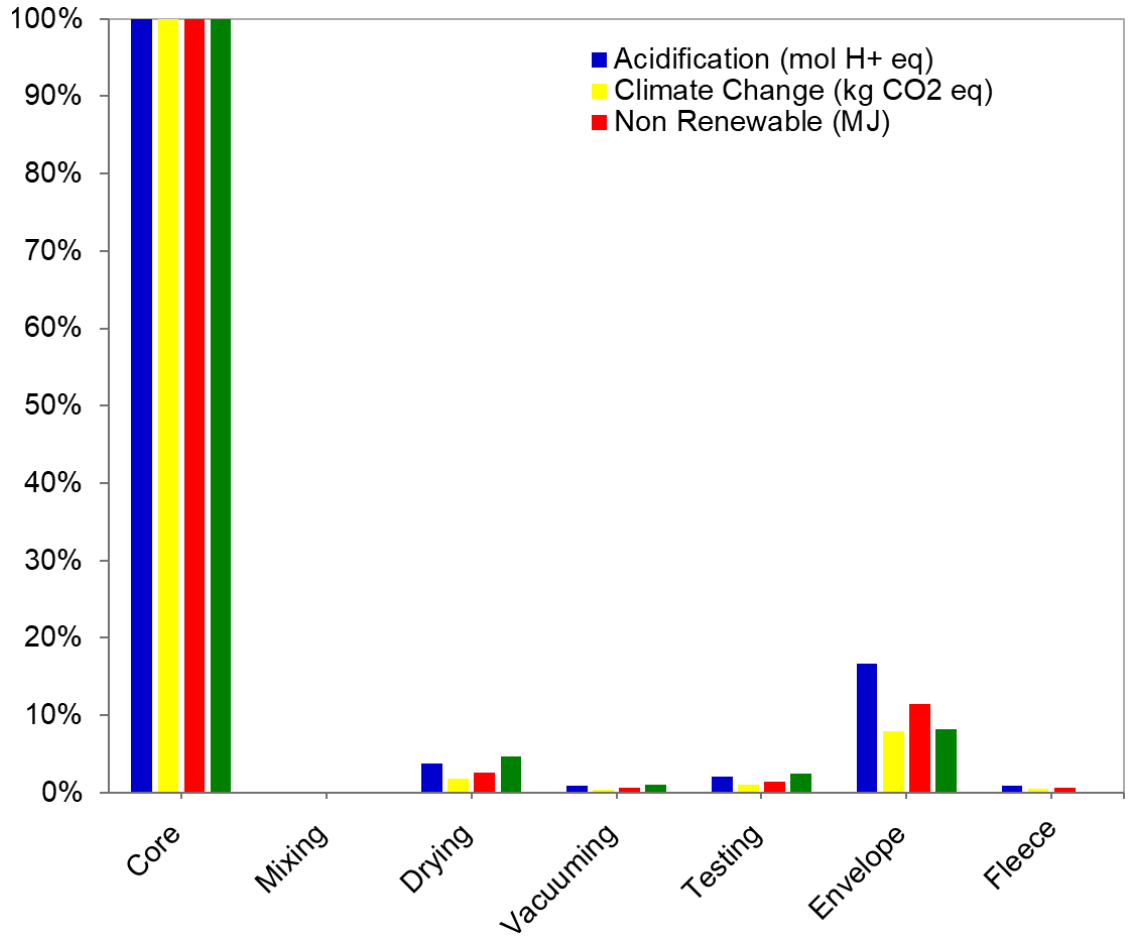

Figure A3.1 LCIA results for the production of different components of VIPs

Table A3.5: Results of the production of different components of VIPs

	Core	Mixing	Drying	Vacuuming	Testing	Envelope	Fleece
Acidification (mol H+ eq)	0.0754	0.0001	0.0029	0.0007	0.0015	0.0125	0.0007
Climate Change (kg CO_2 eq)	27.79	0.01	0.51	0.12	0.27	2.22	0.13
Non-Renewable (MJ)	396.31	0.21	10.40	2.42	5.56	45.40	2.57
Renewable (MJ)	125.76	0.03	5.82	1.35	3.11	10.25	0.12

Appendix 4: LCA results using APOS approach

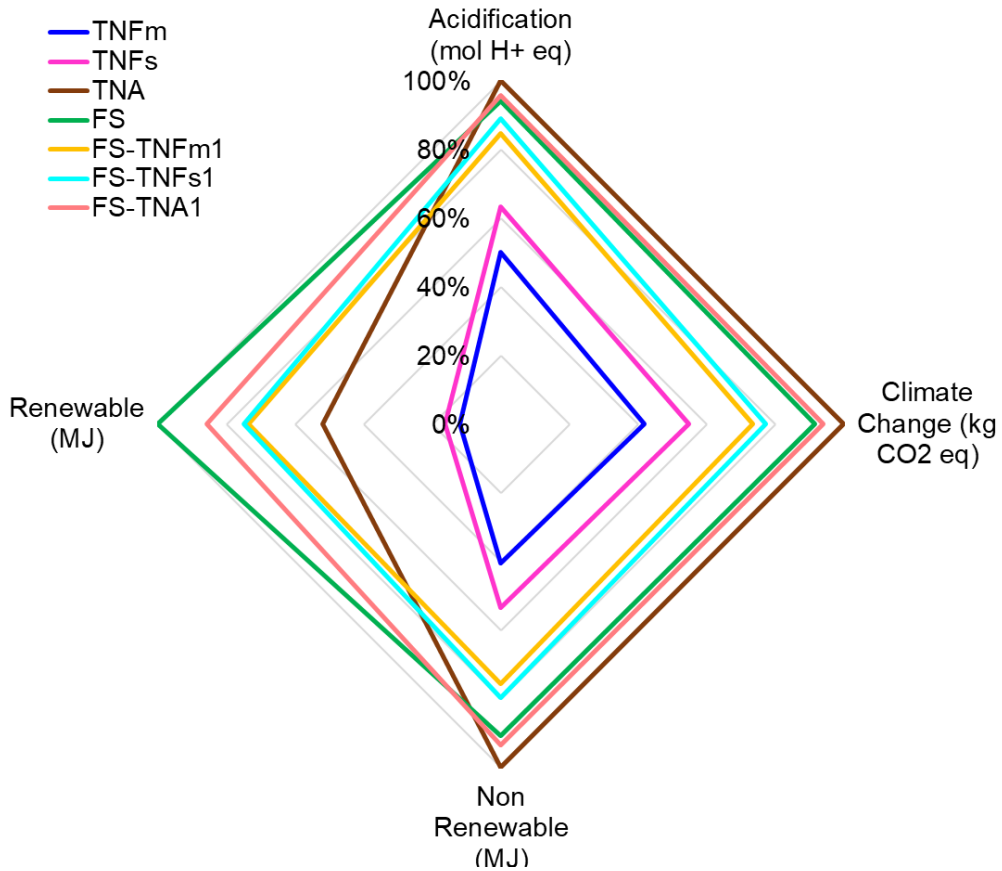

Figure A4.1 Contribution of seven core materials to the four environmental impacts (cradle to gate APOS approach)

Table A4.1 Results of pure core materials VIPs (Cradle to Gate APOS approach)

	FS	TNFm	TNFs	TNA
Acidification (mol H+ eq)	20.2	10.7	13.6	21.5
Climate Change (kg CO_2 eq)	5241.1	2405.5	3135.4	5731.4
Non-Renewable (MJ)	76106.9	33977.6	44821.4	83909.8
Renewable (MJ)	22153.0	2623.0	3604.2	11505.8

Table A4.2 Results of composite core materials VIPs (cradle to gate APOS approach)

	FS-TNFm	FS-TNFs	FS-TNA1
Acidification (mol H+ eq)	18.2	19.1	20.6
Climate Change (kg CO_2 eq)	4214.8	4430.7	5388.2
Non-Renewable (MJ)	63476.1	66728.6	78456.7
Renewable (MJ)	16298.4	16592.4	18963.8

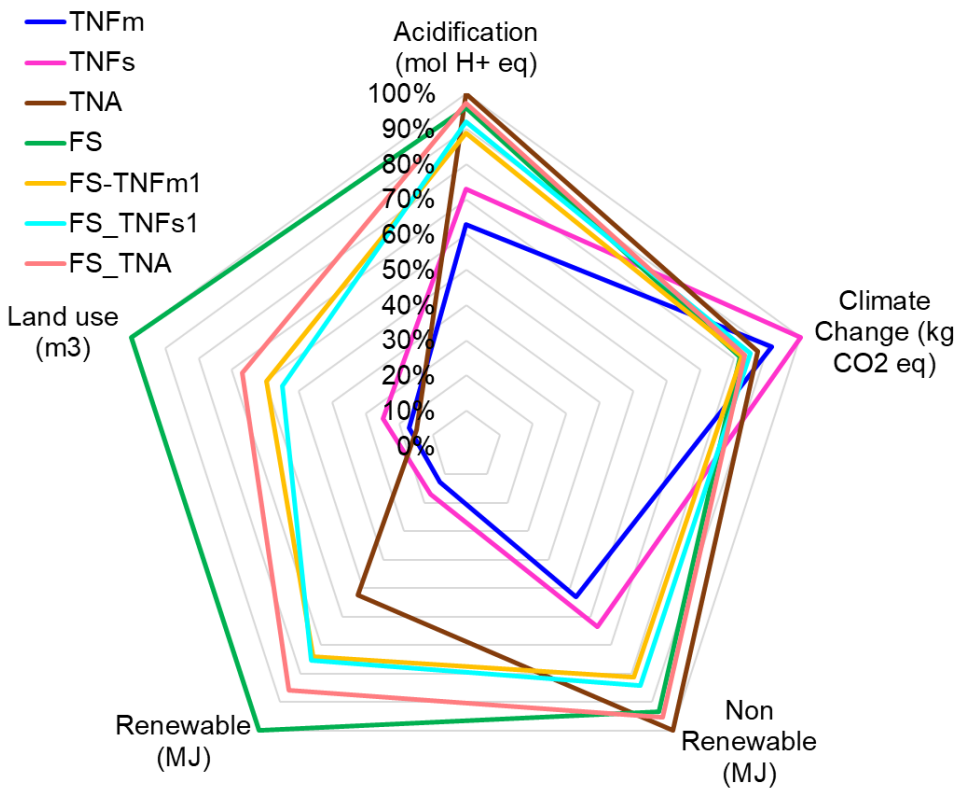

Figure A4.2 Contribution of seven core materials to the five environmental impacts (cradle to grave APOS approach)

Table A4.3 Results of pure core materials VIPs (cradle to grave APOS approach)

	TNFm	TNFs	TNA	FS
Acidification (mol H+ eq)	18.3	21.2	29.1	27.9
Climate Change (kg CO_2 eq)	7736.0	8469.1	7382.7	6928.2
Non-Renewable (MJ)	56459.1	67352.6	106378.0	99112.1
Renewable (MJ)	2850.8	3834.1	11733.0	22402.6
Land use (m3)	2.1	3.0	1.8	12.2

Table A4.4 Results of composite core materials VIPs (cradle to grave APOS approach)

	FS-TNFm1	FS_TNFs1	FS_TNA
Acidification (mol H+ eq)	25.8	26.7	28.2
Climate Change (kg CO_2 eq)	6988.3	7202.3	7061.4
Non-Renewable (MJ)	86226.1	89448.7	101253.1
Renewable (MJ)	16537.4	16830.1	19204.6
Land use (m3)	7.3	6.7	8.1

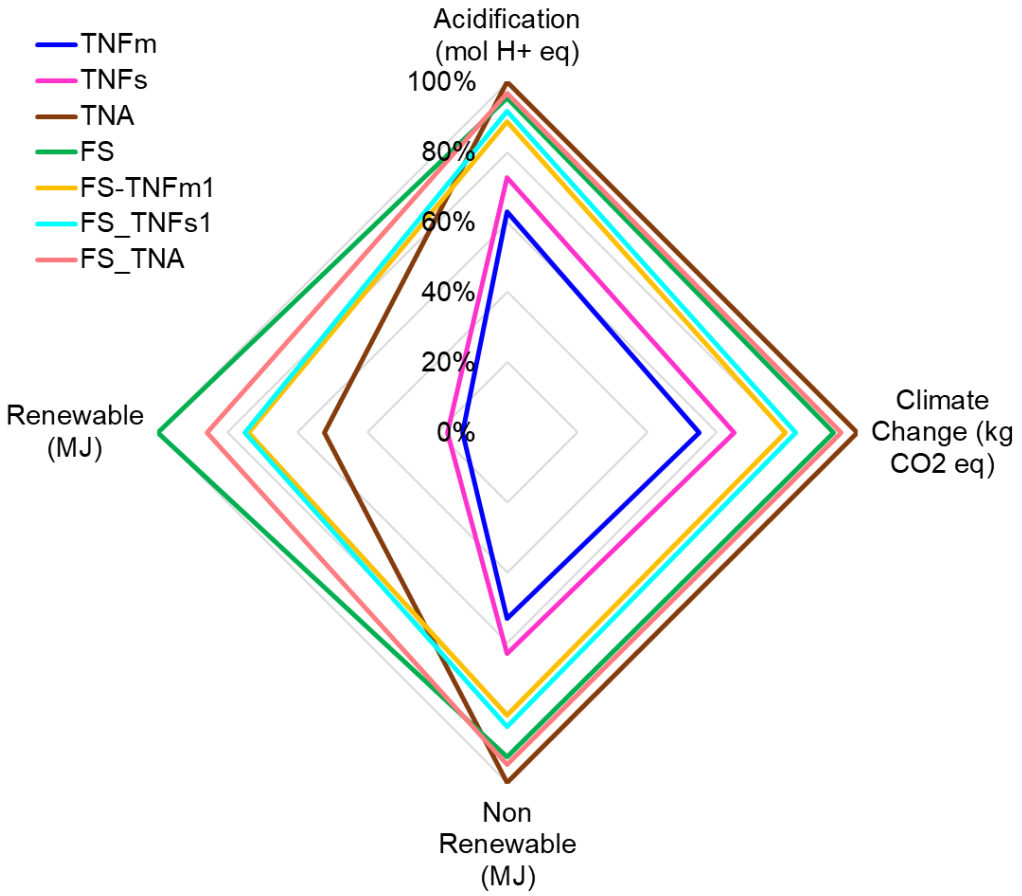

Figure A4.3 Contribution of seven core materials to the four environmental impacts (cradle to cradle APOS approach)

Table A4.5 Results of pure core materials VIPs (cradle to cradle APOS approach)

	TNFm	TNFs	TNA	FS
Acidification (mol H+ eq)	18.3	21.1	29.0	27.7
Climate Change (kg CO_2 eq)	4050.6	4780.5	7376.5	6886.2
Non-Renewable (MJ)	56351.4	67195.2	106283.5	98480.7
Renewable (MJ)	2846.3	3827.5	11729.0	22376.3

Table A4.6 Results of composite core materials VIPs (cradle to cradle APOS approach)

	FS-TNFm1	FS_TNFs1	FS_TNA
Acidification (mol H+ eq)	25.7	26.6	28.1
Climate Change (kg CO_2 eq)	5859.9	6075.8	7033.3
Non-Renewable (MJ)	85849.9	89102.3	100830.4
Renewable (MJ)	16521.7	16815.7	19187.0

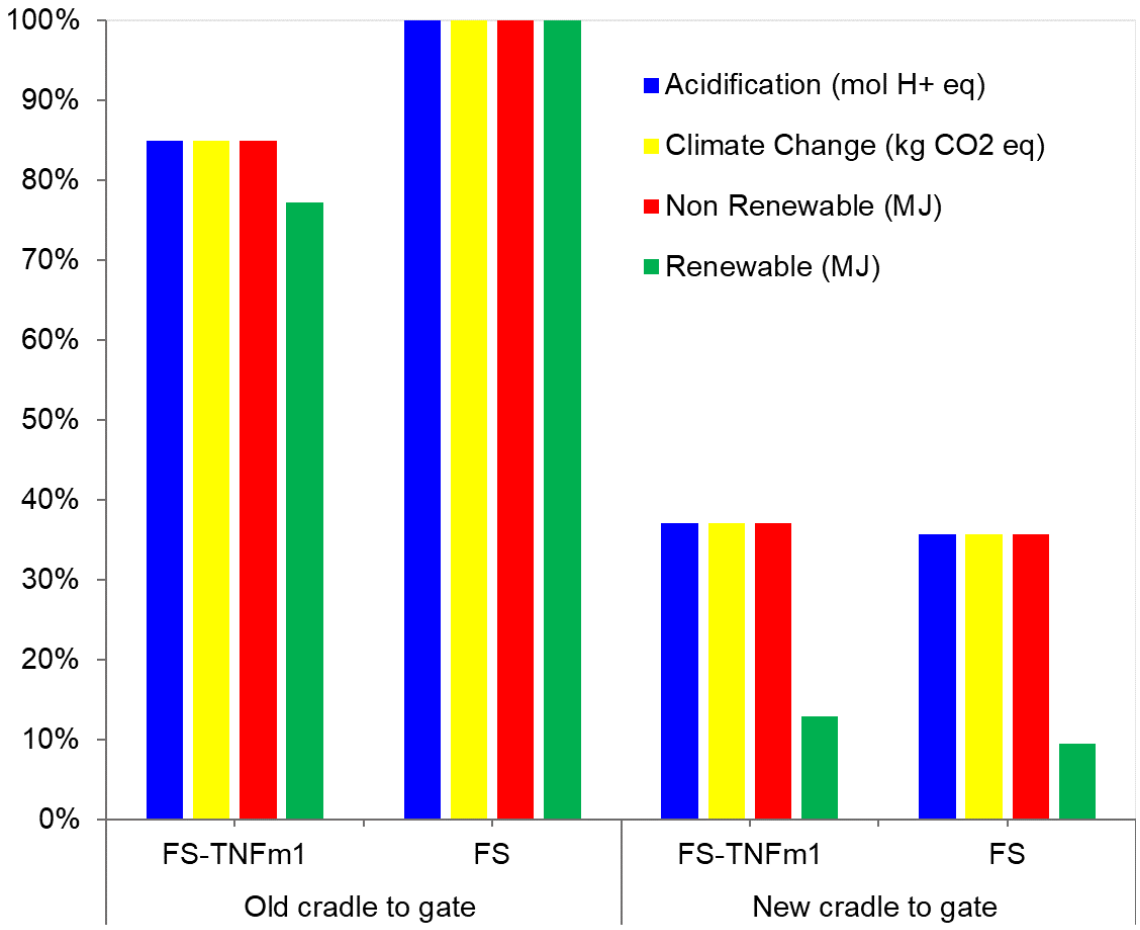

Figure A4.4 LCIA results comparing the old and new cradle to gate - APOS

Table A4.7 Results comparing the old and new cradle to gate - APOS

	Old cradle to gate		New cradle to gate	
	FS-TNFm1	FS	FS-TNFm1	FS
Acidification (mol H+ eq)	18.6	21.8	8.1	7.8
Climate Change (kg CO_2 eq)	4294.8	5053.5	1876.9	1804.6
Non-Renewable (MJ)	64680.1	76106.9	28267.1	27177.9
Renewable (MJ)	17110.0	22153.0	2856.1	2108.1

Appendix 5: LCA SimaPro using Cut-off Approach

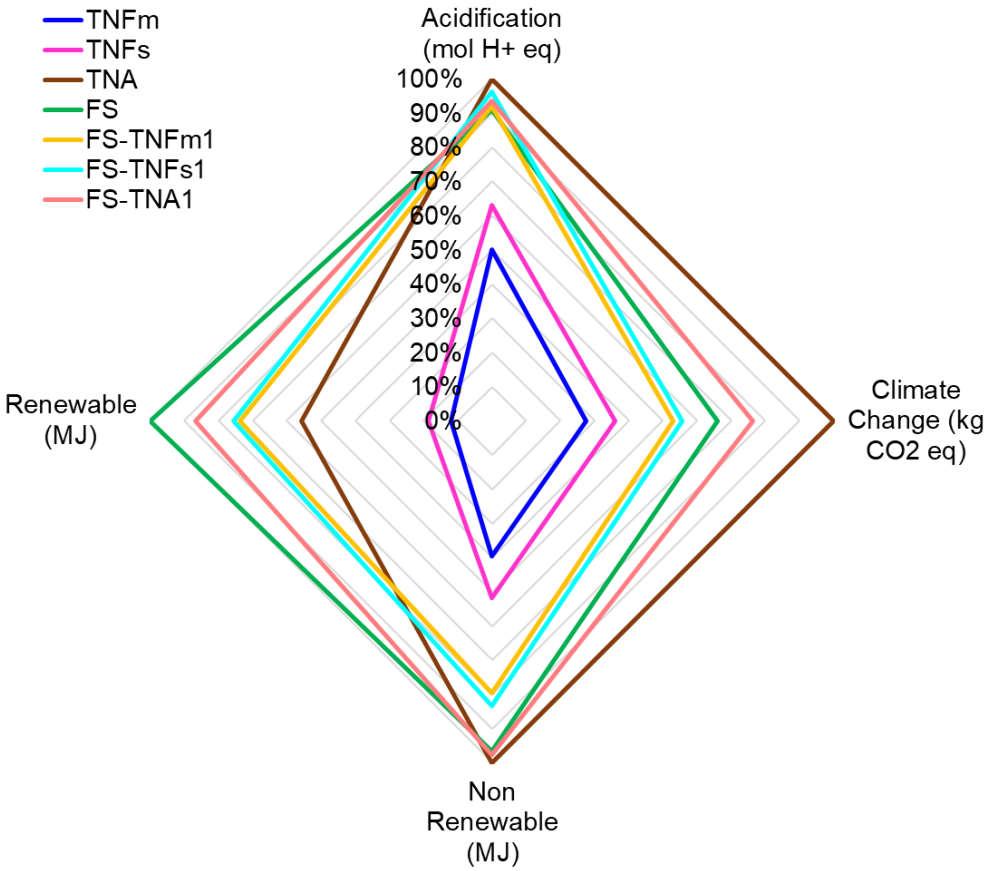

Figure A5.1 Contribution of seven core materials to the four environmental impacts (cradle to gate - SimaPro)

Table A5.1 Results of pure core materials VIPs (cradle to gate - SimaPro)

	FS	TNFm	TNFs	TNA
Acidification (mol H+ eq)	20.2	11.2	14.1	22.3
Climate Change (kg CO_2 eq)	7469.4	3122.0	4075.0	11319.5
Non-Renewable (MJ)	86746.8	35373.5	46503.3	89721.5
Renewable (MJ)	11157.4	1348.7	2076.2	6223.4

Table A5.1 Results of composite core materials VIPs (cradle to gate - SimaPro)

	FS-TNFm	FS-TNFs1	FS-TNA1
Acidification (mol H+ eq)	20.5	21.4	20.8
Climate Change (kg CO_2 eq)	6007.2	6288.3	8624.5
Non-Renewable (MJ)	71344.9	74683.0	87650.5
Renewable (MJ)	8217.3	8435.3	9680.0

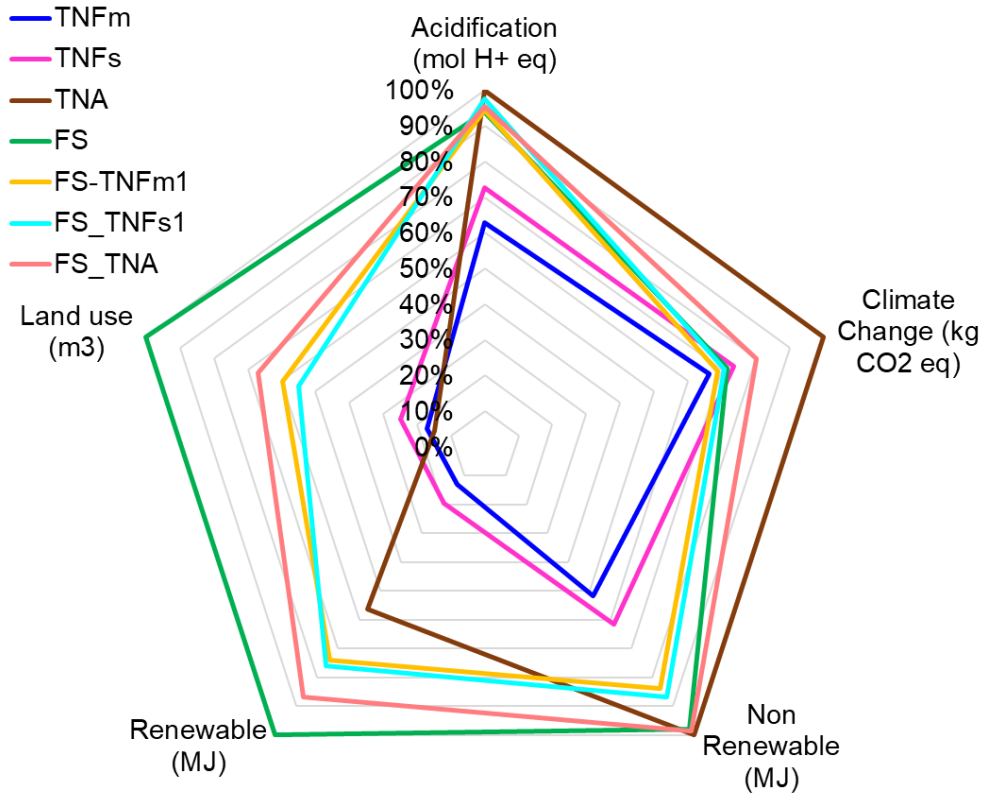

Figure A5.2 Contribution of seven core materials to the five environmental impacts (cradle to grave - SimaPro)

Table A5.3 Results of pure core materials VIPs (cradle to grave - SimaPro)

	TNFm	TNFs	TNA	FS
Acidification (mol H+ eq)	18.8	21.7	29.9	28.0
Climate Change (kg CO_2 eq)	8881.2	9838.8	13399.3	9599.1
Non-Renewable (MJ)	58194.7	69379.5	112528.1	110146.7
Renewable (MJ)	1477.6	2205.9	6352.1	11294.6
Land use (m3)	2.1	3.0	1.8	12.2

Table A5.4 Results of composite core materials VIPs (cradle to grave - SimaPro)

	FS-TNFm1	FS_TNFs1	FS_TNA
Acidification (mol H+ eq)	28.2	29.1	28.6
Climate Change (kg CO_2 eq)	9216.7	9495.0	10734.7
Non-Renewable (MJ)	94462.8	97767.9	110819.6
Renewable (MJ)	8350.4	8568.0	9813.9
Land use (m3)	7.3	6.7	8.1

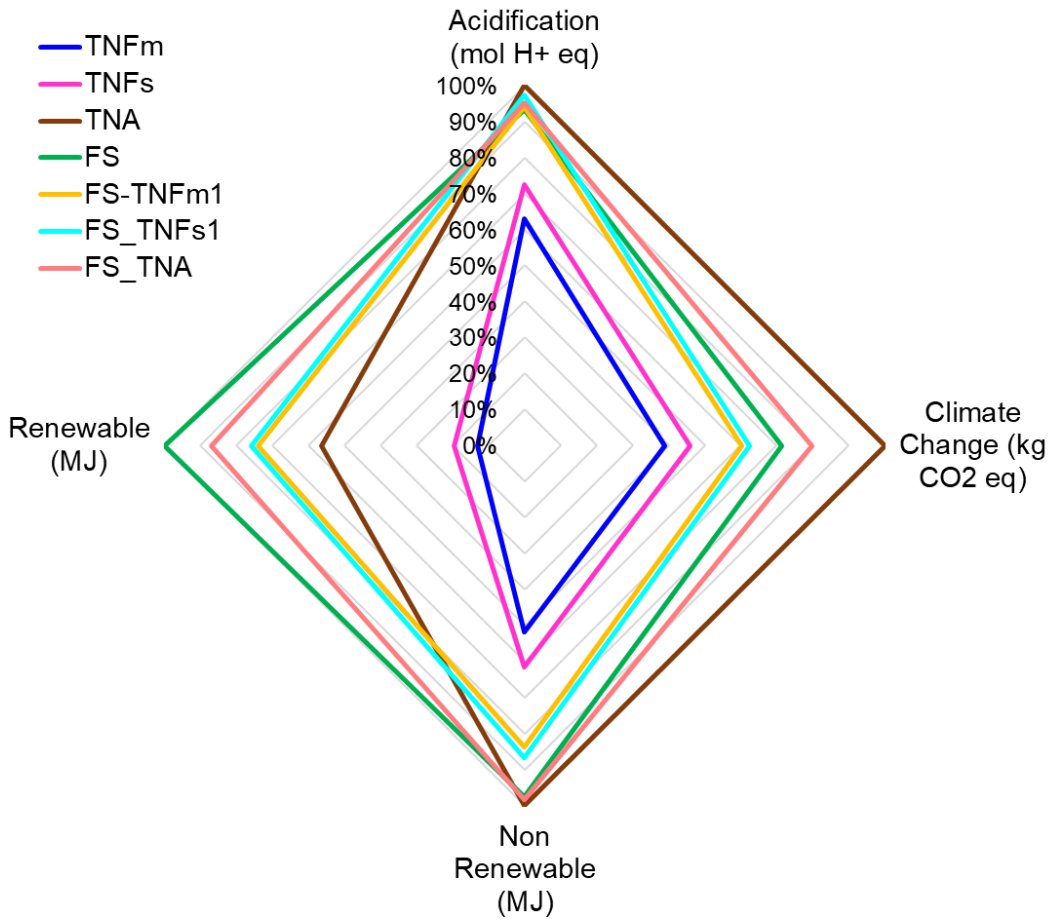

Figure A5.3 Contribution of seven core materials to the four environmental impacts (cradle to cradle - SimaPro)

Table A5.5 Results of pure core materials VIPs (cradle to cradle - SimaPro)

	TNFm	TNFs	TNA	FS
Acidification (mol H+ eq)	18.8	21.6	29.8	27.8
Climate Change (kg CO_2 eq)	5193.0	6146.0	13390.5	9540.4
Non-Renewable (MJ)	58075.7	69205.5	112423.7	109449.1
Renewable (MJ)	1475.9	2203.4	6350.6	11284.6

Table A5.6 Results of composite core materials VIPs (cradle to cradle - SimaPro)

	FS-TNFm1	FS_TNFs1	FS_TNA
Acidification (mol H+ eq)	28.1	29.0	28.4
Climate Change (kg CO_2 eq)	8078.2	8359.3	10695.4
Non-Renewable (MJ)	94047.2	97385.3	110352.8
Renewable (MJ)	8344.5	8562.5	9807.2

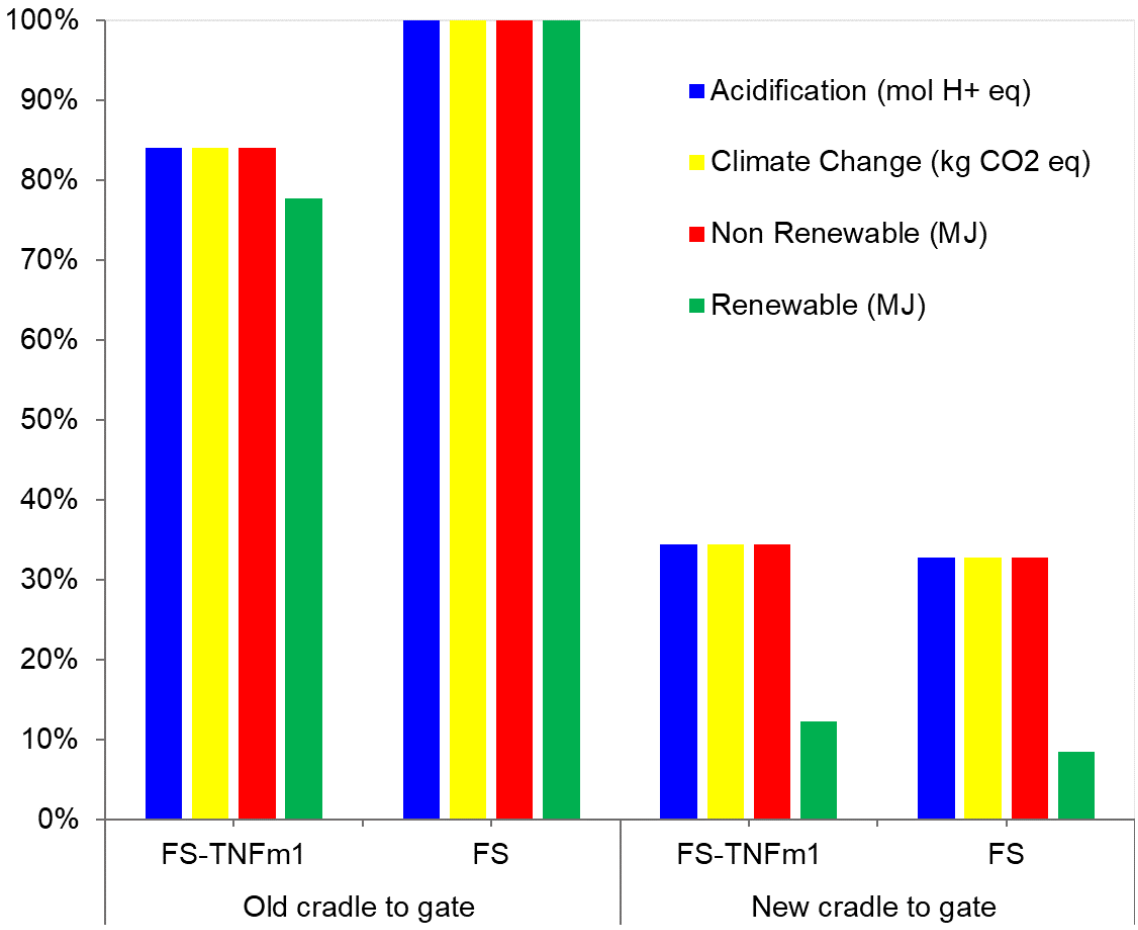

Figure A5.4 LCIA results comparing the old and new cradle to gate – SimaPro

Table A5.7 Results comparing the old and new cradle to gate - SimaPro

	Old cradle to gate		New cradle to gate	
	FS-TNFm1	FS	FS-TNFm1	FS
Acidification (mol H+ eq)	20.9	24.9	8.6	8.2
Climate Change (kg CO_2 eq)	6139.1	7304.1	2514.8	2395.1
Non-Renewable (MJ)	72911.0	86746.8	29866.7	28445.5
Renewable (MJ)	8679.5	11157.4	1372.1	945.8